

**HCCI HEAT RELEASE RATE AND COMBUSTION EFFICIENCY: A
COUPLED KIVA MULTI-ZONE MODELING STUDY**

by

Yanbin Mo

A dissertation submitted in partial fulfillment
of the requirements for the degree of
Doctor of Philosophy
(Mechanical Engineering)
in The University of Michigan
2008

Doctoral Committee:

Professor Dennis N. Assanis, Chair
Professor James F. Driscoll
Professor Margaret S. Wooldridge
Associate Research Professor Zoran S. Filipi
Research Scientist George A. Lavoie

© Yanbin Mo 2008
All Rights Reserved

To Deng

ACKNOWLEDGMENTS

I feel extremely fortunate to be associated with one of the best mentors in the engine society, Professor Assanis. He impacts me tremendously not only in the research subject matter, but well beyond. He has been a role model for me. To possess the same quality as a person will be my goal for the long future to come.

I'm also in great debt to Dr. Lavoie. Dr. Lavoie became my engine "hero" ten years ago and 7900 miles away from this place when I first read his paper on extended Zeldovich mechanism back in China during college. His guidance and patience help me overcome academic growing pains. I would also like to thank Professor Filipi for his help and guidance; he has always made himself available for questions and discussions.

I sincerely thank Professor Wooldridge and Professor Driscoll for serving on my dissertation committee. Professor Wooldridge's heat transfer class is one of my best classroom experiences throughout my student career. Another great class I took is Professor Faeth's combustion class. Unfortunately, Professor Faeth passed away not long after my preliminary exam. Professor Driscoll is kind enough to fill in the void left by Professor Faeth, for that, I'm truly thankful.

Special thanks go to the HCCI circle in the Autolab. Aris has been a mentor for me over my HCCI journey. I can't thank him enough for the help he provided on the subject matter, as well as soccer video clips he offered for relaxing. It has been great environment to work with Kyoungjoon, Junseok, and Orgun. I thank them for their support.

Here are the people in the auto lab making my life much easy and fun: William, Bruno, Stani, Dohoy, Sangjin, Bin, Jason, Pin, Andreas, Chaitanya, the flag football team and the rest of my auto lab friends.

I thank my parents for making me who I am, and always having the patience and encouragement. Also, thank to my daughter Amelia, for giving me so much fun and hope.

Finally, I would like to express my gratitude to my wife, Deng. The only thing she hasn't done for me is becoming a mechanical engineer herself and writing the dissertation for me. Her continuous support and love is beyond appreciation by words.

TABLE OF CONTENTS

DEDICATION	ii
ACKNOWLEDGMENTS	iii
LIST OF FIGURES	xi
LIST OF TABLES	xx
LIST OF ABBREVIATIONS	xxii
ABSTRACT	xxv
CHAPTER 1 INTRODUCTION	1
1.1 Review of near-HCCI Production Engine.....	2
1.1.1 Toyota UNIBUS	2
1.1.2 Nissan MK	3
1.1.3 Honda AR	3
1.2 Review of HCCI Experiment	4
1.3 Review of HCCI Modeling	7
1.3.1 Single-zone Thermo-kinetic Model	7
1.3.2 Multi-zone Thermo-kinetic Models.....	9
1.3.3 Segregated Sequential CFD Multi-zone Thermo-kinetic Models	10
1.3.4 Fully coupled CFD Chemical Kinetics Models	11
1.3.5 Fully Integrated Sequential CFD Multio-zone Models	13
1.4 Thesis Objectives and Anticipated Contributions	14
CHAPTER 2 KIVA-MZ STUDY OF HCCI COMBUSTION	17
2.1 Experiment Evidence of Ignition Dominance	18
2.1.1 UM HCCI Engine	18
2.1.2 Sandia HCCI Engine.....	19

2.2 KIVA-MZ Overview	21
2.2.1 KIVA3V Introduction.....	21
2.2.2 Governing Equations and Flow Models	22
2.2.3 Multi-zone Mapping.....	25
2.3 KIVA-MZ Simulation Setup	26
2.3.1 Chemical Kinetics Mechanism	27
2.3.2 CFD Grid	28
2.4 KIVA-MZ Validation.....	29
2.4.1 Intake Temperature Sweep Study.....	29
2.4.2 Natural Thermal Stratification Study.....	30
2.5 Simulation Design	31
2.5.1 Filtered Parametric Study	32
2.5.2 Intake Temperature Sweep Study.....	33
2.5.3 Structure of Simulation Results	37
2.6 Parametric Study Results.....	41
2.6.1 Equivalence Ratio	41
2.6.2 Load	42
2.6.3 EGR.....	43
2.6.4 Engine Speed	43
2.6.5 Wall Temperature and Swirl.....	44
2.6.6 Piston Geometry.....	44
2.6.7 Crevice Volume	45
2.6.8 Compression Ratio.....	45
CHAPTER 3 ENGINE OPERATING PARAMETERS.....	66
3.1 Equivalence ratio.....	66
3.1.1 Open end parametric study	67

3.1.2	Sweep Study Revisit	69
3.1.3	Filtered Parametric Study	70
3.2	Load.....	71
3.2.1	Open End Parametric Study.....	72
3.2.2	Sweep Study Revisit.....	73
3.2.3	Filtered Parametric Study	73
3.3	EGR.....	74
3.3.1	Open End Parametric Study.....	74
3.3.2	Sweep Study Revisit.....	75
3.3.3	Filtered Parametric Study	76
3.4	Engine speed.....	76
3.4.1	Open End Parametric Study.....	77
3.4.2	Sweep Study Revisit.....	78
3.4.3	Filtered Parametric Study	78
CHAPTER 4 ENGINE DESIGN PARAMETERS.....		105
4.1	Swirl Number and Wall Temperature	105
4.1.1	Open End Parametric Study.....	106
4.1.2	Sweep Study Revisit.....	109
4.1.3	Filtered Parametric Study	109
4.2	Piston Geometry.....	111
4.2.1	Sweep Study Revisit.....	111
4.2.2	Open end Parametric Study	112
4.3	Crevice Volume.....	113
4.3.1	Open End Parametric Study.....	113
4.3.2	Sweep Study Revisit.....	115
4.3.3	Filtered Parametric Study	115

4.4 Compression Ratio	117
4.4.1 Sweep Study Revisit	117
4.4.2 Filtered Parametric Study	117
CHAPTER 5 HCCI COMBUSTION CORRELATIONS	140
5.1 1D HCCI Simulation Characteristics	141
5.1.1 Residual Self Coupling	141
5.1.2 Heterogeneity	142
5.1.3 Thermal Inertial	142
5.2 Ignition Correlation for HCCI	143
5.3 Combustion Efficiency Correlation.....	144
5.3.1 Peak Combustion Efficiency.....	145
5.3.2 Combustion Fall Off Timing	148
5.3.3 Combustion Fall Off Slope	149
5.4 Burning Duration Correlation	150
5.5 Summary of Correlations	152
5.6 Validation with KIVA Data	153
CHAPTER 6 ONE DIMENSIONAL HCCI ENGINE SIMULATION.....	163
6.1 Fluid Flow Modeling.....	164
6.1.1 Manifold.....	164
6.1.2 Valve.....	165
6.1.3 Cylinder.....	166
6.2 Heat Transfer Modeling	168
6.2.1 Manifold.....	168
6.2.2 Cylinder.....	169
6.3 Combustion Modeling.....	170
6.3.1 Ignition.....	170

6.3.2 Combustion Efficiency	171
6.3.3 Burning Duration	171
6.3.4 Burning Profile.....	171
6.4 GT-Power User Model Implementation.....	172
6.4.1 GT-Power User Model Setup.....	173
6.4.2 Fortran Code Modification	173
6.4.3 Solver Subroutine Interaction	174
6.5 1D Engine Simulation Validation	175
6.5.1 GT-Power Model Calibration	175
6.5.2 GT-Power Model Validation	176
6.5.3 Improvement over Marginal Combustion Prediction	177
CHAPTER 7 HCCI TRANSIENT STUDY	185
7.1 Tow Stage Temperature Control Engine.....	186
7.1.1 Intake Mixing Valve	187
7.1.2 Variable Intake Close Timing.....	187
7.2 Steady State Sensitivity Study.....	188
7.2.1 Mixing Angle and Intake Closing Timing	188
7.2.2 Engine Speed and Mixing Angle Interaction.....	191
7.3 Single Step Transient Study	192
7.3.1 RPM Step Change.....	192
7.3.2 Air Fuel Ratio Step Change	193
7.3.3 Mixing Valve Angle	193
7.3.4 Intake Valve Close Timing	193
7.3.5 Summary of Two Stage Temperature Control Strategy	194
CHAPTER 8 CONCLUSIONS AND SUGGESTIONS	204
8.1 Summary and Conclusions.....	204

8.2 Suggestions for Future work	207
BIBLIOGRAPHY	209

LIST OF FIGURES

Figure 2.1 - Relationship between combustion efficiency, burning duration and ignition timing for intake temperature sweep from UM HCCI test engine.....	47
Figure 2.2 - - Relationship between combustion efficiency, burning duration and ignition timing for equivalence ratio sweep from UM HCCI test engine	47
Figure 2.3 - Relationship between combustion efficiency, burning duration and ignition timing for intake temperature sweep from Sandia test engine.....	48
Figure 2.4 - Combustion rate comparison for four iso-octane chemical mechanisms under early ignition timing condition.....	49
Figure 2.5 - Combustion rate comparison for four iso-octane chemical mechanisms under late ignition timing condition.....	49
Figure 2.6 - Combustion rate comparison for three KIVA grid sizes under early ignition timing condition.....	50
Figure 2.7 - Combustion rate comparison for three KIVA grid sizes under late ignition timing condition.....	50
Figure 2.8 – KIVA-MZ validation against Sandia engine data on an intake temperature sweep.....	51
Figure 2.9 - KIVA-MZ heat release rate validation against Sandia engine data on thermal stratification	52
Figure 2.10 - KIVA-MZ pressure validation against Sandia engine data on thermal stratification	52
Figure 2.11 - Cumulative temperature mass distribution of three cases replicating Sandia engine thermal stratification study.....	53
Figure 2.12 – KIVA-MZ engine performance variables comparison for six intake temperature cases.....	54
Figure 2.13 – KIVA-MZ Heat release rate comparison for six intake temperature cases	55
Figure 2.14 – KIVA-MZ cylinder composition comparison for six intake temperature cases.....	56

Figure 2.15 – KIVA-MZ Cylinder temperature mass distribution comparison for three intake temperature cases	57
Figure 2.16 - Relationship between combustion efficiency, burning duration and ignition timing for two intake temperature sweeps with different equivalence ratio.....	58
Figure 2.17 - Relationship between combustion efficiency, burning duration and ignition timing for two intake temperature sweeps with different load	59
Figure 2.18 - Relationship between combustion efficiency, burning duration and ignition timing for three intake temperature sweeps with different EGR	60
Figure 2.19 - Relationship between combustion efficiency, burning duration and ignition timing for two intake temperature sweeps with different rpm.....	61
Figure 2.20 - Relationship between combustion efficiency, burning duration and ignition timing for four intake temperature sweeps with two different wall temperatures and two different swirl numbers	62
Figure 2.21 - Relationship between combustion efficiency, burning duration and ignition timing for two intake temperature sweeps with different piston geometry	63
Figure 2.22 - Relationship between combustion efficiency, burning duration and ignition timing for three intake temperature sweeps with different crevice volume.....	64
Figure 2.23 - Relationship between combustion efficiency, burning duration and ignition timing for two intake temperature sweeps with different compression ratio.....	65
Figure 3.1 - Cumulative temperature mass distribution comparison under open end parametric study for two cases with two different equivalence ratios.....	80
Figure 3.2 - Mass fraction burned comparison under open end parametric study for two cases with two different equivalence ratios	81
Figure 3.3 - Mass fraction burning rate comparison under open end parametric study for two cases with two different equivalence ratios	81
Figure 3.4 - CO composition comparison under open end parametric study for two cases with two different equivalence ratios.....	82
Figure 3.5 - Isooctane composition comparison under open end parametric study for two cases with two different equivalence ratios	82
Figure 3.6 - Cylinder temperature comparison for two equivalence ratios under three simulation conditions (normal, adiabatic, and inert-adiabatic).....	83
Figure 3.7 - Cumulative temperature mass distribution comparison under filtered parametric study for two cases with two different equivalence ratios.....	84

Figure 3.8 - Mass fraction burned comparison under filtered parametric study for two cases with two different equivalence ratios	85
Figure 3.9 - Mass fraction burning rate comparison under filtered parametric study for two cases with two different equivalence ratios	85
Figure 3.10 - CO composition comparison under filtered parametric study for two cases with two different equivalence ratios.....	86
Figure 3.11 - Isooctane composition comparison under filtered parametric study for two cases with two different equivalence ratios	86
Figure 3.12 - Cumulative temperature mass distribution comparison under open end parametric study for two cases with two different loads	87
Figure 3.13 - Mass fraction burned comparison under open end parametric study for two cases with two different loads.....	88
Figure 3.14 - Mass fraction burning rate comparison under open end parametric study for two cases with two different loads.....	88
Figure 3.15 - CO composition comparison under open end parametric study for two cases with two different loads	89
Figure 3.16 - Isooctane composition comparison under open end parametric study for two cases with two different loads.....	89
Figure 3.17 - Cumulative temperature mass distribution comparison under filtered parametric study for two cases with two different loads	90
Figure 3.18 - Mass fraction burned comparison under filtered parametric study for two cases with two different loads.....	91
Figure 3.19 - Mass fraction burning rate comparison under filtered parametric study for two cases with two different loads.....	91
Figure 3.20 - CO composition comparison under filtered parametric study for two cases with two different loads	92
Figure 3.21 - Isooctane composition comparison under filtered parametric study for two cases with two different loads.....	92
Figure 3.22 - Cumulative temperature mass distribution comparison under open end parametric study for three cases with three different EGR.....	93
Figure 3.23 - Mass fraction burned comparison under open end parametric study for three cases with three different EGR	94

Figure 3.24 - Mass fraction burning rate comparison under open end parametric study for three cases with three different EGR	94
Figure 3.25 - CO composition comparison under open end parametric study for three cases with three different EGR	95
Figure 3.26 - Isooctane composition comparison under open end parametric study for three cases with three different EGR	95
Figure 3.27 - Cumulative temperature mass distribution comparison under filtered parametric study for two cases with two different EGR.....	96
Figure 3.28 - Mass fraction burned comparison under filtered parametric study for two cases with two different EGR	97
Figure 3.29 - Mass fraction burning rate comparison under filtered parametric study for two cases with two different EGR	97
Figure 3.30 - CO composition comparison under filtered parametric study for two cases with two different EGR.....	98
Figure 3.31 - Isooctane composition comparison under filtered parametric study for two cases with two different EGR	98
Figure 3.32 - Cumulative temperature mass distribution comparison under open end parametric study for two cases with two different rpm	99
Figure 3.33 - Mass fraction burned comparison under open end parametric study for two cases with two different rpm.....	100
Figure 3.34 - Mass fraction burning rate comparison under open end parametric study for two cases with two different rpm.....	100
Figure 3.35 - CO composition comparison under open end parametric study for two cases with two different rpm	101
Figure 3.36 - Isooctane composition comparison under open end parametric study for two cases with two different rpm.....	101
Figure 3.37 - Cumulative temperature mass distribution comparison under filtered parametric study for two cases with two different rpm	102
Figure 3.38 - Mass fraction burned comparison under filtered parametric study for two cases with two different rpm.....	103
Figure 3.39 - Mass fraction burning rate comparison under filtered parametric study for two cases with two different rpm.....	103

Figure 3.40 - CO composition comparison under filtered parametric study for two cases with two different rpm	104
Figure 3.41 - Isooctane composition comparison under filtered parametric study for two cases with two different rpm.....	104
Figure 4.1 – Cumulative temperature distribution comparison under open end parametric study for four cases with two different wall temperatures and two different swirl numbers.....	120
Figure 4.2 - Mass fraction burned comparison under open end parametric study for four cases with two different wall temperatures and two different swirl numbers	121
Figure 4.3 - Mass fraction burning rate comparison under open end parametric study for four cases with two different wall temperatures and two different swirl numbers.	121
Figure 4.4 - CO composition comparison under open end parametric study for four cases with two different wall temperatures and two different swirl numbers.....	122
Figure 4.5 - Isooctane composition comparison under open end parametric study for four cases with two different wall temperatures and two different swirl numbers	122
Figure 4.6 – Cumulative temperature mass distribution comparison under filtered parametric study for four cases with two different wall temperature and two different swirl numbers.....	123
Figure 4.7 - Mass fraction burned comparison under filtered parametric study for four cases with two different wall temperature and two different swirl numbers.....	124
Figure 4.8 - Mass fraction burning rate comparison under filtered parametric study for four cases with two different wall temperature and two different swirl numbers ..	124
Figure 4.9 - CO composition comparison filtered parametric study for four cases with two different wall temperature and two different swirl numbers	125
Figure 4.10 - Isooctane composition comparison filtered parametric study for four cases with two different wall temperature and two different swirl numbers	125
Figure 4.11 – Cumulative temperature mass distribution comparison under open end parametric study for two cases with two different piston geometries	126
Figure 4.12 - Temperature mass distribution comparison under open end parametric study for two cases with two different piston geometries	127
Figure 4.13 - Mass fraction burned comparison under open end parametric study for two cases with two different piston geometries.....	128

Figure 4.14 - Mass fraction burning rate comparison under open end parametric study for two cases with two different piston geometries	128
Figure 4.15 - CO composition comparison under open end parametric study for two cases with two different piston geometries	129
Figure 4.16 - Isooctane composition comparison under open end parametric study for two cases with two different piston geometries	129
Figure 4.17 - Cumulative temperature mass distribution comparison under open end parametric study for three cases with three different crevice volumes.....	130
Figure 4.18 - Mass fraction burned comparison under open end parametric study for three cases with three different crevice volumes	131
Figure 4.19 - Mass fraction burning rate comparison under open end parametric study for three cases with three different crevice volumes	131
Figure 4.20 - CO composition comparison under open end parametric study for three cases with three different crevice volume.....	132
Figure 4.21 - Isooctane composition comparison under open end parametric study for three cases with three different crevice volume.....	132
Figure 4.22 - Cumulative temperature mass distribution comparison under filtered parametric study for three cases with three different crevice volumes.....	133
Figure 4.23 - Mass fraction burned comparison under filtered parametric study for three cases with three different crevice volumes	134
Figure 4.24 - Mass fraction burning rate comparison under filtered parametric study for three cases with three different crevice volumes	134
Figure 4.25 - CO composition comparison under filtered parametric study for three cases with three different crevice volumes.....	135
Figure 4.26 - Isooctane composition comparison under filtered parametric study for three cases with three different crevice volumes	135
Figure 4.27 - Cumulative temperature mass distribution comparison under filtered parametric study for two cases with two different compression ratios.....	136
Figure 4.28 - Mass fraction burned comparison under filtered parametric study for two cases with two different compression ratios	137
Figure 4.29 - Mass fraction burning rate comparison under filtered parametric study for two cases with two different compression ratios	137

Figure 4.30 - CO composition comparison under filtered parametric study for two cases with two different compression ratios.....	138
Figure 4.31 - Isooctane composition comparison under filtered parametric study for two cases with two different compression ratios	138
Figure 4.32 - Instantaneous compression ratio comparison for two compression ratios	139
Figure 5.1 – KIVA-MZ simulated relationship between combustion efficiency and ignition timing (sweep 1 to sweep 20).....	154
Figure 5.2 - Combustion efficiency correlation model.....	154
Figure 5.3 - KIVA-MZ result of combustion fall off timing versus equivalence ratio under four engine speeds	155
Figure 5.4 - Correlation result of combustion fall off timing versus equivalence ratio under four engine speeds	155
Figure 5.5 – KIVA-MZ simulated relationship burning duration and ignition timing (Sweep 1 to sweep 20).....	156
Figure 5.6 - Burning duration correlation model.....	156
Figure 5.7 – Comparison between original burning duration (left) and equivalence ratio adjusted burning duration (right) versus ignition timing, under three engine speeds (750, 2000, 3750 rpm)	157
Figure 5.8 - Comparison between original burning duration (up) and engine speed adjusted burning duration (below) versus ignition timing.....	158
Figure 5.9 - Comparison between original burning duration (up) and equivalence ratio and engine speed adjusted burning duration (below) versus ignition timing	159
Figure 5.10 - Simulation timeline for HCCI correlations.....	160
Figure 5.11 - Correlation validation with KIVA data at 1250 rpm and 0.2951 equivalence ratio	161
Figure 5.12 - Correlation validation with KIVA data at 1250 rpm and 0.1894 equivalence ratio	161
Figure 5.13 - Correlation validation with KIVA data at 1500 rpm and 0.2438 equivalence ratio	162
Figure 5.14 - Correlation validation with KIVA data at 3000 rpm and 0.2533 equivalence ratio	162
Figure 6.1 – GT-Power model map of UM engine.....	179

Figure 6.2 – GT-Power user subroutine interface.....	179
Figure 6.3 – GT-Power FORTRAN interface.....	180
Figure 6.4 - Pressure comparison for calibration point between GT-Power model and UM HCCI engine	180
Figure 6.5 - Combustion efficiency validation comparison between GT-Power model and UM HCCI engine.....	181
Figure 6.6 - 10% burned location validation comparison between GT-Power model and UM HCCI engine.....	181
Figure 6.7 - 50% burned location validation comparison between GT-Power model and UM HCCI engine.....	182
Figure 6.8 - 90% burned validation comparison between GT-Power model and UM HCCI engine.....	182
Figure 6.9 - Comparison between fixed value model and new combustion model in stable transition	183
Figure 6.10 - Comparison between fixed value model and new combustion model in unstable transition.....	183
Figure 6.11 - Comparison between fixed value model and new combustion model in misfire transition.....	184
Figure 7.1 – GT-Power model map of two stage temperature control engine.....	195
Figure 7.2 – Mixing junction schematics.....	195
Figure 7.3 - Ignition timing map with variations of intake valve close timing and mixing angle under rpm 1000 and air fuel ratio 65.....	196
Figure 7.4 – Volumetric efficiency map with variations of intake valve close timing and mixing angle under rpm 1000 and air fuel ratio 65	196
Figure 7.5 - Ignition timing map with variations of intake valve close timing and mixing angle under rpm 2000 and air fuel ratio 45.....	197
Figure 7.6 – Volumetric efficiency map with variations of intake valve close timing and mixing angle under rpm 2000 and air fuel ratio 45	197
Figure 7.7 - Ignition timing map with variations of engine speed and mixing angle for air fuel ratio at 45	198
Figure 7.8 - Ignition timing map with variations of engine speed and mixing angle for air fuel ratio at 55	198

Figure 7.9 - Ignition timing map with variations of engine speed and mixing angle for air fuel ratio at 65	199
Figure 7.10 - Ignition timing response to sudden increase of engine speed	200
Figure 7.11 - Ignition timing response to sudden decrease of engine speed	200
Figure 7.12 - Ignition timing response to sudden increase of air fuel ratio	201
Figure 7.13 - Ignition timing response to sudden decrease of air fuel ratio	201
Figure 7.14 - Ignition timing response to sudden increase of mixing valve opening	202
Figure 7.15 - Ignition timing response to sudden decrease of mixing valve opening	202
Figure 7.16 - Ignition timing response to sudden increase of intake valve close timing	203
Figure 7.17 - Ignition timing response to sudden increase of intake valve close timing	203

LIST OF TABLES

Table 2.1 - Engine specification of UM HCCI single cylinder test engine	19
Table 2.2 - Engine specifications of Sandia HCCI test engine.....	20
Table 2.3 - Specification of KIVA3V simulation engine	27
Table 2.4 - Parameters for Sandia engine intake temperature sweep	29
Table 2.5 – Parameters of simulation engine for intake temperature sweep	34
Table 2.6 - Combustion parameter comparison for intake temperature sweep	36
Table 2.7 - Parameters for intake temperature sweep study (part one)	37
Table 2.8 - Parameters for intake temperature sweep study (part two)	39
Table 3.1- Parameters for open end parametric study of two cases with two equivalence ratios.....	67
Table 3.2 - Parameters for filtered parametric study of two cases with two equivalence ratio	70
Table 3.3 - Parameters for open end parametric study of two cases with two loads	72
Table 3.4 - Parameters for filtered parametric study of two cases with two load.....	73
Table 3.5 - Parameters for open end parametric study of three cases with three EGR	75
Table 3.6 - Parameters for filtered parametric study of three cases with three EGR	76
Table 3.7 - Parameters for open end parametric study of three cases with two engine speed	77
Table 3.8 - Parameters for filtered parametric study of two cases with two engine speeds	78
Table 4.1 - Parameters for open end parametric study of four cases with two swirl numbers and two wall temperatures	107

Table 4.2 - Parameters for filtered parametric study of four cases with two swirl numbers and two wall temperatures	110
Table 4.3 - Parameters for open end parametric study of two cases with two piston geometries	112
Table 4.4 - Parameters for open end parametric study of three cases with three crevice volumes	114
Table 4.5 - Parameters for filtered parametric study of three cases with three crevice volumes	116
Table 4.6 - Parameters for filtered parametric study of two cases with two compression ratios.....	118
Table 5.1 - Peak combustion efficiency correlation variables	145
Table 5.2 - Equivalence ratio and combustion efficiency correlation data.....	147
Table 5.3 - Correlation validation with KIVA data under four operating conditions.....	153
Table 6.1 - Operation parameter for calibration point	175
Table 6.2 - Combustion results for calibration point	176
Table 7.1 - Simulation engine parameters	189
Table 7.2 - Input parameters for two different speed cases	190

LIST OF ABBREVIATIONS

A/F	air/fuel ratio
ABDC	after bottom dead center
ATDC	after top dead center
BMEP	brake mean effective pressure
BSFC	brake specific fuel consumption
BBDC	before bottom dead center
BTDC	before top dead center
CAI	controlled auto-ignition
Ceff	combustion efficiency
CFD	computational fluid dynamics
CI	compression ignition
CO	carbon monoxide
CR	compression ratio
Cp	specific heat of fuel at constant pressure
Cv	specific heat of fuel at constant volume
DI	direct injection
dP/dCA	pressure rise rate per crank angle degree
dP/dt	pressure rise rate per time
EGR	exhaust gas recirculation
EVC	exhaust valve close
EVO	exhaust valve open
h	heat transfer coefficient

HC	hydrocarbon
HCCI	homogeneous charge compression ignition
IMEP	indicated mean effective pressure
IVC	intake valve close
IVO	intake valve open
L(t)	characteristic stroke
LTC	low temperature combustion
MBT	maximum brake torque
MFB	mass fraction burned
NO _x	nitrogen oxides
P	pressure
P _{mot}	motored cylinder pressure
PCCI	premixed-charge compression ignition
PID	proportional integral derivative control
PM	particulate matter emission
R	universal gas constant
RCF	rapid compression facility
RGF	residual gas fraction
SI	spark ignition
SOC	start of combustion
T	temperature
t	time
T _{in}	intake charge temperature
T _{cool}	coolant temperature
T _{wall}	wall temperature
V	cylinder volume
V _d	displacement volume

VCR	variable compression ratio
VVA	variable valve actuation
VVT	variable valve timing
$W(t)$	characteristic combustion gas velocity
m_f	injected fuel mass
x	mass fraction burned rate
y	mole fraction
$\Delta\theta$	characteristic burn duration
γ	ratio of specific heats
Φ	equivalence ratio
w	shape factor in burn rate model
η_c	combustion efficiency

ABSTRACT

Despite of the abundance of HCCI (Homogeneous Charged Compression Ignition) engine experiments, there are several unknown key characteristics, which are difficult to measure with a conventional test engine setup. First, the cylinder temperature distribution is not readily available from test measurements. Second, the instability and misfire mechanisms can not be easily analyzed by engine testing. Finally, the ability to isolate a particular variable is not always practical in testing. In this thesis, an analytical tool is used to explore HCCI combustion under more controlled conditions. A newly available KIVA-MZ model with a novel mapping scheme between CFD cells and thermodynamic zones, provides a virtual experimental environment to explore the combustion process with respect to various engine operating and design parameters.

Nine engine operating and design parameters were investigated with respect to their effects on ignition timing. Equivalence ratio (0.2~0.4), EGR (5%, 20%, and 40%), Load (7~13 mg/cycle), RPM (750~3750), wall temperature (400K, 450K), swirl (0.93, 3.93), compression ratio (12.5, 16), piston geometry (bowl, pancake), and crevice volume (1%, 4%, and 8%) are those nine parameters. The effects of these parameters on combustion efficiency and burning rate were also investigated with controlled ignition timing.

Based on the model results of cylinder temperature distribution information, the design parameters were found to influence the temperature distribution more than the operating parameters did. The ignition timing is not an independently controlled variable; however, the CFD results showed that ignition timing is the single most important variable for the whole combustion process. Besides ignition timing,

equivalence ratio and engine speed are the second and third most important variables for burning rate. Fast burning rate normally results in higher combustion efficiency, but the peak combustion efficiency is mainly determined by the crevice volume.

In order to use the knowledge from the CFD parametric study results, HCCI combustion correlations were developed. These correlations were implemented into GT-Power, a leading commercial 1D engine simulation software package handling general engine system simulation. This improved GT-Power model is a significant improvement over traditional HCCI engine control models with fixed combustion efficiency and burning duration. In marginal engine operating conditions, the new model is able to predict the combustion instability and misfire, while the traditional model fails.

CHAPTER 1

INTRODUCTION

With increasing concern about fuel economy and emissions, the internal combustion engine industry is constantly looking for better alternatives to spark ignition (SI) and direct injection compression ignition (DICI) engines. Homogeneous charge compression ignition (HCCI) engine is one of the alternatives under extensive research in recent years. It was first identified as a distinct combustion concept by Onishi et al. [1979]. The name demonstrates its two essential characteristics. homogeneous mixture and compression ignition. The HCCI concept promises several advantages. In short, it is more efficient than the SI engine, and cleaner than the DICI engine. Compared with the SI engine, higher compression ratio can be used and leaner fuel air mixture can be applied on a HCCI engine. At the same time, compared with the DICI engine, the cylinder mixture is more evenly distributed in a HCCI engine, where fuel rich pocket is not possible. Without the soot-inducing fuel rich pockets and NO_x-inducing lean regions, the overall result is that the HCCI engine can achieve higher fuel efficiency with lower NO_x and soot emissions [Christensen et al., 1999].

Despite the obvious advantages, the HCCI combustion concept also has its own drawbacks. First, hydrocarbon (HC) emission has been found to be high [Dec and Sjonberg, 2003]; second, the power density is low [Risberg et al., 2004]; third, both

ignition timing and heat release rate can not be directly controlled; finally, because of the lack of control, the transitions between engine operation points are more difficult to achieve. Combustion phasing control is the most important issue for this combustion concept. Unlike the SI engine, which has a spark to initiate the combustion, or a DICI engine, which has a fuel injector to control the injection timing, HCCI ignition is primarily controlled by the temperature time history of the intake charge.

Compared with a conventional engine running with the same fuel, HCCI engine requires a higher mixture temperature. In order to have stable HCCI combustion, either intake charge heating or residue gas recirculation should be applied to get stable HCCI combustion. Due to the challenges associated with controlling the combustion phasing, the use of the HCCI concept has been very limited in production applications. However, there are still several pioneers in this area.

1.1 Review of near-HCCI Production Engine

Even though HCCI concept is still under study to be broadly applicable to vehicle use, there are several production engines that already employ near-HCCI combustion mode in the low load range of the operation. Two applications are based on four stroke diesel engine, and another one is based on two stroke gasoline engine.

1.1.1 Toyota UNIBUS

Toyota uniform bulky combustion system (UNIBUS) is introduced in 2000 in Japanese Market [Hasegawa and Yanagihara, 2003]. The engine is a Toyota 1KD-FTV. It is two-staged injection diesel combustion. The first injection is introduced into cylinder in early compression stroke to form premixed mixture and initiate some low temperature reaction. The second injection is released after TDC to trigger the

combustion. Timing and quantity of the first injection has to be precisely controlled along with boost pressure to avoid premature auto ignition. The main enabling control technologies are common rail injection system and variable nozzle turbo. UNIBUS is only applied under part load and under rpm of 3000. Within UNIBUS operation region, richer mixture is supplied in the first injection under low load condition to ensure there is enough low temperature reaction; while total load is controlled by the second injection.

1.1.2 Nissan MK

Nissan modulated kinetics (MK) combustion mode is introduced to market in 1998 in Nissan YD25DDT engine [Kawamoto et al., 2004]. There is a single injection after TDC. The retarded injection along with high EGR ratio prolongs the ignition delay. At the mean time, no-reentrant bowl in combination with high swirl facilitates the dispersion of the injected fuel outside of the piston bowl. Therefore, the mixing time scale is shorter than the auto ignition time scale, and HCCI combustion occurs. MK mode achieves first success at low load condition, and engine switches to regular diesel operation at high loads. In the effort to expand the MK operating range, one key technical issue is the relationship between injection duration and ignition delay. In order to make the ignition delay longer than the injection duration, high pressure injection, reduced compression ratio and EGR gas cooling are applied for second generation of MK engine. Normally, retarded ignition and combustion has lower efficiency, but low temperature combustion and low piston head heat transfer mitigate the problem.

1.1.3 Honda AR

Honda activated radical (AR) is implemented on a two stroke motorcycle engine [Ishibashi and Asai, 1996]. The AR engine operates on dual-mode. At high load, cool start and idle, it operates as a traditional spark ignited engine, and it transits to HCCI type

combustion at part load. The key control device is exhaust throttling, which traps large amount of hot residual gas to bring up the mixture temperature. With the high temperature in the cylinder, HCCI combustion can be achieved even with a relatively low compression ratio. The performance map has a “transition region” where the engine can operate either in HCCI mode or SI mode. Fuel economy is significantly improved on regular two stroke gasoline engine under real life driving conditions. A hydrocarbon emission is reduced by as far as 50%.

Despite of some successful production models, there are still many experiments going on to better understand the combustion control and to increase the operating range. In the following, important HCCI experiments over the years will be reviewed to give more insight to this combustion mode.

1.2 Review of HCCI Experiment

Onishi et al. [1979] first investigated the HCCI combustion on a two-stroke engine. Then Noguchi et al. [1979] also tested it in a two stroke engine. Both of them found the low emission and high efficiency characteristics of this type of combustion. Following them, numerous experiments [Najt et al. 1983, Thring 1989, Christensen et al. 1999] have been performed to demonstrate that HCCI has better fuel efficiency and lower emission under certain steady state operation condition in a test cell. Now, more and more experiments are aiming at understanding the physics of HCCI combustion, including the causes of temperature and composition in-homogeneities; the effect of in-homogeneities on ignition and burning characteristics; and the relationship between control parameters and the resulting in-homogeneities and combustion characteristics.

Christensen et al. [2002] investigated the effect of in-cylinder flow and turbulence on HCCI operation. He applied two different intake swirl ratios and two different

combustion chamber designs, and looked at the resulting combustion characteristics. The experimental results show that with delayed ignition timing, the burning duration is also prolonged. And under early ignition cases, higher turbulence results in higher combustion efficiency. This was attributed to the thinner boundary layer created by turbulence.

Morimoto et al. [2001] studied the effects of cylinder gas in-homogeneity by supplying EGR at different intake locations. Results show that improved charge mixing results in slightly later ignition timing, but faster burning. This experiment tested the effect on composition in-homogeneity on combustion characteristics. With improved charge mixing, the temperature and composition is more even; while less mixed charge has larger stratification, and some pockets have much more favorable conditions for early ignition compared to more even mixture conditions. On the burning duration side, the more evenly distributed charge has quicker combustion because the better homogeneity makes auto-ignition of different parcels in the cylinder to be closer.

Richter et al. [2000] used PLIF to investigate the inhomogeneity effect on HCCI combustion. They confirmed that fuel preparation method does influence the in-cylinder homogeneity. Even for very homogeneous charge, the onset of combustion had very large local variations which would affect the subsequent combustion, in the sense of spatial variation. However, overall, their study did not quantify the level of variations, so real effects are not known.

Au et al. [2001], using a four cylinder HCCI engine, observed the cylinder-to-cylinder variation. Also, they investigated the effect of EGR fraction on the start of combustion and combustion efficiency. They found that EGR has little effect on start of combustion and combustion efficiency, while it has some effect on burning duration. Note that the EGR applied in their case is external EGR, which is mixed with the fresh charge before going through the intake heater. So there is no thermal effect on this addition of EGR; the only effect is the dilution and heat capacity effects.

Zhao et al. [2001] analyzed the effect of residual gas on HCCI combustion. He identified five effects: charge heating, oxygen dilution, heat capacity, chemical, and stratification. And he concludes that only charge heating and stratification effects advance ignition timing, while dilution and heat capacity effects slow down the burning rate. This work is consistent with the previous observations.

Chang et al. [2004] measured the wall surface temperature and instantaneous heat flux on a single cylinder HCCI engine with re-breathing system and proposed universal modified Woshini heat transfer model that could be applied to understand unique combustion characteristics in HCCI engines. In their expression for the heat transfer coefficient, the effect of the gas velocity term induced by combustion was reduced and the effect of in-cylinder gas temperature was emphasized. They also showed that the coolant temperature has a significant effect in determining ignition timing; warmer coolant temperature was shown to be favorable to initiate combustion.

Dec and Sjöberg [2003] investigated the emission and combustion inefficiency mechanism under low equivalence ratio condition. The experiment was conducted on a single cylinder research engine with 18:1 compression ratio. Intake temperature was swept to maintain the same combustion phasing when fueling rate was changed. The research results showed that combustion inefficiency is mainly caused by the bulk quenching at lean condition, as CO species could contain as much as 65% of the total fuel carbon.

In summary, the absence of a 'natural' ignition control mechanism for HCCI engines has so far led researchers to explore a range of candidate control strategies using a range of experiments on single cylinder research engines, and occasionally on multi-cylinder development engines. Either internal or external EGR has been commonly applied to control combustion. The majority of the studies have used fixed valve timing, modified for HCCI operation, and have mainly focused on understanding the in-cylinder physics and chemistry and the relationship between basic engine design parameters and

engine performance during steady state operation [Christensen et al., 1999]. Only a few experimental setups have used variable valve timing (VVT) capability [Agrell et al. 2003], which can potentially enable SI-HCCI-SI transition.

The studies to date have reported that if EGR is homogeneously mixed with fresh charge, it has a thermal effect on the ignition timing, and dilution and heat capacity effects on combustion efficiency and burning duration. If EGR is not homogeneously mixed with fresh charge, stratification effects affects all the combustion characteristics. Also, turbulence has a limited effect on combustion. Its main effect appears to be on the cylinder wall heat transfer and charge mixing.

Performing such explorations solely in the laboratory would be inefficient, expensive, and impractical, since there are many variables that exhibit complex interactions. Rather, the control problem must be tackled using intelligent experiments guided by a suite of modeling tools to understand the process.

1.3 Review of HCCI Modeling

Ever since the computer began to be used in engine modeling, engine models became more and more sophisticated and accurate over the times. However, computational power still hasn't reached the level that researchers can embed fine-grid CFD in system optimization or system control study. The computational resource has been either allocated to in-depth physical models or large number loop iteration models, but not both.

1.3.1 Single-zone Thermo-kinetic Model

The earliest example of this type of model was developed by Najt and Foster [1983] to help analyze experimental work on a premixed-charge, compression-ignited

CFR engine. Their model employed the Shell ignition model and an empirical Arrhenius single step combustion model. By fitting the model constants to a wide range of engine combustion rate data, the authors were able to suggest that the combustion process was dominated by kinetics, a view that is widely accepted today.

Recent examples of zero-dimensional models use more sophisticated and detailed chemical kinetics [Smith et al. 1997; Christensen et al. 1998; Aceves et al. 1999; Wong and Karim 2000, and Dec 2002]. In general, these models have been successful in exploring the effects of fuel composition, compression ratio, A/F ratio, EGR rates and other operating parameters, as well as the lean limits of HCCI operation.

Hiltner et al. [2000], Ogink and Golovitchev [2001], have combined the single zone approach with existing zero-dimensional engine models to provide accurate estimates of the effects of the gas exchange process and have used the resulting simulations to evaluate unconventional engine concepts or variable valve timing strategies.

Fiveland and Assanis [2000] proposed a full cycle, thermo-kinetic single zone model. The fresh charge was assumed to be perfectly homogeneous, with fluid mechanics assumed to have no impact on combustion phasing and rate besides their effect through cylinder wall heat transfer. Detailed chemical kinetics mechanisms for natural gas (GRI, Warnatz) were applied to predict the ignition timing and heat release rate. Their model contributed to understanding how mixture preparation and in-cylinder thermodynamics conditions affect ignition timing, as well as engine performance.

While the zero-dimensional, single zone, thermo-kinetic models have shown the ability to yield satisfactory accuracy against measurements of engine performance, they suffer significant shortcomings in predicting the rate of heat release, combustion completeness, and emissions, largely due to the simplifying assumption of strict homogeneity throughout the combustion chamber. Inaccurate estimates of residual temperature and species composition critically affect predictions of subsequent cycles,

thus limiting the ability of the simulation to track transients. Thus, this type of model cannot be directly used as a control and design tool, despite its computational efficiency. The potential problem of this type of model is to expand the engine operating range into unrealistic region.

1.3.2 Multi-zone Thermo-kinetic Models

In an effort to overcome the shortcomings of the zero-dimensional single-zone approach, several authors have added computational zones corresponding to different physical regions in the chamber. This approach can include some important geometrical and physical-chemical phenomena, while avoiding the computational demands of a full CFD approach. Noda and Foster [2001] explored the effect of temperature stratification by modeling multiple zones with different temperatures imposed parametrically in an otherwise zero dimensional model. Ogink and Golovitchev [2002] used a similar approach, but introduced an empirical temperature distribution among the zones to better match the experimental energy release data.

A comprehensive quasi-dimensional model was proposed by Fiveland and Assanis [2001, 2002] with the intent to bridge the gap between zero-dimensional and sequential fluid-mechanic – thermo-kinetic models. This model is based on a full-cycle simulation code and includes an adiabatic core, a predictive boundary layer model and a crevice flow model. In particular, the thermal boundary layer is driven by compressible energy considerations, and hence is of varying thickness, and is solved at multiple geometric locations along the piston-liner interface. A full dynamic ring pack model is used to compute the crevice flows. The model provided good agreement with experimental performance data for a natural gas fueled engine, and gave reasonably good agreement for unburned hydrocarbons. CO predictions were less satisfactory due to lack of detailed thermal resolution in the near wall regime.

The key limitation of multi-zone, quasi-dimensional models is their inability to predicatively describe stratification or in-homogeneities in residual fraction that are likely to exist in practical applications, especially in direct injection systems. With suitable calibration, the quasi-dimensional models have shown that they can include key geometric effects without excessive computational times. As such, they show promise as a rapid computational tool which can be used as the basis of practical in-vehicle system simulations.

1.3.3 Segregated Sequential CFD Multi-zone Thermo-kinetic Models

In order to obtain some of the zonal resolution afforded by CFD models and yet reduce the computational time required by detailed kinetics calculations, a segregated, sequential multi-zone modeling approach has been pioneered by Aceves et al. [2000, 2001, 2002]. In this approach, a computational fluid dynamics code was run over part of the engine cycle, typically from Bottom Dead Center (BDC) until a transition point before Top Dead Center (TDC), and then the fluid was binned into ten mass-temperature groups. Detailed combustion kinetics calculations were then carried out in each temperature group, with the groups interacting with each other only by P-dV work and subject to the constraint of the time varying chamber volume. Diffusion of species and heat between zones was thought to be unimportant due to the rapid combustion time, and thus was not considered. The model was the first to show a 100-200K range of temperature variation within the main charge near TDC, and demonstrated the smoothing effect that this has on predicted energy release rates, a recurrent shortcoming with single zone models. The model also succeeded in resolving the low temperature regions of the chamber, along the wall and in the ring crevice, and showed that these zones are responsible for combustion inefficiency, unburned hydrocarbon and CO emissions.

Nevertheless, CFD calculations were limited to the closed valve portion of the engine cycle and the chamber was treated only in 2-dimensions.

Babajimopoulos et al. [2002] have extended the model proposed by Aceves et al. to study the effects of valve events and gas exchange processes in the framework of a full-cycle HCCI engine simulation. The multi-dimensional fluid mechanics code KIVA-3V [Amsden 1997] was used in 3-D to simulate the exhaust, intake and compression strokes up to a transition point, while a multi-zone, thermo-kinetic code computed the combustion event. After validation by comparison with a natural gas Caterpillar engine, the model was used to explore the effects of variable valve actuation. In particular, a strategy was examined to obtain large internal residual fractions by early closing of the exhaust valves accompanied by late intake valve opening. The model was able to identify not only large variations in temperature, but also significant non-homogeneities in residual content throughout the chamber at the beginning of combustion.

This type of model has successfully resolved the low temperature regions of the chamber, along the wall and in the ring crevice, and showed that these zones are responsible for combustion inefficiency, unburned hydrocarbon and CO emissions. However, this type of model is very cumbersome to take on a transient study, which often involves hundreds of cycles.

1.3.4 Fully coupled CFD Chemical Kinetics Models

In an effort to include the best representation of both fluid flow and chemical kinetics, attempts have been made to use three-dimensional CFD models coupled directly with chemical kinetics to study compression ignition under HCCI like-conditions. Agarwal and Assanis [1997, 1998, 2000] reported on the coupling of a detailed chemical kinetic mechanism for natural gas ignition (22 species and 104 elementary reactions) with the multi-dimensional reacting flow code KIVA-3V, and explored the auto-ignition of

natural gas injected in a quiescent chamber under diesel like conditions. Full kinetics were used up to the point of ignition. After this point, in order to take into account the effects of small scale turbulent mixing, a one-step chemical reaction is used to convert fuel to products of complete combustion. The extended Zeldovich mechanism was added to model NO_x formation.

Kong et al. [1992, 2001, 2002] proposed a similar approach up to the point of ignition, while after ignition they introduced a reaction rate incorporating the effects of both chemical kinetics and turbulent mixing through characteristic timescales. The turbulent timescale was defined as the time of eddy break-up, while the kinetic timescale was estimated as the time needed for a species to reach the equilibrium state under perfectly-mixed conditions. However, two simplifying assumptions were imposed in determining the kinetic time scales: (i) fuel concentration was assumed to be zero at equilibrium; (ii) the kinetic timescale for all species was the same as that of the selected reference. Despite these limitations, the model was able to replicate the effects of injection timing changes on NO_x formation.

Recently, Hong et al. [2002a, 2002b] proposed a more computationally demanding model to simultaneously account for the effects of detailed chemistry and mixing on ignition delay within the KIVA 3V CFD code. The combustion model was comprised of a combination of the laminar flame approach, used during the induction time, and a modified Eddy Dissipation Concept (EDC), used subsequently. The EDC model was used to predict the reaction rate based on the interaction between chemical and mixing rates. A transition model was also developed to predict local ignition and transition phenomena between the chemistry-only and chemistry-mixing regimes based on branched-chain explosion and thermal explosion. The model was used to look at the formation of soot and NO_x in a DI natural gas compression ignition engine.

This is certainly the ‘best’ model as far as accuracy is concerned. In this model, no modifications or simplifications are made to the kinetics to take into account the

effects of mixing or turbulence. As a result, even with a simplified grid, the calculations require days!

1.3.5 Fully Integrated Sequential CFD Multio-zone Models

Babajimopoulos et al. [2005] developed a new type of model in pursuit of dramatic deduction of computational time compared with fully coupled CFD-chemical kinetics model while maintaining high accuracy. It is a hybrid model between fully coupled CFD-chemical kinetics model and segregated sequential CFD-multi-zone thermo kinetic model. In this model, a multi-zone model with detailed chemical kinetics is fully integrated with KIVA-3V. The model communicates with KIVA-3V at each computational timestep, and the composition of the cells is mapped back and forth between KIVA-3V and the multi-zone model. The key technique in this model is the mapping process: how to group of KIVA cells into thermo kinetic zones, and how to map back. The authors map KIVA cells into temperature and equivalence ratio zones according to temperature-equivalence ratio-temperature scheme, which guarantees that no zone has more than 1% of total cylinder mass. The novel contribution of this work is the remapping scheme. The authors first distribute the active species into cells according to the cell's original reactivity, which is calculated by the C and H atoms not existing in complete combustion products. Second, CO₂ and H₂O are mapped back to conserve the cell's C and H balance. Then, O₂ is mapped back to conserve O balance. Finally, N₂ is mapped back to conserve the overall cell mass.

By using this model, the reduction of computational time compared to fully coupled CFD-chemical kinetics model is enormous. The test operated on a 2.8 GHz PC shows that running time has been reduced from 30 hours to 3.5 hours [Babajimopoulos et al. 2005].

There are two major considerations in selecting a proper model for a certain application: the simplicity spectrum and accuracy spectrum. Unfortunately, for a given model, its locations on these two spectrums are almost always cross mirrored, which means that the high end of simplicity matches the low end of accuracy. The models described above are more focusing on predicting a single steady-state cycle. However, one of HCCI's pertinent features is the strong coupling between adjacent cycles. So to effectively assist the design and development of the HCCI engine, a proper model should be able to be run for a number of cycles, with good accuracy not only within a cycle, but also between the cycles.

Since all models described above either involve CFD or chemical kinetics, they take fairly long to execute to be useful in the context of control studies requiring many engine cycles. This is true of even the single-zone models containing detailed kinetics schemes. While the running time could be expedited with appropriate simplification of the kinetics, the single zone models that have been reported in the literature have major shortcomings in predicting the proper rate of heat release and the correct combustion efficiency and exhaust species. Hence, a new methodology is needed in order to satisfy simultaneously the requirements for low computational cost and acceptable accuracy for use in studies of HCCI transients, so as to be effective in guiding engine control strategy development.

1.4 Thesis Objectives and Anticipated Contributions

The major objective of this work is to determine the fundamental physical impact of nine engine operating and design parameters on HCCI combustion. This is achieved through the use of a fully integrated CFD-multi-zone thermo kinetic code developed by Babajimopoulos et al. [2005] to understand various engine parameters' effects on HCCI

combustion. For each parameter, fundamental physical insight is gained for both its impact on ignition timing and its effect on the following combustion by analyzing in cylinder temperature distribution data. Based on the knowledge developed in the parametric study, several HCCI combustion correlations are developed and validated. These correlations are integrated into a one dimensional engine system software GT-Power to enable transient HCCI operation simulation. This integrated GT-Power model is validated with engine experiment data from a UM HCCI engine. Finally, one specific HCCI control strategy is evaluated by the integrated GT-Power model. Both steady state and transient characteristics are presented.

For the first time, high fidelity simulation is used to do parametric study with very fine resolution of cylinder temperature distribution, which is the main contribution of this thesis work. Also, the design of parametric study is oriented with the emphasis of ignition timing. Not only parameter's effect on ignition timing is investigated, but also its effect on combustion efficiency and burning rate under the same ignition timing is examined. Again, doing parametric study under the same ignition timing has not been done before. Combined with ignition delay model developed at UM [He et al. 2005], these newly developed HCCI combustion correlations provide a simple but accurate package of predicting HCCI combustion. The existing common practice of 1D HCCI simulation is to assume values of combustion efficiency and burning duration [Shaver 2005, Rausen J. D. et al. 2004]. These correlations greatly benefit transient HCCI simulation and control study, which often require simulation tool with high computational efficiency.

The document is arranged as follows. In Chapter 2, high fidelity simulation tool KIVA-MZ is introduced and set up, and then major findings are presented. Chapter 3 and chapter 4 respectively investigate the details of engine operation and design variables, and explain the observations presented in chapter 2. Chapter 5 developed HCCI combustion correlations based on the results of 2 through 4 and validated with

KIVA data. Chapter 6 introduces the one dimensional engine simulation tool with the newly developed combustion correlations and validation work against engine experiment data. Chapter 7 evaluates a strategy to control HCCI combustion by the 1D GT-Power tool. Finally, summary and suggestions are offered in Chapter 8.

CHAPTER 2

KIVA-MZ STUDY OF HCCI COMBUSTION

One unique feature of HCCI combustion is that heat release rate is strongly coupled with ignition timing, which is apparent from several experimental observations [Chang et al. 2004, Sjöberg et al. 2004]. To investigate the relationship in depth, engine simulation modeling provides a quick and insightful alternative to engine experiment. Even though the single zone model is capable of predicting ignition timing with detailed chemistry, heat release rate is often over predicted due to the lack of temperature gradient [Fiveland et al. 2002]. Therefore, three dimensional CFD code KIVA-3V is integrated with detailed chemistry solver CHEMKIN [Babajimopoulos, 2005]. The resulting product is called KIVA-MZ, which is capable of capturing fine details of HCCI combustion.

In this simulation study, KIVA-MZ program starts from intake valve closing with the assumption that cylinder mixture is homogeneous, and program finishes at 60 degrees ATDC. In a real engine, cylinder mixture is hardly homogeneous at intake valve closing; however, the knowledge developed under homogeneous condition is the foundation for understanding HCCI combustion under higher levels of heterogeneity.

Nine engine design and operating parameters are investigated with respect to their effects on both ignition timing and heat release rate. The parametric study performed here is more than a traditional one. For meaningful comparison, the effects of parameters must be compared under the same ignition timing. Therefore, several parametric values

to be compared, for example, equivalence ratios 0.2 and 0.4, undergo an inlet temperature sweep. By doing this, comparison of two cases of equivalence ratio can be made under the same ignition timing.

This chapter is arranged in the following: First, experiment trends from two engines are shown. Next, the KIVA-MZ is introduced and set up by sensitivity studies of both grid and chemical mechanism. Then, validations are made with some experiment data from the test engine at Sandia National Lab. Finally, individual engine design and operating variable's effect on combustion rate is analyzed by the KIVA-MZ model.

2.1 Experiment Evidence of Ignition Dominance

Motivation to explore the relationship between combustion speed and ignition timing started from some experiment observations. The tight coupling between ignition timing and heat release rate was first noticed from experimental data in the HCCI engine at the University of Michigan [Chang, et al. 2004]. Then at Sandia National Lab, the same trends were produced with vastly different engine configurations.

The strong relationship between combustion duration and ignition timing is very clear: earlier ignition leads to faster combustion. HCCI combustion is temperature driven, and chemical reaction and piston compression are the two major sources of heat addition. The ignition timing relative to piston position determines the interaction between piston compression heating and combustion heating.

2.1.1 UM HCCI Engine

A GM prototype, pentroof shape cylinder head is installed into a modified Ricardo Hydra single cylinder engine [Chang et al. 2004]. Table 2.1 shows the engine specifications.

Table 2.1 - Engine specification of UM HCCI single cylinder test engine

Bore (mm)	86.0
Stroke (mm)	94.6
Compression Ratio	12.5
RPM	2000
IVO / IVC	346 / 592 (ATDC)
Main EVO / EVC	130 / 368 (ATDC)
Second EVO / EVC	394 / 531 (ATDC)

To enable HCCI combustion in this engine, an exhaust re-breathing strategy is applied to provide the necessary hot residual gas. The exhaust valves open for a second time during the intake stroke via an additional lobe on the exhaust cam. During this period, hot residual gas is drawn back into the cylinder from the exhaust ports, which helps ignition.

This experiment is focused on heat transfer analysis, and several parametric studies are performed. Among these variables, two of them create wide span in ignition timing. They are the intake temperature sweep and the equivalence ratio sweep. From intake temperature sweep data, Figure 2.1 shows that combustion efficiency drops with later ignition timings, and the burning durations get longer with later ignition timing. The same trends are observed in Figure 2.2, which is from the equivalence ratio sweep.

2.1.2 Sandia HCCI Engine

A Cummins B-series production six cylinder diesel engine is converted to operate HCCI in one cylinder, and rest five cylinders are deactivated [Dec and Sjöberg, 2003]. The camshaft phasing was modified to improve the volumetric efficiency and to reduce

the amount of residual gas. This modification reduces the sensitivity of cycle to cycle coupling, so the engine can be stable at low combustion efficiency. The Sandia engine configuration is listed in Table 2.2.

Table 2.2 - Engine specifications of Sandia HCCI test engine

Bore (mm)	102
Stroke (mm)	120
Compression Ratio	18
Connecting Rod (mm)	192
Fuel	Iso-octane
IVO / IVC	357 / 565 (ATDC)
EVO / EVC	120 / 368 (ATDC)

The Sandia engine has intake heating system to feed the engine with warm enough air to reach auto ignition with very lean mixture and little residual gas. It also runs intake temperature sweep. Figure 2.3 shows that similar pattern exists for Sandia engine with respect to the trend in combustion efficiency and burning duration with ignition timing.

Both engines show that ignition timing has profound impact on combustion efficiency and burning duration. To what extent ignition timing can determine combustion efficiency and burning duration, and what are other variables' role in the process are the questions need to be addressed in this thesis work.

2.2 KIVA-MZ Overview

Ever since its first release in the mid eighties, KIVA has become “THE” CFD code for engine research. KIVA-3V is applied here as the virtual engine for numerical experiment. CFD normally doesn’t work well with detailed chemistry since both are very computationally expensive. A creative mapping scheme between CFD cells and thermo-kinetic zones is developed by Babajimopoulos [Thesis, 2005] to perform chemistry calculation under CFD framework.

2.2.1 KIVA3V Introduction

The first version of KIVA program [Amsden et al., 1985] was released by Los Alamos National laboratory in 1985, and because it is a freeware, it gained popularity quickly among academic institutions and industrial companies as well. This is particular true in the internal combustion engine field, where the demand for CFD code is right on the rise. KIVA-II was release in 1989 [Amsden et al., 1989] to replace KIVA-I. KIVA-II made improvements in fields of computational efficiency, numerical accuracy, physical submodels and usability. However, these two versions only excel at in-cylinder flows and open combustion systems, but were quite inefficient when applied to complicated geometries, like long transfer ports or prechambers. This handicap stems from the design that the entire simulation region had to be encompassed within a single tensor-product mesh with fixed index offsets in all three directions, which often result in a large number of deactivated cells.

KIVA-3 removed this issue by the use of a block-structured mesh that automatically deletes unused cells [Amsden et al., 1993]. Also, the use of indirect addressing for neighbor connectivity enables data storage arrays to be sorted, minimizing the length of vector loops. The killer application of KVIA-3 to IC engines is ports in the cylinder walls, which included both crankcase-scavenged 2-stroke engines with transfer

and boost ports. KIVA-3V is a significant improvement through the addition of a model for intake and exhaust valves, while inheriting all previous features of KIVA-3 [Amsden et al., 1993]. The valve model treats valves as solid objects that travel through the mesh, applying the same “snapper” technique used for piston motion in KIVA-3.

2.2.2 Governing Equations and Flow Models

The equations of motion for the fluid can be solved for both laminar and turbulent flows. The mass, momentum and energy equations for the two forms differentiate primarily in the form of the transport coefficients (i.e. viscosity, thermal conductivity and species diffusivity), which are much larger in the turbulent formulation because of the additional transport created by turbulent fluctuations. In the turbulent case, the transport coefficients are derived from a turbulent diffusivity that depends on the turbulent kinetic energy and its dissipation rate.

The continuity equation for species i is:

$$\frac{\partial \rho_i}{\partial t} + \nabla \cdot (\rho_i \mathbf{u}) = \nabla \cdot \left[\rho D_i \nabla \left(\frac{\rho_i}{\rho} \right) \right] + \dot{\rho}_i^c + \dot{\rho}^s \delta_{il} \quad (2.1)$$

where ρ_i is the mass density of species i , ρ the total mass density, and \mathbf{u} the fluid velocity. Fick’s Law is used for diffusion with a single coefficient D_i . The terms $\dot{\rho}_i^c$ and $\dot{\rho}^s$ indicate source terms due to chemistry and spray, respectively. Species l is the species of which the spray droplets are composed and δ_{il} is the Dirac delta function.

The momentum equation for the fluid mixture is:

$$\frac{\partial(\rho \mathbf{u})}{\partial t} + \nabla \cdot (\rho \mathbf{u} \mathbf{u}) = -\frac{1}{\alpha^2} \nabla p - A_o \nabla \left(\frac{2}{3} \rho k \right) + \nabla \cdot \boldsymbol{\sigma} + \mathbf{F}^s + \rho \mathbf{g} \quad (2.2)$$

where p is the fluid pressure, k is the turbulent kinetic energy per unit mass, $\boldsymbol{\sigma}$ is the viscous stress tensor, \mathbf{g} is the gravitational acceleration vector, and \mathbf{F}^s is the rate of momentum gain per unit volume due to the spray. The dimensionless quantity α is used

in conjunction with the Pressure Gradient Method (PGS), which enhances computational efficiency in low Mach number flows, where the pressure is nearly uniform. A_o is a computational switch, which is set to zero for laminar and one for turbulent flows.

The viscous stress tensor is Newtonian in form:

$$\boldsymbol{\sigma} = \mu[\nabla\mathbf{u} + \nabla(\mathbf{u}^T)] + \lambda\nabla \cdot \mathbf{u}\mathbf{I} \quad (2.3)$$

where \mathbf{I} is the unit dyadic and λ, μ are the first and second coefficients of viscosity, respectively.

The internal energy equation is:

$$\frac{\partial(\rho I)}{\partial t} + \nabla \cdot (\rho \mathbf{u} I) = -p\nabla \cdot \mathbf{u} + (1 - A_o)\boldsymbol{\sigma} : \nabla\mathbf{u} - \nabla \cdot \mathbf{J} + A_o\rho\varepsilon + \dot{Q}^C + \dot{Q}^S \quad (2.4)$$

where I is the specific internal energy exclusive of chemical energy, $\boldsymbol{\sigma} : \nabla\mathbf{u}$ indicates the double-dot product between the surface tension and velocity gradient tensor, \mathbf{J} is the sum of the contributions due to heat conduction and enthalpy diffusion, ε is the dissipation rate of turbulent kinetic energy k , and \dot{Q}^C and \dot{Q}^S are source terms due to chemical heat release and spray interaction.

The ideal gas relationships are used for the equation of state to relate internal energy to temperature:

$$p = R_o T \sum_i \frac{\rho_i}{M_i} \quad (2.5)$$

$$I(T) = \sum_i \left(\frac{\rho_i}{\rho} \right) I_i(T) \quad (2.6)$$

$$I_i(T) = h_i(T) - \frac{R_o}{M_i} T \quad (2.7)$$

where R_o is the universal gas constant, M_i is the molecular weight of species i , $I_i(T)$ is the specific internal energy of species i at temperature T , and $h_i(T)$ is the specific enthalpy of species i , taken from the JANAF thermodynamic tables.

When one of the turbulence models are in use ($A_o = 1$), two additional transport equations are solved for the turbulent kinetic energy k and its dissipation rate ε . Currently, two turbulence models are included in KIVA-3V.

The k- ε model

The transport equations that are solved for the turbulent kinetic energy k and its dissipation rate ε are:

$$\frac{\partial(\rho k)}{\partial t} + \nabla \cdot (\rho \mathbf{u} k) = -\frac{2}{3} \rho k \nabla \cdot \mathbf{u} + \boldsymbol{\sigma} : \nabla \mathbf{u} + \nabla \cdot \left[\left(\frac{\mu}{Pr_k} \right) \nabla k \right] - \rho \varepsilon + \dot{W}^S \quad (2.8)$$

$$\frac{\partial(\rho \varepsilon)}{\partial t} + \nabla \cdot (\rho \mathbf{u} \varepsilon) = -\left(\frac{2}{3} c_{\varepsilon 1} - c_{\varepsilon 3} \right) \rho \varepsilon \nabla \cdot \mathbf{u} + \nabla \cdot \left[\left(\frac{\mu}{Pr_\varepsilon} \right) \nabla \varepsilon \right] + \frac{\varepsilon}{k} (c_{\varepsilon 1} \boldsymbol{\sigma} : \nabla \mathbf{u} - c_{\varepsilon 2} \rho \varepsilon + c_S \dot{W}^S) \quad (2.9)$$

These are the standard k - ε equations with some additional source terms. The source term $-\left(\frac{2}{3} c_{\varepsilon 1} - c_{\varepsilon 3} \right) \rho \varepsilon \nabla \cdot \mathbf{u}$ in the ε -equation accounts for length scale changes when there is velocity dilatation. Source terms involving the quantity \dot{W}^S arise due to the interaction of the gas with the spray. The quantities $c_{\varepsilon 1}$, $c_{\varepsilon 2}$, $c_{\varepsilon 3}$, c_S , Pr_k , and Pr_ε are constants whose values are determined from experiments and some theoretical considerations.

The SGS Model (RNG k - ε)

The SGS model includes a constraint for the dissipation rate ε :

$$\varepsilon \geq \left[\frac{c_\mu}{Pr_\varepsilon (c_{\varepsilon 2} - c_{\varepsilon 1})} \right]^{1/2} \frac{k^{3/2}}{L_{SGS}} \quad (2.20)$$

where L_{SGS} is a length scale determined by the user in the input file. Typical suggested values for this length scale are 4-5 times a representative computational cell dimension.

The physical reasoning behind this model is that the turbulent length scale has to be less than or equal to L_{SGS} .

2.2.3 Multi-zone Mapping

The most accurate simulation approach toward HCCI combustion analysis could be achieved by fully integrating a CFD code with a detailed chemical kinetics code, which would solve for the chemistry in each computational cell. However, to appropriately resolve the temperature distribution in the cylinder, the grid size is on the order of 10^4 or 10^5 [Babajimopoulos, 2005]. The combination large numbers of cells with chemical kinetics calculations makes such a model very computationally intensive. Kong et al. [2003] reported good results using this approach by implementing one iso-octane mechanism [Ognik and Golovitchev, 2001] into 2244 CFD cells.

In an effort to reduce the computational time required by the solution of detailed chemistry in each computational cell, while maintaining an acceptable degree of accuracy, a new HCCI modeling methodology has been developed by Babajimopoulos [2005]. A multi-zone model with detailed chemical kinetics is fully integrated with KIVA-3V. The model communicates with KIVA-3V at each computational timestep, and the composition of the cells is mapped back and forth between KIVA-3V and the multi-zone model. The zone initialization takes into consideration both the temperature and the equivalence ratio of the cells.

This approach requires two way mapping procedure. Forward mapping mixes CFD cells into a thermodynamic zone; while backward mapping distributes the content in a thermodynamic zone into CFD cells.

The steps for forward mapping are in the following:

a) All cells in the cylinder are sorted from lowest to highest temperature and are divided into five temperature zones. Each zone contains a prescribed fraction of the mass.

b) The cells in each temperature zone are sorted from lowest to highest equivalence ratio. Then sub divided them into equivalence ratio zones with maximum range of 0.02 in each equivalence ratio zone.

c) The last step is to take any T/equivalence ratio zones which contain more than 1% of the cylinder mass, sort the cells in these zones by temperature, and divide them into smaller temperature zones, so that, in the end, the mass fraction in each zone does not exceed 1%.

Once cells are grouped into a zone, and the zone is allowed to react using the average temperature and composition of the cells, it is impossible to know exactly what fraction of each species should be mapped back onto each cell. However, it is possible to distribute the species to the cells, so that the change in thermodynamic properties of the cells is minimized. In order to do that, certain requirements must be met: The mass of each cell in the zone must be conserved; The mass of each individual species in the zone must be conserved; The number of C, H, O and N atoms in each cell must be conserved.

So the backward mapping is described below:

a). First, species except CO_2 , H_2O , O_2 , and N_2 are distributed to the cell based on the original cell's C and H items not in CO_2 and H_2O , which ensure the chemical energy is distributed proportionally.

b). CO_2 and H_2O are distributed to CFD cell conserve the cell's C and H atoms.

c). O_2 is distributed to match cell's O atom number.

d). Finally, N_2 is distributed to balance the total cell mass.

2.3 KIVA-MZ Simulation Setup

Because the simulation is intended to be executed hundreds or even thousands of times, the computational speed has to be acceptable. So the chemical mechanism and

computational grid have to be optimized. Ideally, two engine meshes should be created to match the two test engines at UM and Sandia. However, the focus of the study is parametric study, so one generic engine geometry is created instead. The configuration is listed in Table 2.3.

Table 2.3 - Specification of KIVA3V simulation engine

Bore (mm)	90
Stroke (mm)	105
Compression Ratio	12.5 & 16
Piston Geometry	Pancake & Bowl
Fuel	Isooctane
Crevice volume (%)	1 & 4 & 8

2.3.1 Chemical Kinetics Mechanism

The most comprehensive isooctane mechanism is the LLNL's full mechanism, which has 857 species, and 3606 reactions. This mechanism is not practical for parametric study. Reduced mechanism should be used instead to make computational time affordable.

Sensitivity studies are performed on chemical kinetics mechanism to determine the appropriate one to ensure the best combination of computational efficiency and accuracy. Three reduced mechanisms are compared to the full mechanism. They are Curran skeletal mechanism [Curran et al. 2002], and two other reduced mechanisms. Curran skeletal mechanism has 258 species, and two other reduced mechanisms have 197 and 179 species. Comparisons are performed with a single zone engine model under two operating conditions. One operation point is an early ignition case with 10% EGR

percentage, 0.4 equivalence ratio and 510 K intake temperature. As indicated in Figure 2.4, Curran skeletal case has early ignition, while R197 and R179 match the full mechanism well on ignition with R197 fitting better on the completeness of combustion. The other operation point is late in ignition with 40% EGR percentage, 0.4 equivalence ratio, and 505 K intake temperature. In Figure 2.5, Curran skeletal case over predicts ignition timing again, while both R197 and R179 under predict ignition timing with R197 having clear advantage over R179 both on the heat release profile and combustion efficiency. In the following study, all results are based on R197 mechanism.

2.3.2 CFD Grid

Computational time is also significantly affected by CFD grid size. In order to get the best accuracy out of moderate grid size, another round of sensitivity study is performed.

The three grid sizes under comparison have 4260, 16350, and 65400 cells respectively. Two engine operation conditions with two ignition timings are chosen to explore the behavior of the grid size under both early and late ignition. With ignition timing at about 2 degrees before TDC, Figure 2.6 shows that cumulative burning curves are close to each other except that the coarsest grid with 4260 cells has slightly early burning. Under late ignition timing, which is about 2 degrees after TDC, as shown in Figure 2.7, the coarsest grid with 4260 cells has been separated from the other two curves, while there is no significant difference in the other two grids. For both cases, the middle grid matches well with the finest grid. So, in the following study, the grid size is fixed at 16350 cells.

2.4 KIVA-MZ Validation

Before this simulation code is used as numerical experiment to generate large amounts of data, it is validated against experiment results. Between two available test engines data, Sandia engine is better suited for the validation work. The main reason is the level of homogeneity in the cylinder. Unlike the UM engine, the Sandia engine doesn't apply large amount of residual gas, thus its mixture is more uniform in composition. Composition uniformity is assumed at intake valve closing for the KIVA-MZ simulation. Thus it is an easy choice to use the Sandia engine data to validate the KIVA-MZ.

2.4.1 Intake Temperature Sweep Study

In this research work, the main focus is on the relationship between combustion efficiency, burning duration and ignition timing. Ideally, experimental data should have wide span of ignition timing, thus the intake temperature sweep data is chosen as the benchmarking sweep. Following table lists the parameters for the Sandia intake temperature sweep.

Table 2.4 - Parameters for Sandia engine intake temperature sweep

Compression Ratio	18
IVC (ATDC)	-155
Engine speed (RPM)	1200
Equivalence ratio	0.246
Intake pressure (Bar)	1.2
Intake temperature (K)	367.5~423

For engine testing, conventional definition of ignition timing is the location where 10 percent of energy is released, and burning duration is defined as the crank angle

duration from 10 percent to 90 percent energy released. Figure 2.8 shows the comparison of combustion efficiency and burning duration between KIVA-MZ and the experiment data. Overall, the simulation tool is capable of accurately predicting the trend of combustion efficiency and burning duration with the range of ignition timing. Also, the simulation covers more range in the later ignition region, where combustion efficiency starts to fall and burning duration gets very long.

2.4.2 Natural Thermal Stratification Study

Another important experiment study performed on the Sandia engine is natural thermal stratification [Sjöberg et al 2004]. Three cases are compared with different level of temperature distribution in the cylinder. The baseline case has coolant temperature at 100 degree Celsius and swirl number at 0.9. The second case has lower coolant temperature at 50 degree Celsius and the same swirl number. The third case has the same coolant temperature as the second case, but with a higher swirl number at 3.6. The combustion phasing (10% burned location) is regulated at 5 degrees ATDC for all three cases. The conclusion is that lower coolant temperature and higher swirl number increase the temperature stratification in the cylinder, which slows down the heat release rate.

KIVA-MZ is utilized to replicate the same trend. Instead of the coolant temperature boundary condition, cylinder wall temperature is set as the boundary condition. The baseline case has wall temperature at 450 Kelvin and swirl number at 0.93. The second case has wall temperature at 400 Kelvin and swirl number at 0.93. The third case has wall temperature at 400 Kelvin and swirl number at 3.93.

Both the heat release comparison (Figure 2.9) and the pressure comparison (Figure 2.10) match the experiment trend. The extra information provided by KIVA-MZ simulation is the temperature distribution history (Figure 2.11), which is not available from the experiment. The temperature distribution before combustion has clear

separation in low temperature region, where baseline case has the least mass in this region and third case has the most mass. This pattern of distribution is kept over the whole combustion process.

2.5 Simulation Design

Different research interest determines different data structure to be retrieved. In this study, traditional parametric study data structure can only reveal the relationship between the ignition timing and the parameter under study. Since one of the goals is to explore the relationship between all these parameters and combustion rate barring the effect caused by ignition timing, the parametric study is designed to compare combustion process under the same ignition timing.

In this thesis, “open end parametric study” is defined as that a parametric study only varying the parameter itself without varying any other independent parameters, and there’s no regulation of the final results or intermediate variables.

Opposite to the “open end parametric study” is the “close end parametric study”, which has a targeted constant value for the final result. If a parameter does vary the final result under “open end parametric study”, then another independent variable has to be modified to compensate the original parameter’s effect to achieve the “close end parametric study”.

There’s a third type of parametric study with interest in intermediate variables. What if an intermediate variable needs to be regulated? In this thesis, it is called “filtered parametric study”.

2.5.1 Filtered Parametric Study

The definition for “filtered parametric study” is defined as a parametric study with regulated intermediate value, which may involve the modification of other independent variables. The difference between “filtered parametric study” and “open end parametric study” is the involvement of other independent variables. The difference between “filtered parametric study” and “close end parametric study” is whether the final result is regulated or intermediate variable is regulated.

To embody the concept of “filtered parametric study”, an example is given in HCCI combustion study. The example is about the relationship between result value combustion efficiency and input parameter equivalence ratio. Meanwhile, strong relationship is known between combustion efficiency and ignition timing. Ignition timing, in this case, is an intermediate variable.

So in this example, equivalence ratio is the parameter under study, combustion efficiency is the final result, and ignition timing is the intermediate variable. Under “open end parametric study”, different values of equivalence ratio results in different combustion efficiency, as well as ignition timing.

Now, the question is whether equivalence ratio has effect on combustion efficiency only through its effect on ignition timing, or equivalence ratio has effect on combustion efficiency more than its effect through ignition timing. By doing just “open end parametric study”, the answer won’t be known since ignition timing is not kept constant. The only way to answer the question is to keep the ignition timing constant while varying the equivalence ratio. This requires another independent variable to be varied to compensate the effect of equivalence ratio on ignition timing. And that independent variable is called compensator variable.

The choice of compensator variable is not random. It should have the following two characteristics: First, it can alter the value of intermediate variable, which is obvious;

second, it can alter the final result only through its effect on the intermediate variable. In this example, the compensator variable should be able to change ignition timing and its effect on ignition timing should be the only mechanism that it can change the combustion efficiency.

The compensator variable for HCCI combustion study is intake temperature.

2.5.2 Intake Temperature Sweep Study

The relationship between intake temperature and ignition timing is very straightforward. Higher intake temperature has earlier ignition. The proof that ignition timing is the only mechanism that intake temperature can change combustion efficiency relies on the facts that intake temperature has minimum effect on mixture adiabatic temperature, mixture distribution, and heat transfer characteristics. Higher intake temperature resulting in higher combustion efficiency is predominantly due to earlier ignition.

Parametric study of intake temperature itself can provide important information on misfiring mechanism. By reducing the intake temperature gradually, the ignition gets later and later, and eventually misfiring happens. By looking into the species concentration and temperature profile, more detailed information can be reviewed.

In this thesis work, combustion efficiency is defined as the ratio of the chemical energy eventually released over the total chemical energy available for the cycle. Based on either total available energy or eventually released energy, there are two definitions of percentage fuel burned. Absolute percentage burned is calculated by dividing the current released energy by total available energy in the cylinder; while relative percentage burned is calculated by dividing the current release energy by the energy eventually released. When combustion efficiency is close to 100%, the difference between absolute percentage burned and relative percentage burned is small. However, when combustion

efficiency is significantly below 100%, the difference between these two values can be large. In the following context, two abbreviations are used to address the difference. “% fuel” represents the absolute percentage burned; while “% burned” represents the relative percentage burned. Ignition timing under this study is defined as the crank angle location for “1% fuel”.

Six intake temperature cases (476.5, 480, 485, 492.5, 497.5, and 510 Kelvin) are studies with the following setup:

Table 2.5 – Parameters of simulation engine for intake temperature sweep

Intake Pressure (bar)	1.1
EGR (%)	5
Engine Speed (rpm)	2000
Compression Ratio	12.5
Equivalence Ratio	0.26

The KIVA3V-MZ model calculates thermodynamic and chemical properties within a CFD cell, but to record information to that detail requires huge memory space, which is not practical for studies focusing on the variations of engine operating parameters and design variables, which require many simulation runs. However, the model outputs still provide enough details of the combustion process by recording three major information groups: first is the performance group (Figure 2.12), including: cylinder pressure, cylinder average temperature, cylinder maximum temperature, accumulative mass fraction burned, and derived mass fraction burning rate (Figure 2.13); the second group is species composition group (Figure 2.14), including hydroxyl (OH) , hydrogen peroxide (H₂O₂), hydroperoxy (HO₂), hydrogen (H₂), carbon monoxide (CO), and isooctane. Finally, there is a temperature distribution group, recording the

temperature distribution evolution history in the cylinder (Figure 2.15). The temperature distribution comparison is carried out with three initial temperature cases: good combustion (497.5 K), marginal combustion (480 K), and misfire (476.4 K).

The trend is quite obvious in Figure 2.12. With lower initial temperature, the ignition gets later, and peak pressure and temperature gets lower. The combustion efficiency also gets lower with later ignition. The four higher initial temperature cases finish the combustion at higher combustion efficiency, and the two lower initial temperature cases are distinctively below, especially the lowest initial temperature case. The pressure curves are on top of each other before the case with the earliest ignition takes off. In Figure 2.13, the heat release rate comparison shows that the earlier the ignition, the faster the burning.

Figure 2.14 shows the trends of individual species composition with ignition timing. OH radical composition decreases with later ignition; while H_2O_2 composition increases with later ignition. H_2 and HO_2 radicals' compositions also decrease with later ignition.

Combustion efficiency is close for the four cases with higher temperatures. The case with 480 K intake temperature finishes significantly lower; while the case with 476.5 K intake temperature obviously misfires. For those four cases with good combustion efficiency, the heat release rate (Figure 2.13) differentiates significantly. Higher intake temperature results in earlier ignition and faster heat release rate. The following table shows the importance of ignition timing:

Table 2.6 - Combustion parameter comparison for intake temperature sweep

Intake Temperature	Ignition Timing	Combustion Efficiency	Burning Duration (10%~90% burned)
[K]	[ATDC]	[%]	[CAD]
476.5	1.24	40.46	21.45
480	-0.13	86.97	14.32
485	-1.81	91.57	8.65
492.5	-3.95	92.59	6.08
497.5	-5.23	92.83	5.3
510	-8.04	93.21	4.27

The misfiring case with 476.5 K intake temperature is of great interest. It is obvious that exothermic reactions are happening well into the expansion stroke. The amount of OH is almost negligible. And it is obvious that H₂O₂ stops dissociating at about 30 degrees ATDC. Instead, H₂O₂ has an upward turn since HO₂ keeps cracking the fuel into Alkyl and H₂O₂. At the same time, there is plenty of CO available, however, there's not enough OH radical existing to react with.

The temperature distributions (Figure 2.15) of three intake temperature cases reveal the temperature histories of these three representatives of combustion: good, marginal, and misfire. For good combustion, the fully developed distribution is reached by 5 degrees ATDC; while for marginal combustion, it takes much longer, and there is noticeable mass fraction of intermediate temperature existing in the cylinder; for misfire case, the temperature distribution is more linear, which means that different levels of partial combustion exists in the cylinder. So the misfire pattern in the HCCI is not just the quenching of boundary layer, rather, each temperature and composition region has its own degree of combustion completeness.

2.5.3 Structure of Simulation Results

The simulation is able to investigate the following parameters' effect on combustion other than above mentioned intake temperature: equivalence ratio, load, EGR, RPM, piston geometry, crevice volume, compression ratio, wall temperature and swirl number.

There're 46 intake temperature sweeps with 1422 individual runs. The detailed information of the sweep is listed in the following two tables. For variable kept constant for the intake temperature sweep, a value is shown in the table; for variable with changing value for the sweep, negative sign (-) is presented.

Table 2.7 - Parameters for intake temperature sweep study (part one)

Sweep	Crevice	Piston	CR	Speed	EGR
	[%]		[-]	[RPM]	[%]
1	4	Pancake	12.5	2000	20
2	4	Pancake	12.5	2000	40
3	4	Pancake	12.5	2000	5
4	4	Pancake	16	1200	5
5	4	Pancake	16	1200	5
6	4	Pancake	16	1200	5
7	4	Pancake	16	1200	5
8	4	Pancake	16	1200	5
9	4	Pancake	16	2000	5
10	4	Pancake	12.5	2000	5
11	4	Pancake	12.5	2000	5
12	4	Pancake	12.5	2000	5
13	4	Pancake	12.5	2000	5

14	4	Bowl	12.5	1200	5
15	4	Bowl	12.5	1200	5
16	4	Pancake	12.5	1200	5
17	4	Pancake	12.5	1200	5
18	4	Pancake	12.5	750	0
19	4	Pancake	12.5	750	0
20	4	Pancake	12.5	750	0
21	4	Pancake	12.5	750	0
22	4	Pancake	12.5	750	0
23	4	Pancake	12.5	750	0
24	4	Pancake	12.5	1250	0
25	4	Pancake	12.5	1250	0
26	4	Pancake	12.5	1250	0
27	1	Pancake	12.5	1200	5
28	8	Pancake	12.5	1200	5
29	4	Pancake	12.5	1200	5
30	4	Pancake	12.5	1200	5
31	4	Bowl	12.5	3750	0
32	4	Bowl	12.5	3750	0
33	4	Bowl	12.5	3750	0
34	4	Bowl	12.5	1500	0
35	4	Bowl	12.5	2250	0
36	4	Bowl	12.5	3000	0
37	4	Pancake	12.5	2000	5
38	4	Pancake	12.5	2000	5
39	4	Pancake	12.5	2000	5

40	4	Pancake	12.5	2000	5
41	4	Pancake	12.5	2000	5
42	4	Pancake	12.5	2000	5
43	4	Pancake	12.5	2000	5
44	4	Pancake	12.5	2000	5
45	4	Bowl	12.5	1200	5
46	4	Bowl	12.5	1200	5

Table 2.8 - Parameters for intake temperature sweep study (part two)

Sweep	Phi	Fuel	Pin	Twall	Swirl
	[-]	[mg/cycle]	[bar]	[K]	[-]
1	-	12	1.1	400	0.93
2	-	12	1.1	400	0.93
3	0.26	-	1.1	400	0.93
4	-	9	1.1	400	0.93
5	-	12	1.1	400	0.93
6	-	9	1.1	450	0.93
7	-	13	1.1	400	0.93
8	0.26	-	1.1	400	0.93
9	0.26	-	1.1	400	0.93
10	0.3	12	-	400	0.93
11	0.4	12	-	400	0.93
12	0.3	9	-	400	0.93
13	-	12	1.1	400	0.93
14	-	9	1.1	400	0.93
15	-	9	1.1	450	0.93

16	-	9	1.1	400	0.93
17	-	9	1.1	450	0.93
18	-	9	1.1	400	0.93
19	-	8	1.1	400	0.93
20	-	7	1.1	400	0.93
21	-	10	1.1	400	0.93
22	-	11	1.1	400	0.93
23	-	12	1.1	400	0.93
24	-	7	1.1	400	0.93
25	-	9	1.1	400	0.93
26	-	11	1.1	400	0.93
27	-	9	1.1	400	0.93
28	-	9	1.1	400	0.93
29	-	9	1.1	400	3.93
30	-	9	1.1	400	3.93
31	-	9	1.1	400	0.93
32	-	7	1.1	400	0.93
33	-	11	1.1	400	0.93
34	-	9	1.1	400	0.93
35	-	9	1.1	400	0.93
36	-	9	1.1	400	0.93
37	-	7	1.1	400	0.93
38	-	8	1.1	400	0.93
39	-	9	1.1	400	0.93
40	-	10	1.1	400	0.93
41	-	11	1.1	400	0.93

42	-	12	1.1	400	0.93
43	-	13	1.1	400	0.93
44	-	14	1.1	400	0.93
45	-	9	1.1	400	3.93
46	-	9	1.1	400	3.93

2.6 Parametric Study Results

For each parameter, the first set of data is the relationship between combustion efficiency, burning duration and ignition timing. Because intake temperature sweep naturally creates a span of ignition timing, curves can be obtained for combustion efficiency and burning duration versus ignition timing.

2.6.1 Equivalence Ratio

Intake temperature sweep is performed for each of the two equivalence ratio cases: 0.3 (sweep 10) and 0.4 (sweep 11). Then combustion efficiency (left) and burning duration (right) are plotted against ignition timing (Figure 2.16). When ignition timing is early enough, there's no discernable difference in combustion efficiency between these two equivalence ratio cases, but it is clear that the higher equivalence ratio case can endure later ignition timing to finish burning the majority of the mixture. For the case with equivalence ratio at 0.3, ignition timing later than TDC has lower combustion efficiency than best possible combustion efficiency (peak combustion efficiency). With later ignition timing, the combustion efficiency drops to an even lower number. The combustion efficiency drops slowly in the beginning around TDC, but the slope gets steeper around 1 degree ATDC. So there is a gradual change of the combustion efficiency slope between TDC and 1 degree after. For the case with an equivalence ratio

of 0.4, the critical ignition timing where combustion efficiency starts to fall comes later than the 0.3 case. It is around 4 degrees ATDC, but the change is more dramatic. There is almost no transition period. Combustion efficiency drops sharply from peak value.

For burning duration, which is defined as the crank angle duration from 10% burned to 90% burned, the higher equivalence ratio case is substantially shorter than the lower equivalence ratio case over the span of ignition timing. This means that the higher equivalence ratio case burns much faster than the lower equivalence ratio if ignition timing is about the same.

2.6.2 Load

Since equivalence ratio is already studied above, it is kept constant in the load study. These two load cases have the same equivalence ratio of 0.3, providing that they have matching fueling rate and air supply. One case has 9 milligrams of fuel per engine cycle (sweep 12); the other case has 12 milligrams of fuel per engine cycle (sweep 10).

The result (Figure 2.17) is very encouraging. There's no discernable difference in combustion efficiency. The peak combustion efficiency of three cases match with each other, as well as their transition periods and downward slopes. There's very slight difference in burning duration. The higher load case has very small advantage on the burning speed. Again, the difference is so small that no assertive statement can be made that a higher load burns faster.

The difference between the equivalence ratio and load studies is very striking, which implies that HCCI combustion rate is more related to cylinder temperature, and less related to cylinder pressure. More details are discussed in Chapter 3.

2.6.3 EGR

EGR cases are compared with the same fuel quantity and intake pressure, which means that air is replaced by combustion products. Three cases are compared with EGR level set at 5% (sweep 13), 20% (sweep 1), and 40% (sweep 2).

The traditional definition of equivalence ratio only measures the air surplus, and it varies significantly among these three cases. For 5% EGR, the equivalence ratio is in the range of 0.32 to 0.34; for 20% EGR, the range is about 0.41 to 0.43; and for 40%, the range is about 0.56 to 0.6. However, if converting those combustion products into air with equivalent heat capacity, all three cases have a similar value of around 0.33.

From Figure 2.18, both the combustion efficiency and burning duration are very close to each other across the three EGR cases. Despite these three cases having huge differences in equivalence ratios according to the traditional definition, similar heat capacity of the cylinder charge keeps each combustion rate in pace with the others.

2.6.4 Engine Speed

Two engine speed cases are compared. One has rpm set at 1200 (sweep 8); the other has rpm set at 2000 (sweep 9). The results are shown in Figure 2.19.

At very early ignition timing, peak combustion efficiency of the two cases are very close. As ignition timing gets later, the higher rpm case hits the critical ignition timing first, after which combustion efficiency takes a sharp downturn. The burning duration of the two cases are obviously separated from each other. The difference is smaller when ignition timing is early, but diverges when ignition timing gets later. The effect of engine speed is two-folded. On one hand, it affects the time for chemistry; on the other hand, it alters the time for heat transfer. This is discussed in next chapter.

2.6.5 Wall Temperature and Swirl

Because both wall temperature and swirl impose similar effects on HCCI combustion, it is better to group them together. Four cases with two wall temperatures and two swirl numbers are compared. The case with low wall temperature (400 K) and low swirl number (0.93) is sweep 16; the case with high wall temperature (450 K) and low swirl is sweep 17; the case with low wall temperature and high swirl number (3.93) is sweep 29; and the case with high wall temperature and high swirl number is sweep 30.

Figure 2.20 shows that moderate separation are prevalent for all cases. Peak combustion efficiency is still close across cases when ignition timing is very early. When ignition timing gets later, the first case to undergo combustion deterioration is the case with low wall temperature and high swirl number. On the opposite, the case with high wall temperature and low swirl number endure the latest ignition timing to see its combustion efficiency gets reduced.

The burning duration is consistent with the combustion efficiency trend. The case with high wall temperature and low swirl number burns the fastest; the case with low wall temperature and high swirl number is the slowest.

The relative importance of wall temperature and swirl number is leaning toward swirl number under this study. Both the combustion efficiency and the burning duration curves show that cases with the same swirl number are closer than cases with the same wall temperature.

2.6.6 Piston Geometry

In diesel engines, the piston geometry is a very important factor for combustion. In the HCCI engine, the shape may not bear the same significance as in a diesel engine; but it still alters the heat transfer in certain way. Two geometries are compared. One has a flat piston top (sweep 16), which make the cylinder chamber at TDC look like a

pancake; the other has a bowl shape in the piston (sweep 14). Both compression ratios are kept the same at 12.5.

Again, there's no difference in peak combustion efficiency (Figure 2.21). The bowl shape piston case starts the combustion efficiency downturn earlier, but the slope is less steep. The burning duration of the two cases is moderately separated from each other. The pancake case burns quicker, and on average it spends three less crank angles to burn from 10% to 90%.

2.6.7 Crevice Volume

Crevice volume has been the major contributor to unburned HC in spark ignited engine. For the HCCI engine, it also can be the contributor. Three cases are compared with different crevice volume. Sweep 27 has a crevice volume set at 1% of the cylinder volume when piston is at TDC; sweep 16 has 4%; and sweep 28 has 8%.

This is the only comparison that results in different peak combustion efficiency (Figure 2.22). The critical ignition timing for combustion deterioration is close, the combustion efficiency downward slopes are close, and the burning durations are close.

The difference in peak combustion efficiency is large. The case with 1% crevice has peak combustion efficiency close to 100%; while the case with 8% crevice has peak combustion efficiency only in the mid 80%.

2.6.8 Compression Ratio

Compression ratio is very influential on ignition timing. In fact, a small percentage change in compression ratio results in huge swing of ignition timing. To compare two compression ratios under the same ignition timing requires a large intake temperate compensation for the low compression ratio cases.

One case has a compression ratio set at 12.5 (sweep 3); the other has compression ratio set at 16 (sweep 9).

Figure 2.23 shows that a higher compression ratio has slightly higher peak combustion efficiency, but the difference is very small. The critical ignition timing and combustion efficiency downturn slopes are also very close.

There is a unique feature about compression ratio comparison with regard to burning duration. In all the previous comparisons, the burning duration curves are either close to each other or separated. In this comparison, the burning duration curves are separated when ignition timing is early, but they start to converge when ignition timing gets later, and burning duration becomes identical when ignition timing is right at TDC.

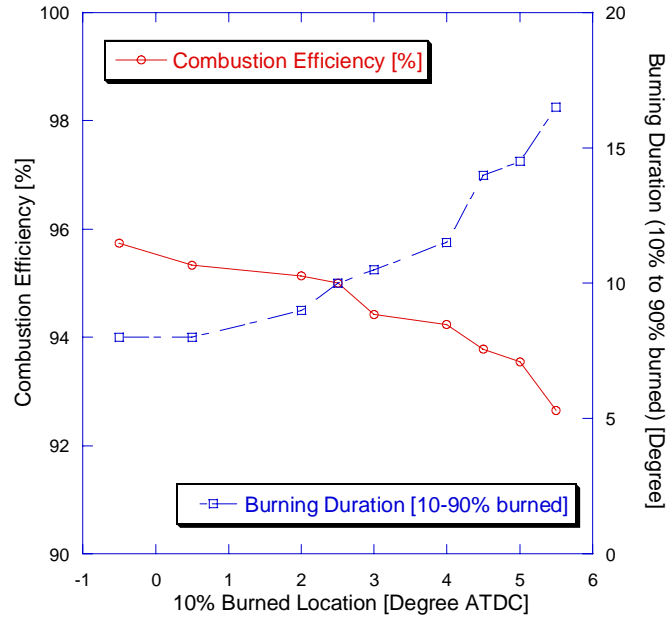


Figure 2.1 - Relationship between combustion efficiency, burning duration and ignition timing for intake temperature sweep from UM HCCI test engine

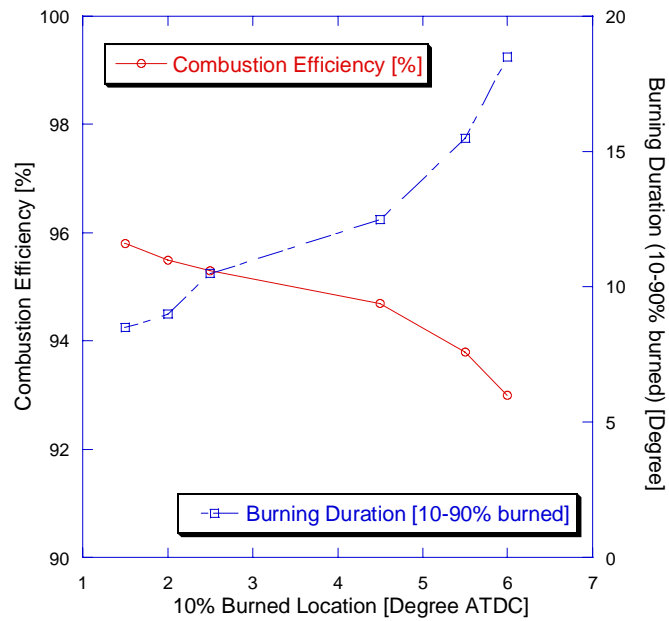


Figure 2.2 - - Relationship between combustion efficiency, burning duration and ignition timing for equivalence ratio sweep from UM HCCI test engine

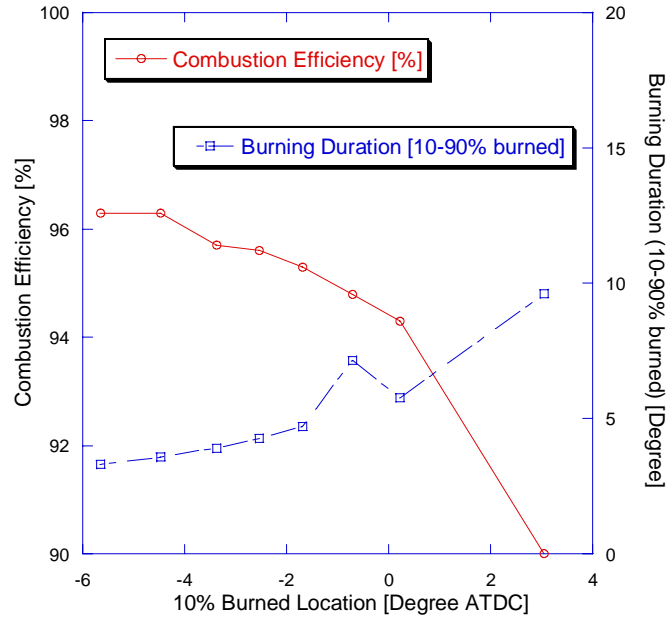


Figure 2.3 - Relationship between combustion efficiency, burning duration and ignition timing for intake temperature sweep from Sandia test engine

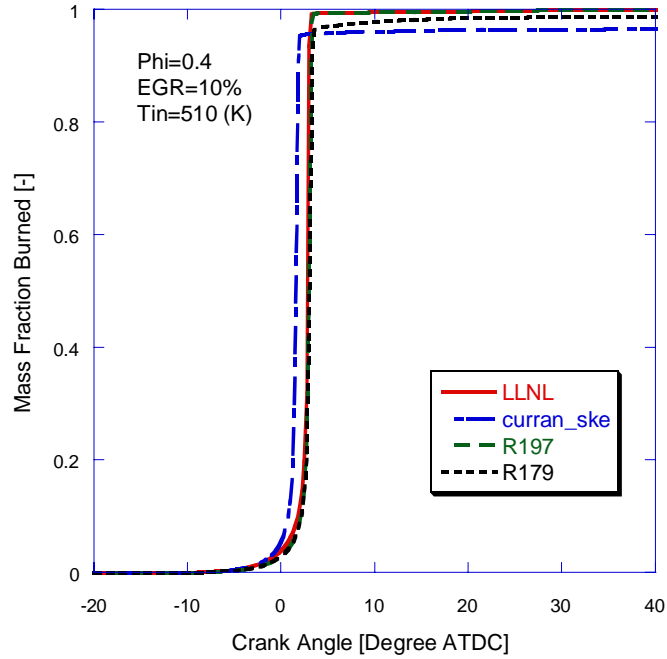


Figure 2.4 - Combustion rate comparison for four iso-octane chemical mechanisms under early ignition timing condition

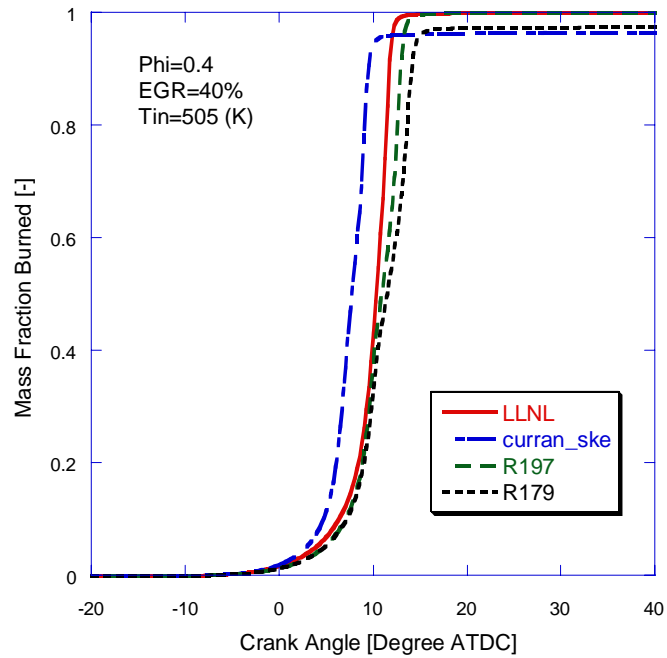


Figure 2.5 - Combustion rate comparison for four iso-octane chemical mechanisms under late ignition timing condition

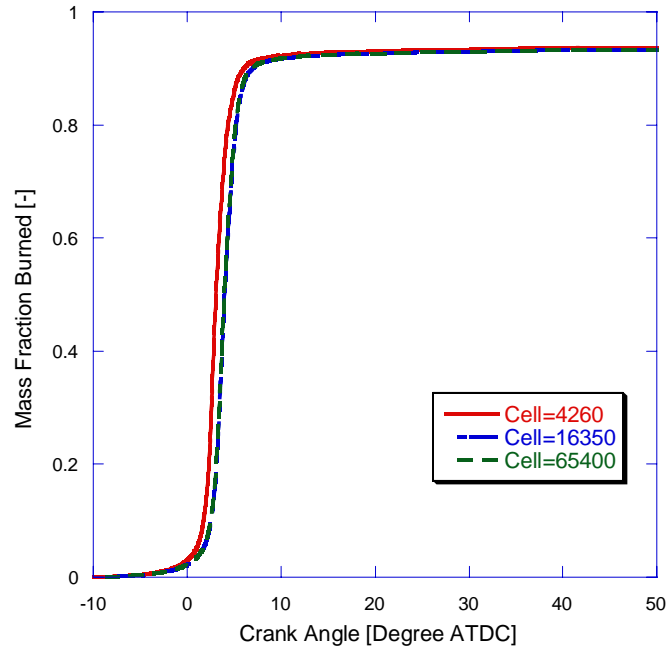


Figure 2.6 - Combustion rate comparison for three KIVA grid sizes under early ignition timing condition

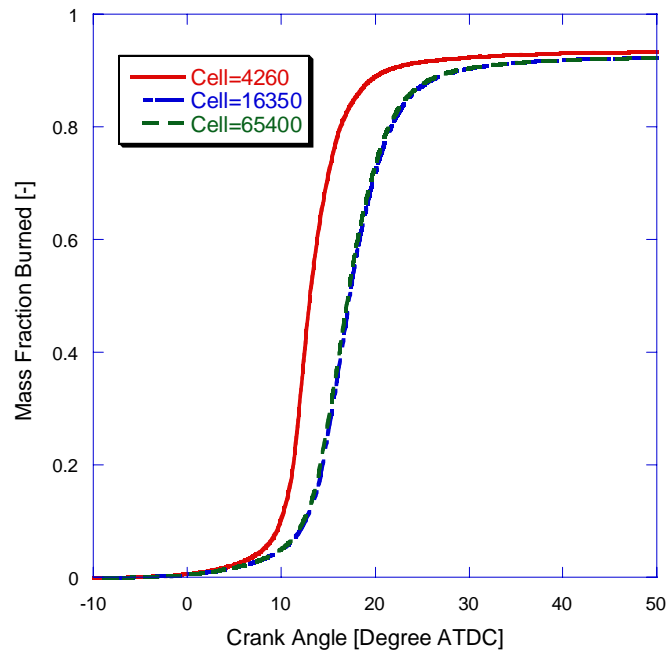


Figure 2.7 - Combustion rate comparison for three KIVA grid sizes under late ignition timing condition

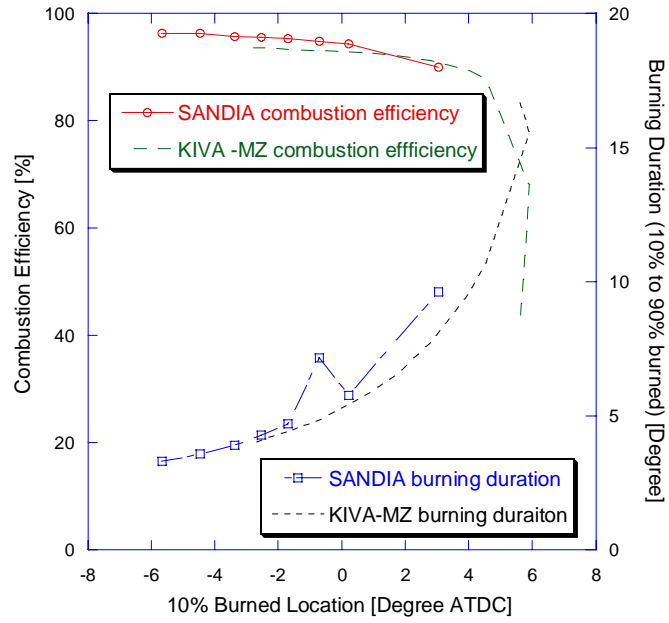


Figure 2.8 – KIVA-MZ validation against Sandia engine data on an intake temperature sweep

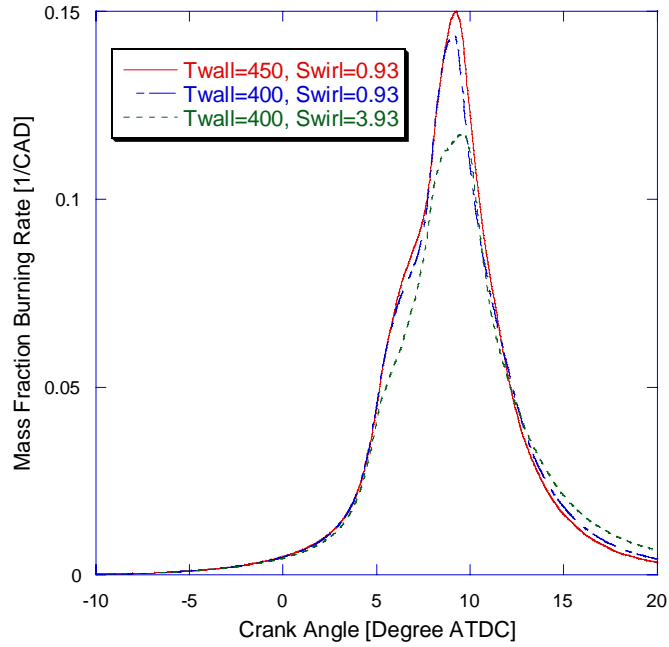


Figure 2.9 - KIVA-MZ heat release rate validation against Sandia engine data on thermal stratification

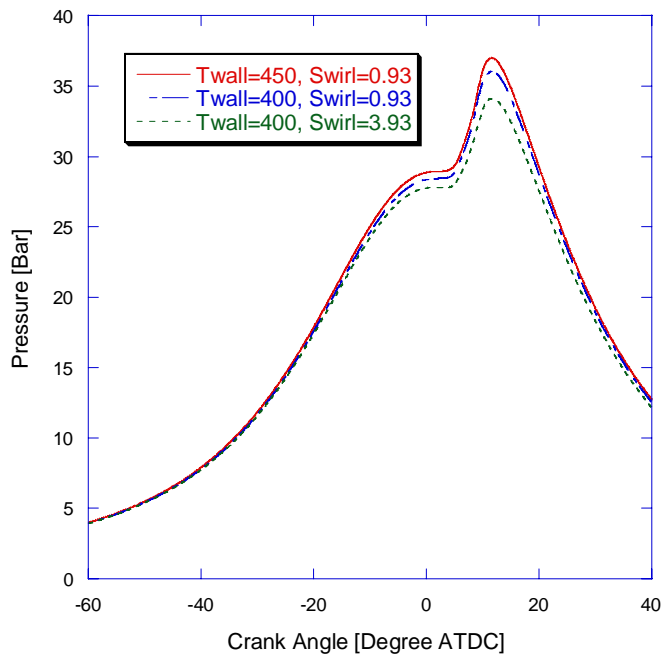


Figure 2.10 - KIVA-MZ pressure validation against Sandia engine data on thermal stratification

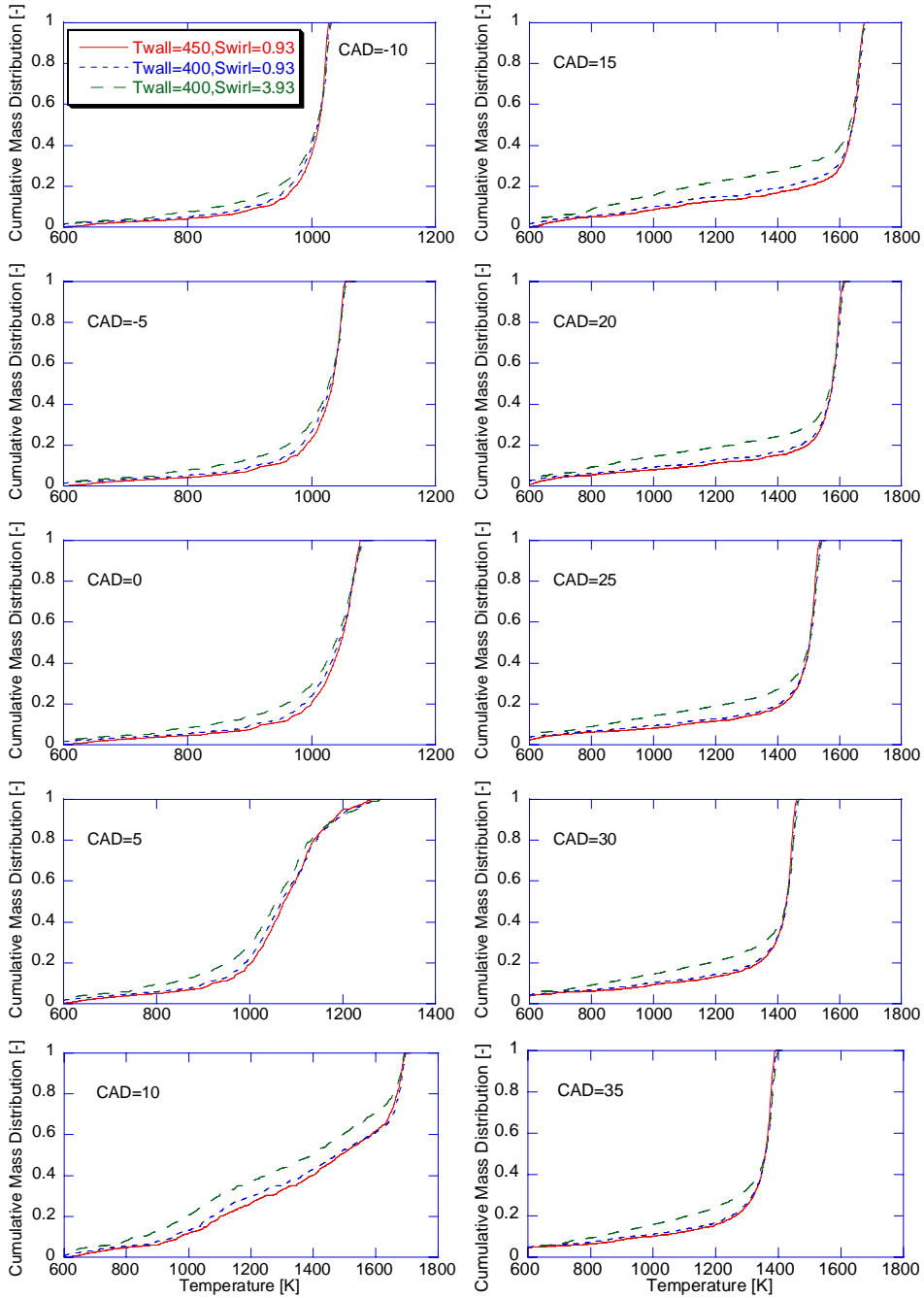


Figure 2.11 - Cumulative temperature mass distribution of three cases replicating Sandia engine thermal stratification study

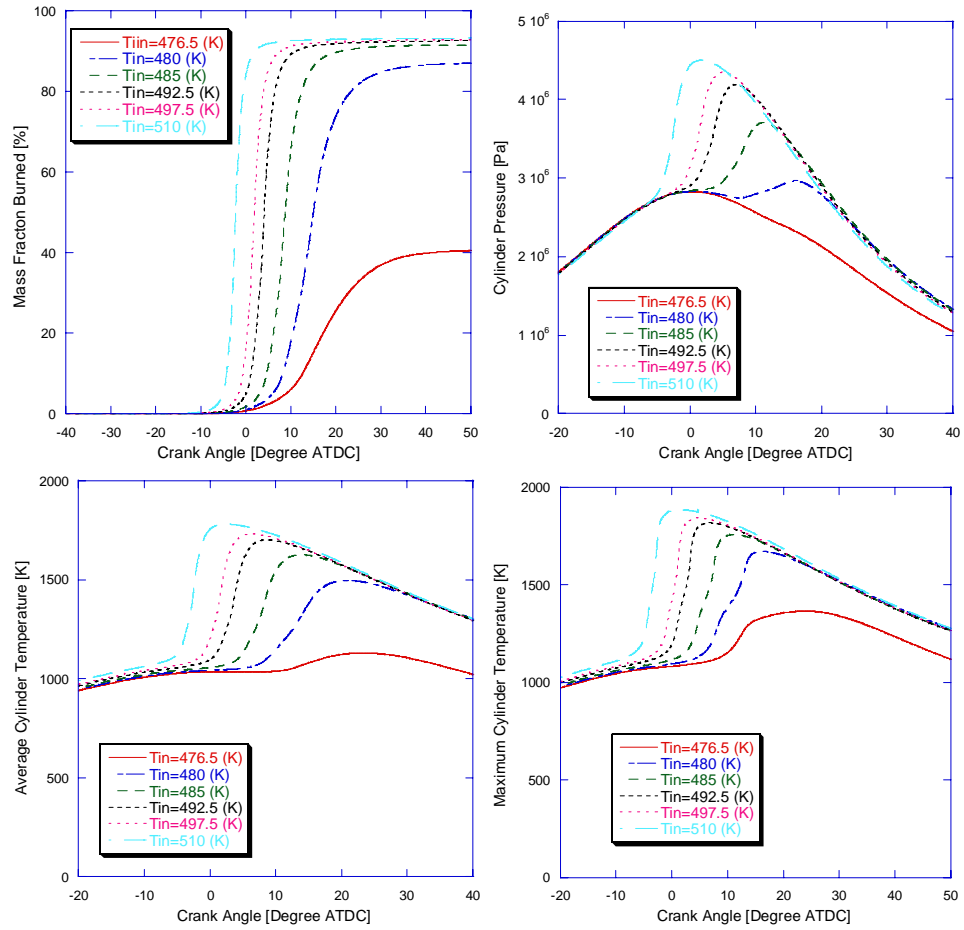


Figure 2.12 – KIVA-MZ engine performance variables comparison for six intake temperature cases

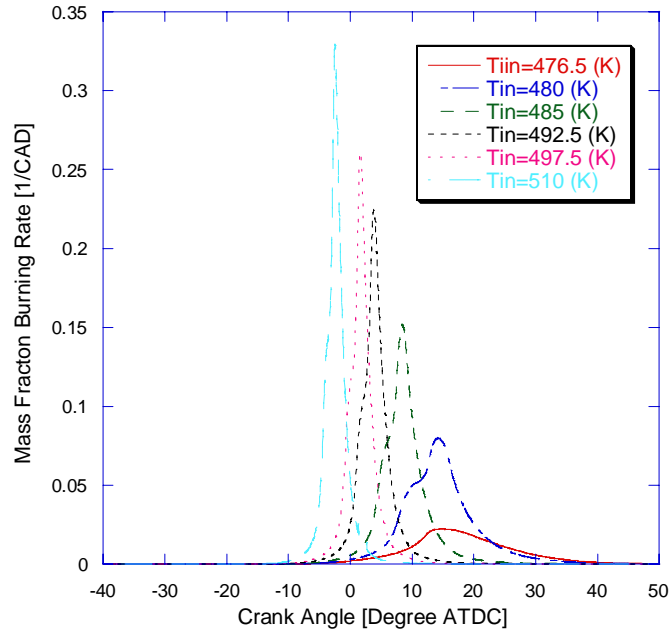


Figure 2.13 – KIVA-MZ Heat release rate comparison for six intake temperature cases

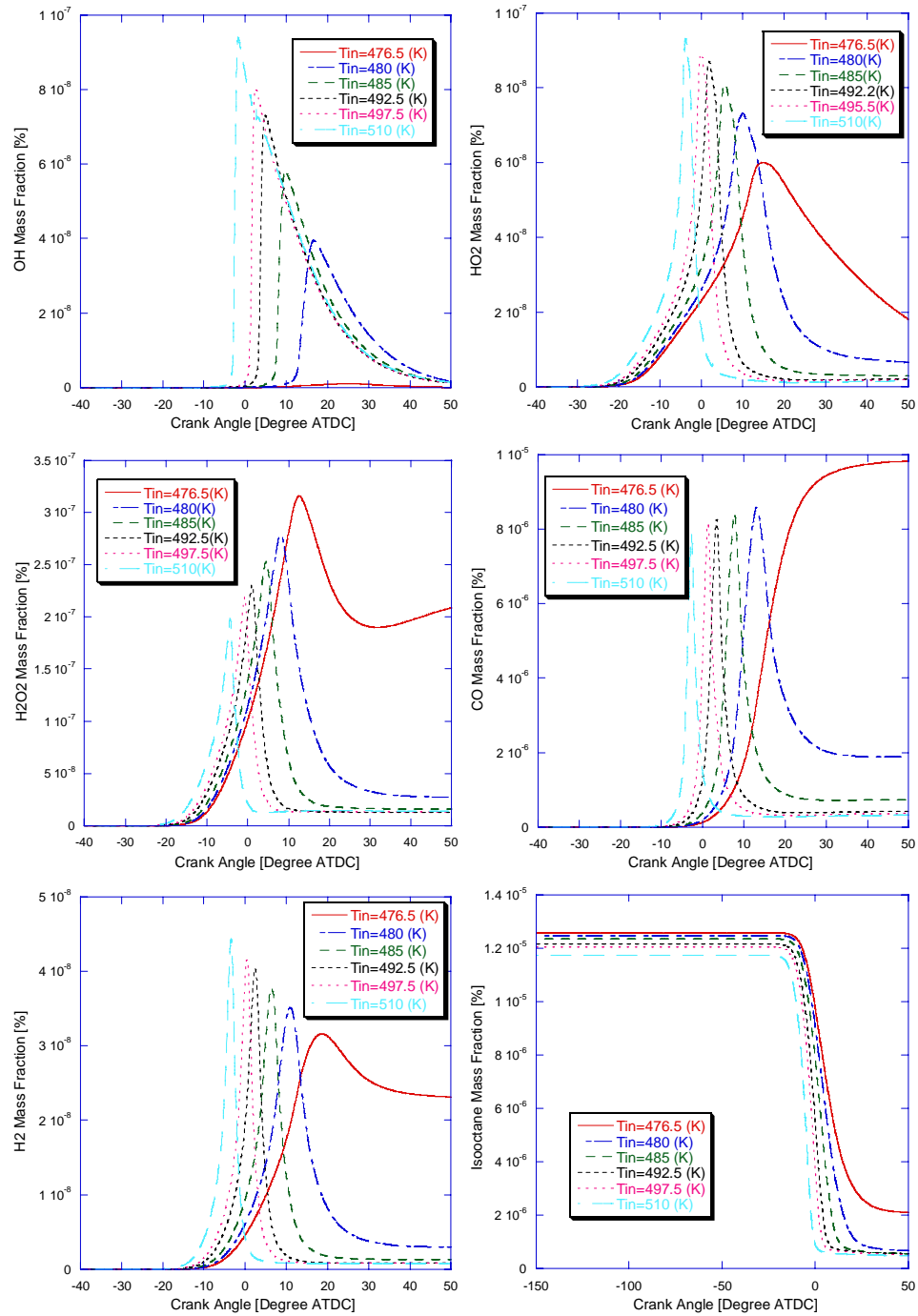


Figure 2.14 – KIVA-MZ cylinder composition comparison for six intake temperature cases

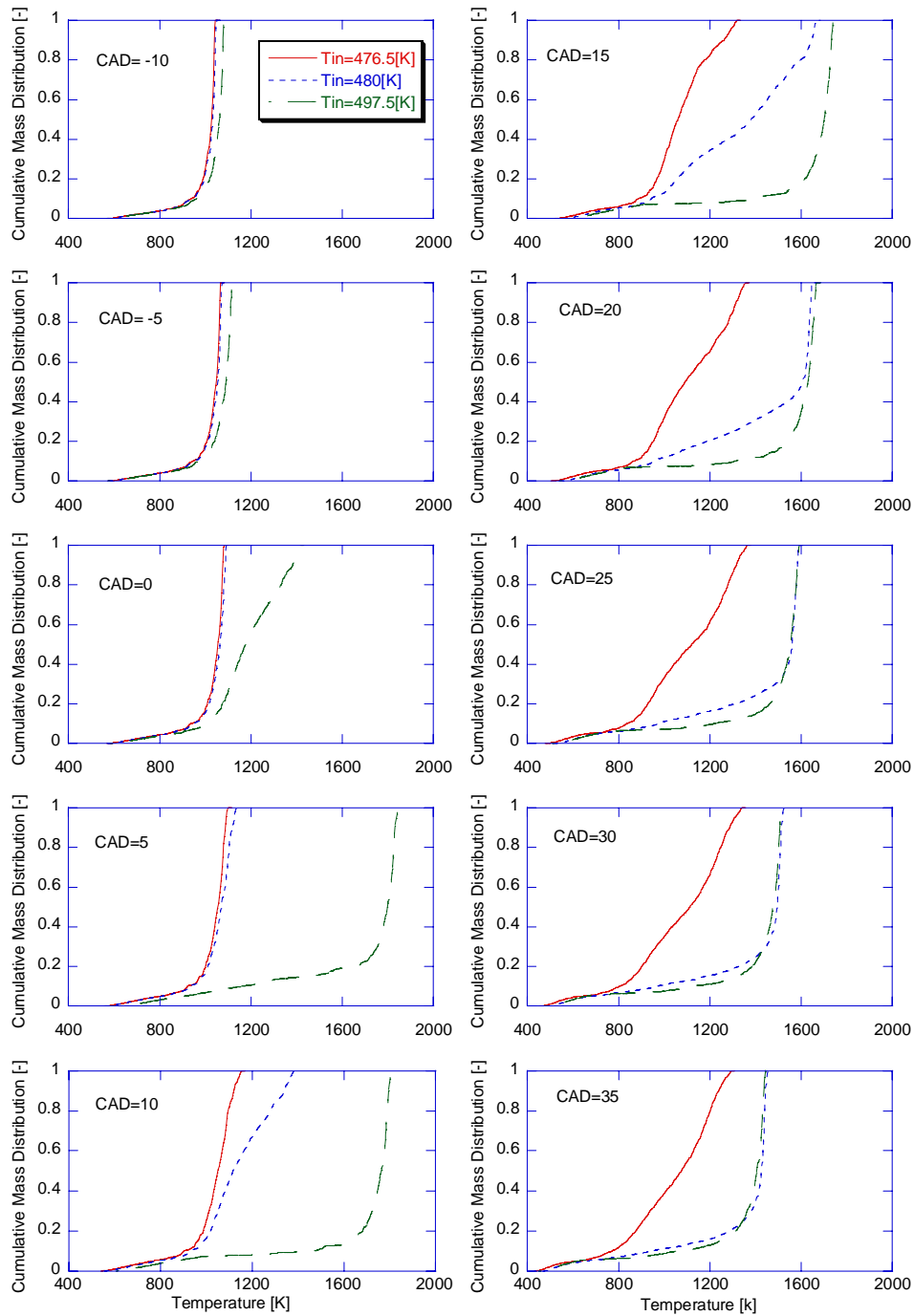


Figure 2.15 – KIVA-MZ Cylinder temperature mass distribution comparison for three intake temperature cases

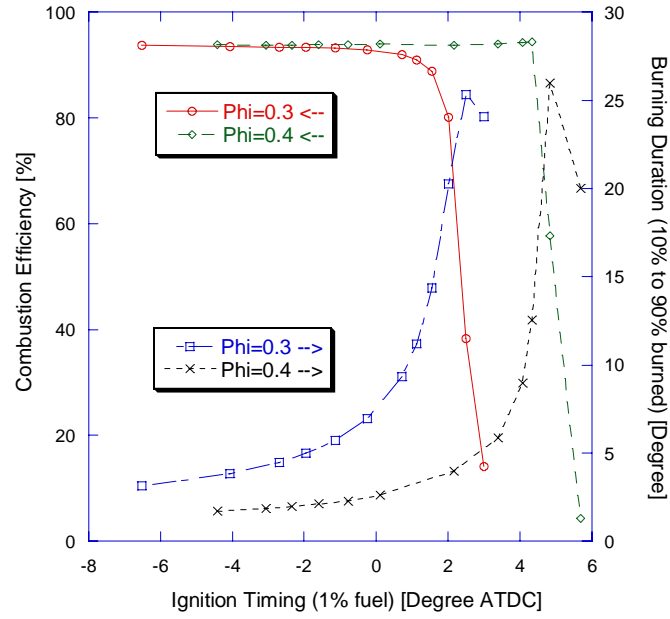


Figure 2.16 - Relationship between combustion efficiency, burning duration and ignition timing for two intake temperature sweeps with different equivalence ratio

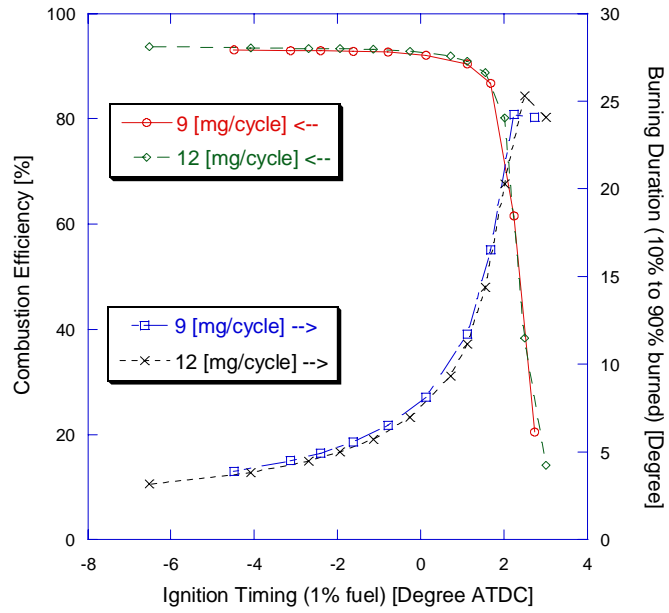


Figure 2.17 - Relationship between combustion efficiency, burning duration and ignition timing for two intake temperature sweeps with different load

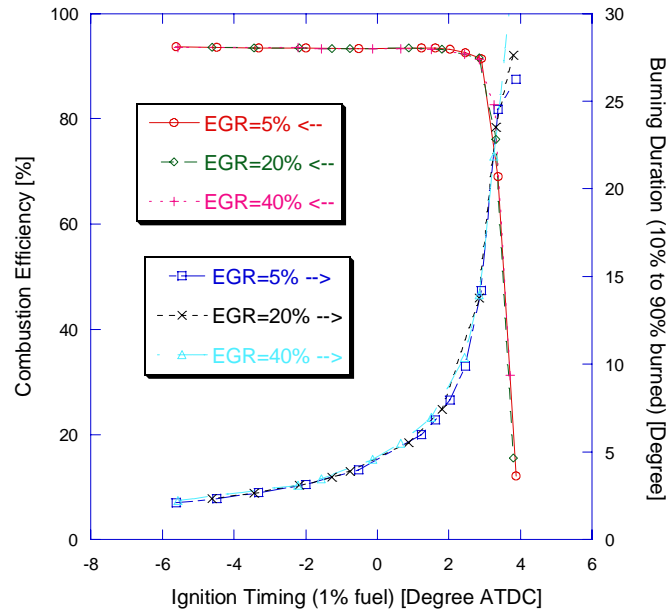


Figure 2.18 - Relationship between combustion efficiency, burning duration and ignition timing for three intake temperature sweeps with different EGR

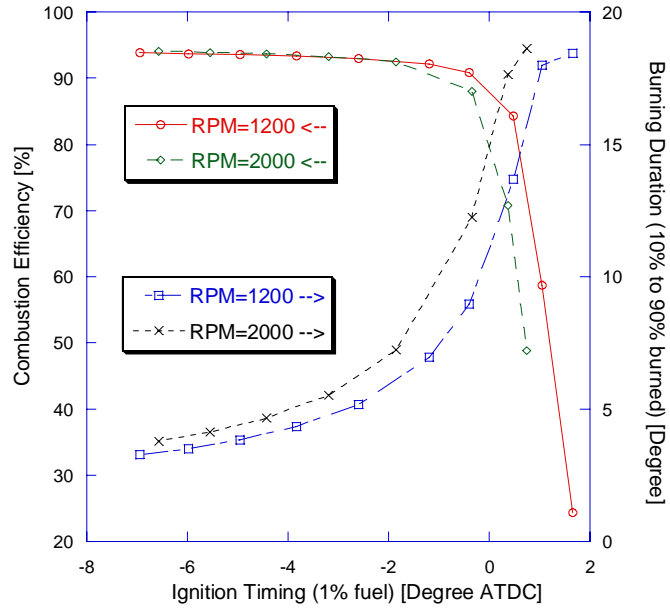


Figure 2.19 - Relationship between combustion efficiency, burning duration and ignition timing for two intake temperature sweeps with different rpm

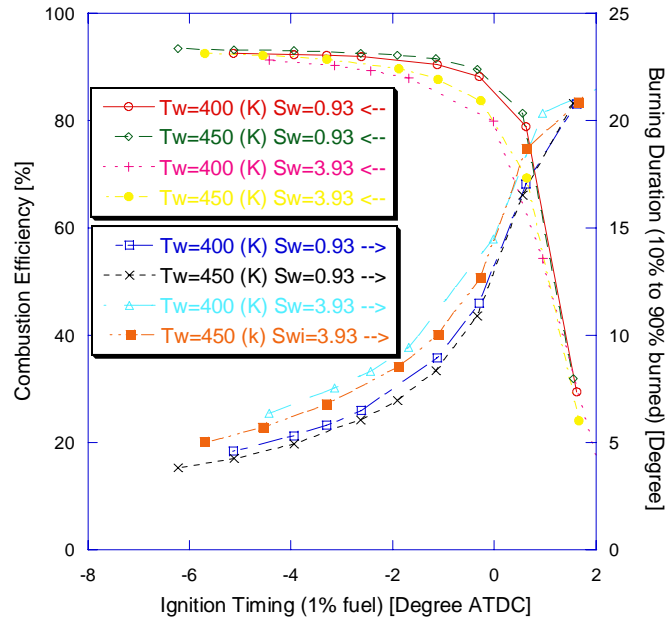


Figure 2.20 - Relationship between combustion efficiency, burning duration and ignition timing for four intake temperature sweeps with two different wall temperatures and two different swirl numbers

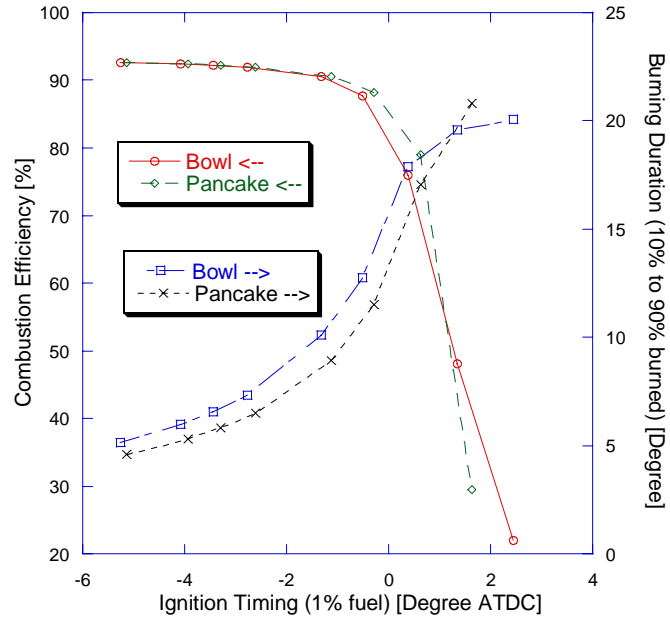


Figure 2.21 - Relationship between combustion efficiency, burning duration and ignition timing for two intake temperature sweeps with different piston geometry

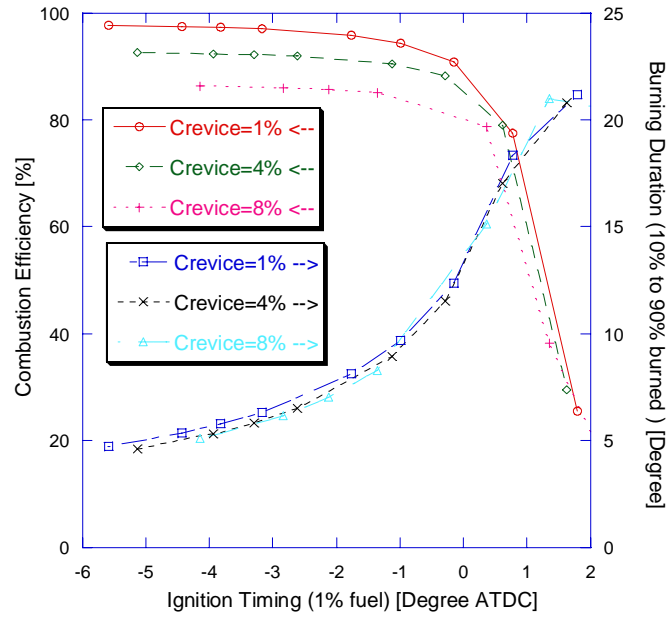


Figure 2.22 - Relationship between combustion efficiency, burning duration and ignition timing for three intake temperature sweeps with different crevice volume

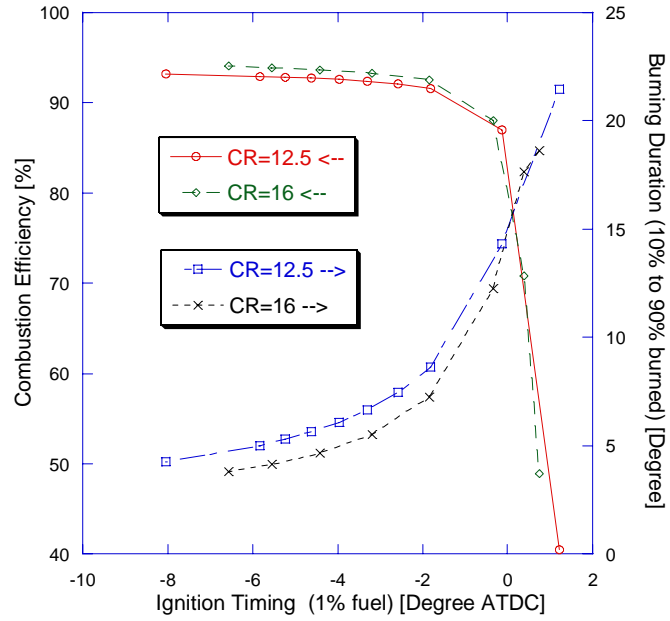


Figure 2.23 - Relationship between combustion efficiency, burning duration and ignition timing for two intake temperature sweeps with different compression ratio

CHAPTER 3

ENGINE OPERATING PARAMETERS

In this chapter, engine operating parameters are analyzed in detail with regard to their effects on ignition timing, combustion efficiency and burning rate. Equivalence ratio, load, EGR, and engine speed are examined with in-cylinder temperature distribution data. Unlike design parameters, operating parameters change frequently during engine operation, so the results in this chapter are more pertinent to engine controller development.

For each parameter, there're two sets of comparisons. First set of comparison focuses on the variation in the parameter itself, and the attention is on how this parameter affects the ignition timing; second set of comparison focus on how the parameter under study can impact combustion speed under the same ignition time.

This chapter and the next are the extensions of the section 2.6 of Chapter 2, where overall sweep results are presented. This chapter and next are focusing on comparison of individual pair of matching points. In-cylinder data is used to support the observation made in the section 2.6 of Chapter 2.

3.1 Equivalence ratio

The main advantages of HCCI are derived from its lean burning, so equivalence ratio is low in HCCI engines. Conceptually, HCCI combustion is a series of auto ignition

happening across the cylinder chamber and over the time period when piston is near the TDC. The adiabatic combustion temperature is very important for overall heat release rate. For a richer mixture, its higher combustion temperature at the beginning can heat up the cylinder mixture in a greater level so that the rest of the unburned mixture reaches ignition criteria earlier. So hotter combustion and earlier ignition get into an escalating effect to speed up the combustion.

3.1.1 Open end parametric study

In this study, the fueling rate is kept at constant of 12 milligrams per cycle, and two values of initial pressure are chosen to supply the cylinder with different air quantities. These two cases have equivalence ratio of 0.3 and 0.4. Case 1098 from sweep 10 has equivalence ratio at 0.3; case 1106 from sweep 11 has equivalence ratio at 0.4. Table 3.1 shows the parameters of these two cases.

Table 3.1- Parameters for open end parametric study of two cases with two equivalence ratios

	CASE 1098	CASE 1106
Intake temperature (K)	485	485
Intake pressure (bar)	1.282	0.963
Equivalence ratio	0.3	0.4
Compression ratio	12.5	12.5
Engine speed (rpm)	2000	2000
Fueling rate (mg/cycle)	12	12
Ignition timing (ATDC)	-2.69	2.16
Combustion efficiency (%)	93.39	93.75

Equivalence ratio is a very important operating variable in HCCI engine with regard to ignition. It can impact the ignition process in two major ways. First, the gamma value affects the compression temperature of the charge during the compression stroke, thus ignition timing is altered. Second, the species concentration varies the temperature threshold of ignition.

Case 1098 with leaner mixture has ignition timing more than 4.5 degrees earlier than case 1106. Figure 3.1 shows that the low equivalence ratio case has higher peak cylinder temperature before ignition, which indicates that the gamma value effect overweighs the composition effect on ignition timing.

To further analyze the reason causing the earlier ignition of leaner mixture, two additional KIVA3V-MZ runs are made. One run has the heat transfer simulation turned off; the other run has both the chemical kinetics simulation and the heat transfer simulation turned off. So, there are three cases for comparison. The original one having all the physics models active is assigned the name “normal”, the second one having no heat transfer model is with name “adiabatic”, and the third one having neither heat transfer nor chemistry model is with name “inert-adiabatic”. Without heat transfer, both “adiabatic” and “inert-adiabatic” have higher cylinder temperature than “normal” (Figure 3.6), but the temperature difference between the lean and the rich mixture still exists, which tells that equivalence ratio difference won’t cause heat transfer variation. The difference between “inert-adiabatic” and “adiabatic” is the chemistry, and it is discernable that richer mixture does ignite at a slightly lower cylinder temperature. However, the chemistry advantage in the high equivalence ratio mixture couldn’t offset the temperature disadvantage. The temperature separation between these two equivalence ratios cases is about 20 Kelvin in all three simulations.

Both cases have good combustion efficiencies, and they are very close in value (Figure 3.2). Figure 3.3 shows that the burning rates for these two cases are very close in shape even though the phasing is widely apart. This observation is quite unique as none

of the parameters in the following analysis has the same pattern. The iso-octane composition plot (Figure 3.5) shows that both cases have about the same level of unburned fuel, while CO composition plot (Figure 3.4) shows that the lean mixture has slightly more freezing CO concentration at the end.

The gamma value of the mixture plays an important role in the ignition timing because of the compression heating effect. Richer mixture has later ignition timing; however, it has higher combustion temperature and can endure much later ignition to finish with good combustion efficiency.

3.1.2 Sweep Study Revisit

In the section 2.6 of Chapter 2, Figure 2.16 has both combustion efficiency and burning duration comparisons for two equivalence ratio. Intake temperature sweep creates a span of ignition timing, which is used as “X” axis. Two “Y” axes are the combustion efficiency and the burning duration.

The shapes of combustion efficiency and burning duration curves are quite different. The burning duration curve is gradually increasing when the ignition timing gets later. The combustion efficiency curve is flat when the ignition timing is earlier than a certain transition point, but the slope changes downward dramatically after that critical ignition timing point. So the comparison between the burning duration is on the base of overall curve matching; while the comparison of the combustion efficiency has three specific matching points: the flat part when ignition timing is early; the ignition timing at the transition point; and the combustion deterioration slope. This comparison framework is applied in all the other parameters.

Figure 2.16 shows that the burning duration curves are widely apart. For any given ignition timing, the rich mixture burns much faster than the lean mixture. Both cases have similar peak combustion efficiency, which is the flat part of the curve. The

lean mixture has the transition point at around TDC; while the rich mixture's transition point is around 4 degrees ATDC. The downward slopes for both cases are similar. With similar ignition timing, the richer mixture has much faster heat release, which helps combustion completeness. The lean mixture misfires at a much earlier ignition timing.

To understand the detailed evolution of the cylinder content, two points are picked up with similar ignition timing, and comparisons are made in the following section.

3.1.3 Filtered Parametric Study

Table 3.2 lists the values for two cases with very close ignition timing. Case 1098 from sweep 10 is with low intake temperature and low equivalence ratio; case 1110 from sweep 11 is with high intake temperature and high equivalence ratio.

Table 3.2 - Parameters for filtered parametric study of two cases with two equivalence ratio

	CASE 1098	CASE 1110
Intake temperature (K)	485	497.5
Intake pressure (bar)	1.2819	0.9878
Equivalence ratio	0.3	0.4
Engine speed (rpm)	2000	2000
Compression ratio	12.5	12.5
Fuelling rate	12	12
Ignition Timing (ATDC)	-2.689	-2.35
Combustion efficiency (%)	93.39	93.78

An addition of 12.5 degrees in intake temperature for the rich mixture is needed to compensate the gamma effect to realize close ignition timings. Figure 3.7 records the temperature distributions from 10 degrees BTDC to 35 degrees ATDC with five degrees increment. Both cases have ignition timing at about 2.5 degrees BTDC, where case 1098 is about 0.3 degrees earlier. The temperature distribution at TDC is close. Most dramatic change happens between TDC and five degrees after. At five degrees ATDC, Case 1110 demonstrates higher degree of combustion completeness, with majority of the mass residing in high temperature region; while Case 1098 shows more even distribution of temperature. Cylinder maximum temperature comparison shows that the peak temperature of Case 1110 is about 300 K lower than that of Case 1098.

The mass fraction burning rate comparison plot (Figure 3.9) shows that Case 1110 has much higher peak heat release rate, which finishes several degrees earlier than Case 1098. The combustion efficiencies (Figure 3.8) are about the same since the ignition timings are early enough to finish the burning. Isooctane compositions match well between these two cases; while CO composition for the rich mixture has much lower peak value and diminishes much earlier.

With similar ignition timing, the richer mixture is burning at a faster pace due to its significantly higher combustion temperature.

3.2 Load

In this load comparison, the fuel quantity and air quantity are changed proportionally to provide the same equivalence ratio, which is 0.3. So intake pressure effect on ignition can be investigated.

3.2.1 Open End Parametric Study

Case 1098 from sweep 10 has 12 milligrams of isooctane per cycle; and Case 1117 from sweep 12 has 9 milligrams of isooctane per cycle. Parameters are listed in the following table.

Table 3.3 - Parameters for open end parametric study of two cases with two loads

	CASE 1098	CASE 1117
Intake temperature (K)	485	485
Intake pressure (bar)	1.282	0.962
Equivalence ratio	0.3	0.3
Compression ratio	12.5	12.5
Engine speed (rpm)	2000	2000
Fueling rate (mg/cycle)	12	9
Ignition timing (ATDC)	-2.69	-0.15
Combustion efficiency	93.39	92.17

Two temperature distribution plots at 10 and 5 degrees BTDC in Figure 3.12 show that there's only slight difference in temperature distribution between these two cases before ignition. Case 1098 has discernable lead on ignition timing due to its much higher cylinder pressure at the intake.

After combustion, the low load case has slightly higher peak cylinder temperature due to its late combustion. Figure 3.13 and Figure 3.14 show cumulative and instantaneous mass burning rate, which are consistent with CO and isooctane composition (Figure 3.15 and Figure 3.16).

Intake pressure does have impact on ignition timing. Higher intake pressure leads to earlier ignition.

3.2.2 Sweep Study Revisit

Figure 2.17 shows very good match between these two load cases. Over the whole span of ignition timing, combustion efficiency and burning duration are almost identical. This observation shows that cylinder pressure can only affect the early part of the ignition. What will happen next is more related to cylinder temperature than cylinder pressure. This load comparison forms sharp contrast to the result of equivalence ratio study (Figure 2.16). The conclusion from this comparison is that cylinder temperature is a much more dominant factor than cylinder pressure for combustion rate after ignition.

3.2.3 Filtered Parametric Study

Case 1093 from sweep 10 has 12 milligrams of iso-octane per cycle; and case 1116 from sweep 12 has 9 milligrams of iso-octane per cycle. Table 3.4 shows the parameters for this comparison.

Table 3.4 - Parameters for filtered parametric study of two cases with two load

	CASE 1093	CASE 1116
Intake temperature (K)	474	482.5
Intake pressure (bar)	1.253	0.9566
Equivalence ratio	0.3	0.3
Engine speed (rpm)	2000	2000
Compression ratio	12.5	12.5
Fuelling rate (mg/cycle)	12	9
Ignition Timing (ATDC)	1.125	1.128
Combustion efficiency	90.99	90.42

It takes about 9 degrees difference in intake temperature to compensate the initial pressure effect to get similar ignition timing. It is not surprising that case 1116 has slightly higher peak cylinder temperature before first ignition. Figure 3.17 shows superb matching between these two cases. The same level of similarity is also evident in Figure 3.18 and Figure 3.19. Isooctane composition (Figure 3.21) starts with slightly different value. However, the timings to reach the freezing value for both cases are very close. So far, the biggest variation between these two cases is the CO composition (Figure 3.20), case 1093 has higher peak value, and declines at a slightly later ignition timing.

The combustion rate under the same ignition timing is amazingly constant. So intake pressure only causes the difference in first ignition timing, but for the same ignition timing, the following combustion rate is independent from initial pressure.

3.3 EGR

Under constant initial pressure and constant fueling rate, the difference of EGR fraction is the trading between fresh air and burned gases. The major change of EGR percentage in HCCI combustion is the gamma value, heat capacity, and oxygen concentration. Since less EGR percentage has higher gamma value and higher oxygen composition, cases with less EGR percentage have earlier ignition timing.

3.3.1 Open End Parametric Study

Table 3.5 lists the parameters of three EGR percentage cases. Case 1131 from sweep 13 has EGR percentage at 5%; case 1006 from sweep 1 has 20% EGR; and case 1014 from sweep 2 has 40% EGR.

Table 3.5 - Parameters for open end parametric study of three cases with three EGR

	CASE 1131	CASE 1006	CASE 1014
Intake temperature (K)	490	490	490
Intake pressure (bar)	1.1	1.1	1.1
Equivalence ratio	0.3535	0.4219	0.5686
Compression ratio	12.5	12.5	12.5
EGR (%)	5	20	40
Engine speed (rpm)	2000	2000	2000
Fueling rate (mg/cycle)	12	12	12
Ignition timing (ATDC)	-1.99	-0.76	2.44
Combustion efficiency	93.46	93.4	92.4

There's some moderate difference in ignition timing. Because of the gamma value effect, the peak cylinder temperature before ignition is in a neat order, as demonstrated by plots at 10 and 5 degrees BTDC in Figure 3.22. Higher EGR percentage cases result in lower peak cylinder temperature before combustion.

The combustion efficiency of all cases are very close (Figure 3.23) despite of the difference in burning rate (Figure 3.24). Also, the CO composition (Figure 3.25) and isooctane composition (Figure 3.26) have similar peak and freezing values.

3.3.2 Sweep Study Revisit

Just like the load study, Figure 2.18 shows amazing overlap between three EGR sweeps. In other words, the combustion rate is invariant to EGR ratio if the ignition timing is the same.

3.3.3 Filtered Parametric Study

Case 1005 from sweep 1 has EGR level at 20%; case 1016 from sweep 2 has EGR level at 40%. Table 3.6 lists the parameters for this comparison.

Table 3.6 - Parameters for filtered parametric study of three cases with three EGR

	CASE 1005	CASE 1016
Intake temperature	485	495
Intake pressure	1.1	1.1
Equivalence ratio	0.33	0.33
Engine speed	2000	2000
Compression ratio	12.5	12.5
Fuelling rate	12	12
EGR (%)	20	40
Ignition Timing (ATDC)	0.872	0.658
Combustion efficiency	93.51	93.41

The temperature compensation is 10 degrees. The temperature distribution curves (Figure 3.27) are strikingly similar. The comparisons on cumulative burned (Figure 3.28) and instant burning rate (Figure 3.29) are also very similar. CO (Figure 3.30) and isooctane (Figure 3.31) composition also match each other very well.

3.4 **Engine speed**

Engine speed has two effects on the HCCI combustion: time for heat transfer and time for chemistry. Slow engine speed gives more time for heat transfer as well as chemical reaction. Generally, these two effects work against each other with respect to ignition timing and combustion speed.

3.4.1 Open End Parametric Study

Case 1078 from sweep 8 has engine speed set at 1200 rpm; and case 1084 from sweep 9 has engine speed set at 2000 rpm.

Table 3.7 - Parameters for open end parametric study of three cases with two engine speed

	CASE 1078	CASE 1084
Intake temperature (K)	440	440
Intake pressure (bar)	1.1	1.1
Equivalence ratio	0.26	0.26
Compression ratio	16	16
Engine speed (rpm)	1200	2000
Fueling rate (mg/cycle)	9.85	9.85
Ignition timing (ATDC)	-4.95	-1.85
Combustion efficiency	93.58	92.50

At 10 degrees BTDC, the temperature distribution (Figure 3.32) is favoring case 1084 to ignite earlier since its curve is on the lower-right side. Shorter heat transfer timing is helping case 1084 retaining the cylinder temperature. However, plot at 5 degrees BTDC center shows that the lower speed case does ignite earlier. Figure 3.35 shows that CO composition rises up much earlier for case 1078.

The final combustion efficiency (Figure 3.33) is close for both speed cases, but the phasing is obviously staged (Figure 3.34). Case 1078 leads ignition timing by about 3 degrees, and its mass fraction burning rate reaches a higher peak value at an earlier ignition timing.

3.4.2 Sweep Study Revisit

Figure 2.19 shows that the comparison of two engine speed sweeps. Burning duration curves have decent separation between them. The difference in burning duration is smaller when the ignition timing is earlier. This trend is consistent with the combustion efficiency invariance at early ignition condition.

When ignition timing gets later, the high engine speed case starts to misfire at an earlier ignition timing.

3.4.3 Filtered Parametric Study

Case 1074 from sweep 1 has engine speed set at 1200; case 1083 from sweep 2 has engine speed set at 2000. Table 3.8 lists their other parameters.

Table 3.8 - Parameters for filtered parametric study of two cases with two engine speeds

	CASE 1074	CASE 1083
Intake temperature (K)	422.5	435
Intake pressure (bar)	1.1	1.1
Equivalence ratio	0.251	0.251
Engine speed (rpm)	1200	2000
Compression ratio	16	16
Ignition Timing (ATDC)	-0.390	-0.334
Combustion efficiency	90.87	88.05

Twelve degrees of intake temperature compensation evens the ignition timings for these two cases. The cylinder temperature difference is quite noticeable before and after combustion (Figure 3.37). Before ignition, case 1083 has higher temperature due to both

less heat loss and higher intake temperature. After combustion, case 1083 has higher temperature due to both less heat transfer and slower heat release (Figure 3.39).

Despite of the same ignition timing, the mass burning rate is different. The low engine speed case has much faster combustion and finishes with higher combustion efficiency (Figure 3.38). The main combustion inefficiency comes from the partial oxidation, as isooctane composition reaches a fairly low level (Figure 3.41), while CO composition (Figure 3.40) for case 1083 freezes at a higher level than case 1074.

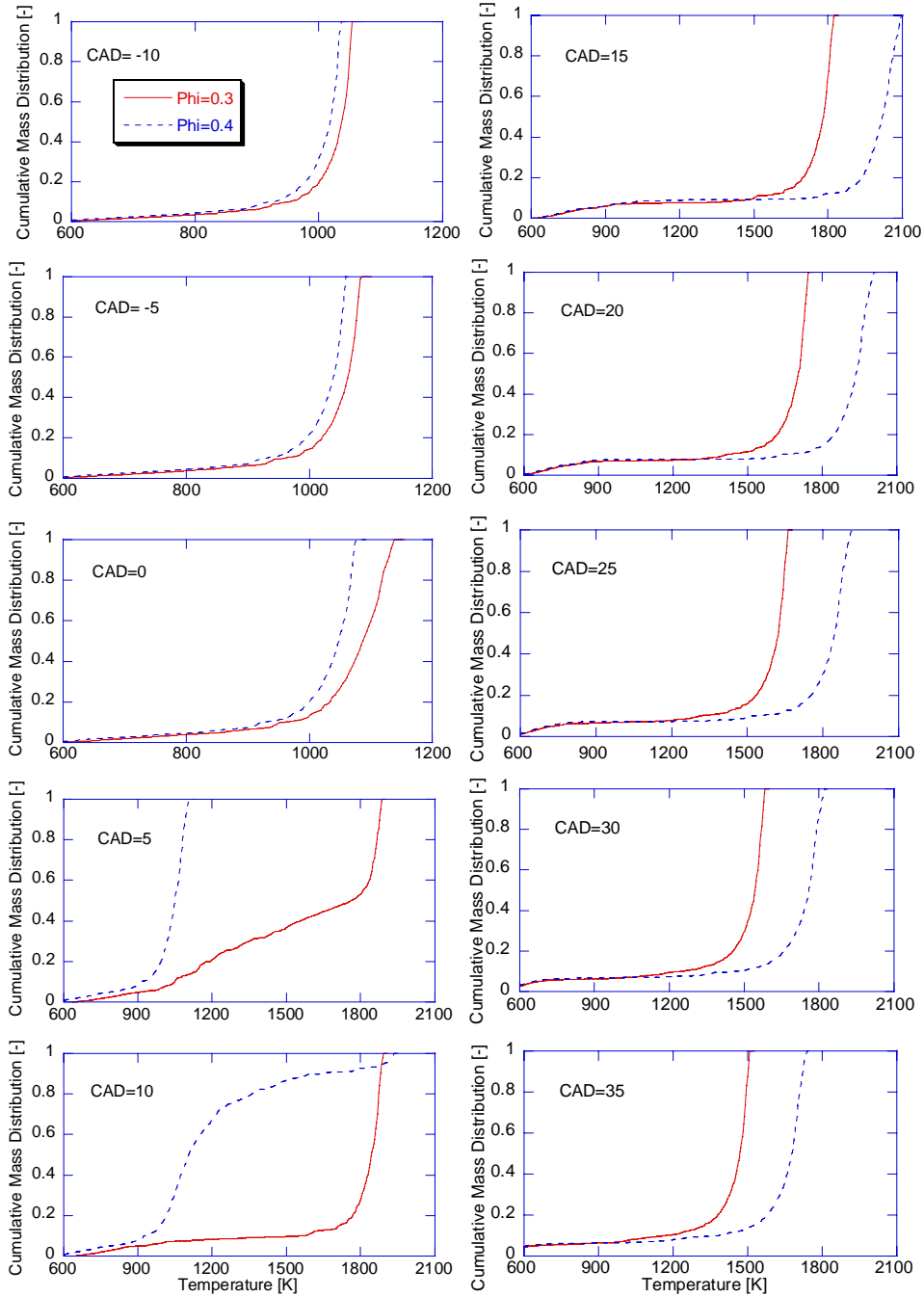


Figure 3.1 - Cumulative temperature mass distribution comparison under open end parametric study for two cases with two different equivalence ratios

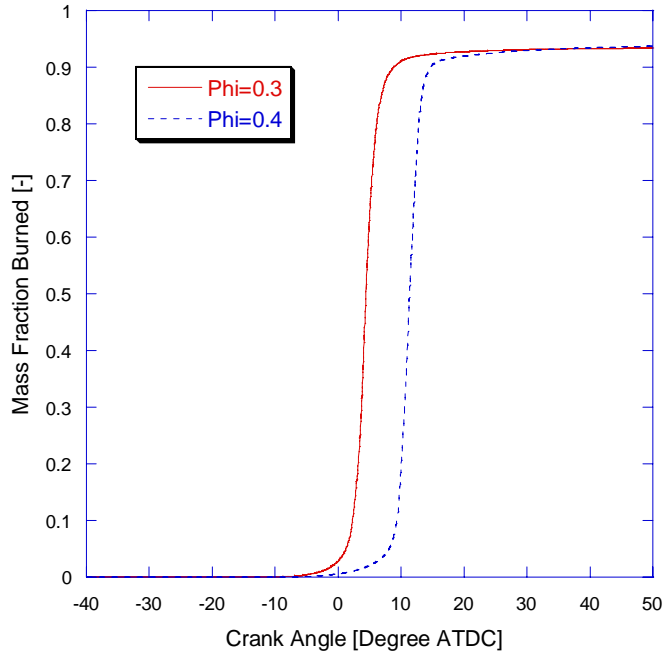


Figure 3.2 - Mass fraction burned comparison under open end parametric study for two cases with two different equivalence ratios

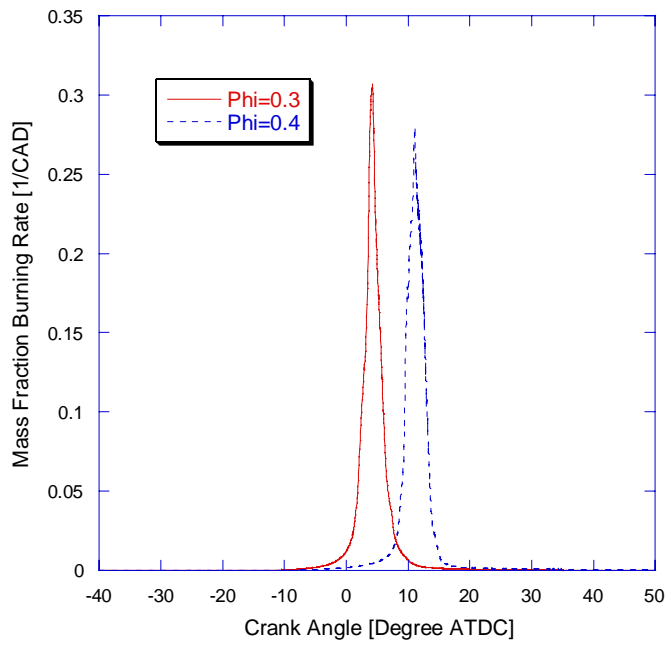


Figure 3.3 - Mass fraction burning rate comparison under open end parametric study for two cases with two different equivalence ratios

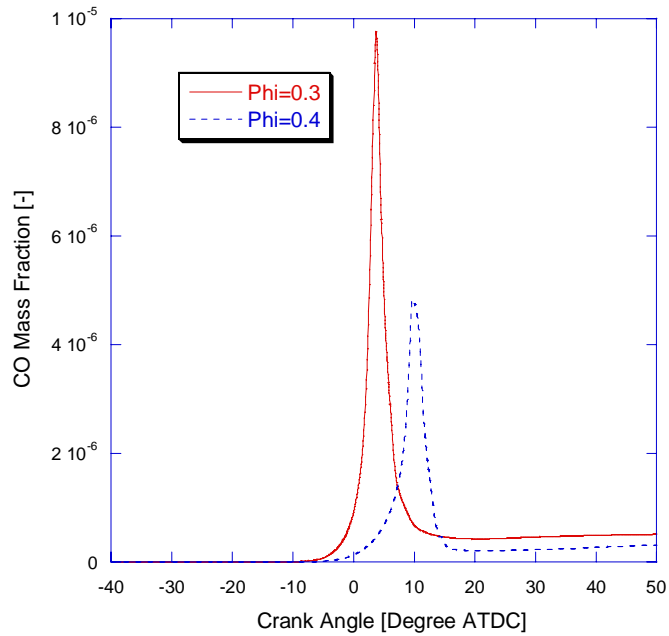


Figure 3.4 - CO composition comparison under open end parametric study for two cases with two different equivalence ratios

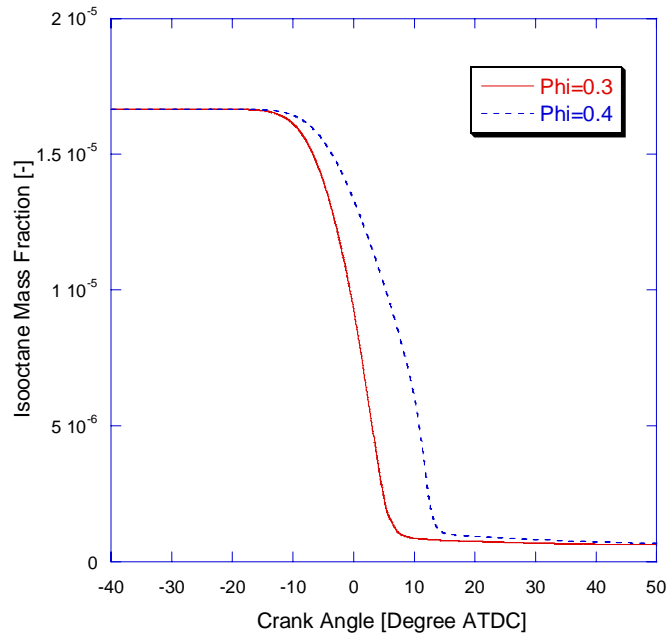


Figure 3.5 - Isooctane composition comparison under open end parametric study for two cases with two different equivalence ratios

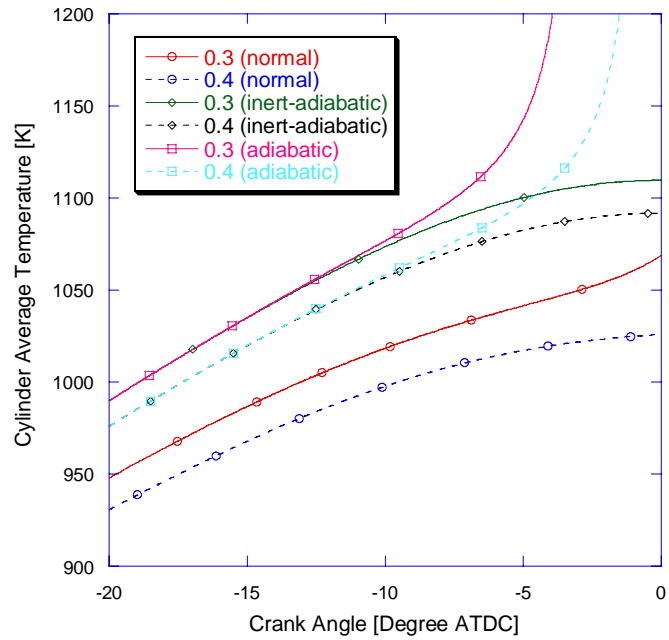


Figure 3.6 - Cylinder temperature comparison for two equivalence ratios under three simulation conditions (normal, adiabatic, and inert-adiabatic)

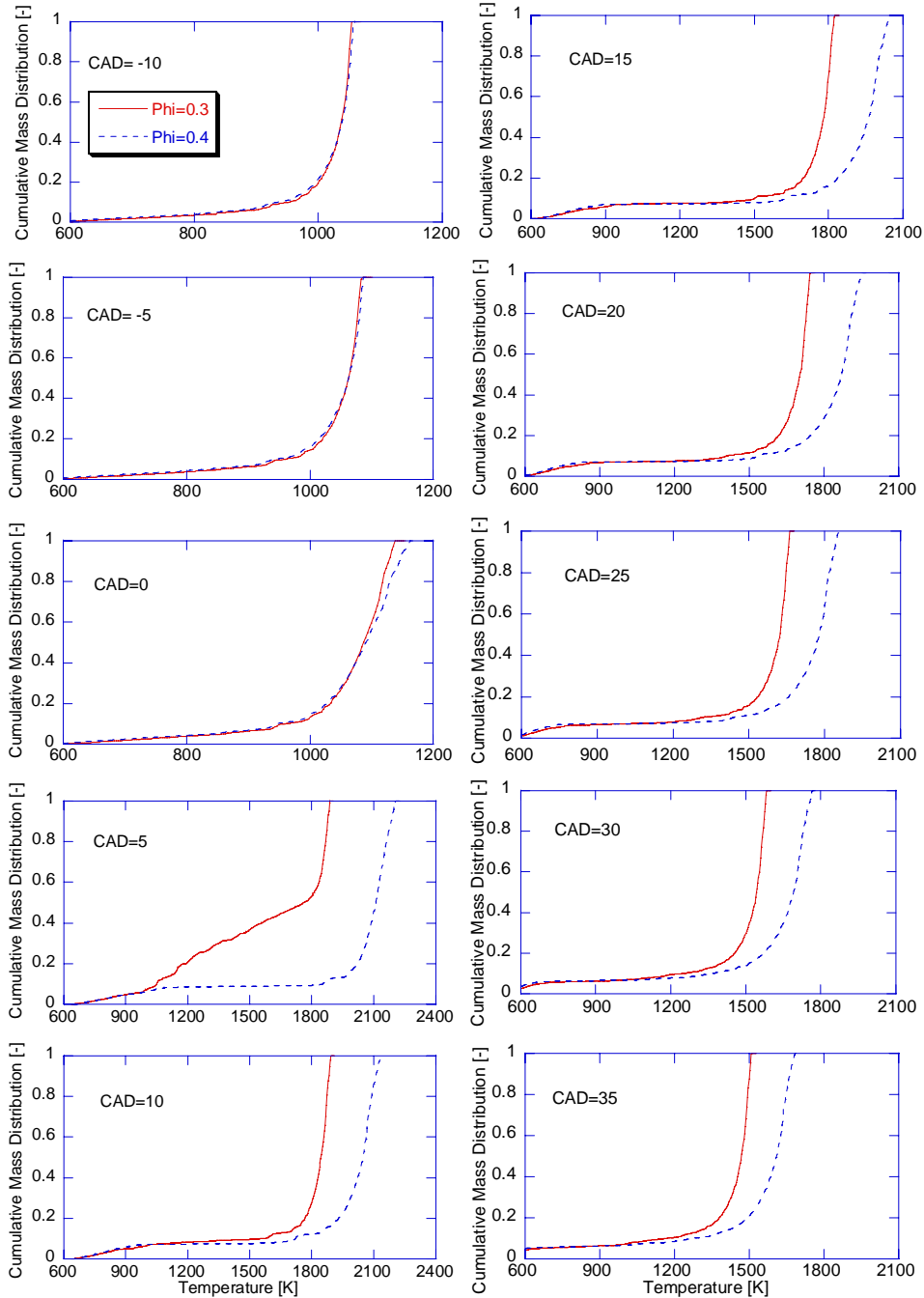


Figure 3.7 - Cumulative temperature mass distribution comparison under filtered parametric study for two cases with two different equivalence ratios

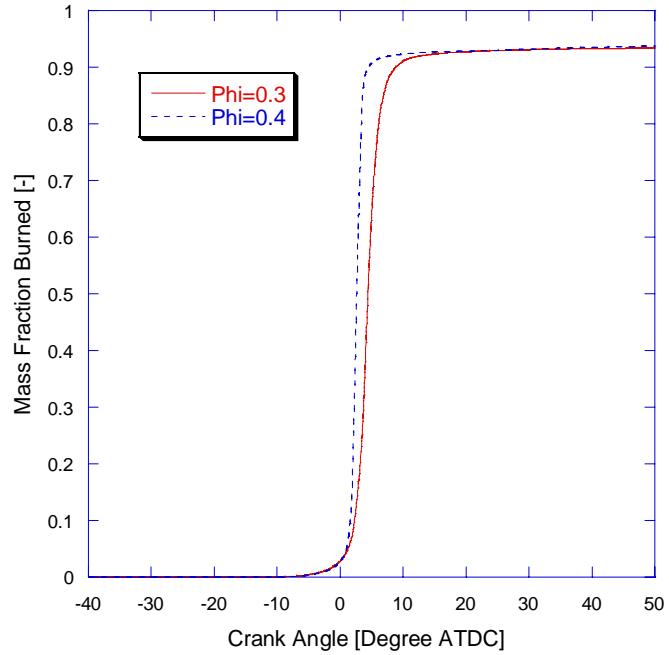


Figure 3.8 - Mass fraction burned comparison under filtered parametric study for two cases with two different equivalence ratios

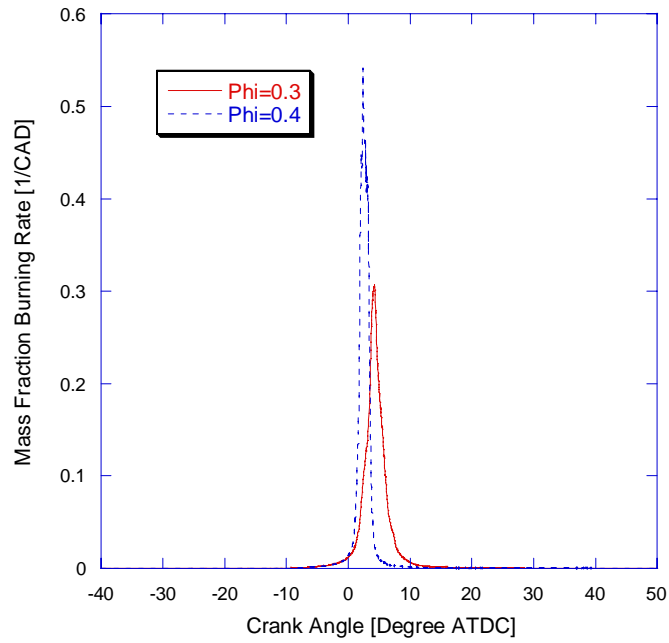


Figure 3.9 - Mass fraction burning rate comparison under filtered parametric study for two cases with two different equivalence ratios

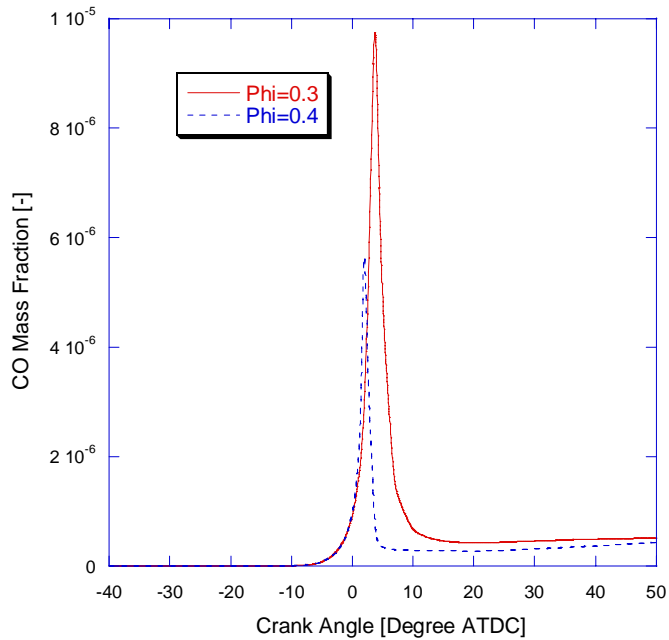


Figure 3.10 - CO composition comparison under filtered parametric study for two cases with two different equivalence ratios

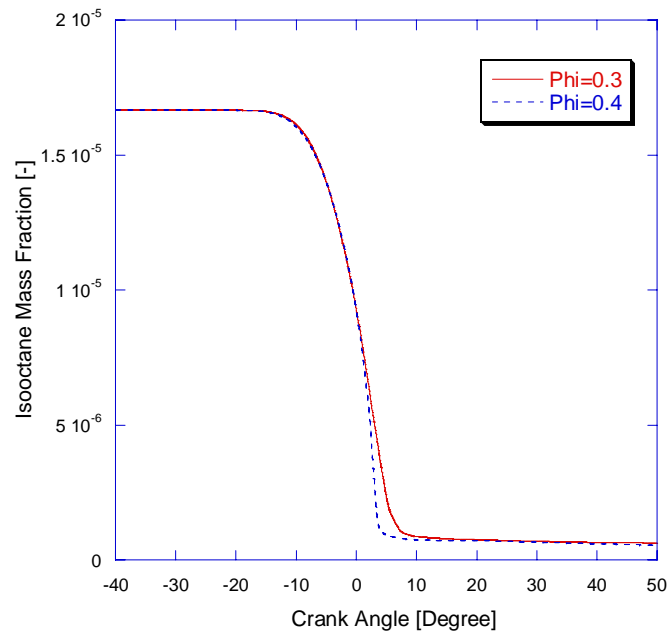


Figure 3.11 - Isooctane composition comparison under filtered parametric study for two cases with two different equivalence ratios

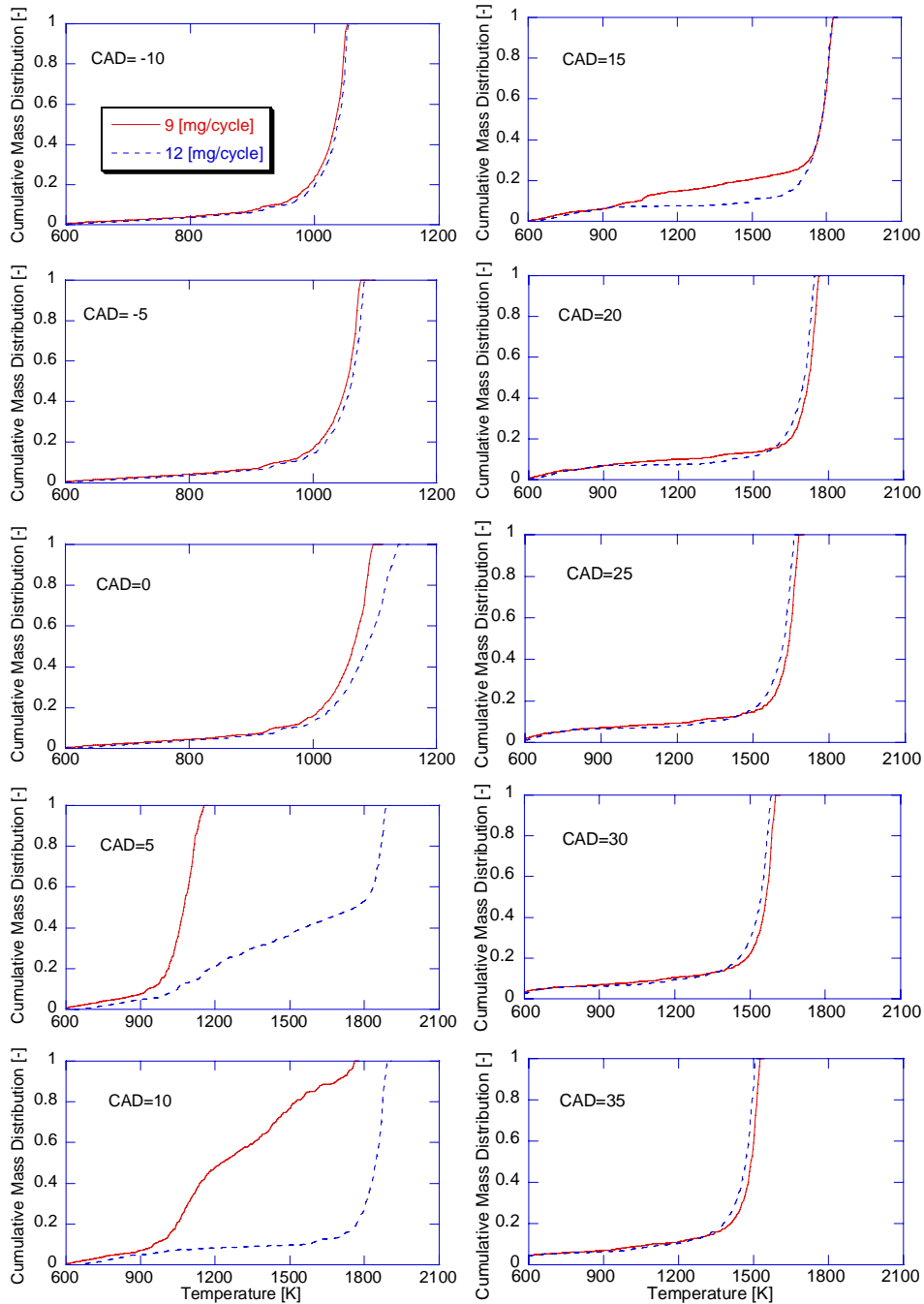


Figure 3.12 - Cumulative temperature mass distribution comparison under open end parametric study for two cases with two different loads

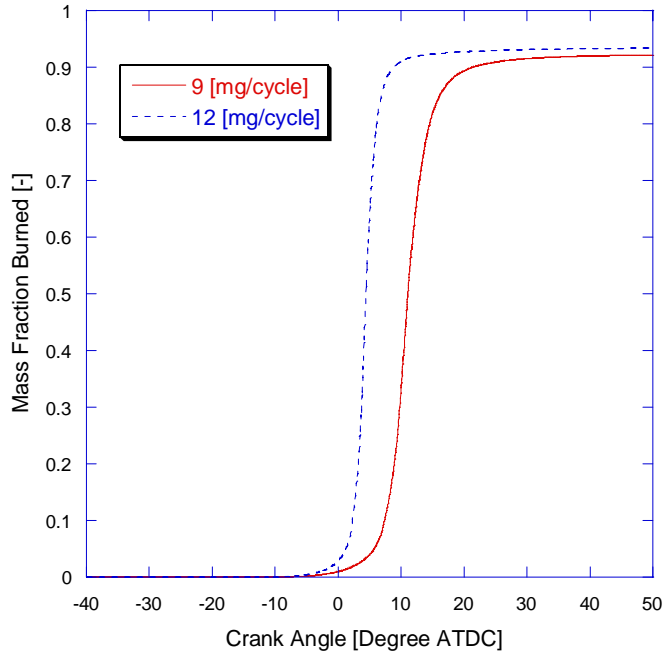


Figure 3.13 - Mass fraction burned comparison under open end parametric study for two cases with two different loads

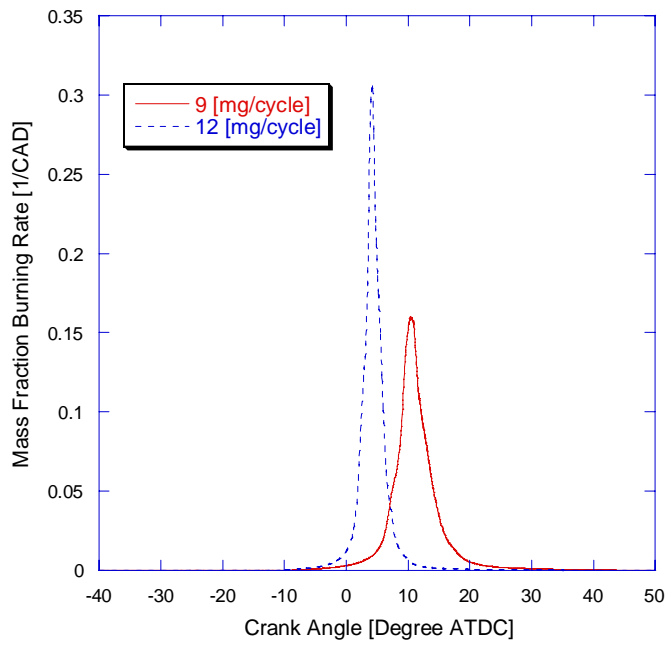


Figure 3.14 - Mass fraction burning rate comparison under open end parametric study for two cases with two different loads

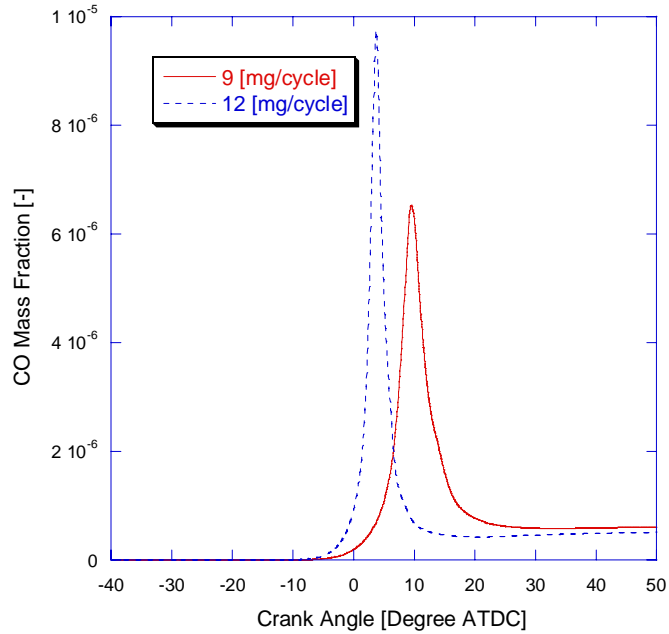


Figure 3.15 - CO composition comparison under open end parametric study for two cases with two different loads

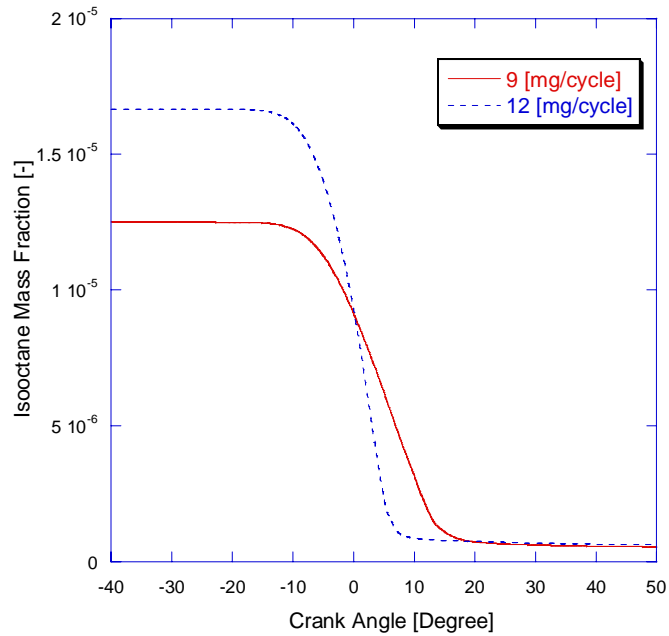


Figure 3.16 - Isooctane composition comparison under open end parametric study for two cases with two different loads

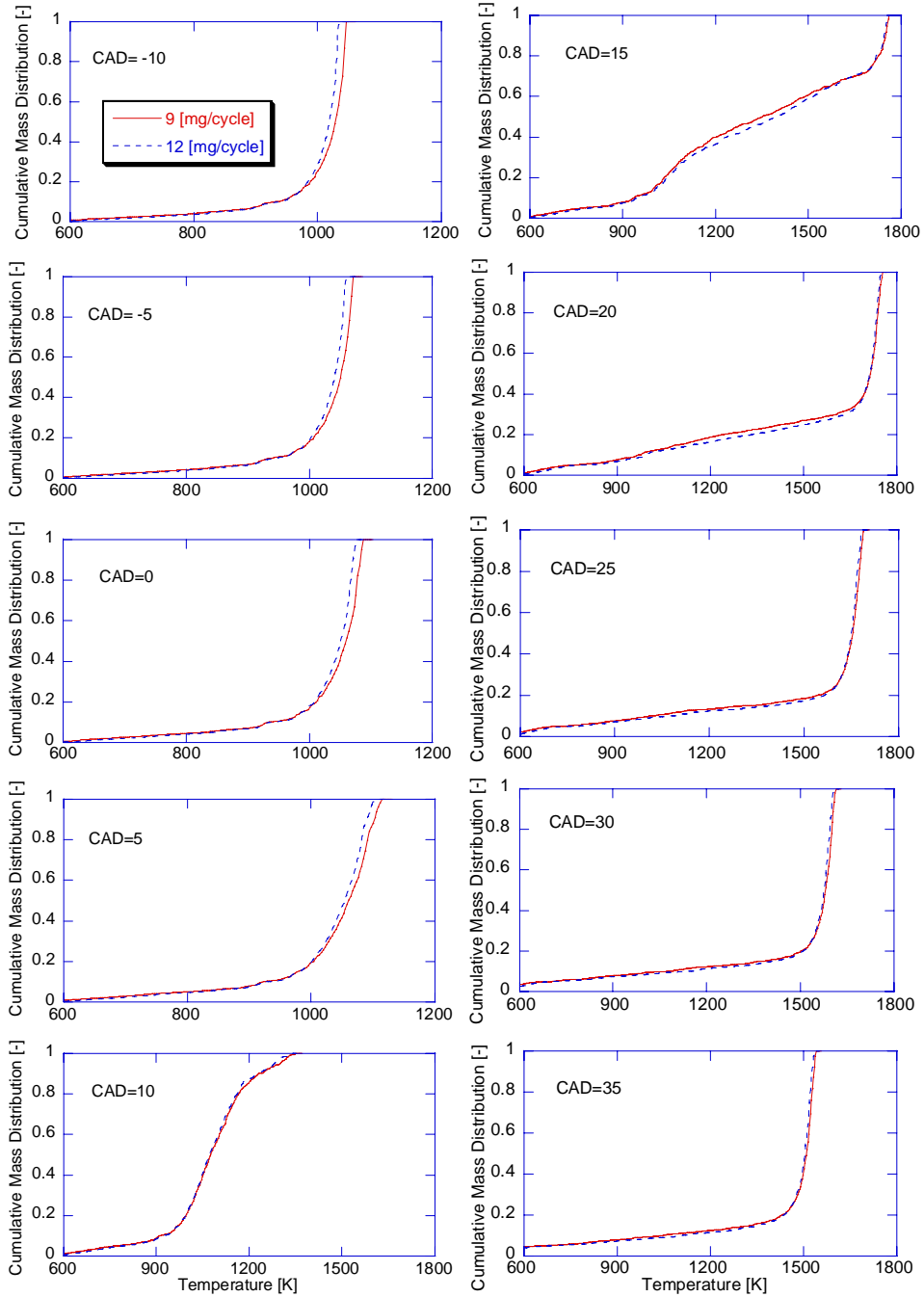


Figure 3.17 - Cumulative temperature mass distribution comparison under filtered parametric study for two cases with two different loads

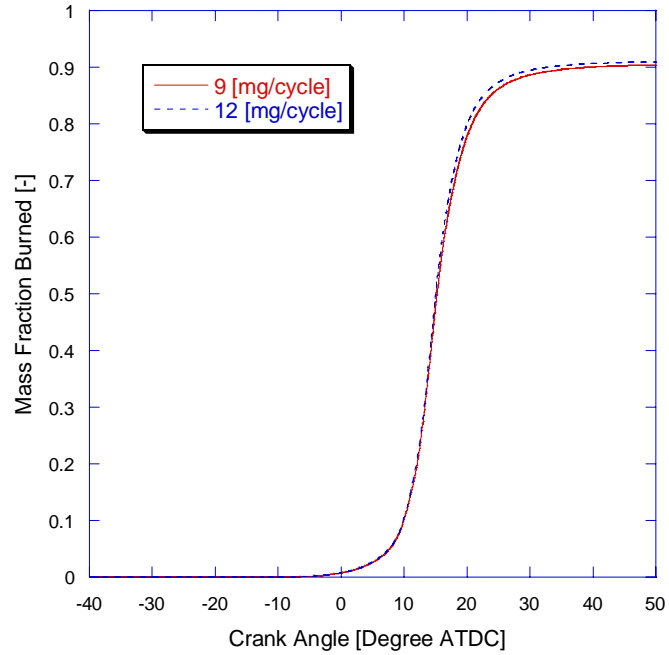


Figure 3.18 - Mass fraction burned comparison under filtered parametric study for two cases with two different loads

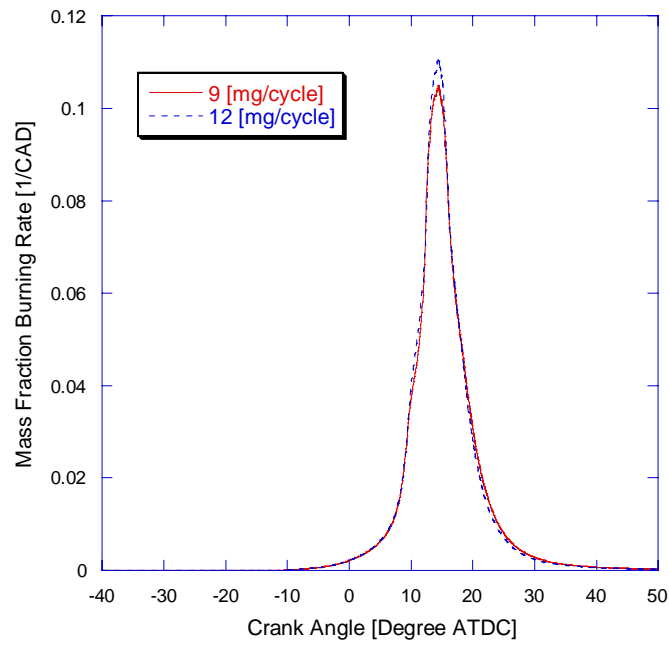


Figure 3.19 - Mass fraction burning rate comparison under filtered parametric study for two cases with two different loads

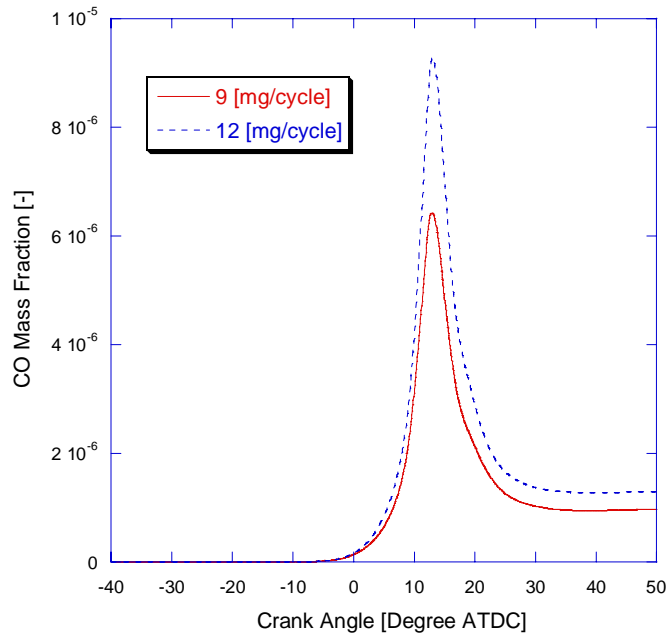


Figure 3.20 - CO composition comparison under filtered parametric study for two cases with two different loads

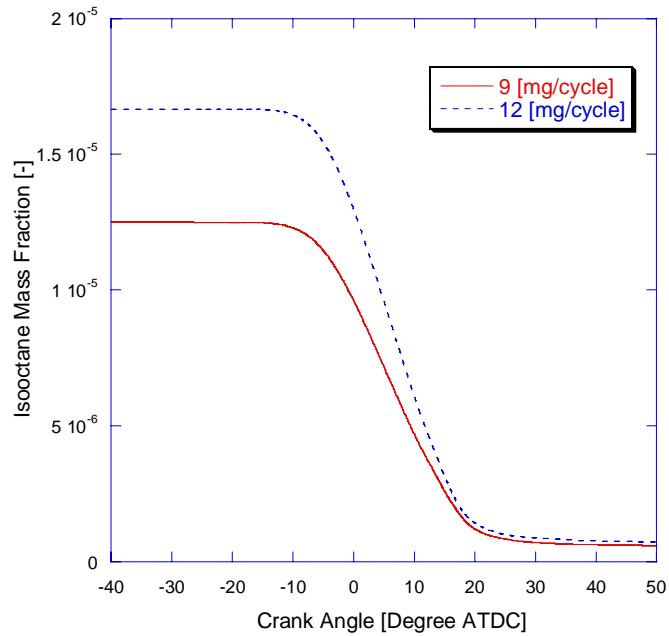


Figure 3.21 - Isooctane composition comparison under filtered parametric study for two cases with two different loads

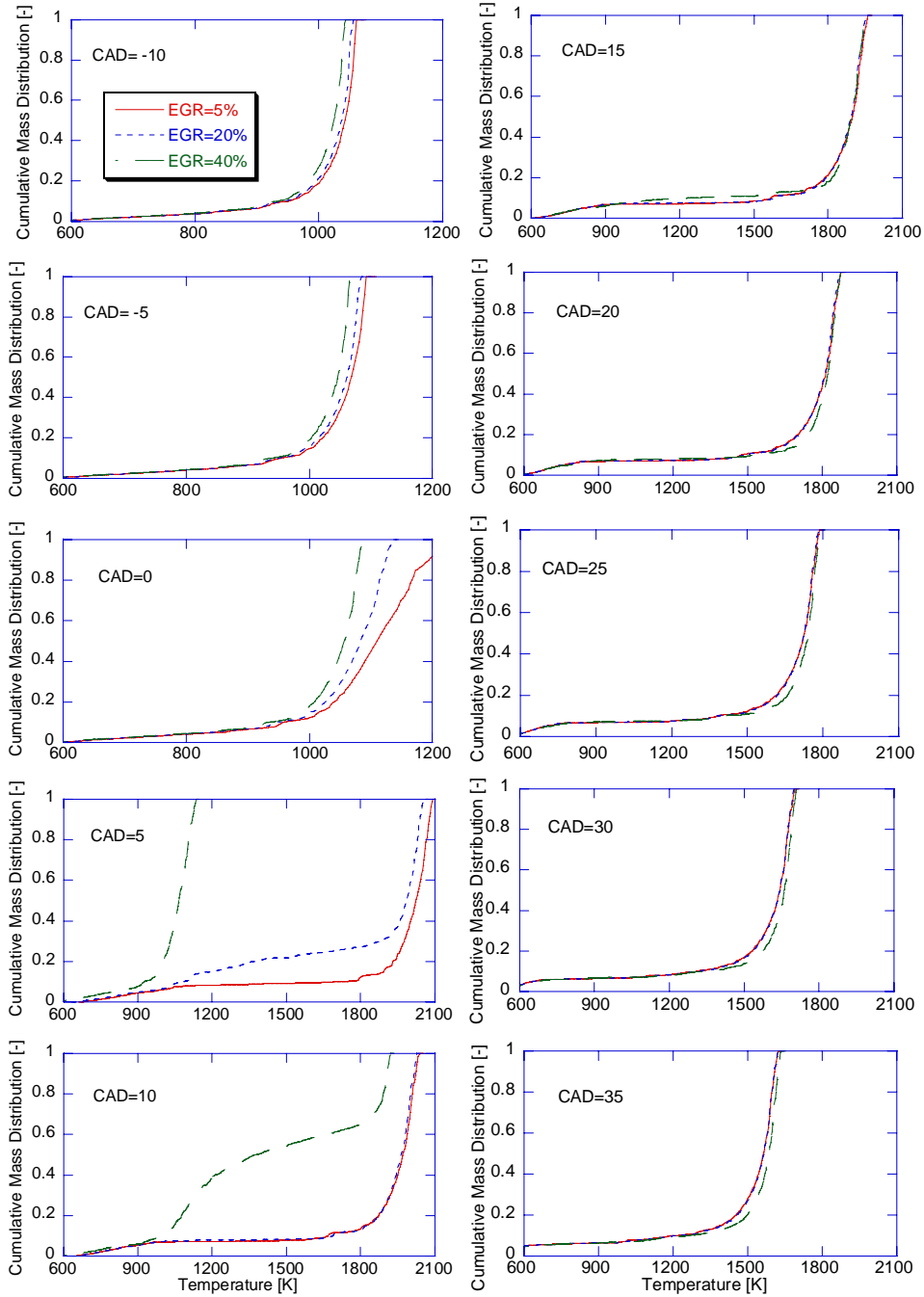


Figure 3.22 - Cumulative temperature mass distribution comparison under open end parametric study for three cases with three different EGR

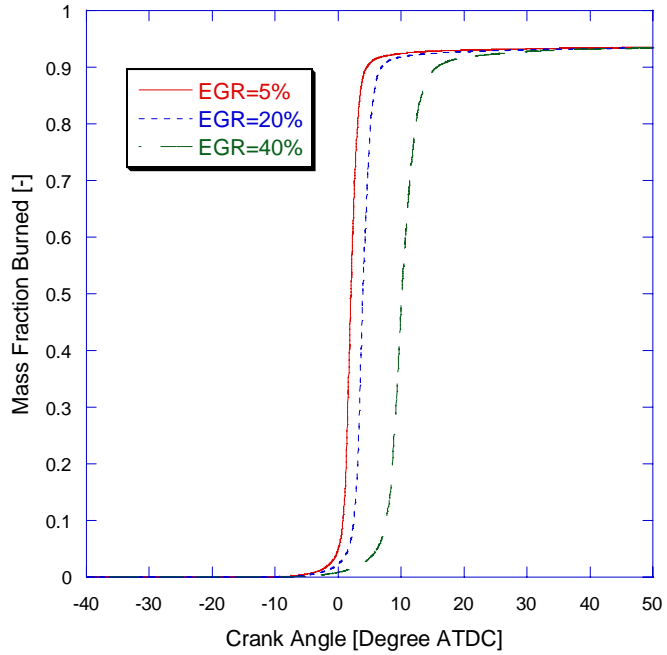


Figure 3.23 - Mass fraction burned comparison under open end parametric study for three cases with three different EGR

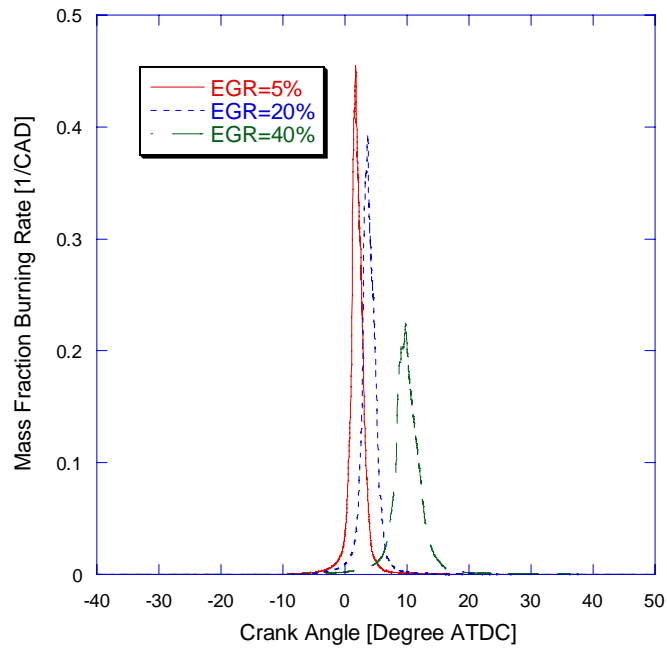


Figure 3.24 - Mass fraction burning rate comparison under open end parametric study for three cases with three different EGR

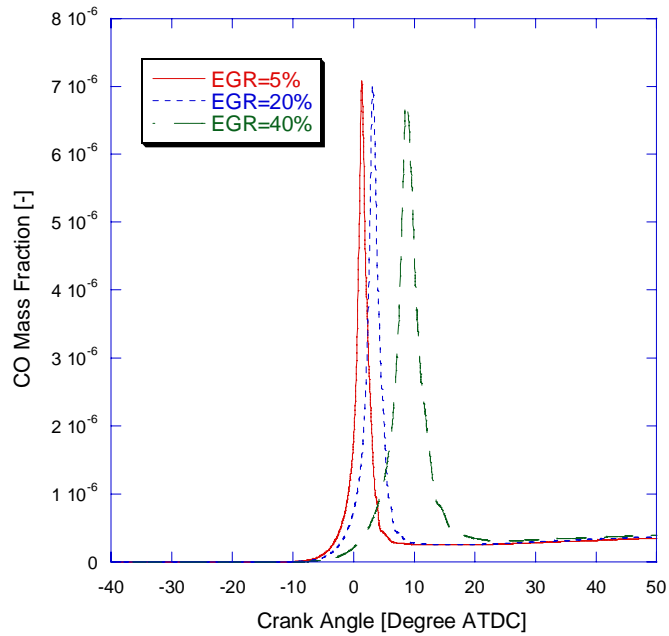


Figure 3.25 - CO composition comparison under open end parametric study for three cases with three different EGR

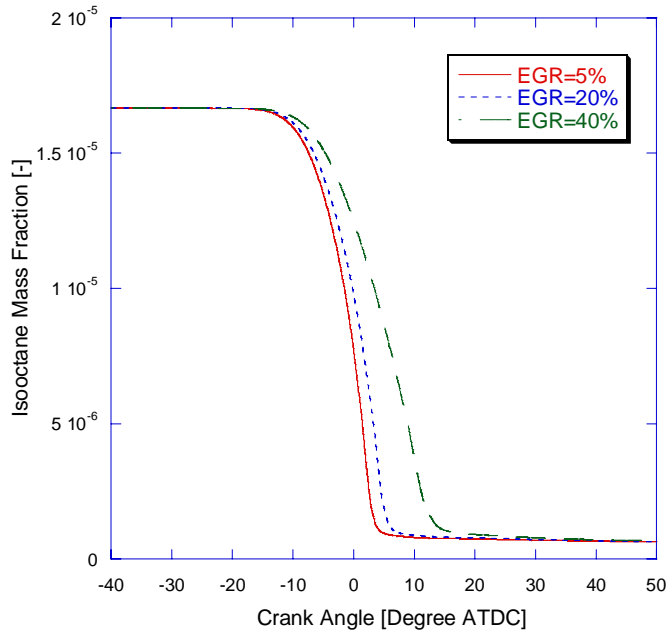


Figure 3.26 - Isooctane composition comparison under open end parametric study for three cases with three different EGR

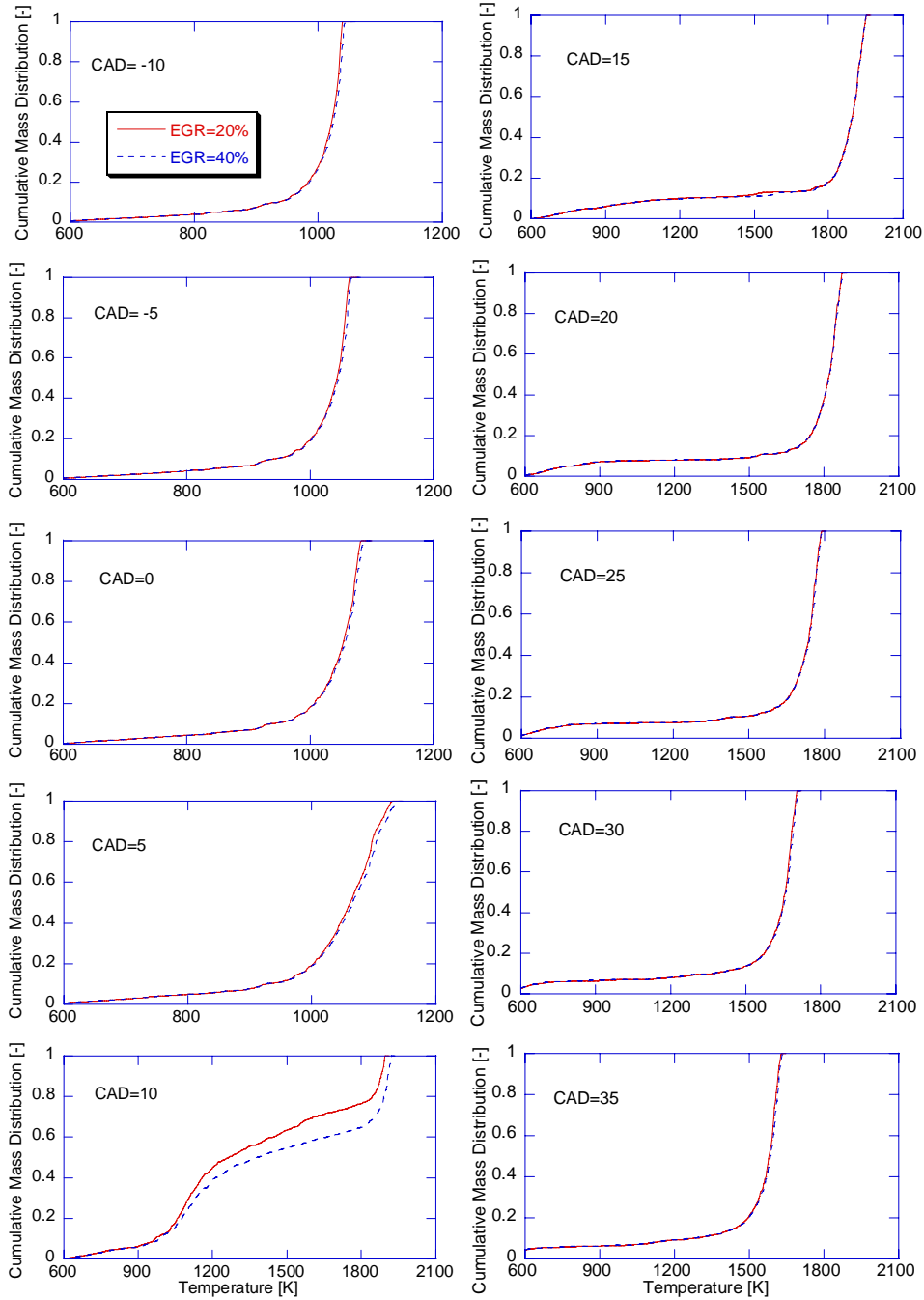


Figure 3.27 - Cumulative temperature mass distribution comparison under filtered parametric study for two cases with two different EGR

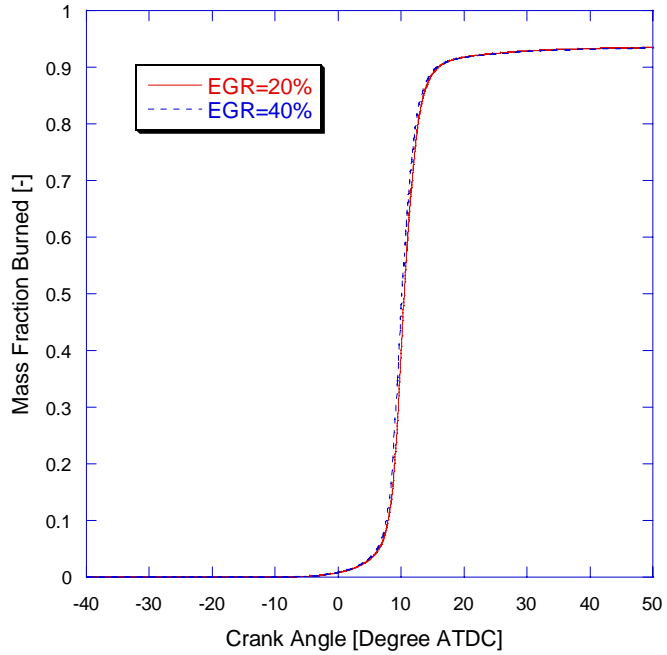


Figure 3.28 - Mass fraction burned comparison under filtered parametric study for two cases with two different EGR

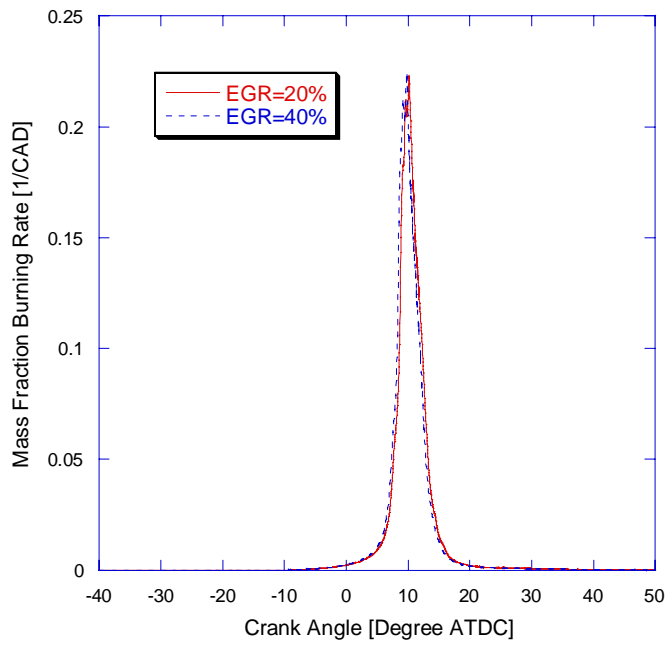


Figure 3.29 - Mass fraction burning rate comparison under filtered parametric study for two cases with two different EGR

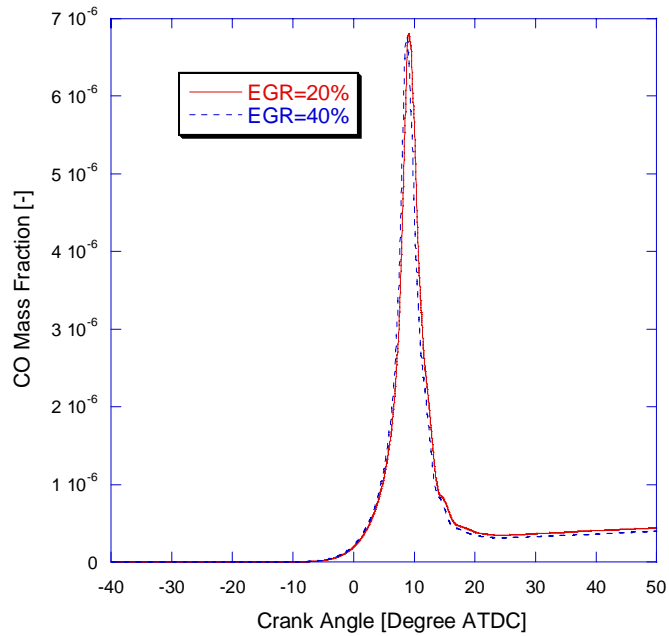


Figure 3.30 - CO composition comparison under filtered parametric study for two cases with two different EGR

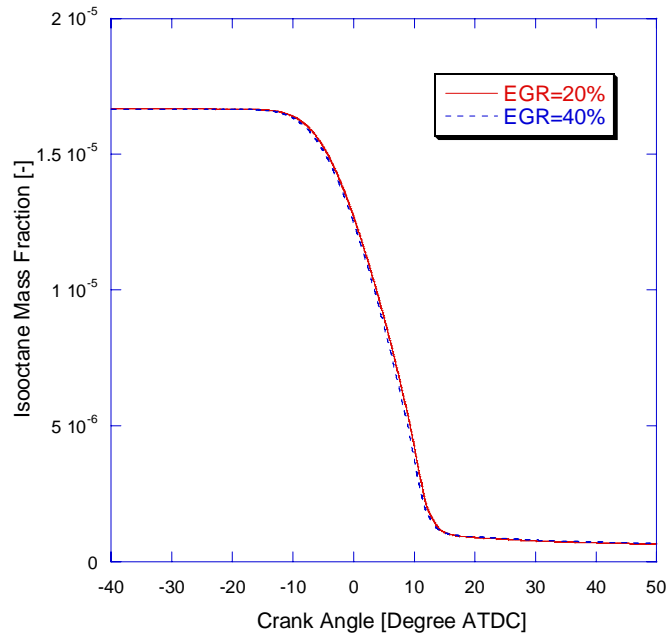


Figure 3.31 - Isooctane composition comparison under filtered parametric study for two cases with two different EGR

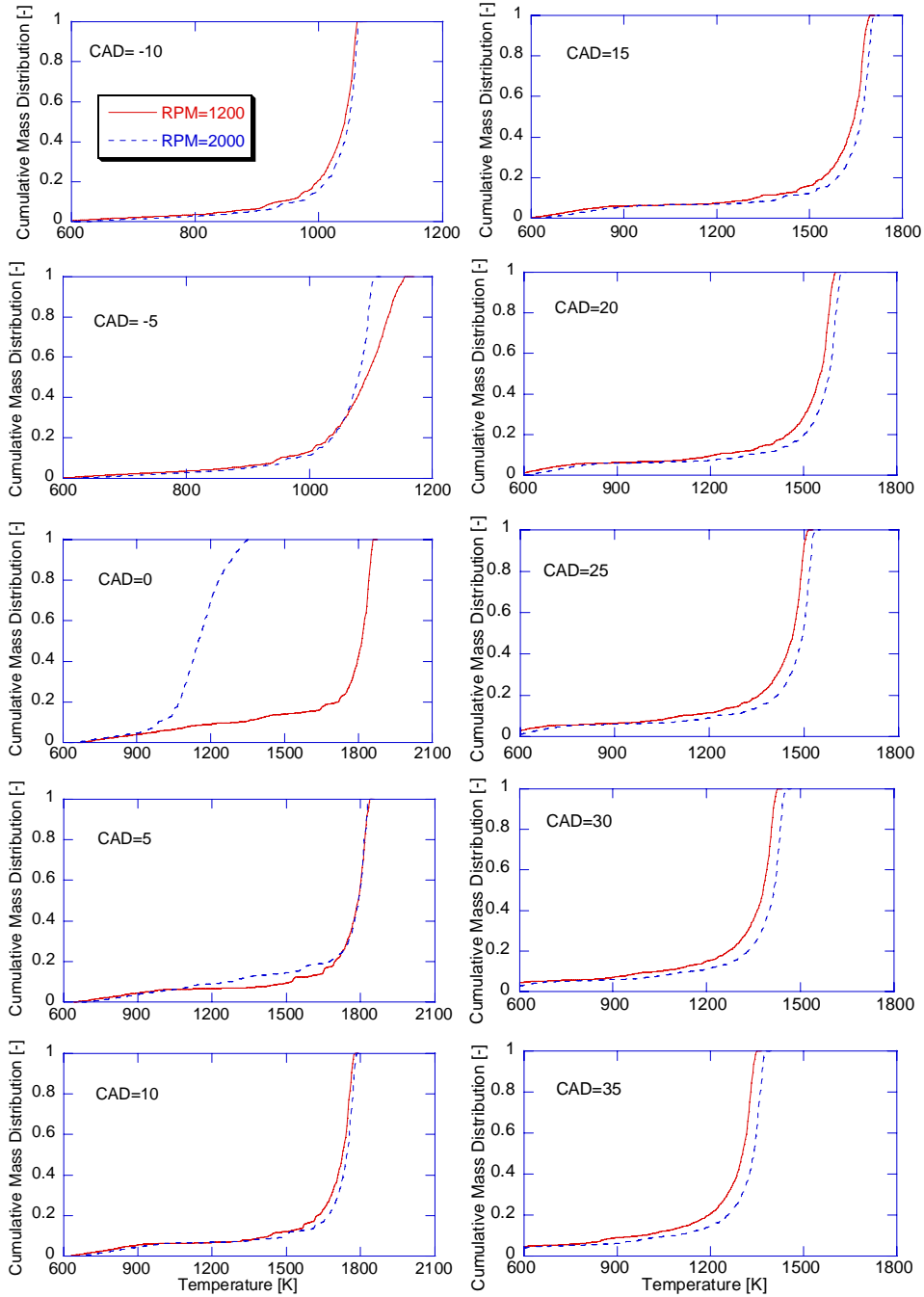


Figure 3.32 - Cumulative temperature mass distribution comparison under open end parametric study for two cases with two different rpm

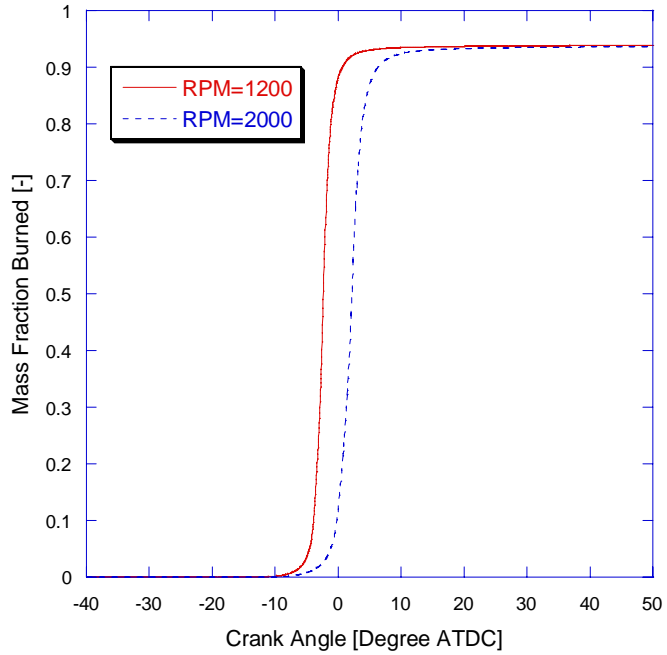


Figure 3.33 - Mass fraction burned comparison under open end parametric study for two cases with two different rpm

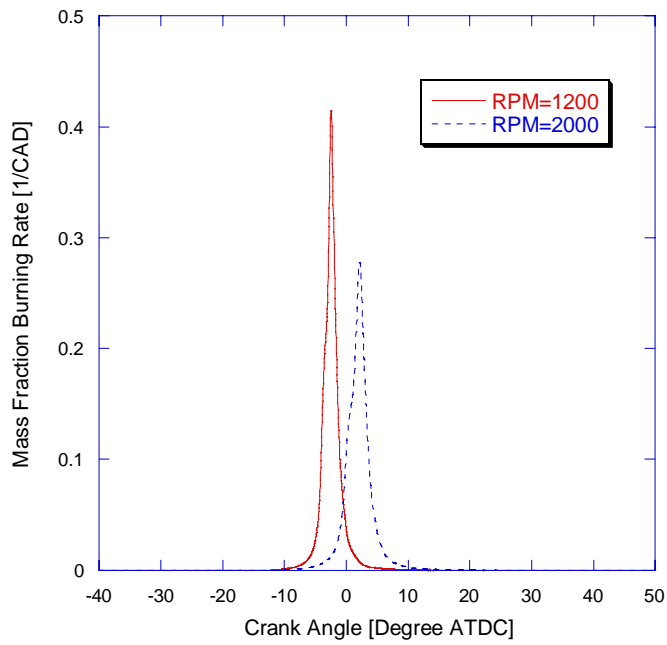


Figure 3.34 - Mass fraction burning rate comparison under open end parametric study for two cases with two different rpm

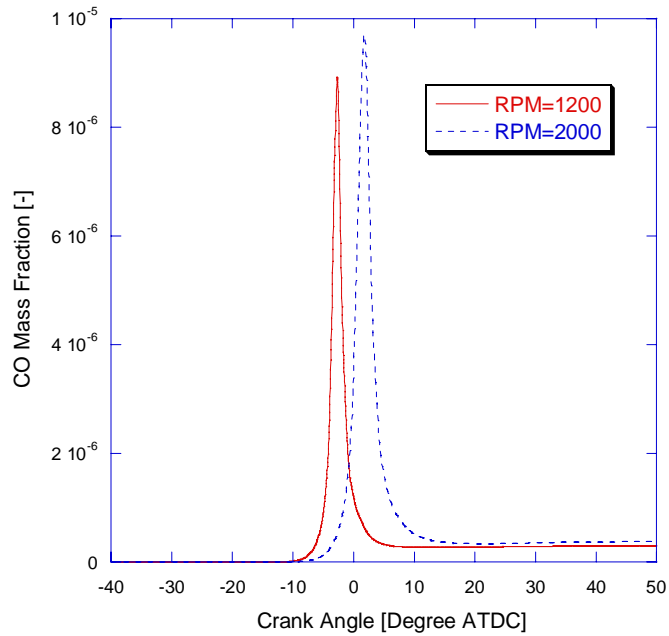


Figure 3.35 - CO composition comparison under open end parametric study for two cases with two different rpm

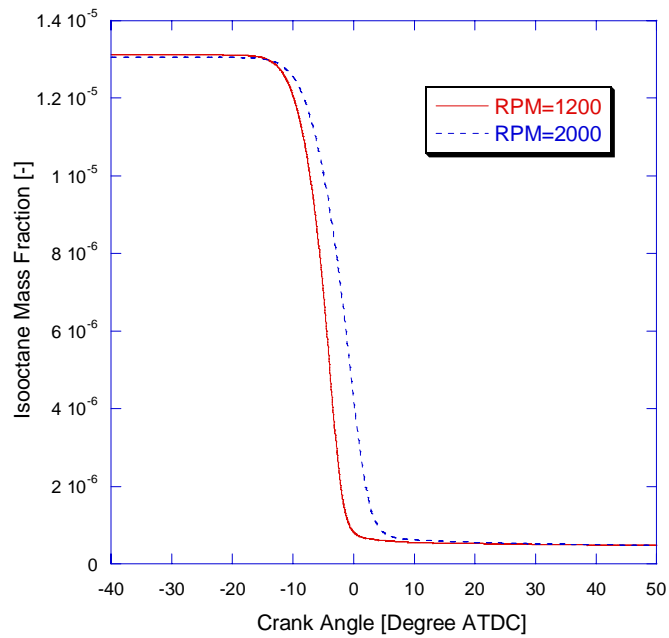


Figure 3.36 - Isooctane composition comparison under open end parametric study for two cases with two different rpm

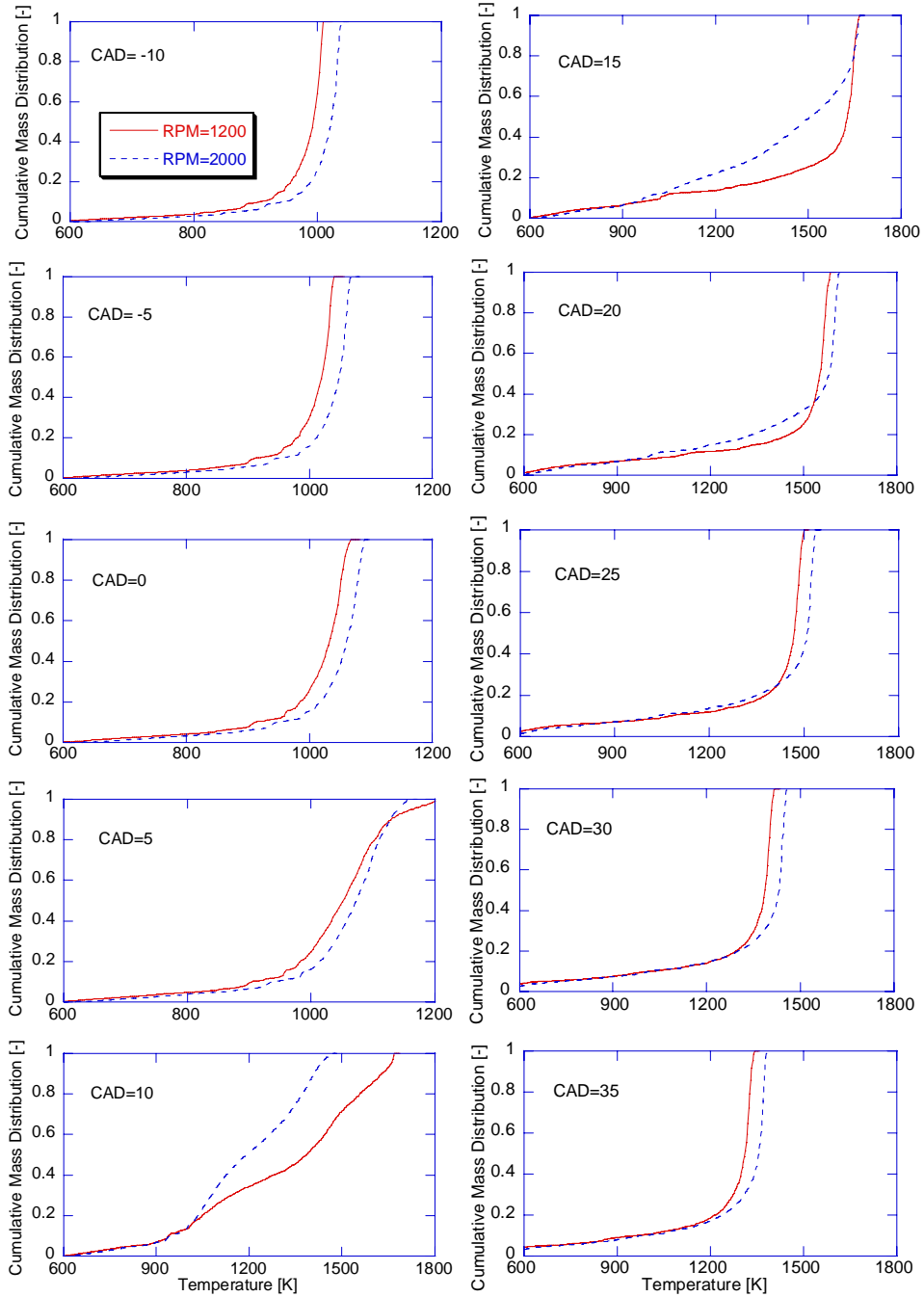


Figure 3.37 - Cumulative temperature mass distribution comparison under filtered parametric study for two cases with two different rpm

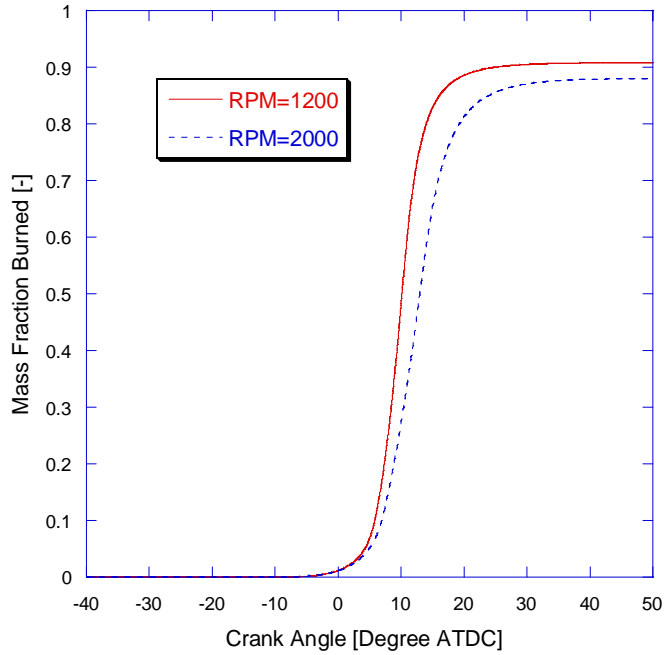


Figure 3.38 - Mass fraction burned comparison under filtered parametric study for two cases with two different rpm

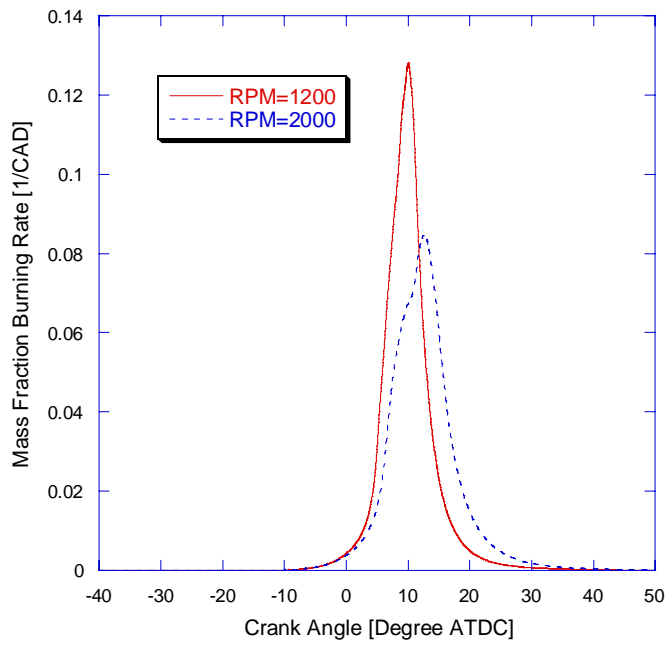


Figure 3.39 - Mass fraction burning rate comparison under filtered parametric study for two cases with two different rpm

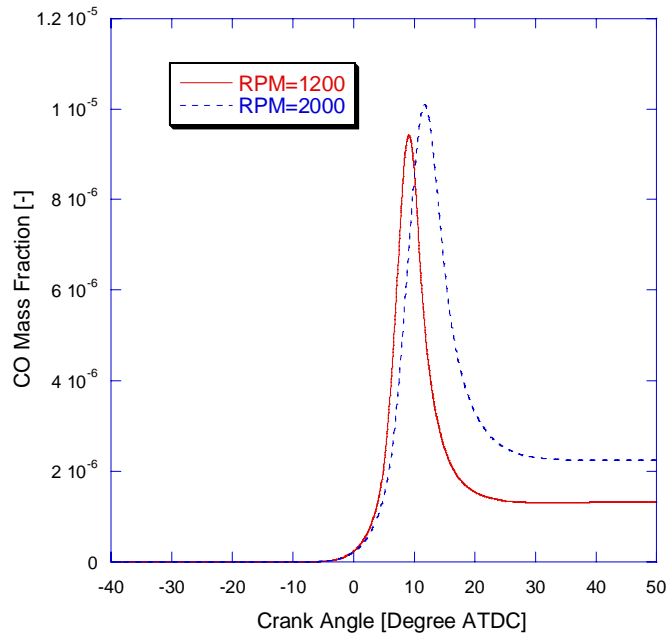


Figure 3.40 - CO composition comparison under filtered parametric study for two cases with two different rpm

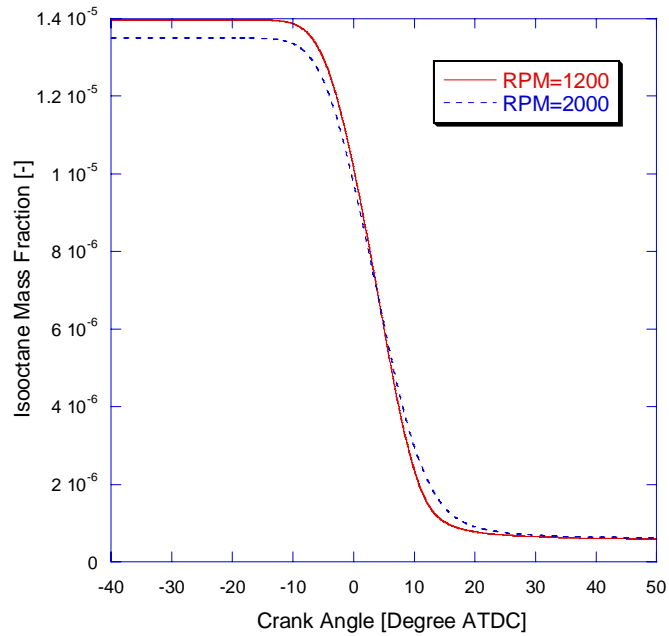


Figure 3.41 - Isooctane composition comparison under filtered parametric study for two cases with two different rpm

CHAPTER 4

ENGINE DESIGN PARAMETERS

In this chapter, five engine design parameters are investigated in detail. Swirl number, piston geometry, crevice volume, and compression ratio are examined with in-cylinder data like species concentration and temperature distribution.

The previous chapter investigated the engine operating parameters; while this chapter focuses on engine design parameters. As demonstrated in the previous chapter, the impact on combustion rate by operating parameters is mainly by the average combustion temperature. Design parameters are believed to be effective in other mechanisms like cylinder temperature distribution. How do these design parameters affect ignition timing? What's the fundamental reason behind the observation made in the section 2.6? For combustion efficiency, what's the contribution from ignition timing and the design parameter? These questions are answered in this chapter.

4.1 Swirl Number and Wall Temperature

Swirl number is defined as the ratio of bulk gas rotational speed to the engine speed. Swirl is a common way to introduce higher level of turbulence in the cylinder. Other than the mixing effect, the other major role swirl can play in HCCI engine is the cylinder wall heat transfer. Higher swirl level can enhance the heat transfer between the cylinder charge and cylinder wall as demonstrated in Chang's thesis [2005]. Because the

swirl number is studied under the context of cylinder wall heat transfer, cylinder wall temperature is also included in this study.

The significance of heat transfer for HCCI is evident from UM HCCI test engine results. Experiment on coolant temperature variation [Chang, 2004] shows that 10 degree Celsius difference of coolant temperature can result in 5 CAD difference in ignition timing.

In this thesis, the term “wall temperature” is used to represent all three temperatures of engine parts: piston, head, and cylinder wall. The cylinder wall temperature is “wall temperature” itself, the head temperature is 10 degrees Kelvin higher than “wall temperature”, and piston temperature is 20 degrees Kelvin higher than “wall temperature”.

4.1.1 Open End Parametric Study

Four cases are picked up with high-low combination of two wall temperatures and two swirl numbers. Case 1157 from sweep 16 has low wall temperature (400 K) and low swirl number(0.93); case 1167 from sweep 17 has high temperature (450 K) and low swirl number; case 1273 from sweep 29 has low temperate and high swirl number(3.93); and case 1282 from sweep 30 has high temperature and high swirl number. Table 4.1 shows the parameters of these four cases.

Table 4.1 - Parameters for open end parametric study of four cases with two swirl numbers and two wall temperatures

	CASE 1157	CASE 1167	CASE 1273	CASE 1282
Intake temperature (K)	470	470	470	470
Intake pressure (bar)	1.1	1.1	1.1	1.1
Equivalence ratio	0.2538	0.2538	0.2538	0.2538
Compression ratio	12.5	12.5	12.5	12.5
Engine speed (rpm)	1200	1200	1200	1200
Wall temperature (K)	400	450	400	450
Swirl ratio	0.93	0.93	3.93	3.93
Fueling rate (mg/cycle)	9	9	9	9
Ignition timing (ATDC)	-1.12	-2.62	-0.01	-1.88
Combustion efficiency (%)	90.53	92.65	79.88	89.72

Case 1167 has the earliest ignition timing at 2.62 BTDC; case 1273 has the latest ignition timing at about the TDC; and case 1157 and 1282 are in between with 0.76 degrees apart in ignition timing. Even though the difference in ignition timing is not large, it is apparent that swirl number and wall temperature do change the ignition timing.

Before ignition, as indicated in the temperature distribution plots at 10 and 5 degrees BTDC in Figure 4.1, case 1167 has the highest peak temperature, and the whole curve is in the lower-right corner, which indicates overall higher temperature mass distribution. On the other hand, case 1273 has the overall lowest temperature. There's a crossover between case 1157 and 1282. Case 1282 has a little bit higher peak temperature, which shows that the cylinder wall temperature does impact on the deepest core of the cylinder charge. However, at the same time; it has more mass in low temperature region due to the stronger swirl level before combustion.

Case 1167 with the earliest ignition has the highest combustion efficiency; and case 1273 has the most sluggish combustion (Figure 4.2 and Figure 4.3), which having combustion efficiency significantly lower than the rest three cases. While case 1167 and 1273 fall into the order of “earlier ignition leading to higher combustion efficiency”, case 1157 and 1282 aren't in that order. The relationship between combustion efficiency and ignition timing is reversed. It's no surprise since the crossover in temperature distribution curve has already been reviewed (Figure 4.1). Case 1282 has higher peak temperature before ignition because of the higher wall temperature, which helps igniting earlier; also, it has more mass in the boundary layer, which contributes to greater combustion inefficiency.

Combustion inefficiency comes from two major sources. One is from crevice volume and boundary layer (boundary layer inefficiency); the other is from the partial oxidation of the bulk gas (partial oxidation inefficiency). When ignition timing is early enough, majority of the combustion inefficiency is from the first source. When ignition timing is later than certain threshold, partial oxidation occurs. The likelihood of each mechanism can be measured by the freezing composition of CO and isooctane concentration. CO concentration is a good indicator for partial oxidation mechanism (Figure 4.4); while isooctane concentration is good indicator for boundary layer mechanism (Figure 4.5).

Figure 4.4 and Figure 4.5 show that the combustion inefficiencies of case 1157 and 1282 are mainly from partial oxidation mechanism, while case 1273 has both mechanisms in effect.

Both wall temperature and swirl number have effects on the peak temperature of the cylinder charge. Higher wall temperature and low swirl number case has higher peak cylinder temperature and earlier ignition.

Higher swirl case has more cylinder mass in low temperature region, which is in the boundary layer. This contributes to combustion inefficiency.

Above study does have variable ignition timing, so it doesn't provide the right information to explain the observation in the Figure 2.20. Following section has four cases with similar ignition timing, and it provides more insight on the combustion efficiency and heat release rate.

4.1.2 Sweep Study Revisit

Either wall temperature or swirl can cause difference in combustion efficiency and burning duration (Figure 2.20). When ignition timing is very early, the peak combustion efficiencies for all four cases are very close. When ignition timing is later than 6 degrees BTDC, combustion efficiency is consistent with burning duration in the order of "faster combustion leading to higher combustion efficiency". The order of combustion efficiency from higher to lower is in the order of "high wall, low swirl", "low wall, low swirl", "high wall, high swirl", and "low wall, high swirl".

4.1.3 Filtered Parametric Study

Table 4.2 lists the parameters for the four cases with very close ignition timing. Ideally, comparison should be made with identical ignition timing, which is the crank angle location where 1% fuel is burned. However, ignition timing is not directly controlled, so trial and error method is used to get similar values in ignition timing, but not identical.

Case 1156 from sweep 16 has low wall temperature (400 K) and low swirl (0.93); case 1164 from sweep 17 has high temperature (450 K) and low swirl; case 1273 from sweep 29 has low temperature and high swirl (3.93); and case 1280 from sweep 30 has high temperature and high swirl.

Table 4.2 - Parameters for filtered parametric study of four cases with two swirl numbers and two wall temperatures

	CASE 1156	CASE 1164	CASE 1273	CASE 1280
Intake temperature (K)	467.5	462.5	470	465
Intake pressure (bar)	1.1	1.1	1.1	1.1
Equivalence ratio	0.2538	0.2538	0.2538	0.2538
Compression ratio	12.5	12.5	12.5	12.5
Engine speed (rpm)	1200	1200	1200	1200
Wall temperature (K)	400	450	400	450
Swirl ratio	0.93	0.93	3.93	3.93
Ignition timing	-0.286	-0.326	-0.01	-0.268
Combustion efficiency	88.2	89.68	79.88	83.81

With intake temperature compensation, the peak cylinder temperatures are very comparable before ignition as shown in the temperature distribution plots at 10 and 5 BTDC in Figure 4.6. When ignition timing is early enough, like 5 degrees BTDC, combustion efficiencies for all four cases are very similar (Figure 2.20). This shows that wall temperature and swirl number only have limited effect on boundary layer inefficiency, but they do have effects on partial oxidation inefficiency and heat release rate when ignition timing isn't very early. Figure 4.7 shows that combustion efficiency of these four cases is separated despite of the similar heat release rate pattern in Figure 4.8. Figure 4.9 shows significant separation in CO composition; while Figure 4.10 doesn't show much difference in isooctane composition. The intake temperatures variation can make the peak cylinder temperatures close for all four cases, but the temperature distribution has its characteristics: high wall temperature and low swirl case has less mass in low temperature region.

Temperature distribution plot at 10 degrees ATDC (Figure 4.6) shows that at the peak of heat release, the cylinder temperature distribution is fairly linear. This implies that substantial mass of each temperature range are present in the cylinder. In HCCI engine, heat release is happening anywhere and everywhere in the cylinder after the first spot of auto ignition, and the temperature distribution before the ignition leads to distribution of oxidation level during combustion. More uniform mixture at high temperature region and less mass in low temperature region has much stronger combustion.

Wall temperature and swirl are important to the temperature distribution in the cylinder. The case with high wall temperature and low swirl results in less mass in the low temperature region. This leads to higher combustion efficiency and faster heat release. When ignition timing is early enough, high wall temperature and low swirl case still has faster heat release rate, but combustion efficiency is close because majority of the fuel is burned BTDC.

4.2 Piston Geometry

In HCCI engine, piston geometry doesn't have the same kind of impact on spark ignited engine with respect to flame-wall interaction. It can still potentially affect the heat transfer and the temperature distribution.

4.2.1 Sweep Study Revisit

The burning duration curves are equally separated over the range of ignition timing under this study (Figure 2.21). However, combustion efficiency is not separated until ignition gets later than 1 degree BTDC. The deteriorating slope is also close in value.

4.2.2 Open end Parametric Study

The effect of piston geometry is investigated by applying two piston shapes under the same operation condition. Case 1158 from sweep 16 has pancake shape chamber; and case 1140 from sweep 14 has bowl shape chamber. Compression ratio is kept identical at 12.5. Table 4.3 lists the parameters of these two cases.

Table 4.3 - Parameters for open end parametric study of two cases with two piston geometries

	CASE 1158	CASE 1140
Intake temperature (K)	475	475
Intake pressure (bar)	1.1	1.1
Equivalence ratio	0.2538	0.2538
Compression ratio	12.5	12.5
Engine speed (rpm)	1200	1200
Fueling rate (mg/cycle)	9	9
Piston top land	Pancake	Bowl
Ignition timing (ATDC)	-2.61	-2.78
Combustion efficiency	91.94	91.90

Apparently, there's little separation between these two cases in ignition timing. Figure 4.11 shows that the temperature mass distributions are very similar for these two cases except there's a point of sudden slope change for case 1140. This pattern is noticeable both before and after combustion. This unusual observation calls for more details. Figure 4.12 gives non-cumulative temperature mass distribution. There are two peaks of cylinder temperature for case 1140, which indicates that the cylinder temperature gradient has two local maximum points.

In Figure 4.13, both cases have very close curves for cumulative heat release. However, there's substantial separation in peak heat release rate (Figure 4.14). Pancake chamber provides much higher peak heat release rate. Some unusual shape exists around the peak of heat release of bowl shape case. The same pattern also exists in CO composition in Figure 4.15. This observation is consistent with the double-peak in temperature mass distribution in Figure 4.12. For more complex chamber geometry, there's possibility of multiple temperature local maxima.

For piston geometry effect, the expected difference is the low end temperature distribution. However, simulation results show that the major change is the high end temperature distribution instead of the low end temperature distribution. Simpler geometry has smoother temperature distribution, thus quicker heat release. Bowl shape geometry creates multiple local temperature maxima, which creates double humps in heat release curve.

4.3 Crevice Volume

Crevice volume is an important source of combustion inefficiency. In HCCI engine, the mechanism of crevice volume on combustion inefficiency is based on heat transfer. Mixture trapped in crevice exposes to more metal surfaces with lower temperatures.

4.3.1 Open End Parametric Study

Table 4.4 lists the parameters of three crevice volume cases. The compression ratio is kept constant at 12.5. Case 1259 from sweep 27 has crevice volume at 1% of the total cylinder volume when piston is at TDC; case 1157 from sweep 16 has 4%; and case 1266 from sweep 28 has 8%.

Table 4.4 - Parameters for open end parametric study of three cases with three crevice volumes

	CASE 1259	CASE 1157	CASE 1266
Intake temperature (K)	470	470	470
Intake pressure (bar)	1.1	1.1	1.1
Equivalence ratio	0.245	0.245	0.245
Compression ratio	12.5	12.5	12.5
Engine speed (rpm)	1200	1200	1200
Crevice volume (%)	1	4	8
Fueling rate (mg/cycle)	9	9	9
Ignition timing (ATDC)	-1.76	-1.12	0.37
Combustion efficiency	95.81	90.53	78.74

Difference in ignition timing is moderate for these three cases. Higher crevice volume case has later ignition timing. The cylinder temperature distribution plots in Figure 4.17 show the reason. At 10 and 5 degrees BTDC, there's discernable difference in the temperature distribution of the cylinder charge. The difference is not limited to low temperature end, which is expected as higher crevice volume case entrains more low temperature mass. For smaller crevice volume case, the whole temperature distribution curve is at lower-right side of the plot, which means that it has higher peak temperature, higher average temperature, and less mass in low temperature region.

The combustion efficiency of these three cases in Figure 4.18 is widely apart. Figure 4.19 shows that the phasing of combustion is clearly differentiated among these cases. Species compositions of CO (Figure 4.20) and isooctane (Figure 4.21) show that case 1266 has higher freezing compositions of both CO and isooctane. So both

combustion inefficiency mechanisms are in play for this case. For case 1259 and 1157, there are moderate separations for both CO and isooctane.

Because of the ignition timing difference, it is premature to say that crevice volume is responsible for the combustion efficiency difference at early ignition. This argument is examined in the following section with close ignition timing comparison.

4.3.2 Sweep Study Revisit

Burning duration curves are on top of each other for the whole span of ignition timing, while combustion efficiency curves are widely separated (Figure 2.22). This implies that combustion inefficiency isn't caused by partial oxidation mechanism. The ignition timing for misfire is similar for all three cases.

4.3.3 Filtered Parametric Study

Case 1261, 1160, and 1270 are chosen with similar ignition timing and with crevice volume at 1%, 4%, and 8% respectively. Table 4.5 lists the parameters for this comparison.

Table 4.5 - Parameters for filtered parametric study of three cases with three crevice volumes

	CASE 1261	CASE 1160	CASE 1270
Intake temperature (K)	477.5	480	485
Intake pressure (bar)	1.1	1.1	1.1
Equivalence ratio	0.245	0.245	0.245
Compression ratio	12.5	12.5	12.5
Engine speed (rpm)	1200	1200	1200
Crevice volume (%)	1	4	8
Ignition timing	-3.818	-3.937	-4.144
Combustion efficiency	97.33	92.42	86.37

The ignition timings are early enough that all three cases have good combustion as indicated by the low freezing CO concentration from Figure 4.25. Mass fraction burned plot from Figure 4.23 shows that despite of similar heat release shape (Figure 4.24), combustion efficiency is reverse proportional to crevice volume.

With early ignition timing, partial oxidation mechanism is eliminated. The difference in combustion efficiency is primarily caused by boundary layer inefficiency. Figure 4.26 clearly shows that the crevice volume dominates the best possible combustion efficiency.

Figure 4.24 shows that the heat release rate is very well matched in phasing for all three cases. The difference in temperature distribution in this comparison doesn't result in obvious separation in heat release rate. In reality, the temperature mass distribution before combustion has two parts: one vertical line containing more than 80% of the cylinder mass, the other horizontal line contains less than 20% cylinder mass. The heat release rate is mainly determined by the vertical one, but combustion efficiency is mainly determined by the horizontal one. The temperature distribution in Figure 4.22 isn't very

different from the comparison from “open end parametric study”. Case 1270 with the largest crevice volume has more mass in low temperature region.

4.4 Compression Ratio

Two compression ratios are studied, and they are 12.5 and 16. Under these two compression ratios, the ranges of meaningful intake temperature are so widely apart that they don't overlap. So the constant intake temperature study for compression ratio is neglected.

4.4.1 Sweep Study Revisit

The burning duration curves have converging shape when ignition timing gets later (Figure 2.23). When ignition timing is at TDC, the difference in burning duration and combustion efficiency are minimal. Combustion efficiency curves match well in magnitude, and the ignition timings for misfire are also close.

4.4.2 Filtered Parametric Study

Case 1027 from sweep 3 has compression ratio set at 12.5; and case 1086 from sweep 9 has compression ratio set at 16. Table 4.6 lists their other parameters.

Table 4.6 - Parameters for filtered parametric study of two cases with two compression ratios

	CASE 1027	CASE 1086
Intake temperature (K)	495	450
Intake pressure (bar)	1.1	1.1
Equivalence ratio	0.251	0.251
Engine speed (rpm)	2000	2000
Compression ratio	12.5	16
Ignition Timing	-4.62	-4.42
Combustion efficiency	92.74	93.65

Forth five degrees of temperature difference in intake temperature makes these two cases having about the same ignition timing. The low compression ratio case 1027 has higher cylinder temperature for most of the compression stroke. When the piston is moving toward TDC, the difference is diminishing as shown in Figure 4.27.

The temperature distribution plots from 5 degrees ATDC to 15 degrees ATDC show some interesting transition. At 5 degrees ATDC, both cases have similar distribution in high temperature region, but the high compression ratio case has less mass in low temperature region. This is caused by fast heat release rate of high compression ratio, which is evident from Figure 4.31 where iso-octane is depleting at a faster pace. At 15 degrees ATDC, both cases have about the same mass in the low temperature region, but low compression ratio case has higher peak temperature. The reason is that the high compression ratio case have larger expansion ratio to convert the thermal energy into piston work.

As shown in Table 4.6, both cases have very similar combustion efficiency. CO (Figure 4.30) and iso-octane (Figure 4.31) compositions also demonstrate that both cases

have quite complete combustion. Figure 2.23 shows that combustion efficiency of these two cases is close over the whole range of ignition timing under study; however, it is still discernable that the high compression ratio case has slightly higher combustion efficiency. This is caused by slightly faster heat release rate of high compression ratio.

In this study, higher compression ratio case has slightly higher heat release rate. It is difficult to explain this observation with the temperature distribution information. However, Figure 2.23 helps find the reason. The difference in heat release rate disappears as ignition timing is going toward TDC. The converging trend of the difference in heat release rate reflects the essence of compression ratio. Figure 4.32 shows the instantaneous compression ratio for 12.5 and 16. Under normal definition, compression ratio is the ratio of the maximum and minimum cylinder volume, which always corresponding to bottom and top location for the piston. Instantaneous compression ratio is defined as the volume ratio of the minimum cylinder volume and current cylinder volume. For cases with different compression ratio, their instantaneous compression ratios are also different with piston at the same crank angle position. Higher compression ratio case has higher instantaneous compression ratio at any point except the TDC, where instantaneous compression ratio is always unity.

The pattern of the instantaneous compression ratio matches well with the burning rate. When ignition timing is early, the difference in instantaneous compression ratio for these two cases are larger, thus the compression heating is larger, which accelerates the heat release process. The difference in burning rate disappears when ignition timing is close to TDC.

Compression ratio's effect on combustion isn't on temperature distribution. In reality, it hardly changes the temperature distribution pattern. The main impact by compression ratio is its instantaneous compression ratio and its compression heating effect on cylinder mixture.

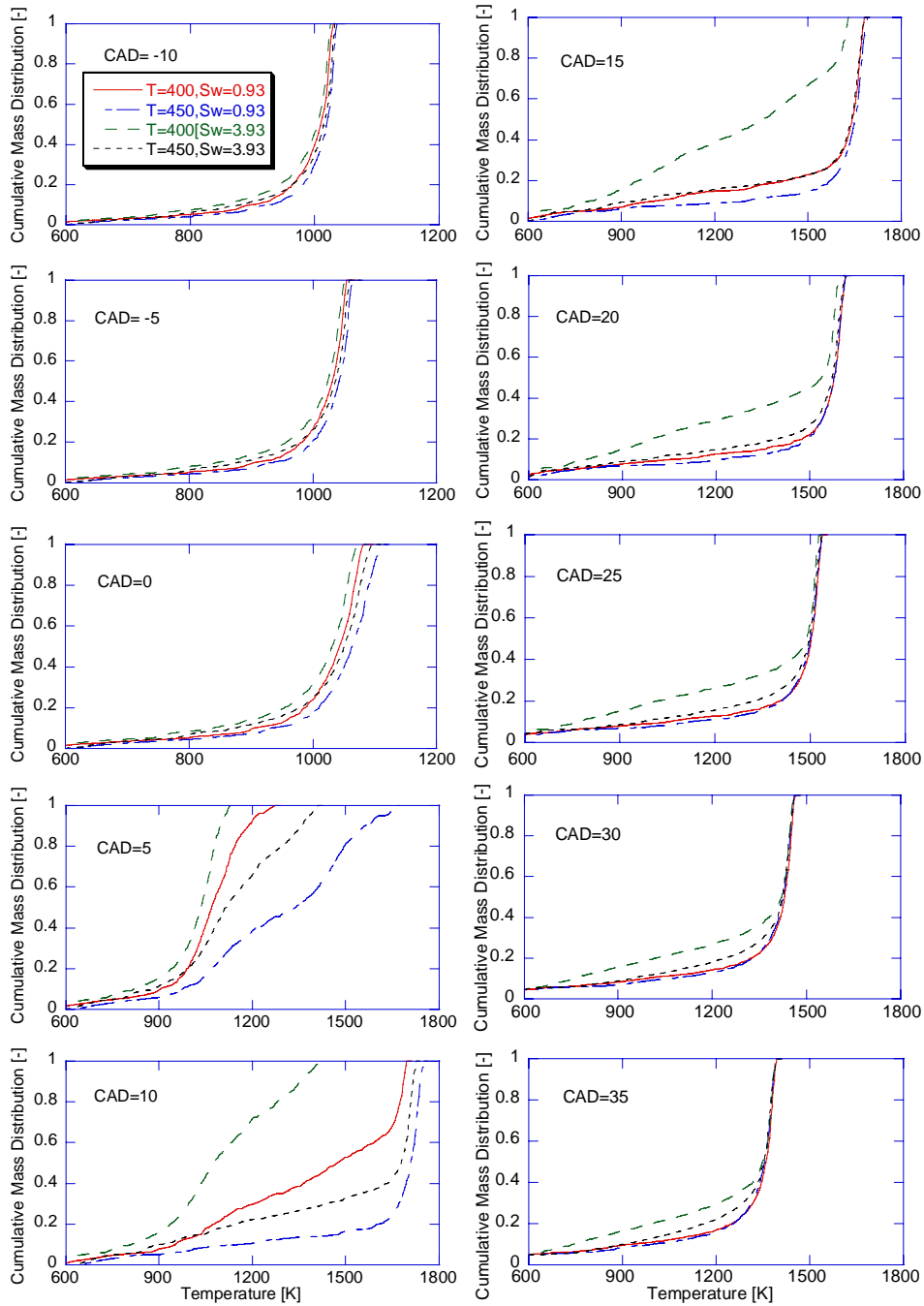


Figure 4.1 – Cumulative temperature distribution comparison under open end parametric study for four cases with two different wall temperatures and two different swirl numbers

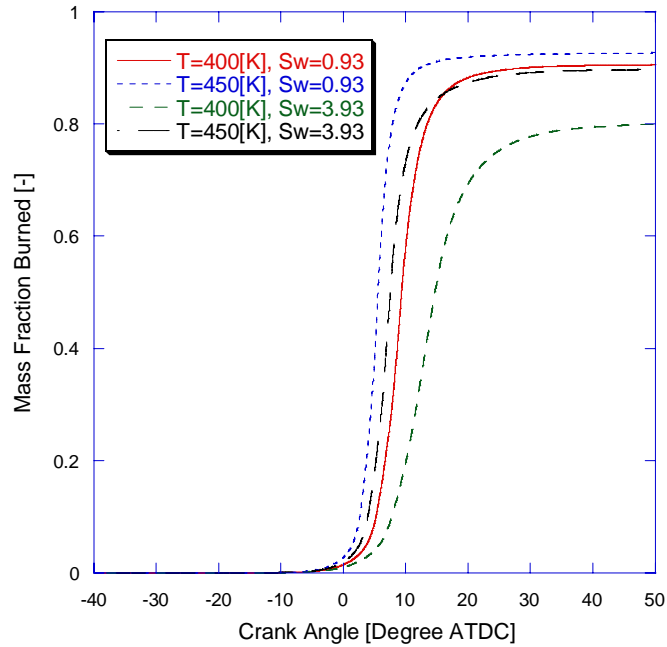


Figure 4.2 - Mass fraction burned comparison under open end parametric study for four cases with two different wall temperatures and two different swirl numbers

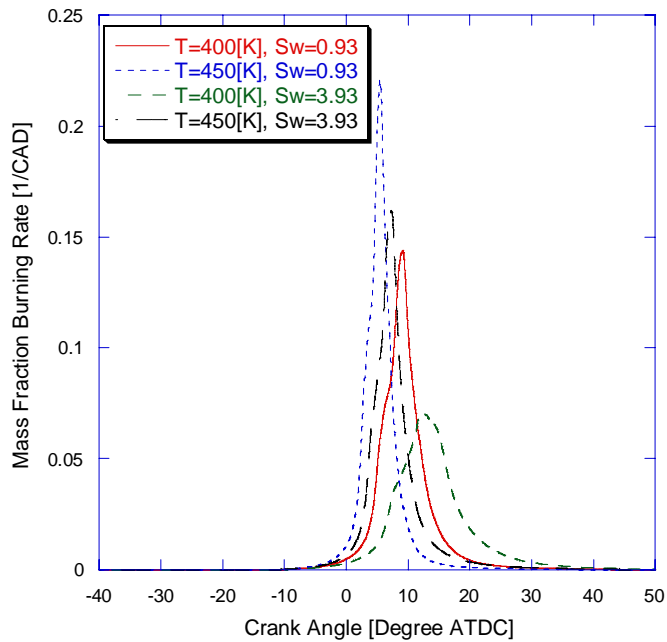


Figure 4.3 - Mass fraction burning rate comparison under open end parametric study for four cases with two different wall temperatures and two different swirl numbers

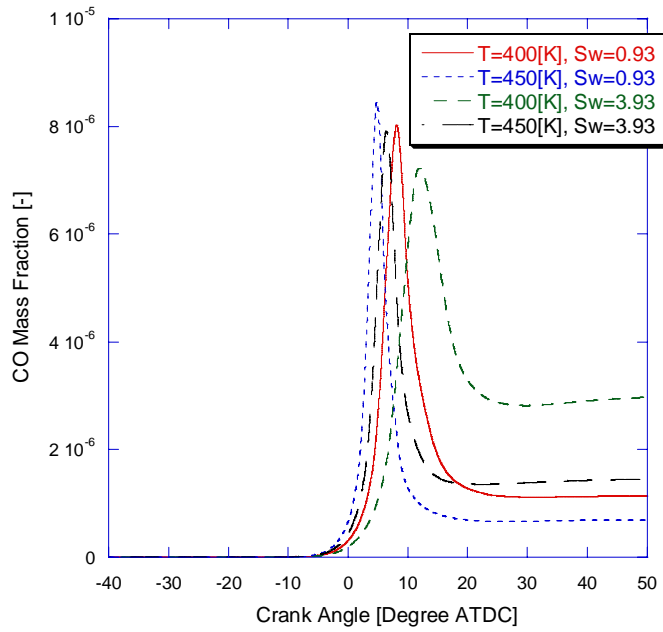


Figure 4.4 - CO composition comparison under open end parametric study for four cases with two different wall temperatures and two different swirl numbers

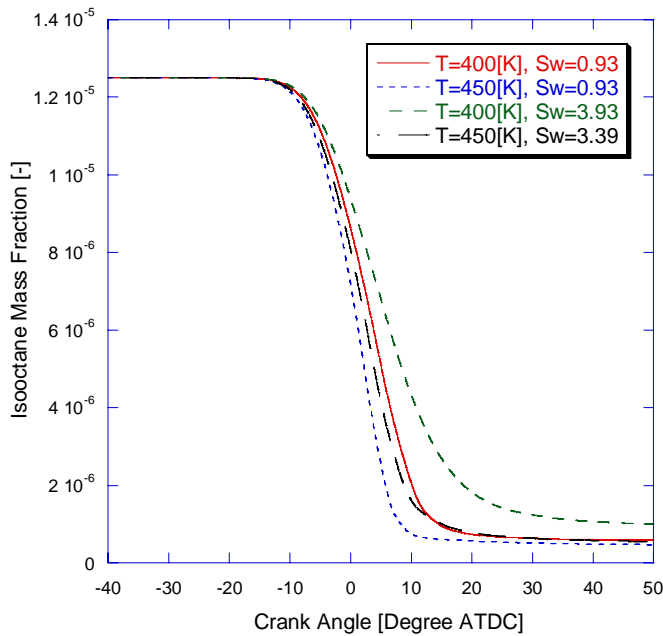


Figure 4.5 - Isooctane composition comparison under open end parametric study for four cases with two different wall temperatures and two different swirl numbers

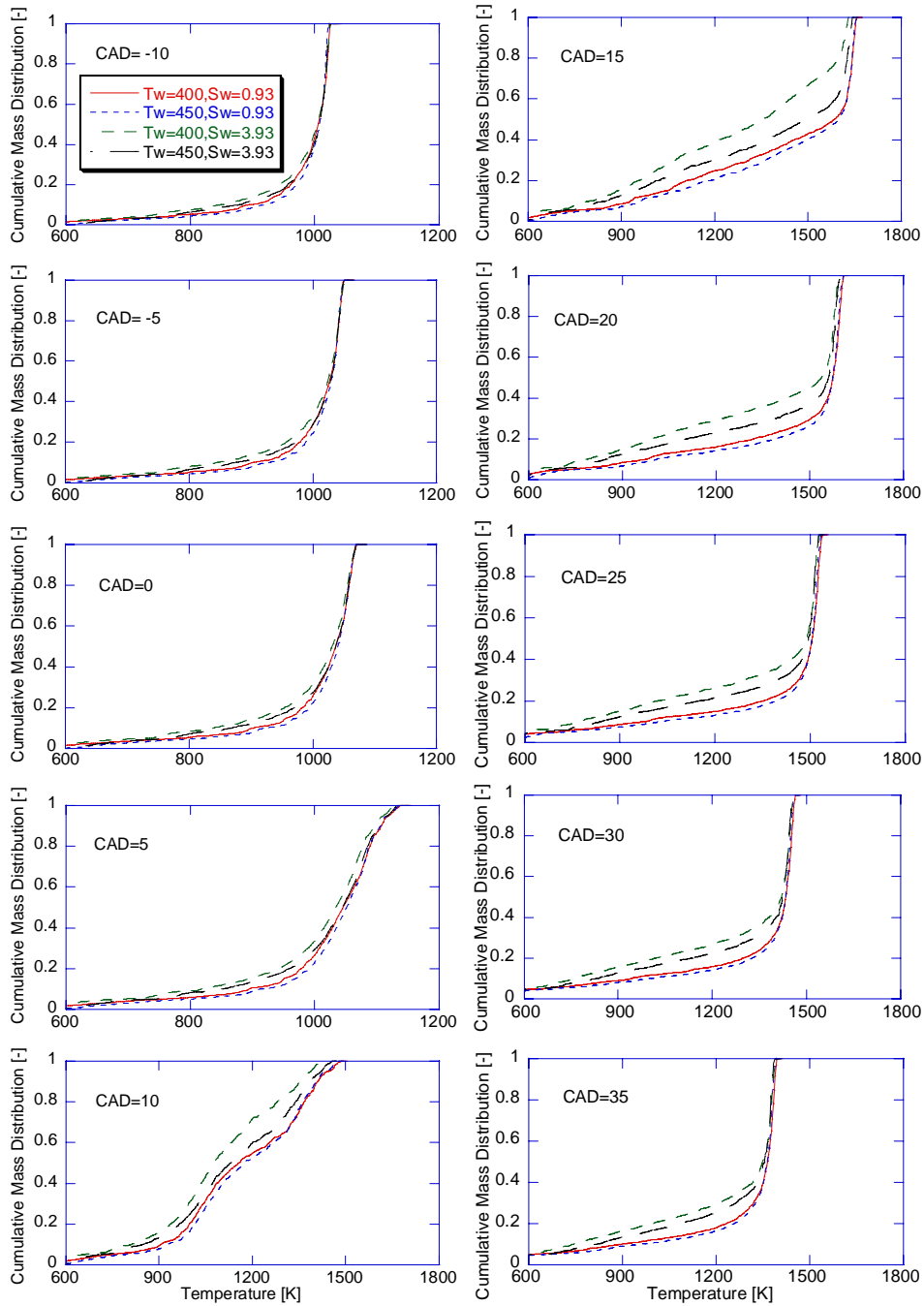


Figure 4.6 – Cumulative temperature mass distribution comparison under filtered parametric study for four cases with two different wall temperature and two different swirl numbers

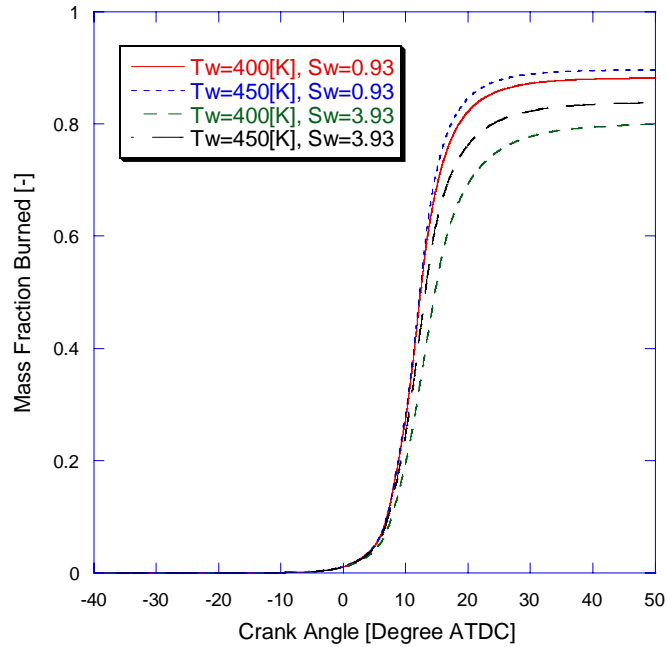


Figure 4.7 - Mass fraction burned comparison under filtered parametric study for four cases with two different wall temperature and two different swirl numbers

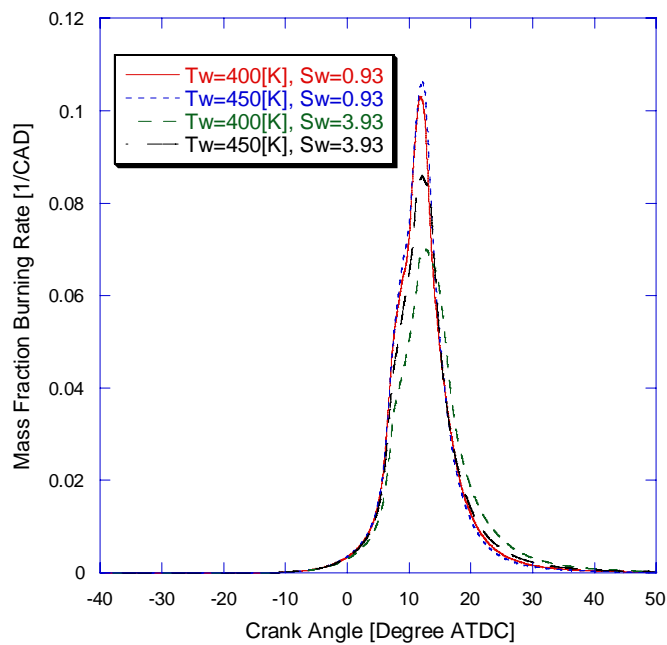


Figure 4.8 - Mass fraction burning rate comparison under filtered parametric study for four cases with two different wall temperature and two different swirl numbers

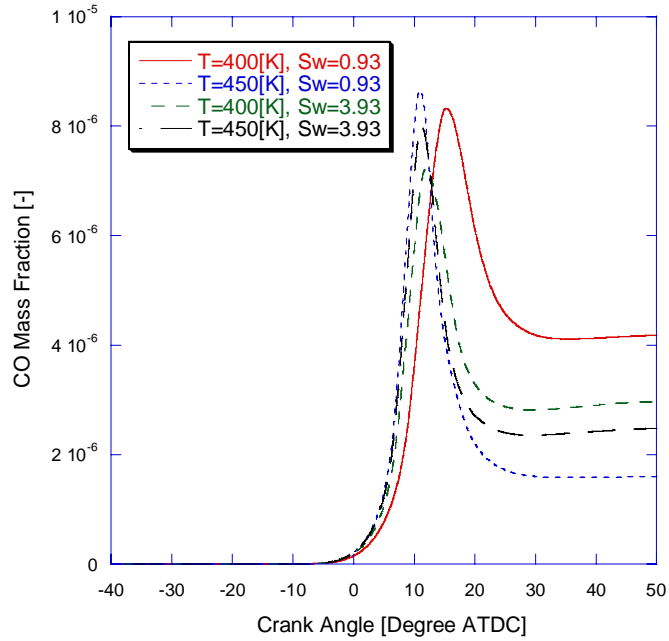


Figure 4.9 - CO composition comparison filtered parametric study for four cases with two different wall temperature and two different swirl numbers

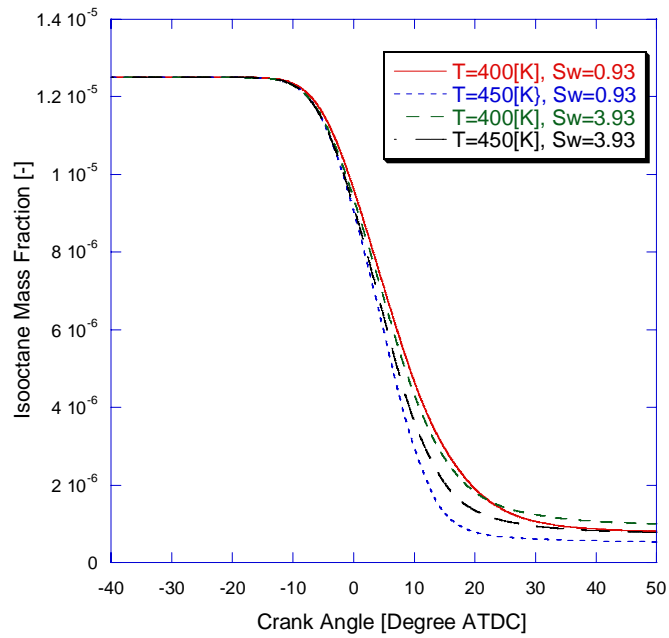


Figure 4.10 - Isooctane composition comparison filtered parametric study for four cases with two different wall temperature and two different swirl numbers

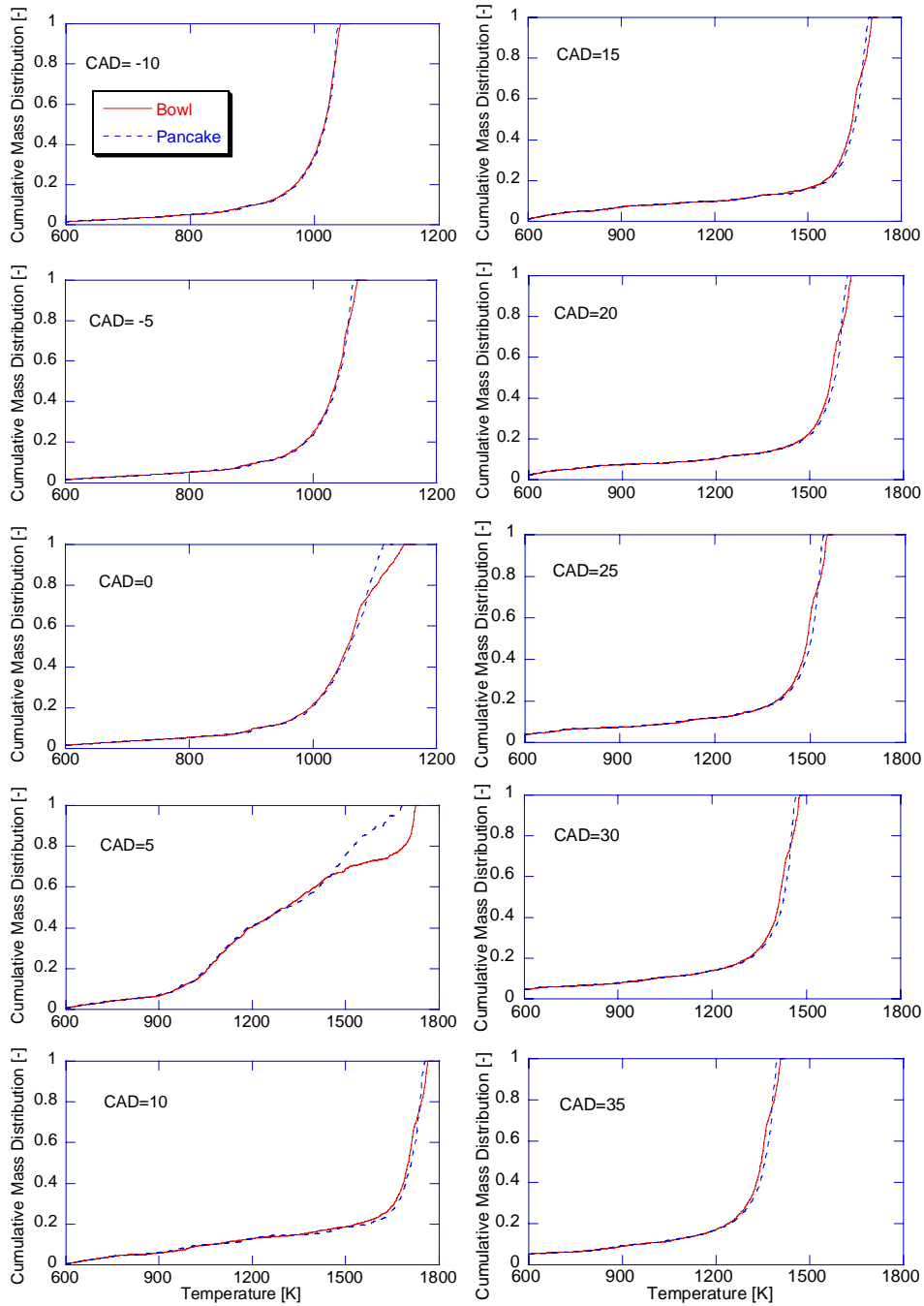


Figure 4.11 – Cumulative temperature mass distribution comparison under open end parametric study for two cases with two different piston geometries

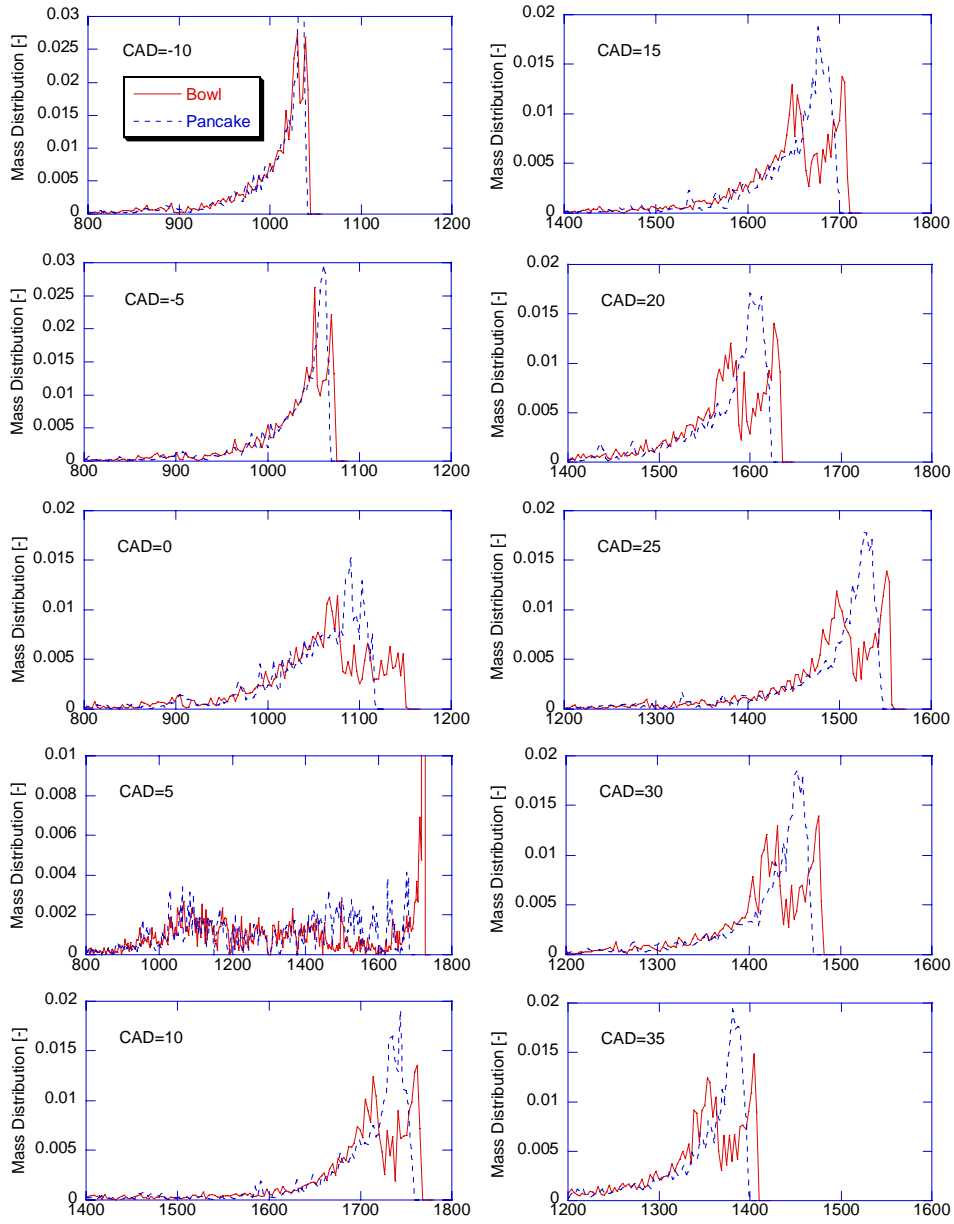


Figure 4.12 - Temperature mass distribution comparison under open end parametric study for two cases with two different piston geometries

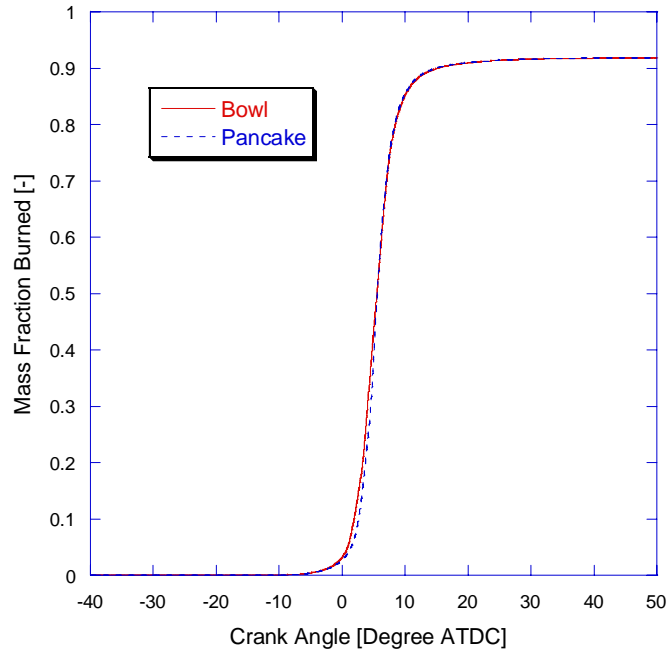


Figure 4.13 - Mass fraction burned comparison under open end parametric study for two cases with two different piston geometries

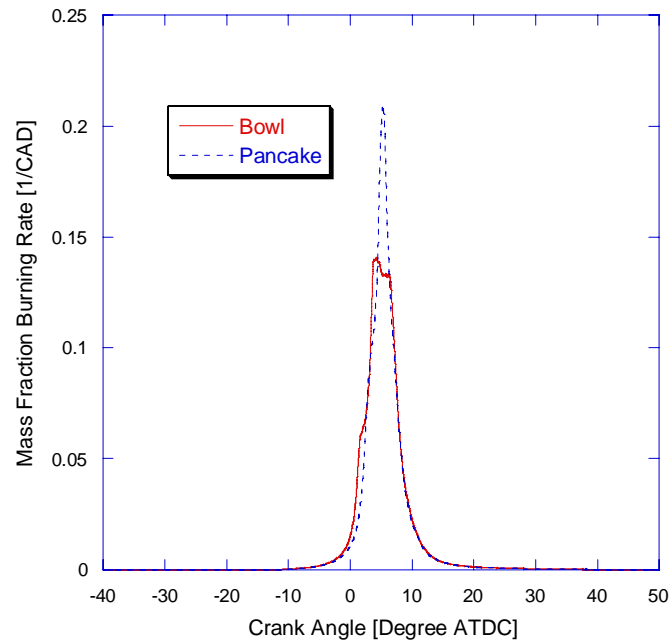


Figure 4.14 - Mass fraction burning rate comparison under open end parametric study for two cases with two different piston geometries

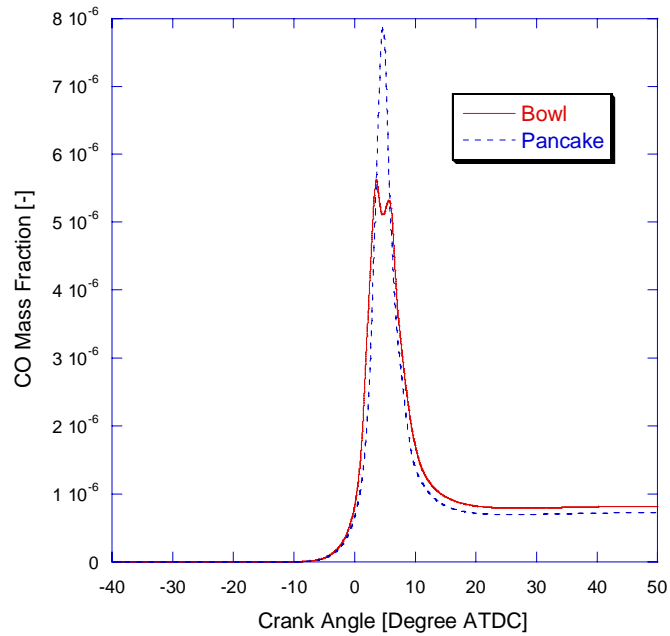


Figure 4.15 - CO composition comparison under open end parametric study for two cases with two different piston geometries

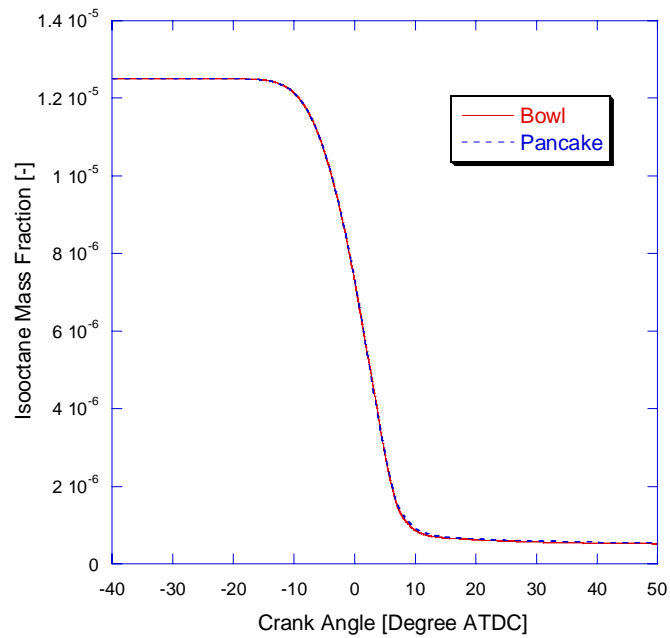


Figure 4.16 - Isooctane composition comparison under open end parametric study for two cases with two different piston geometries

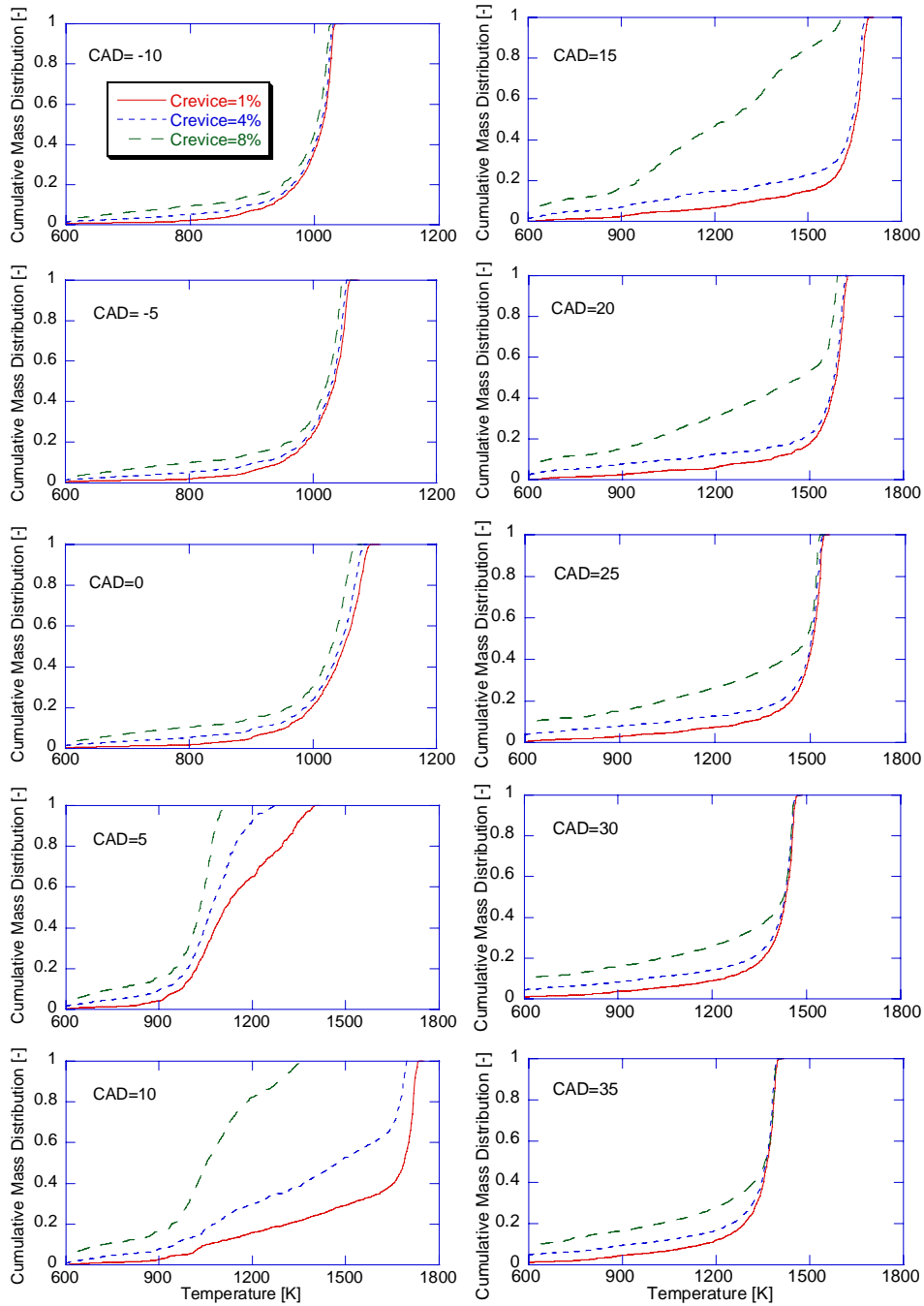


Figure 4.17 - Cumulative temperature mass distribution comparison under open end parametric study for three cases with three different crevice volumes

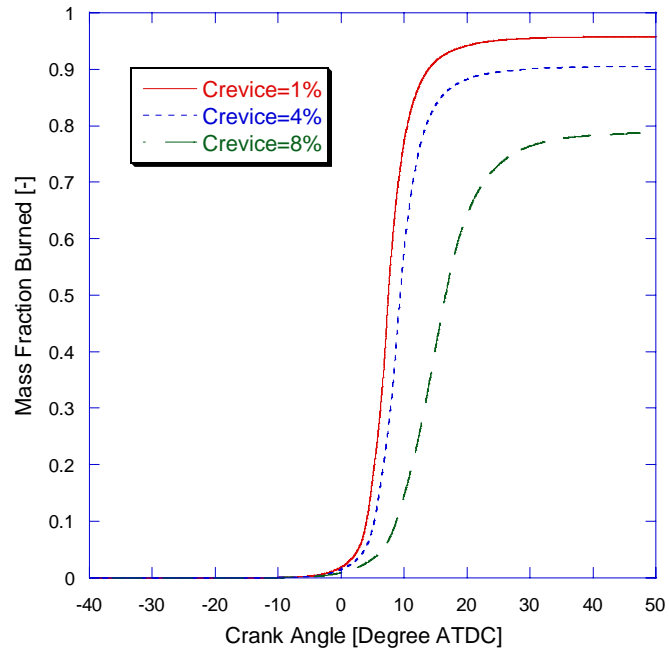


Figure 4.18 - Mass fraction burned comparison under open end parametric study for three cases with three different crevice volumes

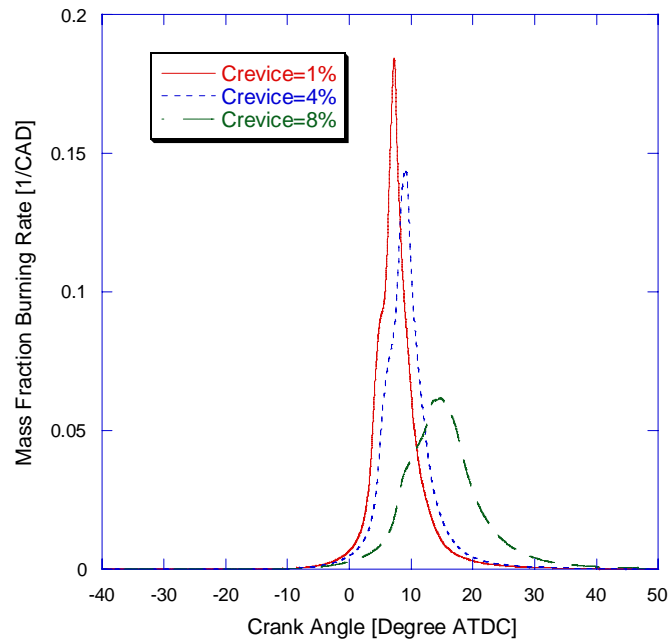


Figure 4.19 - Mass fraction burning rate comparison under open end parametric study for three cases with three different crevice volumes

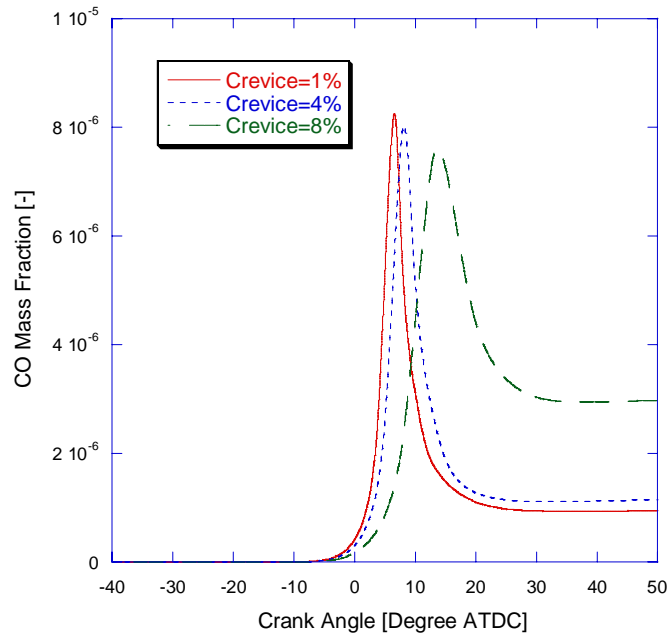


Figure 4.20 - CO composition comparison under open end parametric study for three cases with three different crevice volume

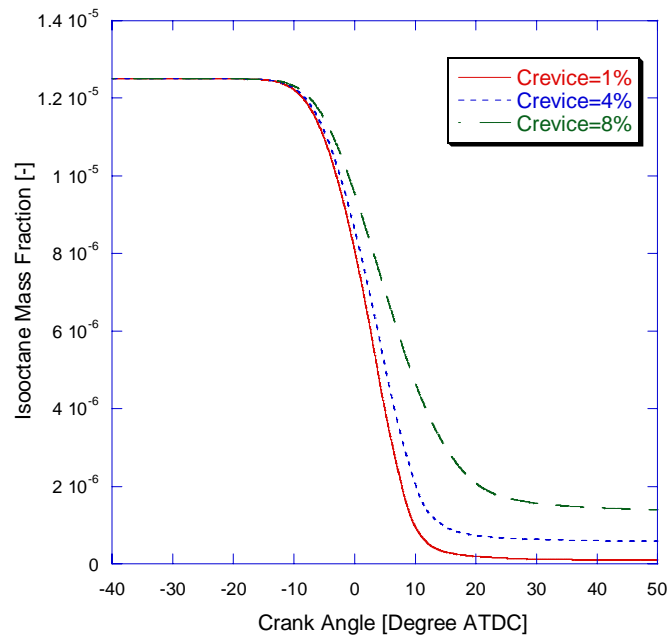


Figure 4.21 - Isooctane composition comparison under open end parametric study for three cases with three different crevice volume

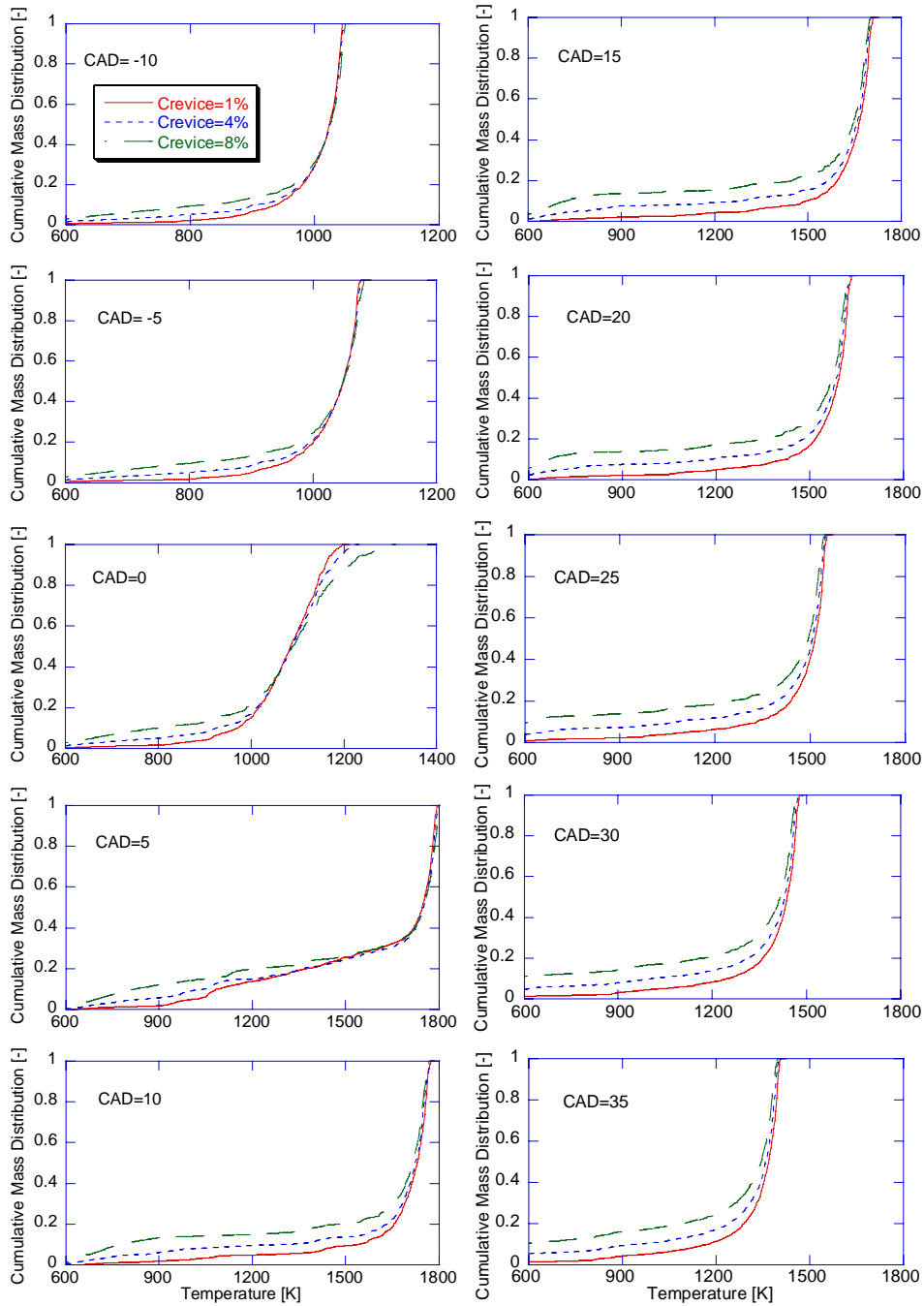


Figure 4.22 - Cumulative temperature mass distribution comparison under filtered parametric study for three cases with three different crevice volumes

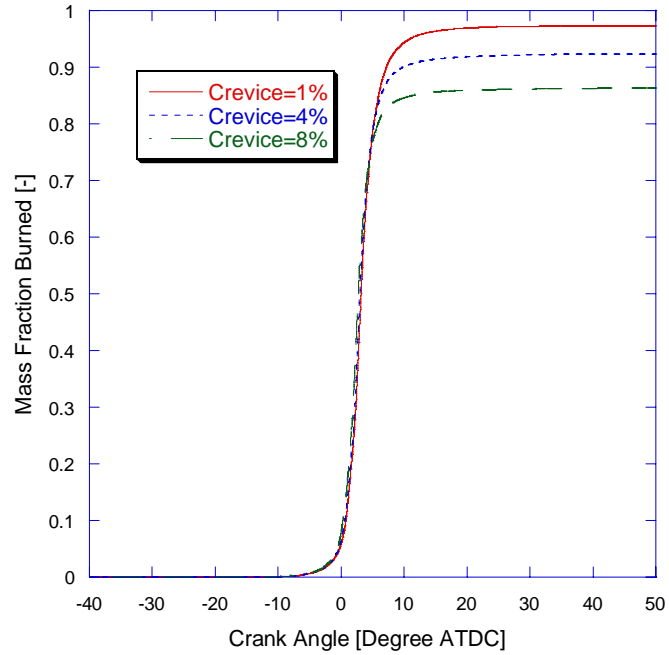


Figure 4.23 - Mass fraction burned comparison under filtered parametric study for three cases with three different crevice volumes

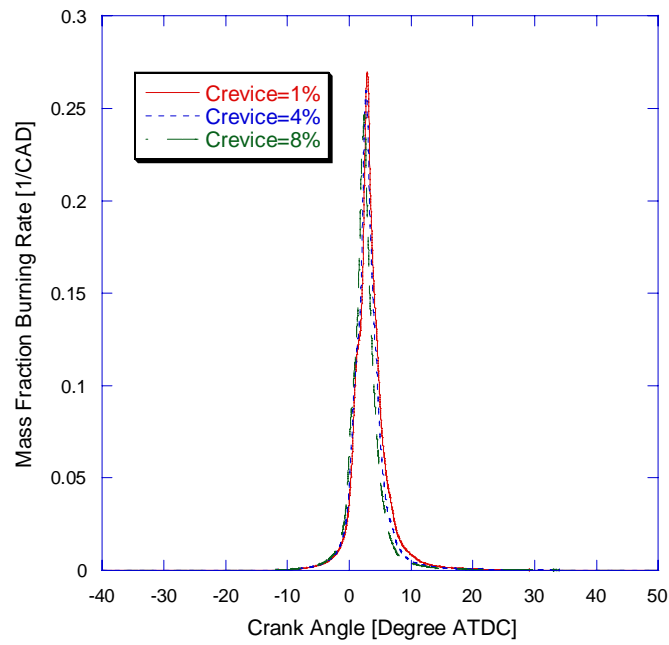


Figure 4.24 - Mass fraction burning rate comparison under filtered parametric study for three cases with three different crevice volumes

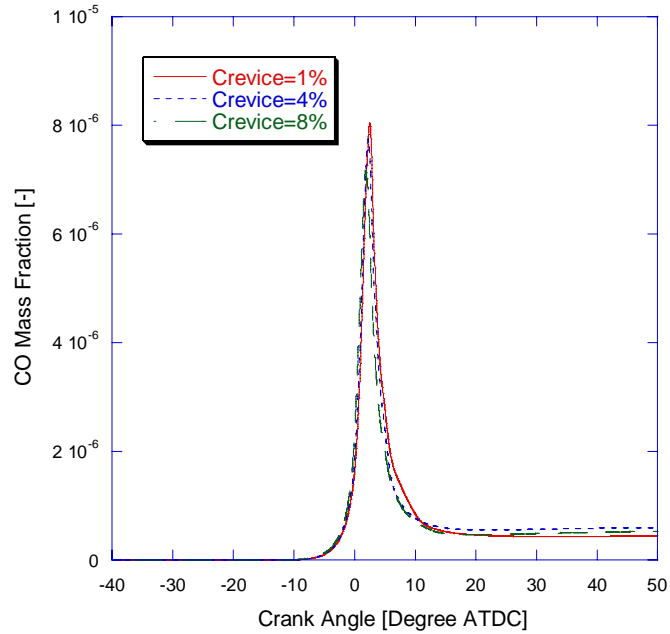


Figure 4.25 - CO composition comparison under filtered parametric study for three cases with three different crevice volumes

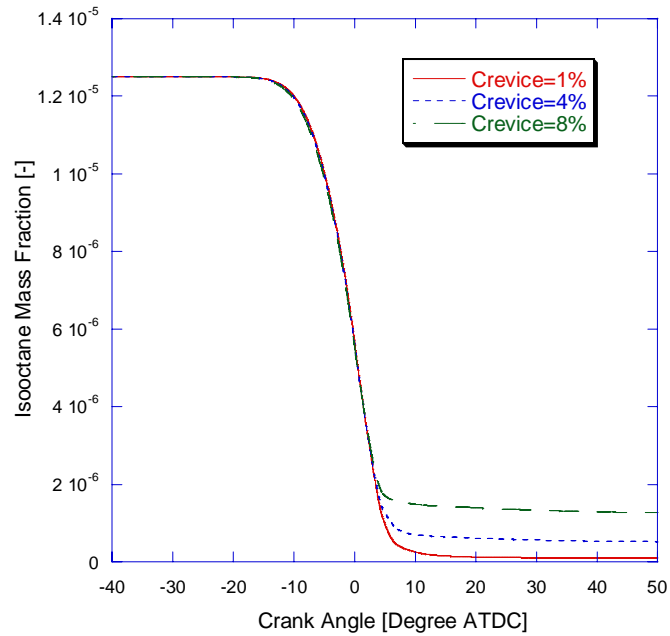


Figure 4.26 - Isooctane composition comparison under filtered parametric study for three cases with three different crevice volumes

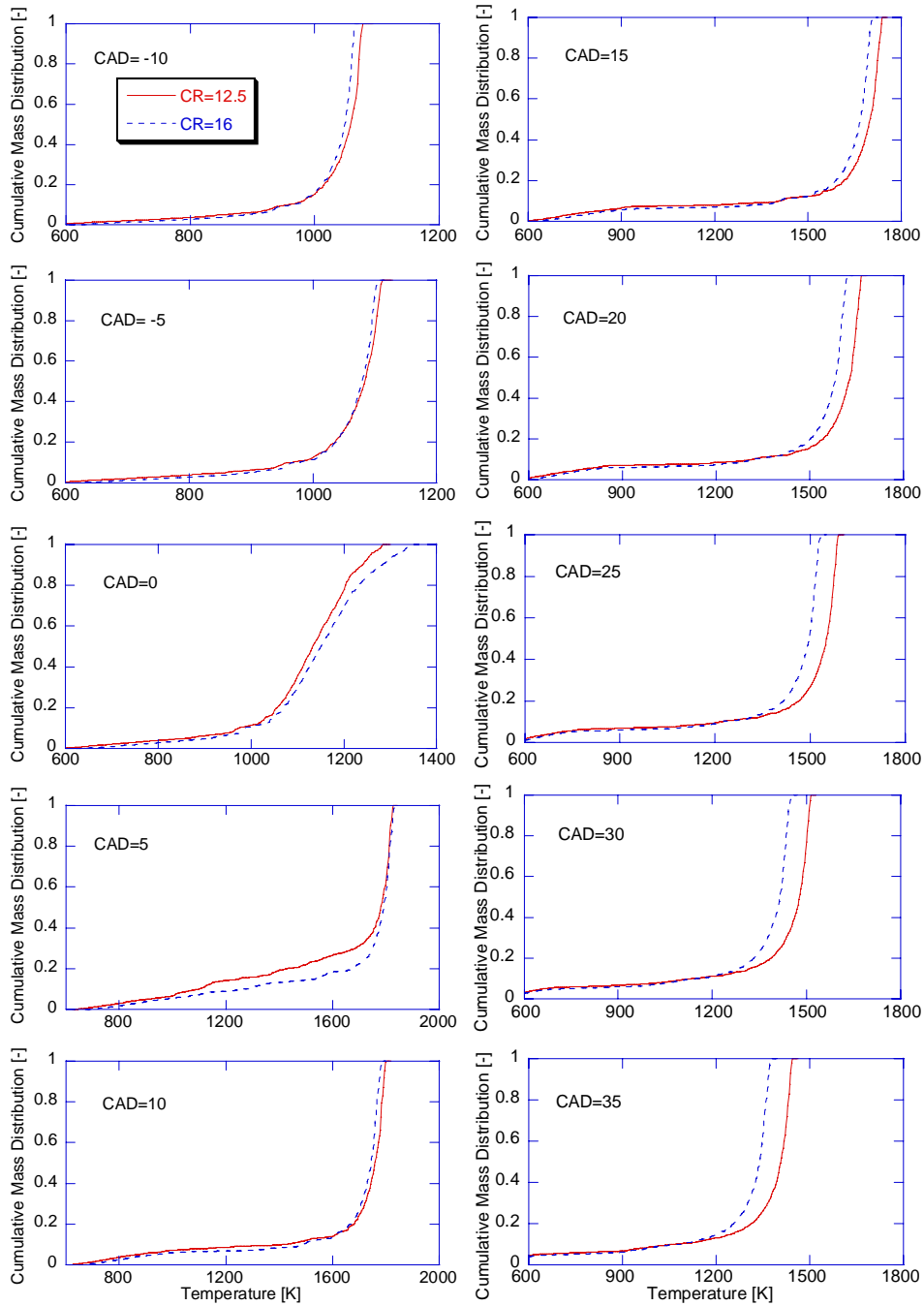


Figure 4.27 - Cumulative temperature mass distribution comparison under filtered parametric study for two cases with two different compression ratios

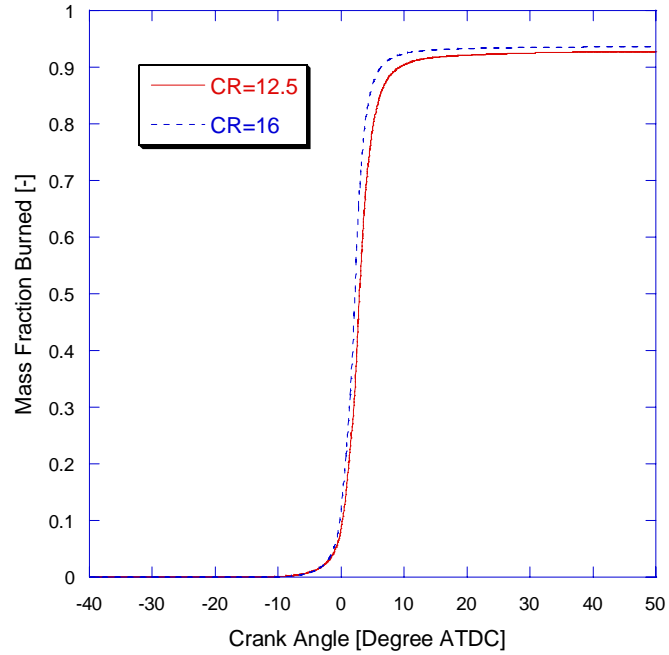


Figure 4.28 - Mass fraction burned comparison under filtered parametric study for two cases with two different compression ratios

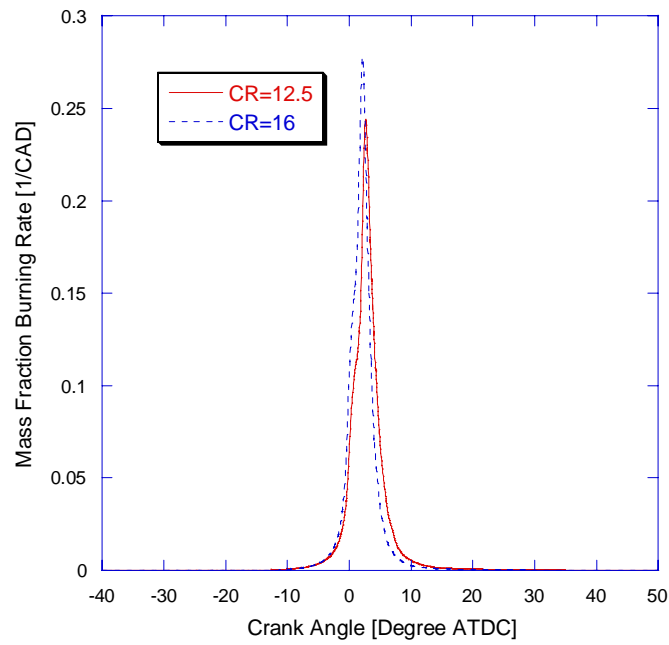


Figure 4.29 - Mass fraction burning rate comparison under filtered parametric study for two cases with two different compression ratios

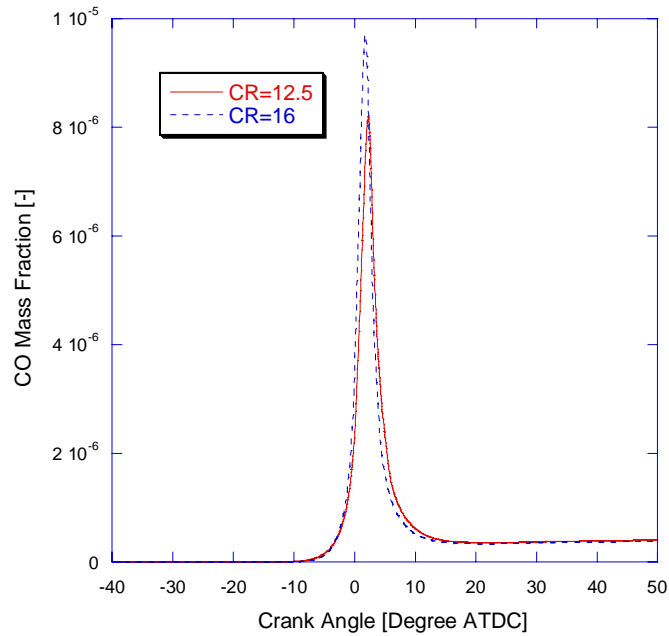


Figure 4.30 - CO composition comparison under filtered parametric study for two cases with two different compression ratios

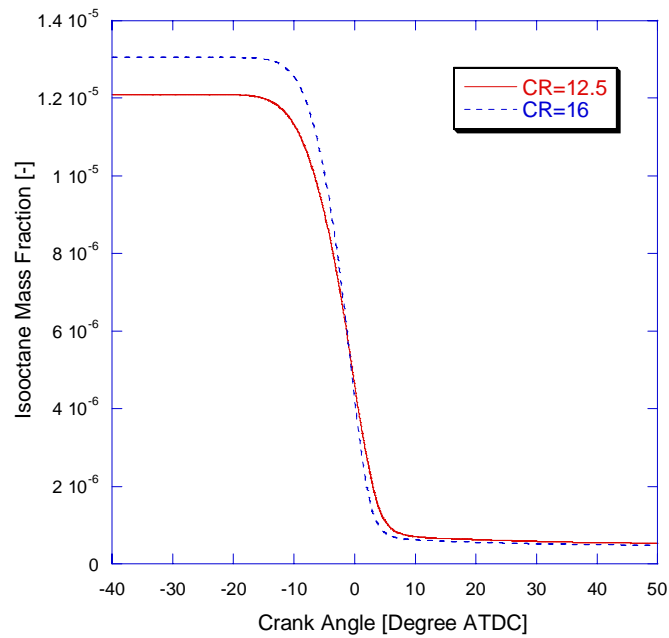


Figure 4.31 - Isooctane composition comparison under filtered parametric study for two cases with two different compression ratios

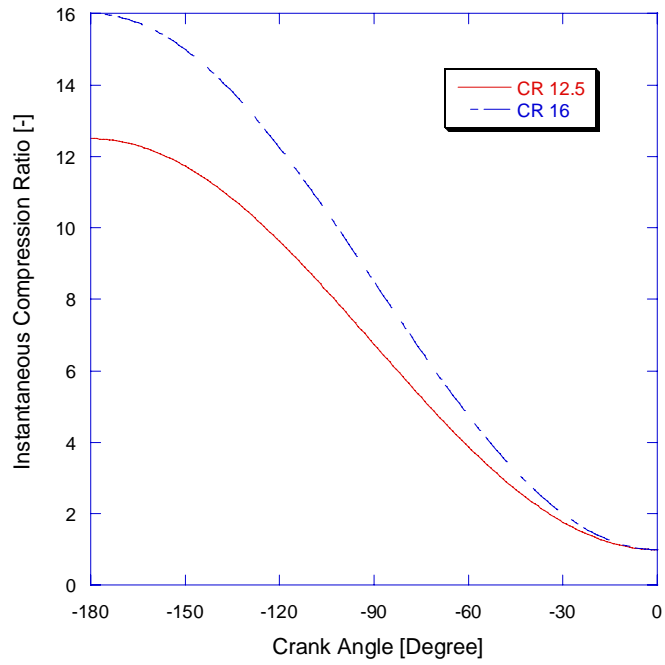


Figure 4.32 - Instantaneous compression ratio comparison for two compression ratios

CHAPTER 5

HCCI COMBUSTION CORRELATIONS

There's no correlation in existing literature predicting HCCI combustion efficiency and burning duration. Most HCCI transient control simulation studies use predetermined values for combustion efficiency and burning duration (Rausen et al, 2004 and Shaver 2005). Wiebe function has been the combustion correlation for diesel and spark ignited engine over many years, and it gives reasonable heat release profile once all the critical parameters are provided. Ignition timing is normally given and combustion efficiency is always assumed to be close to 100%. This type of correlation can work for traditional engine, but is not suitable for HCCI engine simulation, where ignition timing and combustion efficiency are much more volatile. To leverage the capability KIVA-MZ and its parametric study results, new HCCI combustion efficiency and burning duration correlations are proposed. The key components are: ignition correlation, combustion efficiency correlation, and burning duration correlation.

The correlation for ignition timing is the single most important correlation in the whole process because it determines not only the combustion phasing but also combustion efficiency and burning duration. The key component of ignition timing prediction is an ignition delay correlation developed from a rapid compression machine. Combustion efficiency and burning duration correlations are developed from the KIVA-MZ results.

5.1 1D HCCI Simulation Characteristics

1D engine simulation has been evolving over the years. Both the number of engine components and the quality of each component have been improved dramatically. In the past, the pressure in the intake manifold is given as boundary condition for engine simulation, now ambient pressure is the boundary condition because of the availability of pipe model, throttle model, flow split model, and heat exchanger model, et al. At the same time, engine control study using 1 D engine simulation is more and more popular. Once steady state simulation dominates the 1D engine simulation application; now transient simulation becomes the main application. Engine simulation nowadays is more capable, faster and yet more accurate. However, for HCCI simulation, there are several unique characteristics.

5.1.1 Residual Self Coupling

Steady state HCCI operation can be very stable with very small cycle to cycle variation (Richter et al. 1999). This is due to the weak role of turbulence on combustion. In the mean time, HCCI engine can experience large variation from cycle to cycle during transition when large amount of EGR is present, which is due to residual self coupling (Santoso et al. 2005). The coupling phenomenon comes from the relationship between the ignition timing and the residual temperature. Early ignition leads to lower burned temperature, which makes ignition of next cycle later; later ignition results in higher burned temperature. It seems that the dynamics of the relationship makes it a stable one, but when ignition gets really retarded, combustion efficiency starts to drop and burned temperature decreases. So the coupling between ignition timing and residual temperature is not perfectly stable.

When transient engine simulation is concerned, good prediction of ignition timing is not enough; combustion efficiency and burning duration predictions should also be on target to ensure the right residual temperature.

5.1.2 Heterogeneity

Both temperature and composition stratification can impact ignition timing as indicated by Babajimopoulos (2005). Heterogeneity is mainly caused by three factors: cylinder wall heat transfer, mixing with residual gas, and mixing with fuel. Cylinder wall heat transfer is inevitable for any metal block engine. Residue and fuel mixing effect on mixture heterogeneity depends on specific engine setup. Engine with well premixed air fuel charge and little residue has the least degree of heterogeneity. However, this kind of engine still has temperature distribution from core to boundary layer. In real HCCI engine, maintaining a certain level of heterogeneity is a remedy for too rapid heat release.

Engine composition non-uniformity is an area that 1 D engine simulation is not able to address with physical models. And its effect can only be approximated by correlations.

5.1.3 Thermal Inertial

Cylinder liner, piston and head temperatures can affect ignition timing significantly. Chang (2004) increased coolant temperatures by 15 degrees, and the results show that 10% burned location gets advanced by 2 degrees, and overall duration is 30% shorter. This clearly demonstrates the sensitivity of ignition timing to wall temperatures. Steady state cylinder block temperature can vary more than 15 degrees between low load and high load. These factors impose a new challenge for HCCI transient control. Accounting for the temperature variation, and implementing it in the ignition control algorithm become a necessity.

5.2 Ignition Correlation for HCCI

There are two options to predict ignition timing for a single zone engine model. One is to use chemical kinetics solver like Chemkin with detailed or reduce reaction mechanisms. The other is to use some form of knock integral, which is often based on ignition delay correlation developed from shock tube or rapid compression machine. The ignition delay correlation used in this study is developed by a rapid compression machine at the University of Michigan (He et al, 2005).

$$\tau = 1.3 \times 10^{-7} \cdot P^{-1.05} \cdot \phi^{-0.77} \cdot \chi_{O_2}^{-1.41} \cdot \exp(33700/RT) \quad (5.1)$$

Where P is pressure in “atm”, T is temperature in “Kelvin”, ϕ is the fuel to oxygen equivalence ratio, χ_{O_2} is the oxygen mole fraction in percentage, R is the universal gas constant in “cal/mol-K”, and τ is the ignition delay time in “second”.

As obvious in Equation 5.1, the temperature term is the most dominant variable in the equation because of its exponential effect on ignition delay. In order to predict ignition timing with accuracy from this ignition delay model, the cylinder temperature prediction has to be on target.

The major forces to decide the core temperature in the cylinder are compression heating and heat transfer. The accuracy of piston compression heating relies on the value of γ (ratio of specific heat). This value depends on equivalence ratio, initial pressure, compression ratio and EGR percentage.

The accuracy of heat transfer relies on the heat transfer model and it relies on engine speed, wall temperature, swirl ratio, and piston geometry. At the University of Michigan, a new heat transfer correlation is developed for HCCI (Chang, 2004).

$$h(t) = \alpha \cdot L(t)^{-0.2} \cdot p(t)^{0.8} \cdot T(t)^{-0.73} \cdot (C_1 \overline{S_p} + \frac{C_2}{6} \frac{V_d T_r}{p_r V_r} (p - p_{mot}))^{0.8} \quad (5.2)$$

α is a new scaling factor, and L is the instantaneous chamber height.

In summary, single zone engine model has enough sub models to predict the cylinder average temperature, and ignition delay converted knock integral model is used to give estimation on ignition timing.

However, a good ignition prediction doesn't automatically extend to good prediction for overall combustion. Indeed, good ignition prediction only gives a good beginning, and the rest task relies on the prediction of combustion efficiency and burning duration.

5.3 Combustion Efficiency Correlation

As shown in Figure 5.1, the pattern of combustion efficiency versus ignition timing is consistent among all the cases. When ignition timing is early, the combustion efficiency line is flat. As ignition gets later, there is a transition point where combustion efficiency starts to fall down. So there are three essential values: the peak combustion efficiency; the fall off timing, and the fall off slope. The peak combustion efficiency represents the healthy and stable combustion efficiency when ignition timing is early; the fall off timing represents the critical ignition timing when combustion efficiency starts to deteriorate; and fall off slope represents how fast the combustion efficiency deterioration can process with more retarded ignition timing.

Figure 5.2 shows the proposed combustion efficiency model. Three individual correlations is developed in the following sections.

5.3.1 Peak Combustion Efficiency

Without any question, the major factor in peak combustion efficiency is the crevice volume. Three crevice volume geometries are tested under engine setup with 1200 rpm, 12.5 compression ratio, 5% EGR, and 9 milligram of fuel, which corresponding to equivalence ratio of 0.2486 . Intake temperature is swept from low to high to obtain a sweep of combustion efficiency. Overall, combustion efficiency increases with higher intake temperature. However, at some point, the combustion efficiency does not keep increasing as intake temperature keeps increasing. The stabilized combustion efficiency is recorded as peak combustion efficiency.

Table 5.1 lists the variables involving in the correlation.

Table 5.1 - Peak combustion efficiency correlation variables

Crevice Volume (%)	Crevice Log by 2	Non-Crevice Volume (%)	Peak Combustion Efficiency (%)	Combustible Volume Inefficiency
$V_{\%c}$	C_{e2}	$V_{\%nc}$	η_{pc}	$V_{\%nc} - \eta_{pc}$
1	0	99	97.74	1.26
4	2	96	92.63	3.37
8	3	92	86.37	5.63

First column is the crevice volume, which is the volume percentage of the crevice of the total cylinder volume when piston is at TDC. Second column is the log value of the crevice volume divided by the log value of 2, which is defined in Equation 5.3.

$$C_{e2} = \frac{\text{Ln}(V_{\%c})}{\text{Ln}(2)} \quad (5.3)$$

Third column is the non crevice volume, which accounts the cylinder volume not belong to the crevice volume. Fourth column is the peak combustion efficiency. Fifth column is the difference between the non crevice volume and the peak combustion efficiency, which is given name of combustible volume inefficiency.

Ideally, the combustible volume inefficiency ($V_{\%nc} - \eta_{pc}$) should be zero, which means that the combustion efficiency is equal to the non crevice volume. In reality, mixture in the wall boundary and higher mixture density in the crevice volume contribute to the inefficiency. This inefficiency value increases with crevice volume. With higher crevice volume, peak combustion efficiency deteriorates much faster. This inefficiency value is quite linear with the crevice log by 2 in value.

Curve fitting the relationship between crevice log by 2 and combustible volume inefficiency results in the following equation:

$$V_{\%nc} - \eta_{pc} = (1.26 + 0.25 \cdot C_{e2} + 0.4 \cdot C_{e2}^2) \quad (5.4)$$

Meanwhile, for the same crevice volume, equivalence ratio seems to have some weak effect on combustion efficiency. Following table shows the relationship between equivalence ratio and combustion efficiency for engine setup with 4% crevice volume, 2000 rpm, 5% EGR, and 12.5 compression ratio.

Table 5.2 - Equivalence ratio and combustion efficiency correlation data

Equivalence ratio	Combustion efficiency
0.201	92.44%
0.227	92.81%
0.256	93.27%
0.284	93.40%
0.313	93.46%
0.342	93.61%
0.370	93.92%
0.399	94.26%

When equivalence ratio goes from 0.2 to 0.4, the combustion efficiency increases less than 2%. And the relationship is fairly linear.

$$\eta_{pc} = 90.96 + 8.1 \cdot \varphi \quad (5.5)$$

This equation matches well with the previous study. The case with 4% crevice volume has equivalence ratio of 0.2486 and peak combustion efficiency of 92.63%. This equation gives combustion efficiency of 92.97% with equivalence ratio at 0.2486. So using this point as the base point is a natural choice. The overall peak combustion efficiency correlation is presented here with second term accounting for crevice volume, third term for volume inefficiency and final term for equivalence ratio adjustment.

$$\eta_{pc} = 100 - V_{\%c} - (1.26 + 0.25 \cdot C_{e2} + 0.4 \cdot C_{e2}^2) + (\varphi - 0.2486) \cdot 8.1 \quad (5.6)$$

One other variable has demonstrates some effect on peak combustion efficiency is the cylinder wall temperature. Because this study is focusing on peak combustion efficiency, the ignition is fairly early. Fifty degree Celsius difference in wall temperature carries about one percent of combustion efficiency difference. However, bringing in another dimension of variable to have a small gain is not worth to pursue in this effort.

5.3.2 Combustion Fall Off Timing

Among all the lines in Figure 5.1, some have very sharp turns in combustion efficiency, especially those cases that combustion efficiency falling off at a later timing. It is relatively easy to define the fall off point for those lines. But for other lines which have earlier combustion efficiency deterioration, the transition is more gradual and there's no clear choice of fall off point. A universal definition for fall off point is needed. The combustion fall off timing is defined as the ignition timing where combustion efficiency is equal to 93 percent of peak combustion efficiency.

The fall off timing is a strong function of equivalence ratio and engine speed. As shown in Figure 5.3, all the other variables can only cause up to 1 degree of deviation with the same speed and equivalence ratio. So the fall off timing can be adequately correlated by equivalence ratio and engine speed with confidence zone about one degree. Even though there's slight curvature for the speed lines, linear representation is adequate.

For the data point being collected, most have engine speed at 1200 rpm and 2000 rpm, and equivalence ratio is around 0.24, which is evident from Figure 5.3, where point is concentrated in that area.. The top and bottom speed in this study is 3750 and 750 respectively, and each of them has equivalence ratio sweep study. From Figure 5.3, for each speed line, the relationship between fall off timing and equivalence ratio is fairly linear, so two linear correlations are obtained. For rpm at 3750, the correlation is:

$y=53.923*\varphi-14.763$; while for rpm at 750, the correlation is: $y=66.83*\varphi-16.316$. And these two coefficients are differentiated by engine speed.

A simple correlation for fall off timing is in the following:

$$\theta_{fo} = a \cdot \varphi - b \tag{5.7}$$

$$a = 66.83 - 12.907 \cdot \frac{rpm - 750}{3750}$$

$$b = 16.316 - 1.553 \cdot \frac{rpm - 750}{3750}$$

With this correlation, the predicted fall off timing is shown in Figure 5.4. Compared with Figure 5.3, the largest error is around 1 degree.

5.3.3 Combustion Fall Off Slope

From Figure 5.1, the fall off slope (l_{fo}) gets steeper when the fall off timing becomes more retarded. The slope value is not as critical as the fall off timing when engine performance prediction is concerned, and the deviation from point to point is relatively small. So a simple approach is used. Two extremes are chosen, and then linear interpolation is applied for the region in between these two extremes. The least steep case has fall off timing at -3.5, and the slope is 21.45; while the steepest case has fall off timing at 4.5, and the slope is 66.94. So a linear equation for fall off slope is obtained in the following.

$$l_{fo} = 5.685 \cdot \theta_{fo} + 41.227 \tag{5.8}$$

At this point, combustion efficiency is ready to be correlated. When the actual ignition timing is earlier than fall off timing, combustion efficiency is the peak combustion efficiency. If actual ignition timing is later than the fall off timing; the actual combustion efficiency is based on the peak combustion efficiency and the fall off slope as in the following equation.

$$\eta_{com} = \eta_{pc} - l_{fo} \cdot (\theta_{ign} - \theta_{fo}) \quad (5.9)$$

5.4 Burning Duration Correlation

Even if combustion efficiency prediction is correct, many simulation results can be off with erratic heat release rate. A practical way is to have a good prediction of heat release is to provide a burning duration combined with a Wiebe profile. So in this section, burning duration is correlated by the data sets generated by KIVA-MZ.

From Figure 5.5, the pattern of burning duration versus ignition timing is monotonically increasing for all the cases before combustion efficiency deteriorates. The duration is short when ignition timing is early, then the duration increase gradually with later ignition timing. Eventually, the burning duration curve takes a sharp downward turn, which strongly mirrors the falling off of combustion efficiency.

Variations of some parameters do not cause the burning duration curves separate from each other; while others do. The most significant parameter is equivalence ratio (Figure 2.16). Case with richer mixture has much shorter burning duration. The second strongest parameter to deviate the burning duration curve is engine speed (Figure 2.19). Case of higher engine speed has longer burning duration with the same ignition timing. Among other parameters, piston geometry (Figure 2.21) also causes consistent separation between duration curves. Compression ratio (Figure 2.23) also causes some degree of separation between duration curves. Swirl ratio and cylinder wall temperature (Figure 2.20) in this study are the two methods altering cylinder temperature distribution. Swirl ratio can impact the burning duration in a noticeable level. The importance of cylinder temperature and composition distribution is well documented for burning duration.

Ideally, burning duration should be a function of ignition timing and any other variables, which can cause difference in burning duration with the same ignition timing. This means that variables like equivalence ratio, engine speed, compression ratio, piston geometry and temperature distribution should all be included. However, only equivalence ratio and engine speed can cause significant difference, while all other variable have much less impact. Also, the data size of this study is not big enough to support a correlation involving many variables. In this preliminary correlation of burning duration, only equivalence ratio and engine speed are included.

The tuning factor for equivalence ratio and engine speed is obtained separately. There is an equivalence ratio sweep under three engine speeds: 750, 2000, and 3750. Figure 5.7 shows that the equivalence ratio has a power factor of 2. And speed, which is normalized by 2000 has a power factor of -0.15 (Figure 5.8).

Applying these two adjusting factors in overall data pool, the adjusted burning durations collapse into a narrow region (Figure 5.9). Since the effects of other parameters haven't been separated, it is impossible to get a single line. A line is needed for correlation purpose, so average value is computed in the middle of the narrow region.

A fifth order polynomial seems to be enough to correlate the data, which represents the adjusted burning duration.

So, the general correlation for burning duration is in the following:

$$\theta_{duration} = f_{bd}(\theta_{ign}) \cdot \varphi^{-2} \cdot \left(\frac{rpm}{2000}\right)^{0.15} \quad (5.10)$$

$$f_{bd}(\theta_{ign}) = (1.1948 + 0.1698 \cdot \theta_{ign} + 0.0214 \cdot \theta_{ign}^2 + 0.0115 \cdot \theta_{ign}^3 + 0.0026 \cdot \theta_{ign}^4 + 0.0002 \cdot \theta_{ign}^5)$$

Equation 5.10 is only good for combustion efficiency at or close to peak value. Once ignition timing is substantially later than the combustion fall off timing, the burning duration becomes shorter. It is noticed that the point where burning duration becomes

shorter is not the point where combustion efficiency starts to deteriorate, but rather combustion efficiency gets lower than 50%. There's a potential correlation for burning duration under severe misfire condition, but it is of less importance to the overall simulation accuracy, and the CFD data don't cover that region well. So a fixed value of 20 degrees crank angle burning duration is applied for any case running combustion efficiency lower than 50%.

5.5 Summary of Correlations

There are several independent correlations in this whole package, so they have to be presented in a logical way that users can understand easily and implant them into a simulation code.

First of all, this work identifies the supreme importance of ignition timing on overall combustion performance, so most plots and correlations are based on ignition timing. The schematic is in Figure 5.6. Important parameters like peak combustion efficiency and fall off timing are correlated with some engine design and operating parameters.

Figure 5.10 shows the flow chart of the correlations in actual engine simulation. There are two crank angle locations that correlation computations are performed. First one is the intake valve closing timing. Engine speed, equivalence ratio, crevice volume, and residual fraction are all known at this time, so peak combustion efficiency (η_{cpk}) and fall off timing (θ_{fo}) can be calculated. The second one is the ignition timing, which is a result of both constant variables like equivalence ratio and residual fraction and progressing variables like pressure and temperature. This ignition timing is compared with the fall off timing to determine the combustion efficiency and burning duration.

5.6 Validation with KIVA Data

During the course of establishing these correlations, not all data generated by KIVA-MZ is used. Some of the reserved data is used to validate the correlation.

The following table lists four validation cases cover speed range from 1250 to 3000, and equivalence ratio from 0.1894 to 0.2951.

Table 5.3 - Correlation validation with KIVA data under four operating conditions

	RPM	PHI
CASE 1	1500	0.2438
CASE 2	3000	0.2533
CASE 3	1250	0.1894
CASE 4	1250	0.2951

The overall performance of the correlation is acceptable (Figure 5.11 through Figure 5.14). Both peak combustion efficiency and fall off slope is very close to the KIVA-MZ result. More importantly, the fall off timing is on target, even though the transition curvature is neglected.

Case 4 has the best match up among these four validation points (Figure 5.11). This case has the highest equivalence ratio, thus the latest fall off timing. The ignition timing range covers most of the timing range used to construct the correlation. Both combustion efficiency and burning duration curves match very well.

The rest three cases don't have as good match up as case one. Relative speaking, combustion efficiency prediction is satisfactory. The biggest error is caused by the transition curvature, which is neglected in correlation. For burning duration, all three cases have better prediction when ignition timing is around 2 degrees BTDC, where large portion of data existing in the pool used to make the correlation.

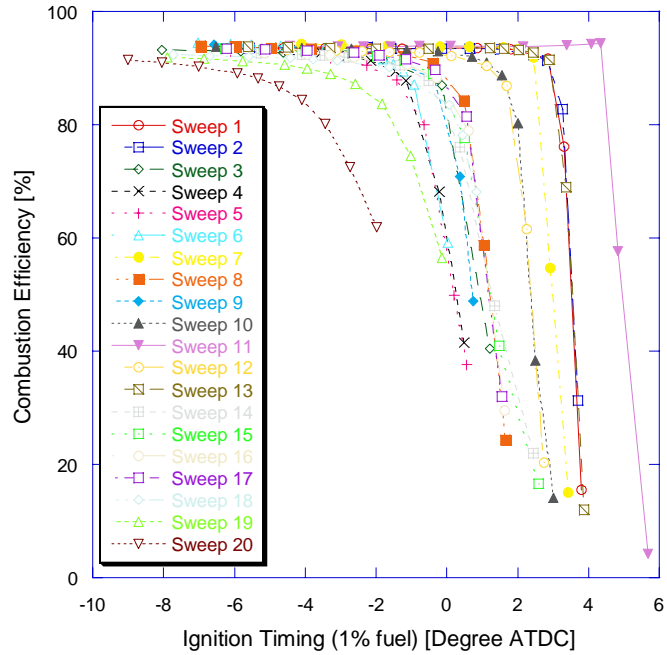


Figure 5.1 – KIVA-MZ simulated relationship between combustion efficiency and ignition timing (sweep 1 to sweep 20)

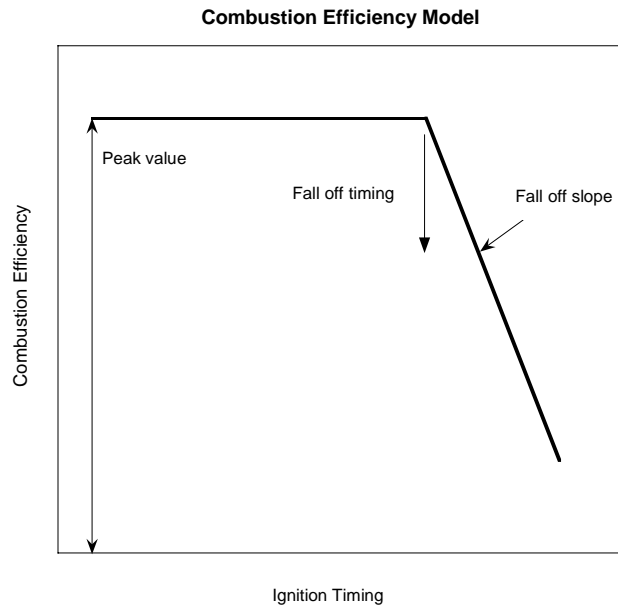


Figure 5.2 - Combustion efficiency correlation model

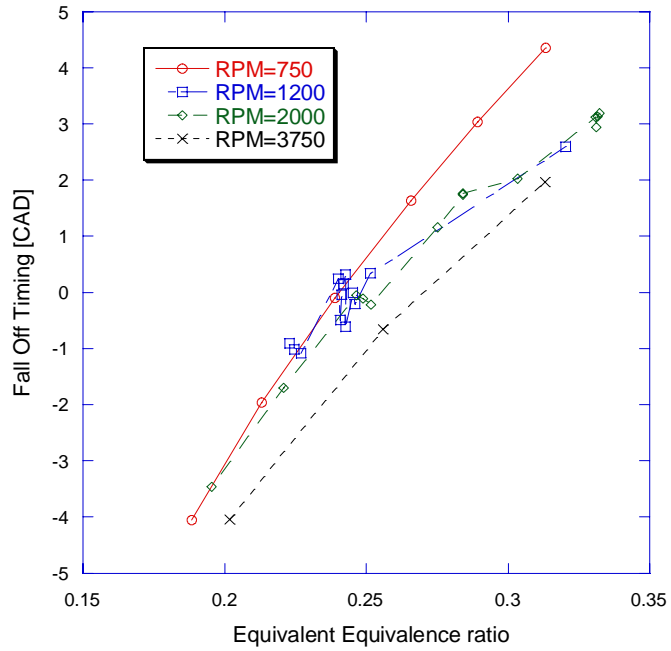


Figure 5.3 - KIVA-MZ result of combustion fall off timing versus equivalence ratio under four engine speeds

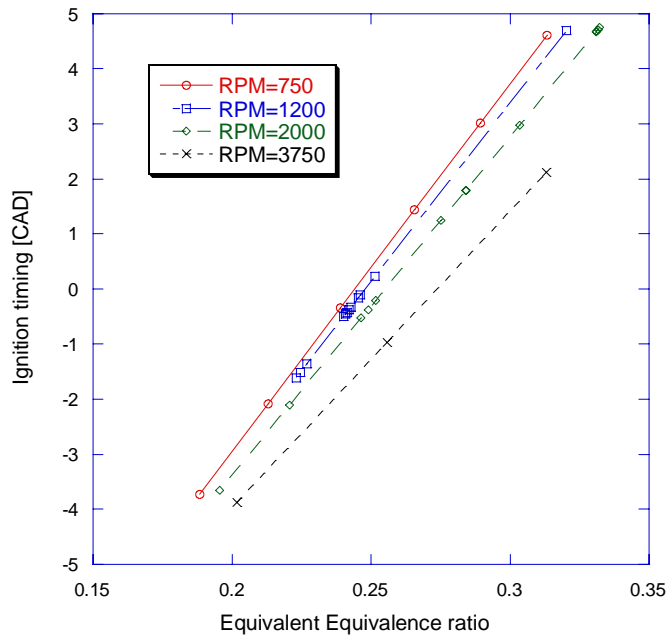


Figure 5.4 - Correlation result of combustion fall off timing versus equivalence ratio under four engine speeds

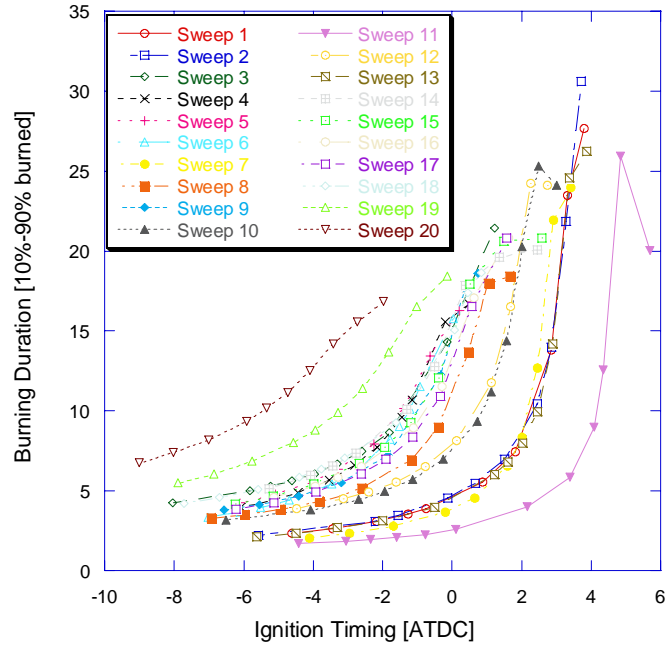


Figure 5.5 – KIVA-MZ simulated relationship burning duration and ignition timing (Sweep 1 to sweep 20)

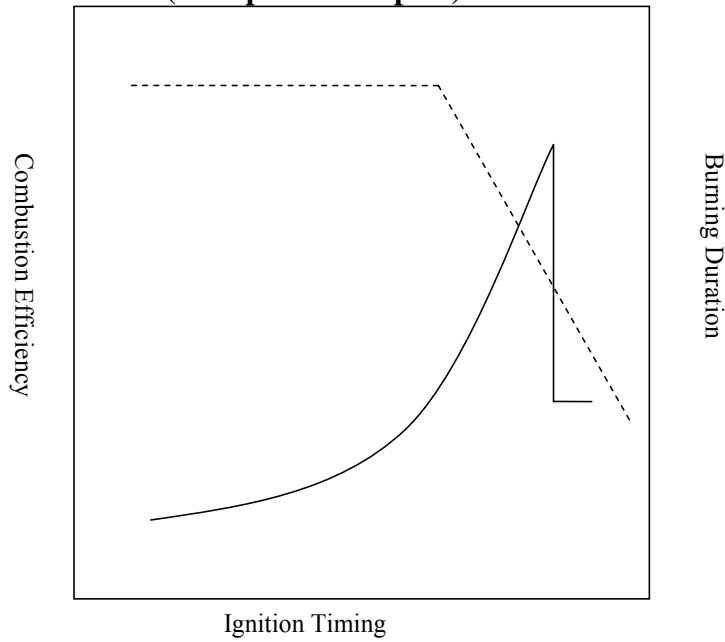


Figure 5.6 - Burning duration correlation model

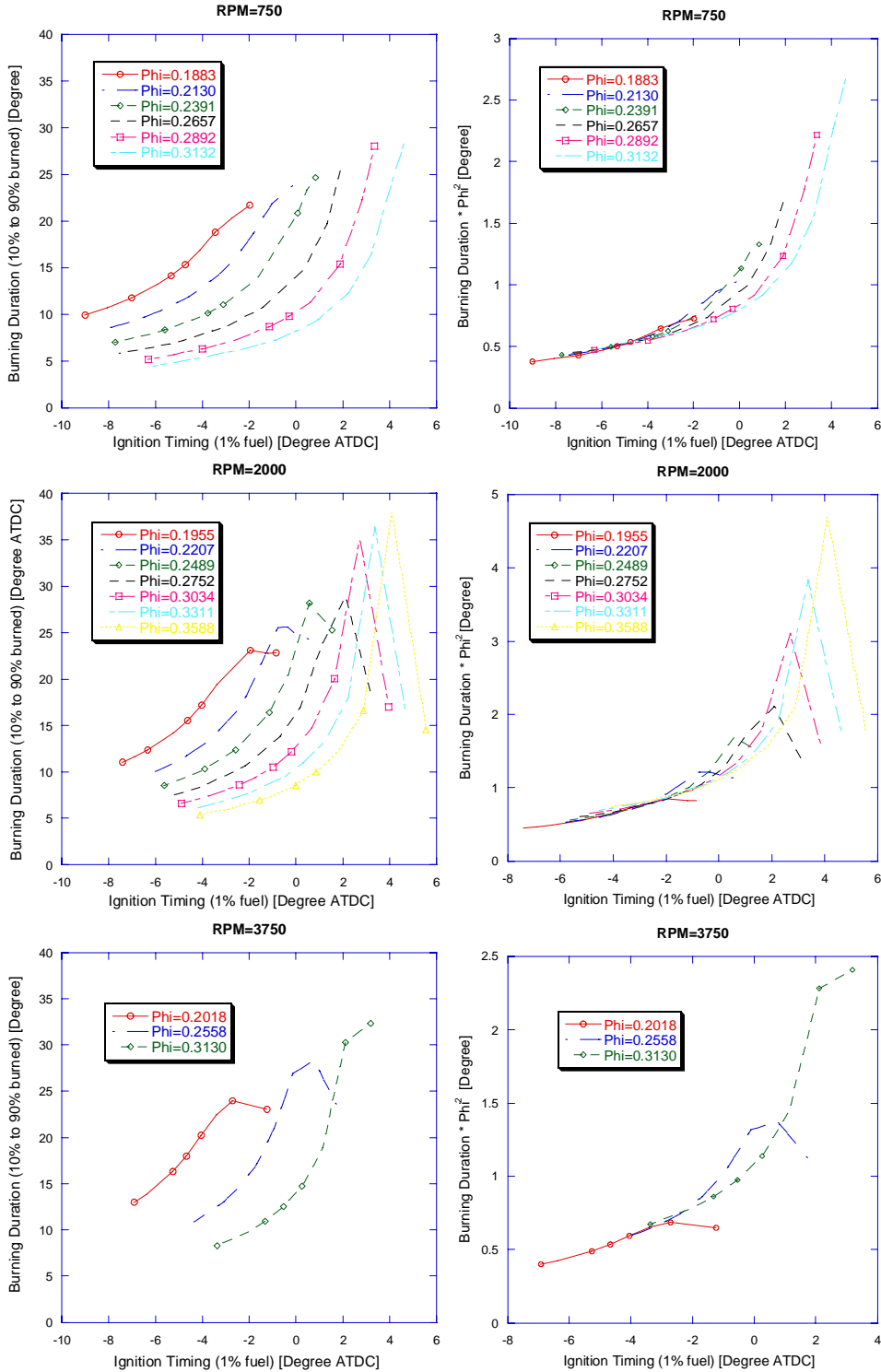


Figure 5.7 – Comparison between original burning duration (left) and equivalence ratio adjusted burning duration (right) versus ignition timing, under three engine speeds (750, 2000, 3750 rpm)

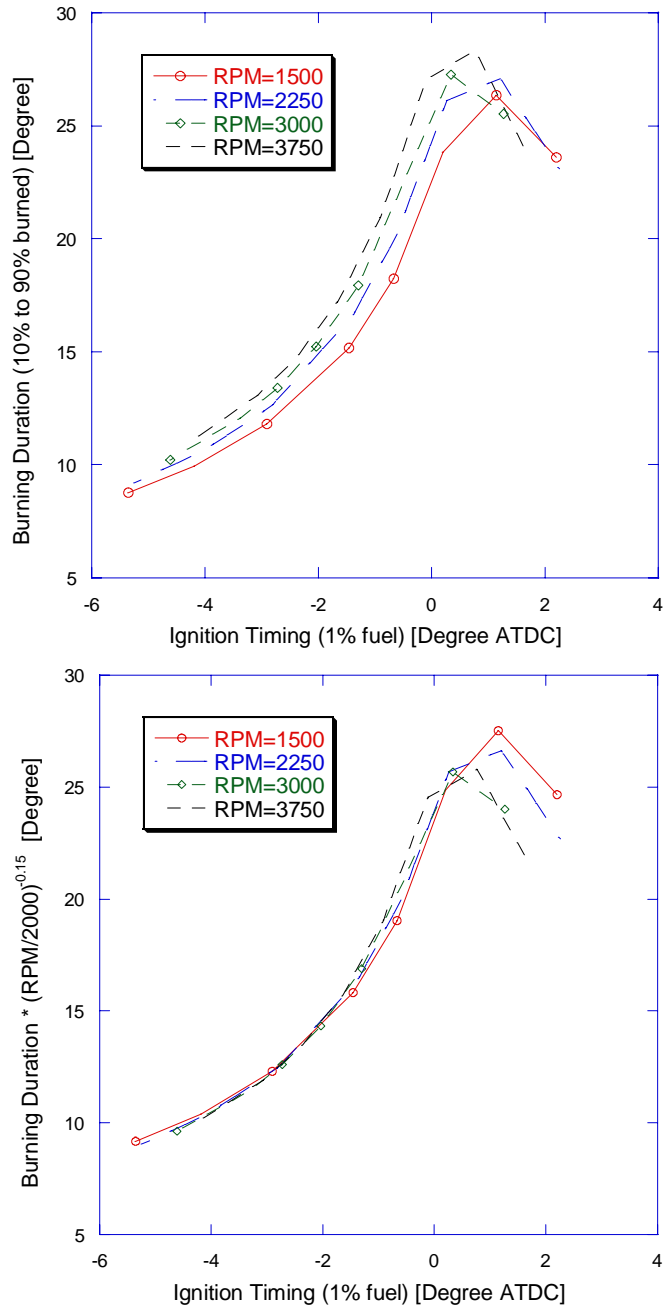


Figure 5.8 - Comparison between original burning duration (up) and engine speed adjusted burning duration (below) versus ignition timing

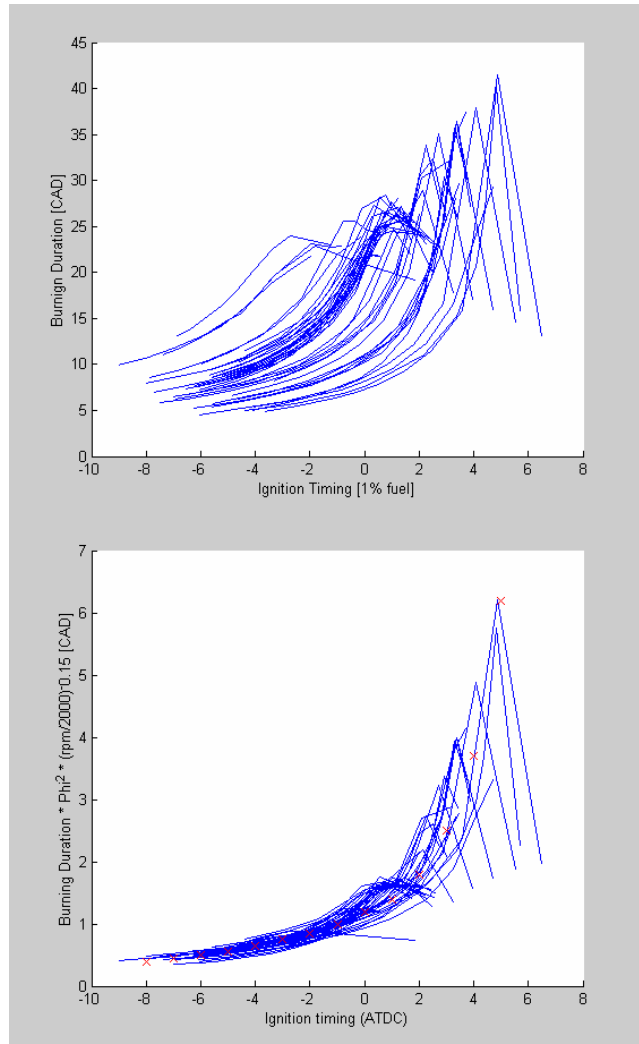


Figure 5.9 - Comparison between original burning duration (up) and equivalence ratio and engine speed adjusted burning duration (below) versus ignition timing

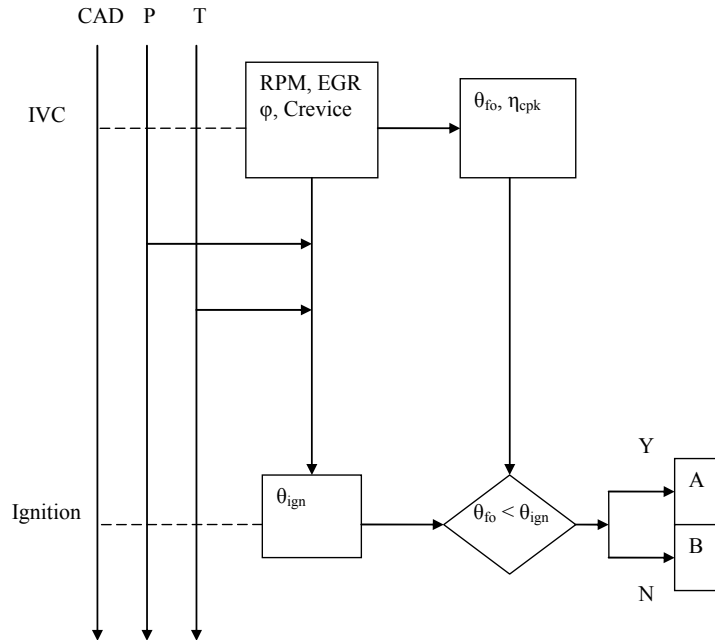


Figure 5.10 - Simulation timeline for HCCI correlations

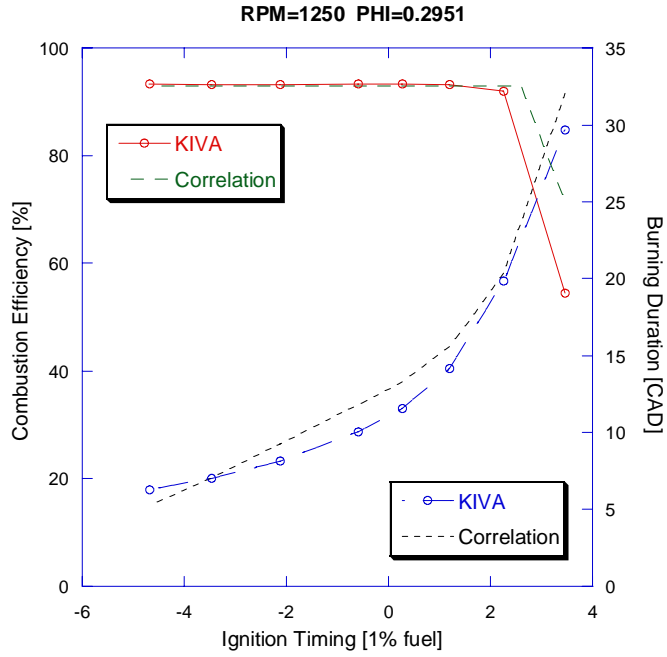


Figure 5.11 - Correlation validation with KIVA data at 1250 rpm and 0.2951 equivalence ratio

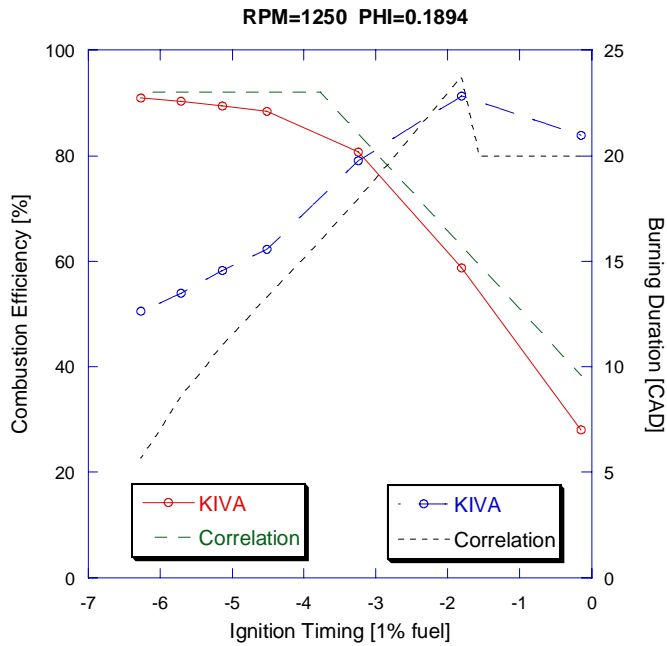


Figure 5.12 - Correlation validation with KIVA data at 1250 rpm and 0.1894 equivalence ratio

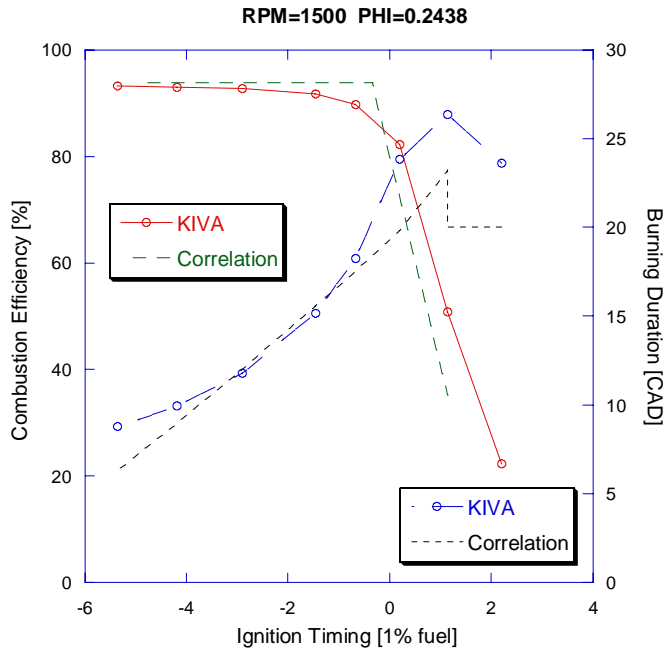


Figure 5.13 - Correlation validation with KIVA data at 1500 rpm and 0.2438 equivalence ratio

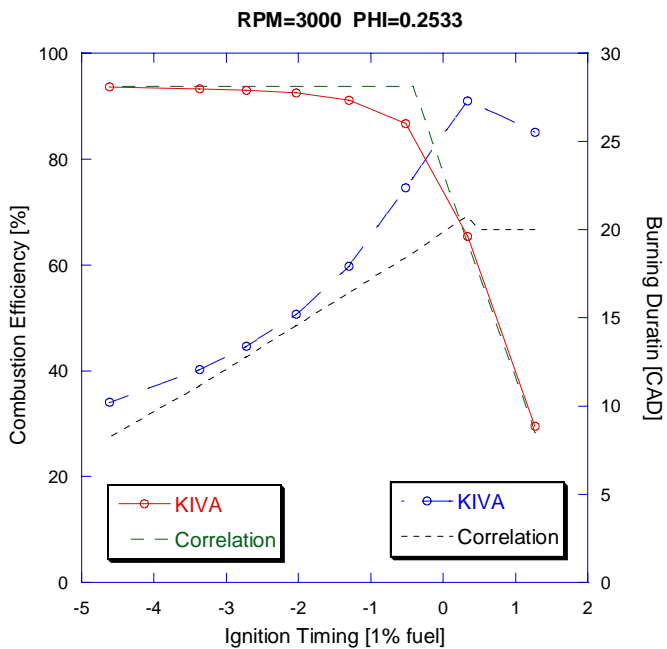


Figure 5.14 - Correlation validation with KIVA data at 3000 rpm and 0.2533 equivalence ratio

CHAPTER 6

ONE DIMENSIONAL HCCI ENGINE SIMULATION

Just like any other computer modeling in science and engineering world, internal combustion engine simulation has evolved from in-house private command-line code to off-the-shelf multimedia commodity. GT-Power, a commercial engine simulation tool developed by Gamma Technologies, is the current market leader in one dimensional engine system simulation software. GT-Power provides wide variety of component models, as well as user friendly interface. However, as a commercial product, its development is more industry driven, rather than academic driven. New combustion concept like HCCI is not included in its combustion model library. Fortunately, GT-Power has open access design so that users are able to provide their own models for certain process not already in the GT-Power library. User models can be built into a DLL (dynamic link library), which communicates with GT-Power's main solver. In the DLL, there are many FORTRAN subroutines dealing with varies engine processes. GT-Power provides the calling arguments and skeleton of the program body, where users have to fill up the code with their own formulations.

This chapter first covers the important formulations in flow, heat transfer and combustion for GT-Power. Then the user subroutine implementation process is introduced. Finally, a virtual UM HCCI engine model is built and validated against experiment data.

6.1 Fluid Flow Modeling

In 1D frame work, flow through pipes and valves are critical to engine simulation. Volumetric efficiency is one of the major matching factors in engine simulation. To get the right amount of air and fuel into cylinder is the prerequisite for any meaningful engine simulation work.

6.1.1 Manifold

The fundamental component for flow system is a pipe. One dimensional flow equation is solved with and across the pipes. A pipe can be further discretized into many nodes, and the flow equations is solved at node level. Since it is one dimensional flow, variables are uniform at pipe cross section. Each scalar variable is assumed to be uniform over each node, and each vector variable is calculated at each boundary. Accordingly, the equations being solved are:

$$\text{Continuity: } \frac{dm}{dt} = \sum_{\text{boundaries}} \rho Av \quad (6.1)$$

$$\text{Energy: } \frac{d(me)}{dt} = p \frac{dV}{dt} + \sum_{\text{boundaries}} (\dot{m} \times H) - h_g A (T_{\text{gas}} - T_{\text{wall}}) \quad (6.2)$$

$$\text{Momentum:} \quad (6.3)$$

$$\frac{d(\rho Av)}{dt} = \frac{dpA + \sum_{\text{boundaries}} (\rho Av \times v) - 4C_f \frac{\rho v^2}{2} \frac{dxA}{D} - C_p \left(\frac{1}{2} \rho v^2\right) A}{dx}$$

Friction loss factor is based on the Reynolds number and the surface roughness of the walls. In Laminar region when Reynolds number is less than 2000, $C_f = 16/Re_D$. In turbulent region, $C_f = 0.08/Re_D^{0.25}$. When the surface is rough and the flow is not laminar, the friction coefficient is calculated below:

$$C_{f_{rough}} = \frac{0.25}{(2 \log_{10}(\frac{D}{2h}) + 1.74)^2} \quad (6.4)$$

6.1.2 Valve

Flow through valves requires discharge coefficients for flow in both directions. They originate from the isentropic velocity equation for flow through an orifice and are defined as the ratio of effective flow area to the reference flow area. They include friction losses and errors in assumptions of velocity profiles in the orifice equations.

For gases, discharge coefficient may be calculated using the following formulas:

$$\begin{aligned} \dot{m} &= A_{eff} \rho_{is} U_{is} = C_D A_R \rho_{is} U_{is} \\ \rho_{is} &= \rho_o (P_r)^{\frac{1}{\gamma}} \\ U_{is} &= \sqrt{RT_o} \left(\frac{2\gamma}{\gamma-1} (1 - P_r^{\frac{\gamma-1}{\gamma}}) \right)^{\frac{1}{2}} \end{aligned} \quad (6.5)$$

Where:

\dot{m} = mass flowrate

A_{eff} = effective flow area

ρ_{is} = density at the valve

ρ_o = upstream stagnation density

U_{is} = isentropic velocity at valve

C_D = discharge coefficient

A_R = reference flow area

P_r = absolute pressure ratio

R = gas constant

T_o = upstream stagnation temperature

γ = specific heat ratio

The reference area should remain unchanged regardless of the angle or position. For cam-driven valves, there are two options available:

C_D may be calculated with the reference area, A_R , which is held constant for all L/D values at

$$A_R = \frac{\pi}{4} \times d_{ref}^2 \quad (6.6)$$

C_D may be calculated with the reference area, A_R , which is uniquely calculated for each lift position in the L/D array as the valve curtain area:

$$A_R = \pi \times d_{ref} \times L \quad (6.7)$$

6.1.3 Cylinder

The main focus of in cylinder flow is the turbulence level, which affects the heat transfer and flame propagation processes. Even though the turbulence level doesn't influence HCCI combustion in a direct way like SI engine, the heat transfer part does play an important role in the cylinder temperature history, which on the contrary, affecting the chemistry.

The in-cylinder flow breaks the cylinder into multiple regions: the central core region, the squish region, the head recess region, and the piston cup region. In each region, the mean radial velocity, axial velocity, and swirl velocity are calculated taking into account the cylinder chamber geometry, the piston motion, and flow rate/swirl/tumble of the incoming and exiting gases through the valves. These velocities are used in the heat transfer model. The flow model also contains single zone turbulence and tumble models. The turbulence model solves the turbulence kinetic energy equation

and the turbulence dissipation rate equation (Morel and Keriba, 1985). From this data, the instantaneous mean turbulence intensity and turbulence length scale are calculated.

Swirl and tumble is generated by the fluids entering the cylinder through the intake valves. The swirl and tumble coefficients are defined as the ratio of the angular momentum flux to the linear momentum flux, which is used to calculate the swirl and tumble torque, which is applied to the in-cylinder gases. Swirl and Tumble coefficients are specified by the user versus L/D (lift over diameter). The swirl and tumble coefficients may be calculated as follows if swirl or tumble torque have been measured in the laboratory:

$$\omega = \frac{2T_s}{\dot{m} \times U_{is} \times D} \quad (6.8)$$

$$\tau = \frac{2T_t}{\dot{m} \times U_{is} \times D}$$

$$U_{is} = \sqrt{RT_o} \left(\frac{2\gamma}{\gamma-1} (1 - P_r^{\frac{\gamma-1}{\gamma}}) \right)^{\frac{1}{2}}$$

Where:

- ω = swirl torque
- τ = tumble torque
- \dot{m} = mass flowrate
- U_{is} = isentropic valve velocity
- D = cylinder bore
- P_r = absolute pressure ratio
- R = gas constant
- T_o = upstream stagnation temperature
- γ = specific heat ratio

6.2 Heat Transfer Modeling

Heat transfer is another critical factor in engine simulation. It not only affects the overall energy flow, but also the heat release rate, which is especially true for HCCI engine. Therein cylinder heat transfer is utilizing the recent work at the University of Michigan [Chang et al. 2004].

6.2.1 Manifold

The heat transfer from fluids inside of pipes to their walls is calculated using a heat transfer coefficient. The heat transfer coefficient is calculated at every timestep from the fluid velocity, the thermo-physical properties and the wall surface finish. The heat transfer coefficient of smooth pipes is calculated using the Colburn analogy.

$$h_g = \frac{1}{2} C_f \rho U_{eff} C_p P_r^{-\frac{2}{3}} \quad (6.9)$$

Where:

C_f = friction coefficient of smooth pipe

ρ = density

U_{eff} = effective velocity outside boundary layer

C_p = specific heat

P_r = Prandtl number

The Colburn analogy is used for turbulent, laminar and transitional flow.

The surface roughness can have a very strong influence on the heat transfer coefficient, especially for very rough surfaces such as cast iron or cast aluminum. The heat transfer coefficient of rough pipes is calculated by using the heat transfer coefficient shown above, then increasing it using the following correlation:

$$h_{g,rough} = h_g \left(\frac{C_{f,rough}}{C_f} \right)^n \quad (6.10)$$
$$n = 0.68 \times P_r^{0.215}$$

Where:

$h_{g,rough}$ = *heat transfer coefficient of rough pipe*

$C_{f,rough}$ = *friction coefficient of rough pipe*

6.2.2 Cylinder

The dominant heat transfer mechanism in the HCCI engine is forced convection from the bulk gas to combustion chamber walls. The radiation effect is very small because of low-soot, low temperature from premixed lean combustion.

The instantaneous heat transfer coefficient from gas to cylinder wall has been extensively studied over the years. These studies are normally dimensional analysis based, and they correlate turbulent flow to Nusselt, Reynolds, and Prandtl numbers. One class of correlation providing spatial average heat transfer coefficient is particular popular for their simplicity. Examples are Annand, Woschni and Hohenberg. In particular, the Woschni correlation has frequently been used for HCCI engine studies, even though the correlation was developed under direct injection diesel engine.

The global heat transfer coefficient depends on characteristic length, transport properties, pressure, temperature, and characteristic velocity. A scaling factor α scaling is used for tuning of the coefficient to match specific engine geometry. A unique feature of Woschni correlation is the gas velocity term. While most other correlations use a time-averaged gas velocity proportional to the mean piston speed, Woschni separated the gas velocity into two parts: the unfired gas velocity that is proportional to the mean piston speed, and the time-dependent, combustion induced gas velocity that is a function of the difference between the motoring and firing pressures.

$$v(t)_{woschni} = C_1 \bar{S}_p + C_2 \frac{V_d T_r}{p_r V_r} (p - p_{motoring}) \quad (6.11)$$

This approach keeps the velocity constant during the unfired period of the cycle, and then imposes a steep velocity rise once combustion pressure departs from motoring pressure. The subscript r denotes a reference crank angle, such as intake valve closing time. The original Woschni model can be rewritten as

$$h_{hcci}(t) = \alpha_{scaling} \times L(t)^{-0.2} \times p(t)^{0.8} \times T(t)^{-0.73} \times v(t)^{0.8} \quad (6.12)$$

$$v(t) = C_1 \bar{S}_p + \frac{C_2}{6} \frac{V_d T_r}{p_r V_r} (p - p_{mot})$$

The HCCI heat transfer experiment at UM proposed three improvements over the original Woschni model: the instantaneous chamber height is used as the characteristic length scale, the temperature exponent is modified to be 0.73, and C2 is reduced to 1/6 of the original value.

6.3 Combustion Modeling

The complete HCCI combustion correlations include ignition timing, combustion efficiency, and burning duration. The detailed burning profile is represented by a wiebe function.

6.3.1 Ignition

Ignition is calculated using knock integral approach based on the ignition delay model developed by a rapid compression machine at the University of Michigan (He et al, 2005).

$$\tau = 1.3 \times 10^{-7} \cdot P^{-1.05} \cdot \phi^{-0.77} \cdot \chi_{O_2}^{-1.41} \cdot \exp(33700/RT) \quad (6.13)$$

Where P is pressure in “atm”, T is temperature in “Kelvin”, ϕ is the fuel to oxygen equivalence ratio, χ_{O_2} is the oxygen mole fraction in percentage, R is the universal gas constant in “cal/mol-K”, and τ is the ignition delay time in “second”.

Above equation gives the ignition delay timing for constant environment. In a real engine, the temperature and pressure are changing, so knock integral approach is used. At the time of intake valve is closed, integration calculation is made for the inverse of the ignition delay until the integration value reaches 1, which flags the ignition.

$$\int_{\theta_{ivc}}^{\theta_{ign}} \frac{1}{\tau} d\theta = 1 \quad (6.14)$$

6.3.2 Combustion Efficiency

Combustion efficiency in HCCI has a critical ignition timing associated with each set of design and operation variables. When ignition timing is earlier than that critical ignition timing, combustion efficiency is mainly determined by crevice volume. When ignition timing is later than the critical ignition timing, the combustion efficiency is predominantly influenced by the ignition timing itself.

At the time of intake valve closing, the peak combustion efficiency is known from Equation 3.7. The real combustion efficiency won't be available until the conclusion of the ignition timing, which is calculated from knock integral of equation 3.2.

With the occurrence of ignition timing, the combustion efficiency is calculated from equation 3.10.

6.3.3 Burning Duration

Burning duration is calculated along with combustion efficiency at the time of ignition with equation 3.11.

6.3.4 Burning Profile

The burning profile applies the format of wiebe function

$$f(\theta) = \eta_{comb} \times \exp\left(-\left(\frac{\theta - \theta_{ign}}{\theta_{duration}}\right)^{w+1}\right) \quad (6.15)$$

The exponent value w is depended on the ignition timing with following table

θ_{ign}	-9	-8	-7	-6	-5	-4	-3	-2	-1	0	1	2	3	4	5	6	7	8	9
w	2	2	2	2	2	2	2	1.7	1.4	1.1	1.1	1.1	1.1	1.1	1.1	1	1	1	1

6.4 GT-Power User Model Implementation

GT-Power is a graphic object based engine and powertrain simulation tool. A virtual engine is built from varies graphic blocks (Figure 6.1), which represent individual physical component. These graphic blocks are called “parts” in GT-Power terminology. And “parts” are derived from “objects”. One “object” can derive many “parts” as long as all these “parts” are identical. One example, intake valve “object” can have two intake valve “parts” if the engine has two identical intake valves. “Objects” themselves are derived from “templates”. Both intake valve “object” and exhaust valve “object” are derived from valve “template”.

Creation of each piece of graphic block in the simulation window has to go through “template->object->part” process. However, parts can be copied and pasted within a model or across different models.

Once proper engine pieces have been put together and correctly linked, users have to go into individual part to setup the configuration and formulation. If all the desired component models are within default GT-Power model library, user can run the model from this point. However, if users need some special model not already in the GT-Power library, users have to set up their own user model and link to GT-Power’s main solver.

6.4.1 GT-Power User Model Setup

In order to make GT-Power execute the user defined combustion and heat transfer models, users have to put the user model names into the process object lines. Users need open an engine cylinder “part”, go to “models” tab, and input the user model names for both heat transfer and combustion objects (Figure 6.2). Then users need double click open the user model to fill in the data that users want to pass to their FORTRAN subroutine.

There are many ways to provide data to the user FORTRAN subroutine, which is described in the next section. The most fundamental and flexible way is to provide data in the user model window. Four arrays (integer, real, string, RLT) are created and passed to user subroutine. RLT is a GT-Power defined variable, which has the following characteristics: one value per engine cycle. It can be an integration value like BMEP (brake mean effective pressure), or a maximum value like peak pressure, or a spot value like ignition timing.

6.4.2 Fortran Code Modification

With GT-Power installation, a FORTRAN DLL project is also copied to the installation directory (Figure 6.3). There’s only one FORTRAN file under the project. Usually, it has name like GTIusr62.f90. “62” means version 6.2, and this is subjected to change over the GT-Power version evolution.

In the FORTRN file, there’re about 30 subroutines, each of which deals with different engine process models. GT-Power does provide default models for these processes, but this DLL provides users the option to formulate their own equations to describe the process.

In the subroutines, user can obtain input values through calling arguments, user model arrays (real, integer, string, RLT), and sensor data. And results can be output through calling arguments and actuator data.

6.4.3 Solver Subroutine Interaction

Among 30 user subroutines in the DLL, two user subroutines have been significantly modified in this thesis work: user cylinder heat transfer (ENGHEATTRUSER) and user combustion (ENGCOMBUSER).

The communication between GT-Power solver and DLL occurs at every calculation step. For heat transfer, the interaction is on for the whole cycle; while for combustion, the interaction happens during the closed cycle from intake valve closing to exhaust valve opening.

GT-Power starts calculation of each engine cycle at intake valve closing. Both combustion and heat transfer models are engaged at that time. In the combustion model, the knock integral starts to accumulate, and there's a flag for ignition. This flag is shared across subroutines through a FORTRAN module structure. The heat transfer model is also monitoring the ignition flag to determine which formulation it uses at current step.

After intake valve closing, GT-POWER starts to communicate with the DLL. The DLL has much smaller calculation step size for CHEMKIN, and the calculation progress up to the GT calculation step size; then the DLL estimates the heat release during this period, and converts to fuel mass burned and passes back to GT-Power, which calculates the energy equation in the cylinder.

6.5 1D Engine Simulation Validation

The combustion model is calibrated and validated with the UM HCCI engine data. The experiment data set chosen for the calibration and validation work is the intake temperature sweep, because this sweep provides the biggest span of ignition timing. The procedure of the calibration and validation has two steps. First, the model is calibrated against the experiment point with the most advanced ignition timing. Then the model is validated against the rest points with later ignition and weaker combustion. The reason to choose the most advanced ignition timing point as the calibration point is to validate the predictive capability of the model on later combustion and misfire.

6.5.1 GT-Power Model Calibration

The experiment data is from the UM HCCI engine, and the engine configuration is listed in Table 2.1. The operation parameter for the calibration point is listed in Table 6.1.

Table 6.1 - Operation parameter for calibration point

Intake Pressure (kPa)	93.99
Intake Temperature (K)	388.96
Air/Fuel Ratio	19.04
Engine Speed (RPM)	1995.7
Fuel Flow Rate (mg/cycle)	10.94
Exhaust Pressure (kPa)	103.27

This operation point is from one sweep study on intake temperature, which ranges from 75 to 115 degree Celsius.

A simple GT-Power model (Figure 6.1) is build according to the UM HCCI engine specifications. Based on the locations of experiment measurement of pressure and temperature in the intake and exhaust system, the model starts from intake plenum, and finishes at exhaust plenum. Both combustion correlation and heat transfer correlation described in Chapter 3 are fully implemented.

The only tuning parameter on combustion side is the temperature adjustment for ignition timing, which is calibrated to match the experiment data.

Figure 6.4 shows the pressure comparison of the simulation against experiment data. After matching the ignition timing, there's no further tuning on combustion efficiency and burning duration. The combustion comparisons are listed in Table 6.2.

Table 6.2 - Combustion results for calibration point

	Experiment	Simulation
Combustion Efficiency (%)	95.74	94.36
10% burned location (ATDC)	-0.5	-0.1
50% burned location (ATDC)	3.5	3.8
90% burned location (ATDC)	7.5	7.8

6.5.2 GT-Power Model Validation

The experiment data used for validation is the intake temperature sweep, which ranges from 75 degree to 135 degree Celsius. The simulation data is compared with experiment data on diagonal plots, which means a diagonal straight line is the perfect match.

Figure 6.5 through Figure 6.8 show that simulation data has good agreement with the experiment data for the combustion efficiency and burning rate. The combustion efficiency is slightly under predicting. 10% burned location has very good agreement, which means that the ignition delay does a good job of predicting ignition timing; then 50% burned location is slightly over predicting and 90% burned location is a little more over predicting.

6.5.3 Improvement over Marginal Combustion Prediction

The improvement of this new combustion model over fixed value correlations used by Rausen [2004] and Shaver [2005] is in the area of marginal combustion and misfire. The weakness of fixed combustion efficiency model is the lack of realistic prediction of combustion efficiency under late ignition timing conditions. The simplification of the combustion efficiency can miscalculate the steady state engine operation range. More importantly, impossible engine transients could go undetected under these simulations. In short, traditional HCCI combustion models for control study have ignition timing as the only prediction of the combustion, and it is an on/off system.

The strong coupling between the residual temperature and ignition timing makes HCCI combustion very intriguing. The consequences of late ignition for one engine cycle can impact the next cycle in many ways. If the combustion efficiency is good, the combustion temperature is higher due to later heat release, which advances the ignition timing of the next cycle; however, if the combustion efficiency goes lower, the combustion temperature drops, and the cylinder temperature drops too, and engine might get stalled. Once combustion efficiency is fixed, the occurrence of ignition is the only prediction to make or break the combustion

To demonstrate the model's improvement over fixed value model, comparisons are made at three distinctive engine transition conditions. The intake mixing throttle angle changes from 30 degrees to 20 degrees at cycle number 20 to create a transition from high intake temperature to a slightly lower mixture temperature, which can delay the ignition timing.

In Figure 6.9, the temperature for hot intake air is 500 Kelvin. Both simulations have stable combustion after transition. Despite the difference in the combustion efficiency, both simulations have stable ignition timing and combustion efficiency after the transition.

In Figure 6.10, the temperature for hot intake air is 495 Kelvin. Fixed value model has stable combustion after transition; while new model has oscillation in combustion efficiency and ignition timing. In this comparison, the ignition timing is in the vicinity of the critical ignition timing, so oscillation in combustion efficiency is present for the new model.

In Figure 6.11, the temperature for hot intake air is 490 Kelvin. Fixed value model has stable combustion after transition; while new model misfires. This is a situation where the knock integral barely reaches unity. The fixed model can still survive since combustion efficiency is still 100%; while the new model dies out due to very poor combustion efficiency.

This series of comparison demonstrate that the old fixed combustion efficiency and burning duration model can operate the model engine in unrealistic region, thus it falsely expands the engine operation range.

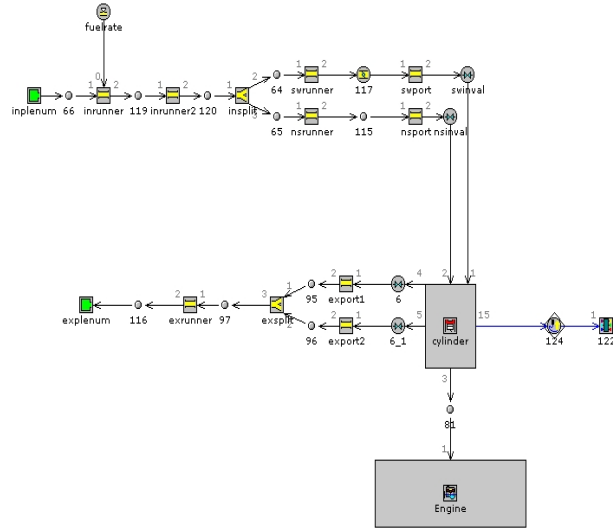


Figure 6.1 – GT-Power model map of UM engine

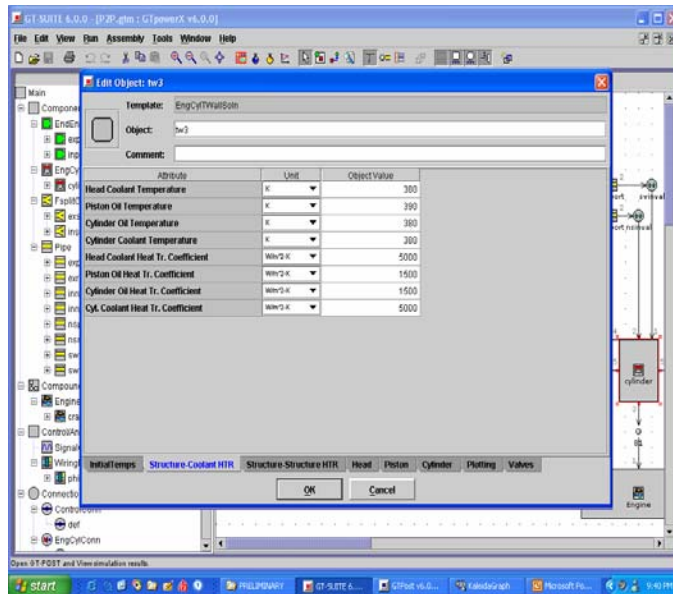


Figure 6.2 – GT-Power user subroutine interface

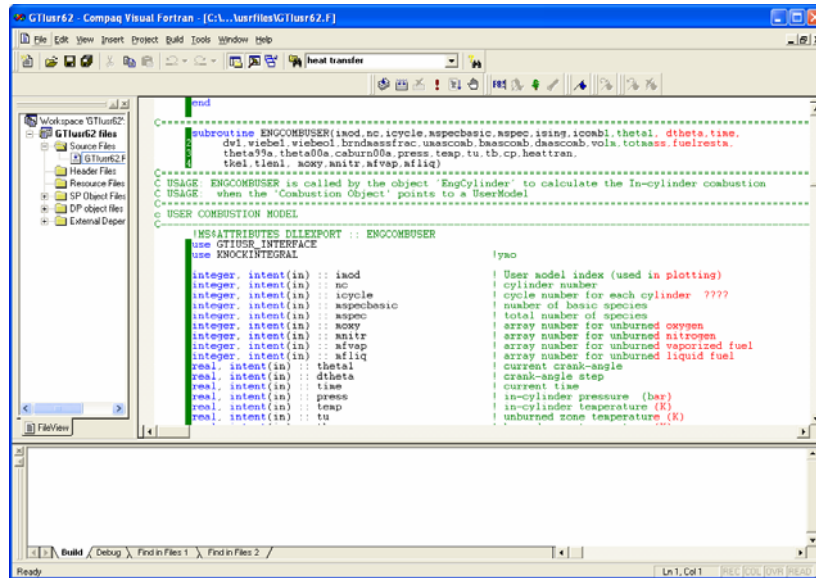


Figure 6.3 – GT-Power FORTRAN interface

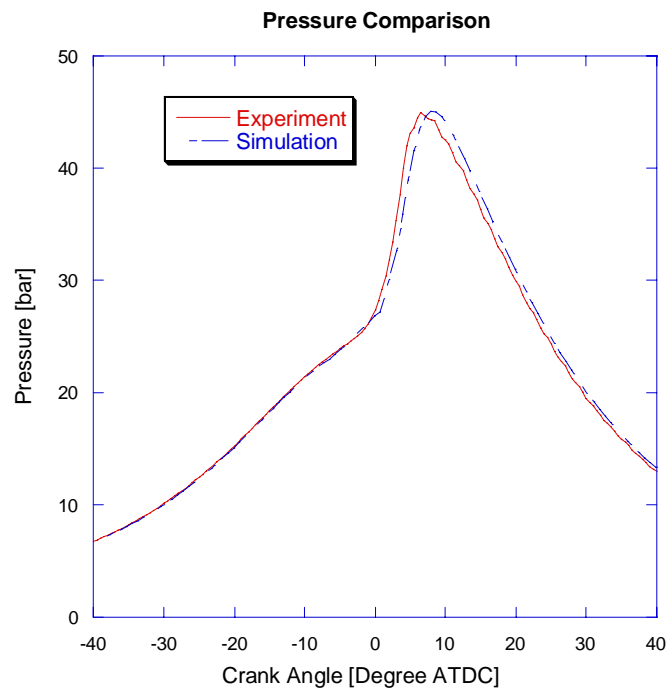


Figure 6.4 - Pressure comparison for calibration point between GT-Power model and UM HCCI engine

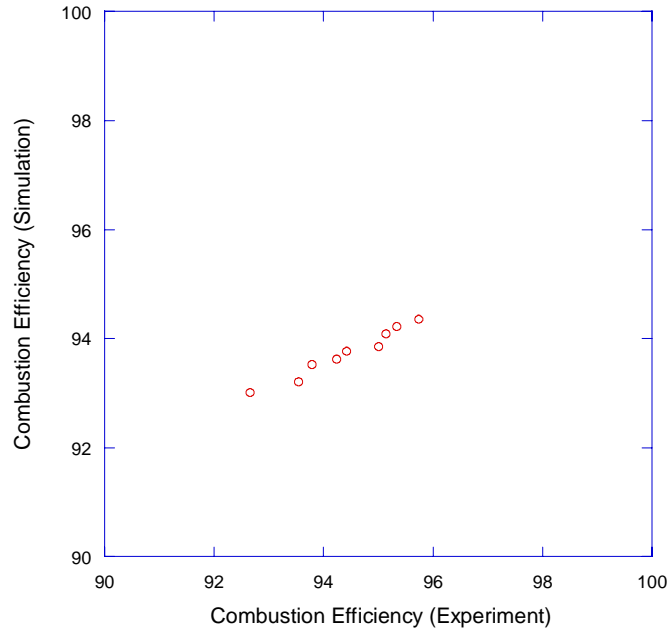


Figure 6.5 - Combustion efficiency validation comparison between GT-Power model and UM HCCI engine

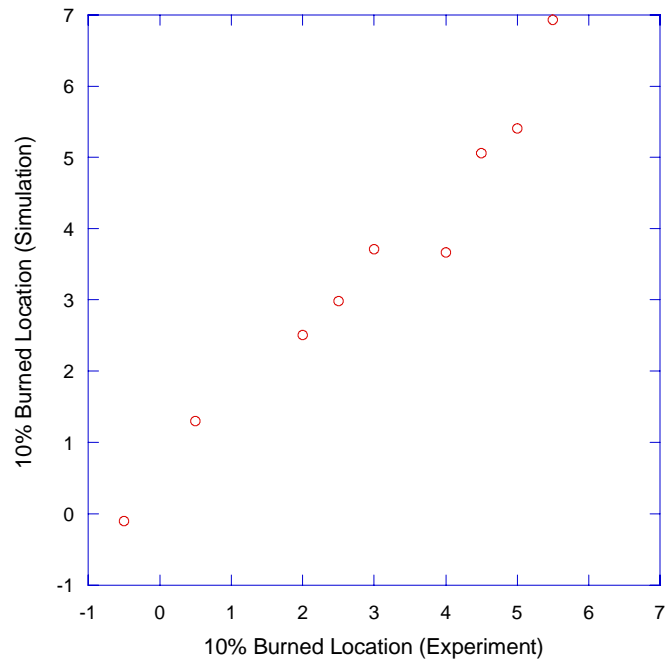


Figure 6.6 - 10% burned location validation comparison between GT-Power model and UM HCCI engine

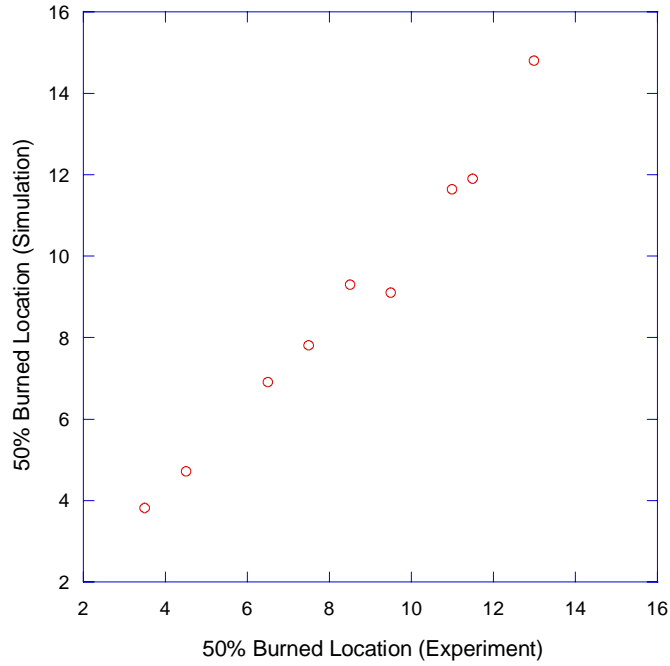


Figure 6.7 - 50% burned location validation comparison between GT-Power model and UM HCCI engine

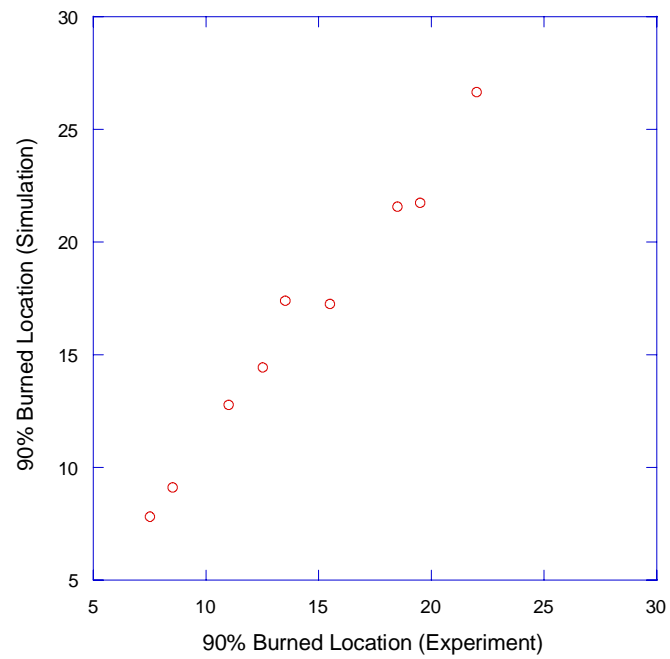


Figure 6.8 - 90% burned validation comparison between GT-Power model and UM HCCI engine

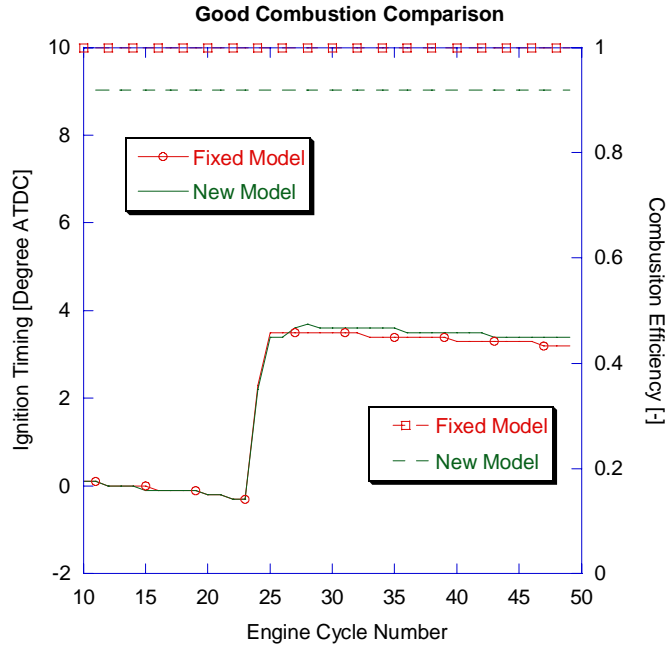


Figure 6.9 - Comparison between fixed value model and new combustion model in stable transition

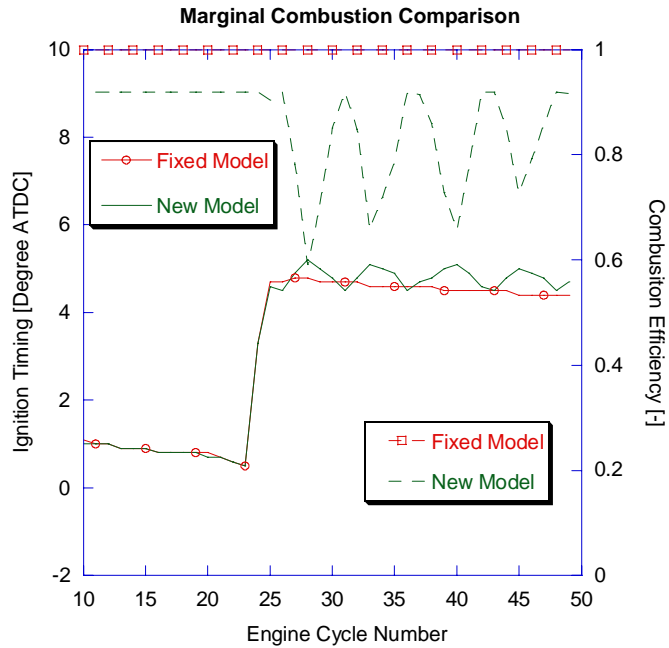


Figure 6.10 - Comparison between fixed value model and new combustion model in unstable transition

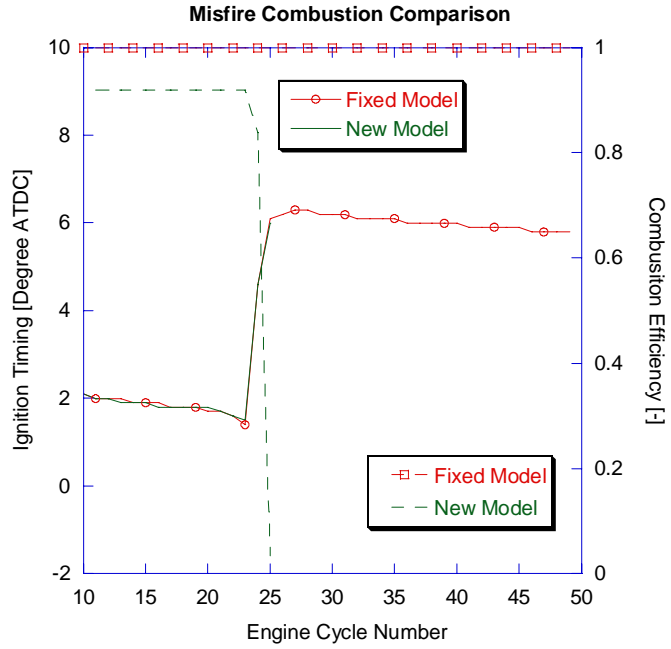


Figure 6.11 - Comparison between fixed value model and new combustion model in misfire transition

CHAPTER 7

HCCI TRANSIENT STUDY

Among all the challenges to HCCI implementation, the most difficult one is the ignition timing control. As demonstrated in the previous chapters, many factors can affect ignition timing. These factors take effect in a wide spectrum of frequency. For example, sudden increase of fuel quantity can take effect within a couple of cycles for its equivalence ratio impact; while its effect on ignition timing by engine wall temperature change won't take effect until much later. The fact that many variables affects ignition timing and they work in different timings makes ignition timing control extremely difficult. The important factors regarding ignition control mechanism are timing and range.

Timing measures the duration from the change of actuator to the actual effect take place. Obviously, shorter timing is desired. Range measures the extents that ignition timing can be changed from the two end values of actuator. This can be limited by the physical dimension and other engine operating and performance constraints.

The GT-Power engine model with new HCCI correlations developed in this research work provides an engine simulation capable of more realistic misfire prediction, thus provides more credible evaluation of control strategy.

Residual gas reuse has been a popular approach for heating up the cylinder charge to assist ignition. However, this approach has fairly large temperature and composition gradients. The correlations developed with KIVA-MZ are under relatively homogeneous

conditions. The correlations won't be able to capture the effects caused by severe non-homogeneity. Thus, in the strategy analyzed below, engine is running at relatively low residual fraction.

The objective of this chapter is to investigate the characteristics of a specific control strategy. First, the control concept is introduced, and then steady state operations data is obtained. Finally, engine transient operation is examined.

7.1 Tow Stage Temperature Control Engine

A model engine is built within GT-Power framework. The simulation engine uses most of the configuration of the UM HCCI engine except the valve train. Solenoid valves are used instead of rebreathing valves to give flexible control of intake valve closing timing. Figure 7.1 shows the schematic of the engine model. The two streams of air mix together before the fuel supply (Figure 7.2).

The ignition timing control is not through residue trapping, instead, there are two mechanisms to regulate the cylinder temperature: intake mixing valve and variable intake valve closing timing. Intake mixing valve is used to regulate the intake air temperature, and variable intake valve closing timing is used to control the effective compression ratio.

The idea to use the combination of intake temperature and effective compression ratio is from the KIVA parametric study. The intake temperature and compression ratio are the two most important factors for ignition timing. However, the responds timings of intake temperature change by mixing valve may not quick enough for engine transient. To compensate for the response timing, effective compression ratio can be achieved by varying the intake valve closing timing.

7.1.1 Intake Mixing Valve

The intake mixing valve regulates two streams of intake air with different temperatures. One is at ambient temperature with ambient pressure; the other is at 500 Kelvin with higher pressure. The mixing valve is on the high temperature side since this stream has higher pressure. Fully closing this valve turns this engine system back to normal aspiration intake system. The valve opening angle is the main parameter determining the flow rate from the high temperature stream. However, the pressure at the engine intake ports can not only influence the overall intake flow rate, but also the relative ratio of the mixture. So the dynamics between the valve angle and the intake port vacuum can be a critical factor for the control of this type of engine.

7.1.2 Variable Intake Close Timing

Compression ratio is very important for HCCI engine, if not more important than in traditional diesel and gasoline engines. The temperature requirement for auto ignition is achieved by piston compression. There are two major ways to vary the piston compression heating on cylinder charger: geometrically and effectively.

The definition of compression ratio is geometry based, and there are three ways to vary the geometric compression ratio: cylinder head, crank shaft, and piston. Moving cylinder head or crank shaft up and down relative to each other can change the engine sweep volume, clearance volume, and their ratio. Reactive piston can increase the clearance volume over the compression stroke. All these geometric based methods involve complicated structure in the engine system, and are very expensive to implement.

Other than geometric compression ratio, real compression heating to the cylinder charger also involves the valve timing. Late intake valve closing can effectively reduce the compression heating, thus reduce the charge temperature. In this chapter, the intake

valve closing timing is controlled by solenoid valve, and it is one of the two major control mechanisms.

7.2 Steady State Sensitivity Study

The main focus of the study is to investigate the combustion characteristics of different combination of mixing angle and intake close timing under different engine speed and load conditions. Under this study, the effective range of each control method is measured under certain engine operating conditions.

There are two parts of the study. First part presents results of two dimensional sweeps of mixing angle and intake closing timing. This study is performed under two engine operating conditions: one with lower engine speed and leaner mixture; the other with higher engine speed and richer mixture. Second part reveals the interactions between engine speed and mixing valve, which stands out in the study of the first part.

7.2.1 Mixing Angle and Intake Closing Timing

The effect of mixing angle and intake closing timing on combustion is investigated under two engine operating conditions. One has engine speed set at 1000 rpm, and air fuel ratio set at 65, the other with engine speed set at 2000 rpm and air fuel ratio set at 45.

The mixing angle ranges from 5 degrees open to 75 degrees open with 5 degree increments. At the fully close position, the engine is running with pure ambient air. With more valve opening, more hot air gets into the intake system. Intake closing timing varies from BDC to 60 degrees after BDC with 10 degree increments. In this study, “0 degree” is assigned to gas exchange TDC. So gas exchange BDC is 540 in crank angle

measurement (-180 is the same as 540 as cycle period is 720). Table 7.1 lists the engine geometry:

Table 7.1 - Simulation engine parameters

Engine Bore (mm)	86
Engine Stroke (mm)	94.6
Connecting Rod Length (mm)	152.2
Compression Ratio	14
TDC Clearance Height (mm)	1
Intake Valve Diameter (mm)	34.5
Exhaust Valve Diameter (mm)	31

It is a single cylinder engine with two intake valves and two exhaust valves. Two streams of intake air merges together before fuel injector delivering the fuel based on air fuel ratio. Fuel air mixture then splits into two intake runners.

Table 7.2 - Input parameters for two different speed cases

Profile	Low speed, lean mixture	High speed, rich mixture
Engine Speed	1000	2000
Air to Fuel Ratio	65	45
Mixing Angle	5~75	5~75
Intake Valve Close	540~600	540~600
Intake Valve Open	350	350
Exhaust Valve Close	370	370
Exhaust Valve Open	170	170
Intake Temperature (ambient)	300 (K)	300 (K)
Intake pressure (ambient)	0.95 (Bar)	0.95 (Bar)
Intake Temperature (hot)	500	500
Intake Pressure (hot)	1.25	1.25
Exhaust Temperature	750	750
Exhaust Pressure	1.006	1.006

The effect of mixing angle is obvious, as more opening introduces more hot air in the cylinder. The range of this control method can vary the intake temperature from 300 K to near 500 K. This can effectively shift the ignition timing by a large extent.

The range of intake valve closing timing is from 540 to 600, which is corresponding to effective compression ratio from 14 to 10.75.

Figure 7.7 shows characteristics of ignition timing map for low engine speed case. It is found that the effect of mixing angle gets saturated right after 20 degrees. More opening of the mixing valve won't bring more hot air into the cylinder. On the other hand, the effect of intake valve close timing has very significant contribution to ignition timing over its whole range.

Figure 7.5 shows different characteristics of ignition timing than Figure 7.7. Mainly, the effective range of mixing angle has been expanded into wider range. Not like the low engine speed case, continuous opening of the mixing angle introduces more hot air to advance the ignition timing.

Figure 7.4 and Figure 7.6 show that the volumetric efficiency of both cases, which is consistent with ignition timing observation. More mixing valve opening generally reduces the volumetric efficiency since the intake air gets hotter and less dense in density. Again, the low speed case reaches saturation point around 20 degrees, where further opening of mixing valve won't have effect on the flow rate of individual stream of intake.

7.2.2 Engine Speed and Mixing Angle Interaction

As apparent from the previous section, the effect of intake close timing is fairly stable by itself, but the interaction between engine speed and mixing angle is very strong, higher engine speed expands the effective range of mixing angle on ignition timing. So a study covering wider range of engine speed is performed.

In the following study, intake valve close timing is fixed at 560, which is 20 degrees ABDC.

Three air fuel ratio cases are investigated with variations of engine speed and mixing angle.

Figure 7.7 shows the interactions between engine speed and mixing angle on ignition timing with air fuel ratio around 45. At the low speed end, when engine speed is lower than 1500, there's a saturation point where more mixing angle won't introduce more hot air. The saturation point is about 10 degrees for 500 rpm, and 20 degrees for 1000 rpm. At the high speed end, the lines for 2500 and 3000 rpm are significantly closer than other neighboring lines, so there's also a speed saturation point. Before

engine speed hits the saturation point, increasing engine speed always improves low pressure ambient intake.

Figure 7.8 and Figure 7.9 show the similar patterns except the effective range of mixing angle is shorter at higher engine speed. With leaner mixture, the minimum mixing angle to avoid misfire is increased.

7.3 Single Step Transient Study

In order to examine the relative response times of each parameter in this engine system, single step change study is performed. Temperature measurements are made right before intake valve. By measuring the temperatures of this spot, the dynamic effects of engine speed, load, mixing angle, and intake valve closing timing can be better reviewed.

For each parameter, two step changes is made with one upward step and one downward step.

7.3.1 RPM Step Change

GT-Power simulation is used to capture the transitions between two engine speeds: 1000 rpm and 2000 rpm. For the engine speed step change, the mixing angle is fixed at 30 degrees, air fuel mixture is fixed at 45, and intake valve close timing is fixed at 20 degrees ABDC.

For both upward and downward step change, the transition happens between 20th and 21th engine cycle.

As shown in Figure 7.10 and Figure 7.11, change of engine speed creates a peak immediately, and then it stabilizes after several cycles. The peak is opposite in the direction of the stabilized trend of engine speed effect. This transition study reflects the

observation in Figure 7.8, which says that higher engine speed creates higher vacuum to enhance the low pressure intake. Both results are apparent in the transition study.

7.3.2 Air Fuel Ratio Step Change

Air fuel ratio step change switches value between 45 and 55. The mixing angle is fixed at 30 degrees, engine speed is fixed at 2000, and intake valve close timing is fixed at 20 degrees ABDC.

The main effect of equivalence ratio is based on two factors: one is the chemical kinetics effect on ignition; the other is the combustion temperature effect on the intake system. Both upward and downward transitions (Figure 7.12 and Figure 7.13) show very small variations in ignition timing.

7.3.3 Mixing Valve Angle

Mixing valve shifts between 20 degrees and 30 degrees. The air fuel ratio is fixed at 45, engine speed is fixed at 2000, and intake valve close timing is fixed at 20 degrees ABDC.

The effect of mixing valve is quite simple. It is all about the temperature of the intake. The response time is about 6 or 7 cycles for both upward and downward shifts (Figure 7.14 and Figure 7.15). This cycle value is mainly determined by the total volume of the intake system. Larger volume the intake system is, longer the response time is.

7.3.4 Intake Valve Close Timing

Intake valve close timing shifts between 10 degrees ABDC and 30 degrees ABDC. For mixing angle step change, the air fuel ratio is fixed at 45, engine speed is fixed at 2000, and mixing valve angle is fixed at 30 degrees.

Again, Figure 7.16 and Figure 7.17 show that immediate response is in active, the immediate overshoot is caused by the immediate change of effective compression ratio. The stabilized value is based on the reduced vacuum been build up with delayed close timing.

7.3.5 Summary of Two Stage Temperature Control Strategy

The time delay of the mixing valve is determined by the total volume in the intake system. Larger volume has longer delay. In the same time, the interaction between the mixing valve and engine speed is quite complicated. When engine speed is very low, the overall flow rate is low, and the pressure difference between the high pressure steam and the cylinder is comparable to the difference between the high pressure steam and the low pressure steam. So the opening angle of the mixing valve almost has no effect on the flow rate. On the other hand, when the engine speed is very high, the flow rate is proportional to the valve opening. However, the engine speed itself reaches certain limit that higher engine speed cannot enhance the flow rate further.

The intake valve closing timing is a viable method to stabilize HCCI transition process because of its quick response. There are two major mechanisms that intake valve closing timing can affect HCCI combustion. One is the effective compression ratio; the other is its effect on engine vacuum. Effective compression ratio takes effect instantaneously, while engine vacuum effect has similar response time scale as mixing valve.

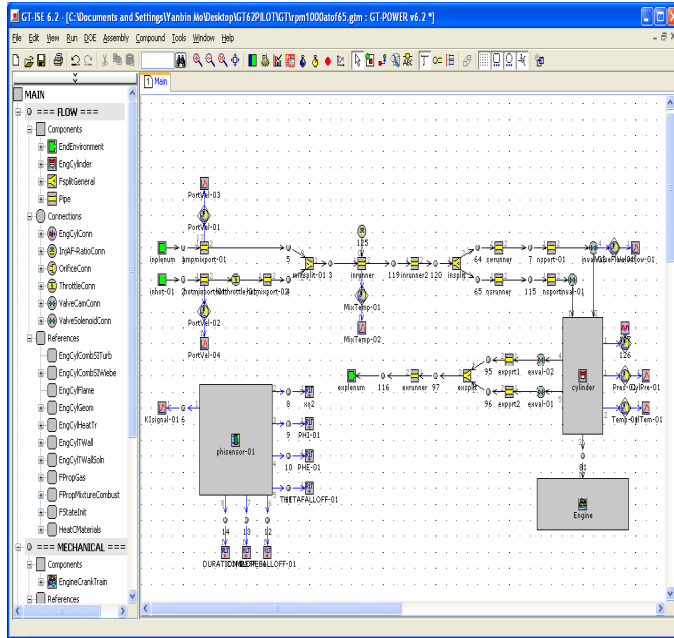


Figure 7.1 – GT-Power model map of two stage temperature control engine

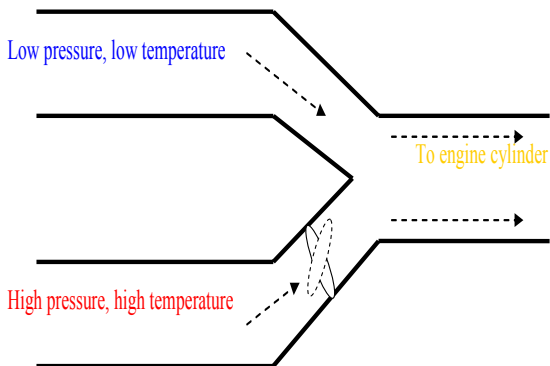


Figure 7.2 – Mixing junction schematics

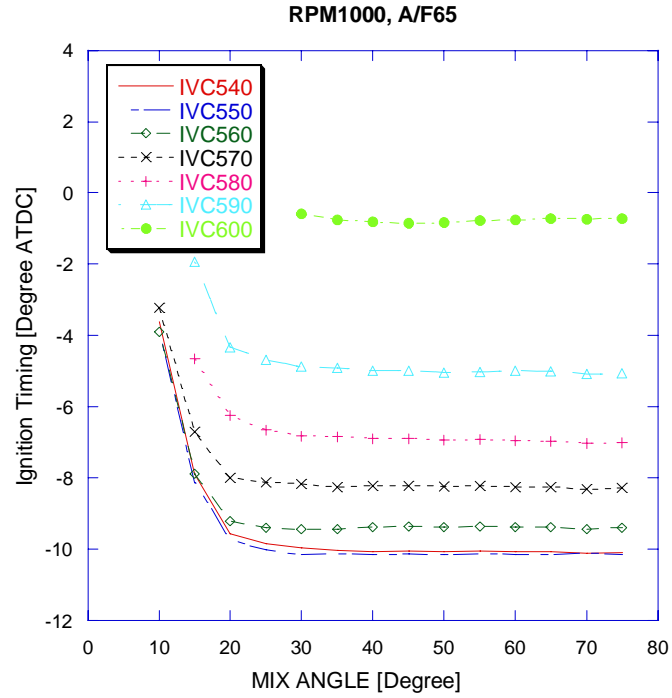


Figure 7.3 - Ignition timing map with variations of intake valve close timing and mixing angle under rpm 1000 and air fuel ratio 65

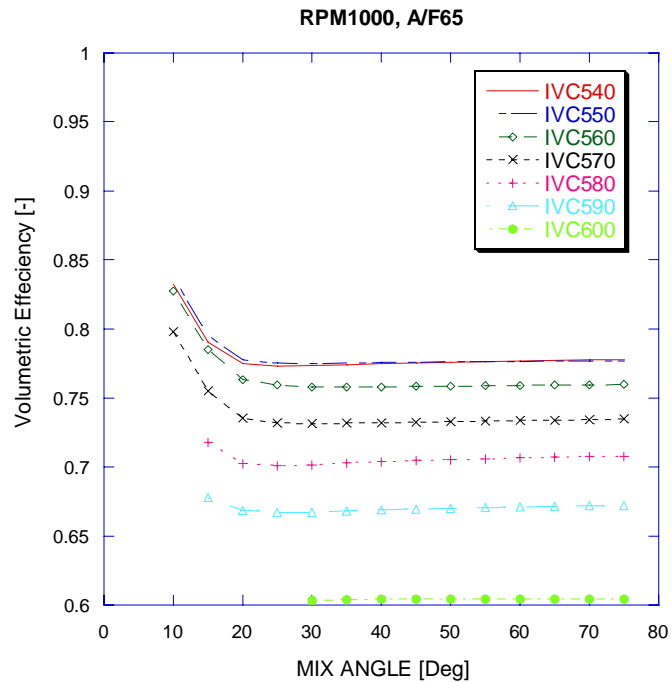


Figure 7.4 – Volumetric efficiency map with variations of intake valve close timing and mixing angle under rpm 1000 and air fuel ratio 65

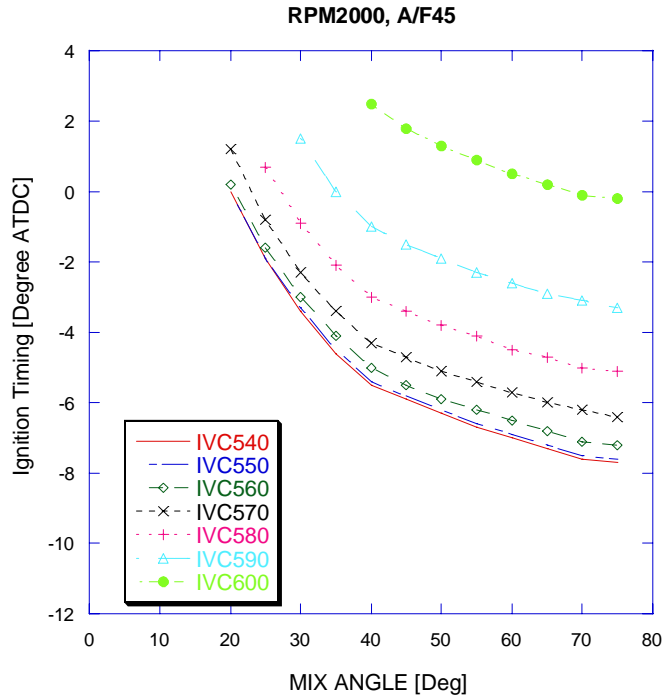


Figure 7.5 - Ignition timing map with variations of intake valve close timing and mixing angle under rpm 2000 and air fuel ratio 45

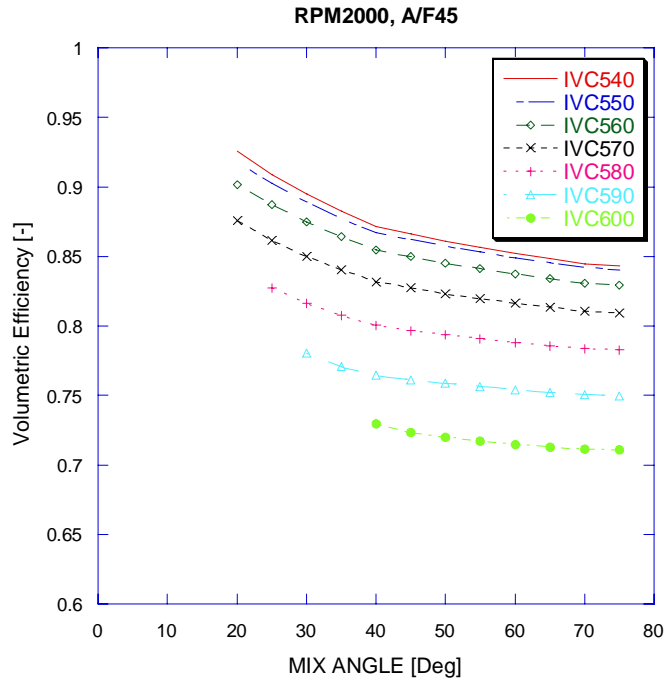


Figure 7.6 – Volumetric efficiency map with variations of intake valve close timing and mixing angle under rpm 2000 and air fuel ratio 45

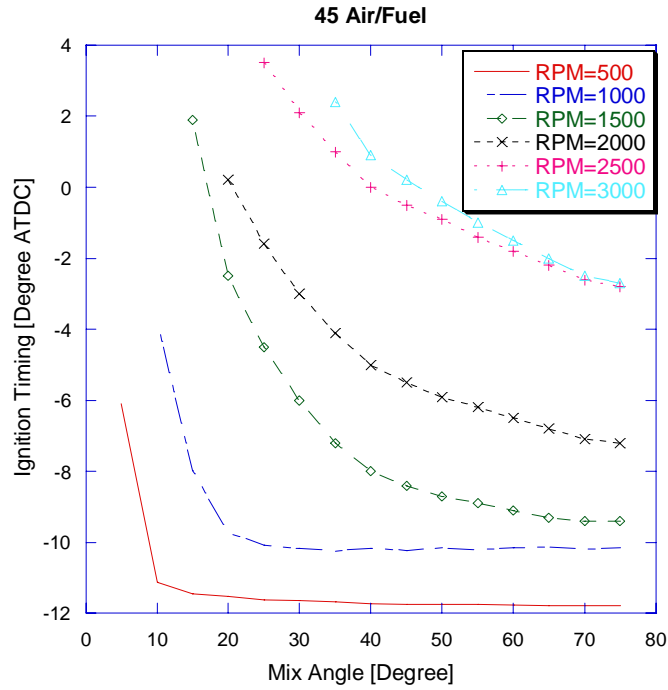


Figure 7.7 - Ignition timing map with variations of engine speed and mixing angle for air fuel ratio at 45

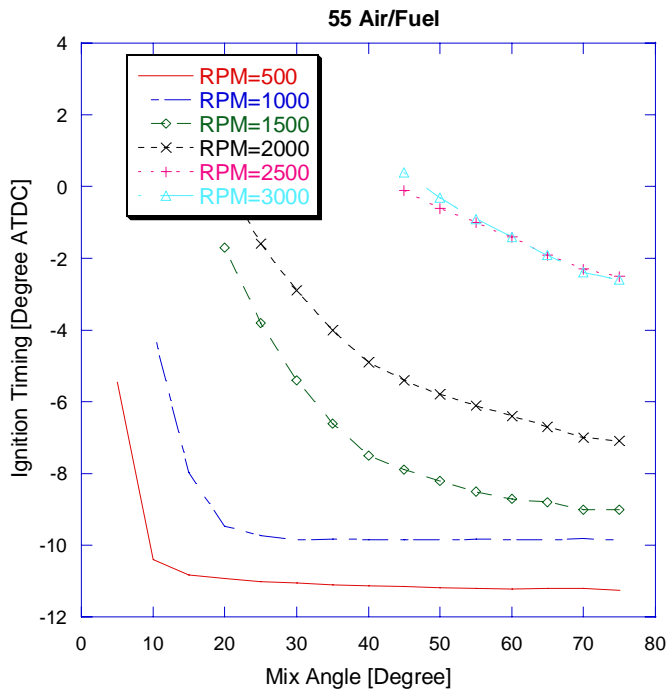


Figure 7.8 - Ignition timing map with variations of engine speed and mixing angle for air fuel ratio at 55

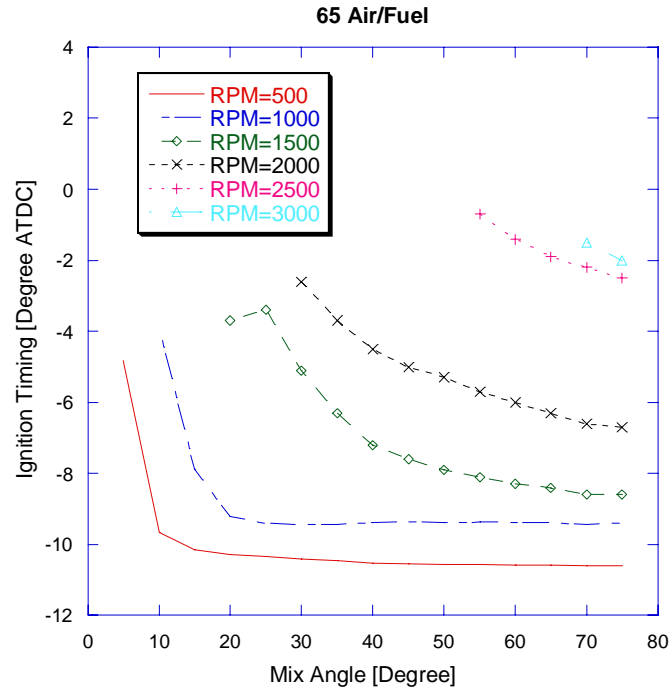


Figure 7.9 - Ignition timing map with variations of engine speed and mixing angle for air fuel ratio at 65

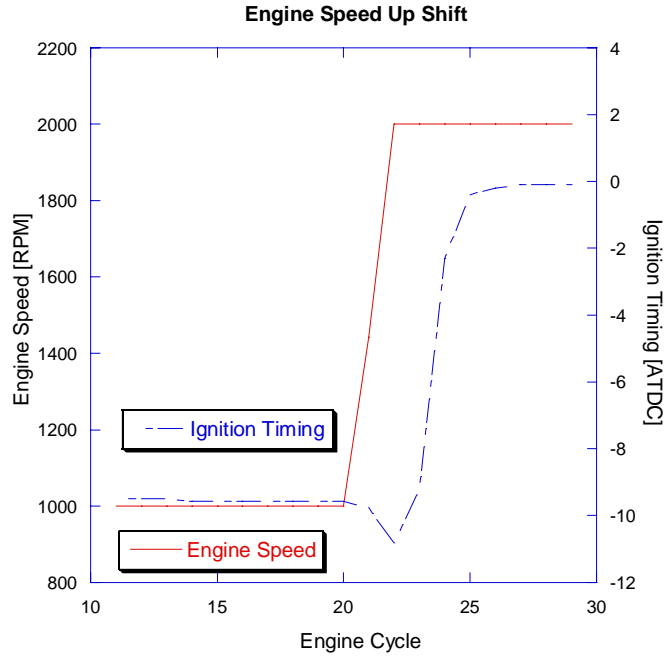


Figure 7.10 - Ignition timing response to sudden increase of engine speed

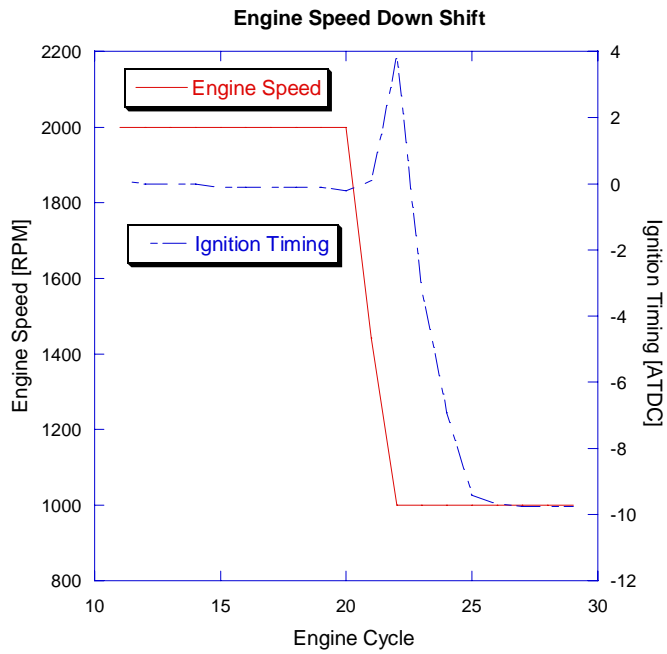


Figure 7.11 - Ignition timing response to sudden decrease of engine speed

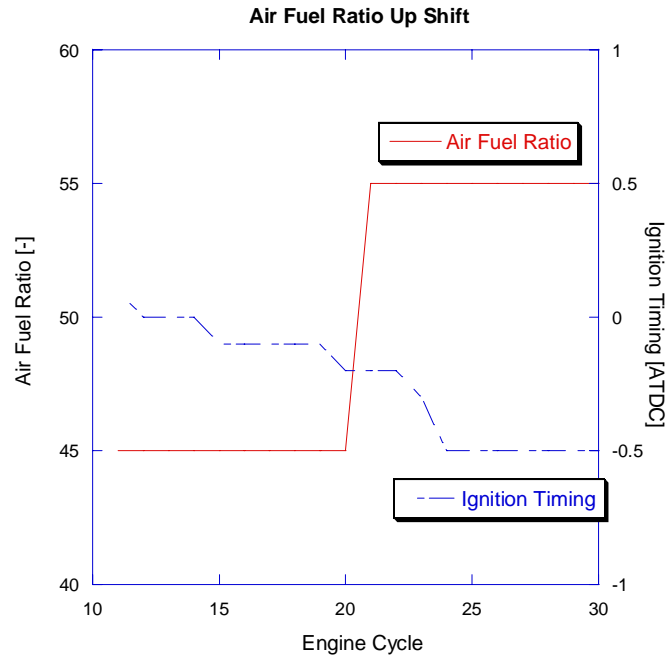


Figure 7.12 - Ignition timing response to sudden increase of air fuel ratio

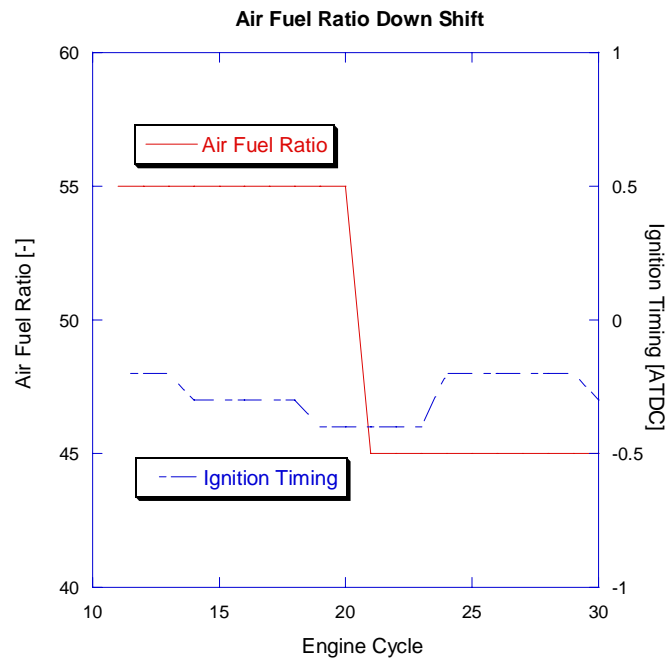


Figure 7.13 - Ignition timing response to sudden decrease of air fuel ratio

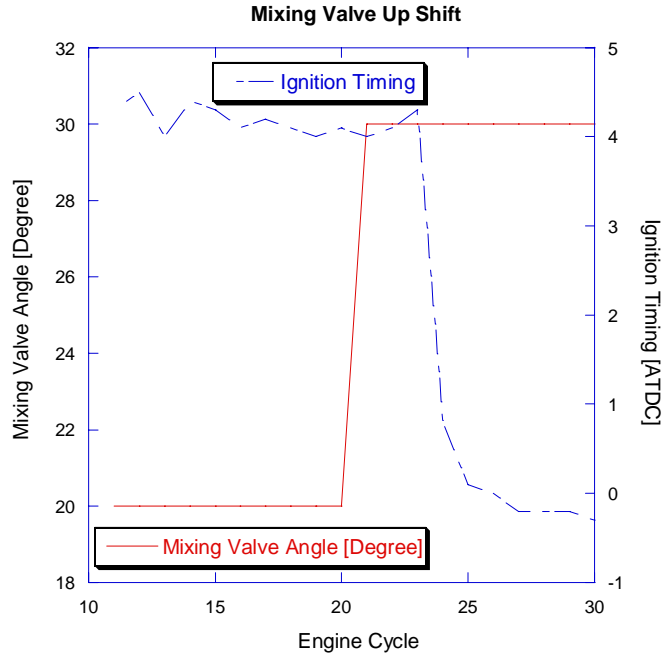


Figure 7.14 - Ignition timing response to sudden increase of mixing valve opening

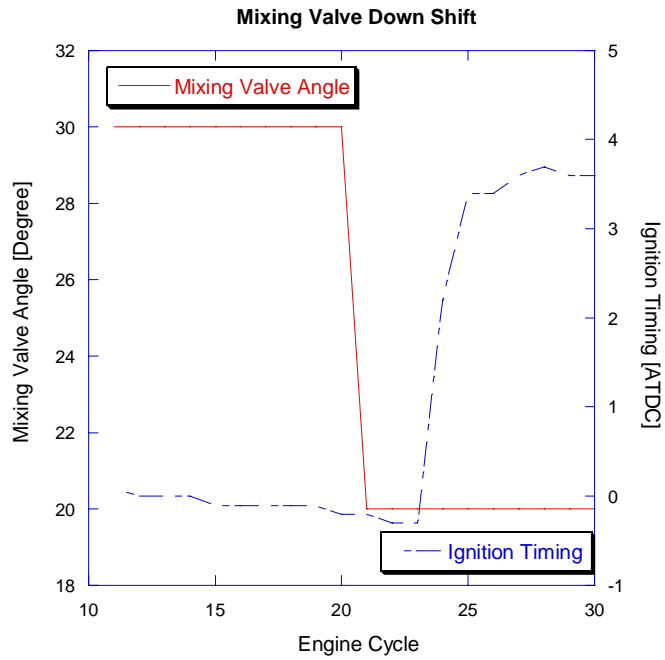


Figure 7.15 - Ignition timing response to sudden decrease of mixing valve opening

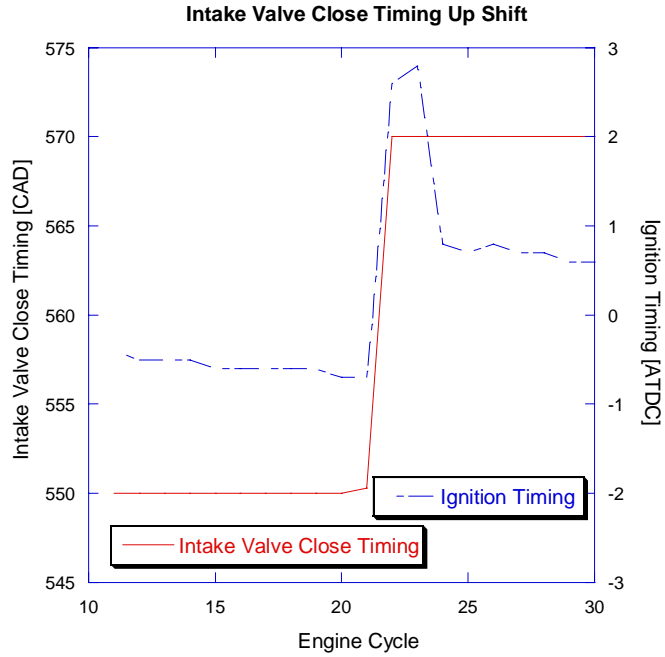


Figure 7.16 - Ignition timing response to sudden increase of intake valve close timing

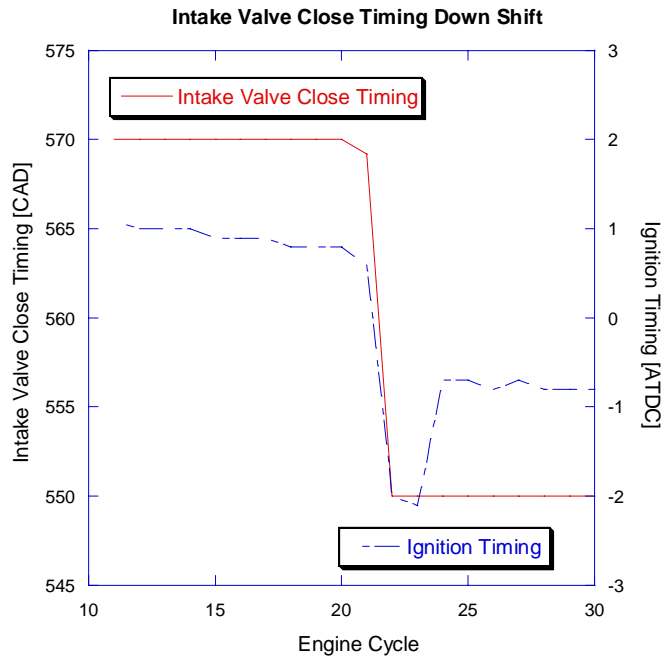


Figure 7.17 - Ignition timing response to sudden increase of intake valve close timing

CHAPTER 8

CONCLUSIONS AND SUGGESTIONS

In the chapters above, the relationship between ignition timing and rate of heat release is investigated using CFD simulation tool KIVA-MZ with fully integrated chemical kinetics. The dominance of ignition timing on combustion rate is demonstrated. Other parameters' effects on heat release are also examined, both with the same intake temperature and the same ignition timing. Utilizing the KIVA results, correlations are developed for HCCI combustions. These correlations are implemented into GT-Power, a commercial engine simulation software. This new 1-D simulation tool is utilized for a control strategy study.

8.1 Summary and Conclusions

Because of the lack of direct control of ignition timing on HCCI engine, the requirement of control study on HCCI engine is far more than the requirement of any other conventional engine. Typical engine control study involves thousand of engine cycles, which demands a very efficient engine simulation. Current HCCI combustion models are based on very simple formations. The ignition timing is predicted by a knock integral equation. Then prefixed combustion efficiency and burning duration values are applied if the ignition does occur. Overall, current correlations are an “on” and “off”

systems according to ignition. In reality, earlier ignition leads to more complete combustion and shorter burning duration; later ignition results in less complete combustion and longer duration. In current literature, there's no HCCI combustion correlation that accounts for the variability of combustion efficiency and burning duration according to ignition timing.

The significance of ignition timing on combustion rate in HCCI engine is obvious from various experimental data. However, ignition timing itself is not enough to correlate combustion efficiency and burning duration. What are the other variables? How are they determined? What are the structures for the correlations? These questions are solved by using CFD simulation tool KIVA-MZ. The engine model only calculates the closed part of the engine cycle.

Each engine design and operation variable goes through two or more sets of sweep studies. For each set of study, each of the variable under study gets an intake temperature swept. These studies can not only reveal how one variable can affect the combustion as a whole, but also give information on how it affects combustion efficiency and burning rate at similar ignition timing

Intake temperature is a unique variable because its effect on combustion is purely depended on its influence on ignition timing. So intake temperature can be used as a compensator to ensure similar ignition timing out of two cases when comparing two values of another variable.

Sweep studies of 9 engine design and operation variables show that each of them changes ignition timing more or less, thus combustion efficiency and burning duration. In general, earlier ignition case has faster and more complete combustion. Individual case is discussed in the following.

Equivalence ratio comparison shows some counter-intuitive results. Under the same intake temperature, leaner mixture has much stronger combustion. The reason is that leaner mixture has higher gamma value, thus reaches higher compression

temperature, which leads to earlier ignition. The advanced phasing of leaner mixture helps reach higher peak pressure; however, richer mixture still has higher peak temperature. When comparing two equivalence ratio cases with similar ignition timing, the trend is reversed. Richer mixture has much faster combustion and it has higher pressure and temperature.

Engine load is investigated under the same equivalence ratio to eliminate the known effect of equivalence ratio. The focus is solely on the effect of fuel quantity. Under the same intake temperature condition, the higher load case has earlier ignition and faster combustion. With the same equivalence ratio, more fuel means more air, so the initial pressure is higher for the higher load case. However, when comparing two load cases with similar ignition timing, the combustion progress is very close.

EGR gas, residual gas, or more straightforward, combustion product gas is used to reduce combustion temperature in diesel engine. In this study, initial pressure is maintained at constant and fresh air is replaced with EGR gas. Higher EGR gas has smaller value of gamma and lower concentration of oxygen, so the higher EGR case has later ignition timing, thus slower combustion. The study under the same ignition timing reveals that gamma value and oxygen concentration only have significant effect on ignition timing itself, but not the whole combustion process.

Engine speed is quite complicated to analyze because the result is a tradeoff of two counteracting factors. Lower engine speed allows more time for heat loss to the cylinder wall, but at the same time, it allows more time for chemical reaction. Under current study, the lower engine speed case has earlier ignition, which seems that chemical reaction time is the more dominating force. Under similar ignition timing, the advantage of slower engine speed allowing more reaction time is even more obvious.

Cylinder wall temperature and swirl number are studied together. As expected, higher wall temperature and lower swirl number result in earlier ignition because of less

heat loss to the wall. This is also true when comparing under similar ignition, higher wall temperature and lower swirl case ends up with faster combustion.

Overall, piston geometry doesn't cause high degree of variation on ignition and combustion rate. But there's apparent difference in peak heat release rate. Pancake chamber has higher peak heat release rate, while bowl shape has a double hump and lower peak heat release rate. This implies that because of simple geometry, pancake combustion chamber has more uniform temperature distribution, while bowl in piston shape chamber have multiple local temperature maxima.

Crevice volume can have very big impact on ignition and combustion. First of all, the combustion efficiency is highly correlated to the crevice volume since most mixture trapped in the crevice won't react and combust. With the same intake temperature, smaller crevice volume has earlier and faster combustion. With similar ignition timing, the combustion rate is comparable despite of difference in combustion efficiency.

Compression ratio is by far the biggest difference maker. There's no comparison with the same intake temperature because the reasonable intake temperature ranges for both cases don't overlap. The comparison with similar ignition shows that combustion rate is comparable. With higher compression ratio, the combustion rate is a little faster. This advantage gets diminished when ignition timing is closer to TDC. The explanation is that higher compression ratio case has higher effective compression from the point of ignition to TDC.

8.2 Suggestions for Future work

This dissertation work provides the foundation for future research on simulation study of HCCI engine control. The combustion efficiency and burning duration

correlations provide realistic behavior of misfire and combustion rate, yet high computational efficiency. The future work will involve both improvement on the correlations and applications of these correlations:

- For engines with different degree of composition heterogeneity, the relationship between ignition timing and subsequent combustion process will be different. KIVA-MZ will be employed to understand the phenomena and quantify a variable to represent composition heterogeneity. The added composition heterogeneity variable will be examined by the same methodology applied in this work and implemented into the correlations.

- Integrate the combustion correlations into GT-Power engine model with transient cylinder wall thermal network and cooling system. This will provide accurate prediction for transient HCCI engine operation.

- Evaluate various HCCI control concepts, including turbo-charged dual model HCCI engine. With variable valve timing and throttle valve controlling the mixture of ambient air and charged air, combustion phasing can be controlled by altering both the effective compression ratio and the intake temperature.

BIBLIOGRAPHY

Aceves, S. M., Flowers, D. L., Espinosa-Loza, F., Babajimopoulos, A., and Assanis, D. N., "Analysis of Premixed Charge Compression Ignition Combustion with a Sequential Fluid Mechanics-Multizone Chemical Kinetics Model," SAE Paper 2005-01-0115, 2005.

Aceves, S. M. Flowers, D. L., Espinosa-Loza, F., Martinez-Frias, J., Dibble, R., Christensen, M., and Johansson, B., and Hessel. R. P., "Cylinder Geometry Effects on HCCI Combustion by Multi-Zone Analysis," SAE paper 2002-01-2869.

Aceves, S. M., Flowers, D. L., Martinez-Frias, J., Smith, J. R., Westbrook, C. K., Pitz, W. J., Dibble, R., Wright, J. F., Akinyemi, W. C., and Hessel, R. P., "A Sequential Fluid-Mechanic Chemical Kinetic Model for Propane HCCI Combustion," SAE paper 2001-01-1027.

Aceves, S., M., Flowers, D. L., Westbrook, C. K., Smith, J. R., Pitz, W. J., Dibble, R., Christensen, M., and Johansson, B., "A Multi-Zone Model for Prediction of HCCI Combustion and Emissions," SAE paper 2000-01-0327.

Aceves, S. M., Martinez-Frias, J., Flowers, D. L., Smith, J. R., Dibble, R. W., and Chen, J. Y., "A Computer Generated Reduced Iso-Octane Chemical Kinetic Mechanism Applied to Simulation of HCCI Combustion," SAE Paper 2002-01-2870, 2002.
Aceves, S. M., Martinez-Frias, J., Flowers, D. L., Smith, J. R., Dibble, R. W.,

Wright, J. F., and Hessel, R. P., "A Decoupled Model of Detailed Fluid Mechanics Followed by Detailed Chemical Kinetics for Prediction of Iso-octane HCCI Combustion," SAE Paper 2001-01-3612, 2001.

Aceves, S. M., Smith, J. R., Westbrook, C. K., and Pitz, W. J., "Compression Ratio Effect on Methane HCCI Combustion," Journal of Engineering for Gas Turbine and Power, Vol. 121, 569-574, 1999.

- Agarwal, A., and Assanis, D., "Multi-Dimensional Modeling of Natural Gas Ignition under Compression Ignition Conditions Using Detailed Chemistry," SAE Paper 980136, 1998.
- Agrell, F., Angstrom, H., Eriksson, B., Wikander, J., and Linderyd, J., "Integrated Simulation and Engine Test of Close loop HCCI Control by Aid of Variable Valve Timing," SAE paper 2003-01-0748.
- Agrell, F., Angstrom, H., Eriksson, B., Wikander, J., and Linderyd, J., "Transient Control of HCCI through Combined Intake and Exhaust Valve Actuation," SAE paper 2003-01-3172.
- Agrell, F., Angstrom, H., Eriksson, B., Wikander, J., and Linderyd, J., "Transient Control of HCCI Combustion by Aid of Variable Valve Timing Through the Use of an Engine State Corrected CA50-Controller Combined With an In-Cylinder State Estimator Estimating Lambda," SAE paper 2005-01-2128.
- Allen, J., and Law, D., "Variable Valve Actuated Controlled Auto-Ignition: Speed Load Maps and Strategic Regimes of Operation," SAE Paper 2002-01-0422
- Amsden, A. A., "KIVA-3: A KIVA Program with Block-Structured Mesh for Complex Geometries", Los Alamos National Laboratory Report LA-12503-MS, 1993.
- Amsden, A. A., "KIVA-3V: A Block-Structured KIVA Program for Engines with Vertical or Canted Valves", Los Alamos National Laboratory Report LA-13313-MS, 1997.
- Amsden, A. A., "KIVA-3V: A Block-Structured KIVA Program for Engines with Vertical or Canted Valves", Los Alamos National Laboratory Report LA-13313-MS, 1997.
- Amsden, A. A., Ramshaw, J. D., O'Rourke, P. J., and Dukowicz, J. K., "KIVA: A Computer Program for Two- and Three-Dimensional Fluid Flows with Chemical Reactions and Fuel Sprays", Los Alamos National Laboratory Report LA-10245-MS, 1985.

- Amsden, A. A., O'Rourke, P. J., and Butler, T. D., "KIVA-II: A Computer Program for Chemically Reactive Flows with Sprays", Los Alamos National Laboratory Report LA-11560-MS, 1989.
- Amsden, A. A., "KIVA-3: A KIVA Program with Block-Structured Mesh for Complex Geometries", Los Alamos National Laboratory Report LA-12503-MS, 1993.
- Aoyama, T., Hattori, Y., Mizuta, J., and Sato, Y., "An Experimental Study on Premixed-Charge Compression Ignition Gasoline Engine," SAE paper 960081.
- Babajimopoulos, A., Assanis, D. A., and Fiveland, S. B., "Modeling the Effects of Gas Exchange Process on HCCI Combustion and an Evaluation of Potential Control through Variable Valve Actuation," SAE paper 2002-01-2829.
- Babajimopoulos, A., Lavoie, G. A., and Assanis, D. N., "Modeling HCCI Combustion with High Levels of Residual Gas Fraction - A Comparison of Two VVA Strategies," SAE paper 2003-01-3220.
- Bengtsson, J., Strandh, P., Johansson, R., Tunestal, P., and Johansson, B., "Multi-Output Control of a Heavy Duty HCCI Engine Using Variable Valve Actuation and Model Predictive Control," SAE paper 2006-01-0873.
- Bhave, A., Kraft, M., Mauss, F., Oakley, A., and Zhao, H., "Evaluating the EGR-AFR Operating Range of a HCCI Engine", SAE paper 2005-01-0161.
- Cairns, A., and Blaxill, H., "The Effects of Combined Internal and External Exhaust Gas Recirculation on Gasoline Controlled Auto-Ignition," SAE paper 2005-01-0133.
- Caton, P. A., Song, H., Kaahaaina, N. B., and Edwards, C. F., "Strategies for Achieving Residual-Effected Homogeneous Charge Compression Ignition Using Variable Valve Actuation," SAE paper 2005-01-0165.

- Chang, J., "Thermal Characterization and Heat Transfer Study of a Gasoline Homogeneous Charge Compression Ignition Engine via Measurements of Instantaneous Wall Temperature and Heat Flux in the Combustion Chamber," Ph.D. Thesis, 2004, The University of Michigan, Ann Arbor.
- Chang, J., Filipi, Z. S., and Assanis, D. N., "New Heat Transfer Correlation for an HCCI Engine Derived from Measurements of Instantaneous Surface Heat Flux," SAE paper 2004-01-2996.
- Chang, J., Filipi, Z. S., Assanis, D. N., Kuo, T-W., Najt, P., and Rask, R., "Characterizing the Thermal Sensitivity of a Gasoline Homogeneous Charge Compression Ignition Engine with Measurement of Instantaneous Wall Temperature and Heat Flux," International Journal Engine Research, Vol. 6, pp. 289-309, 2005.
- Chang, K., Babajimopoulos, A., Lavoie, G. A., Filipi, Z. S., and Assanis, D. N., "Analysis of Load and Speed Transitions in an HCCI Engine Using 1-D Cycle Simulation and Thermal Networks," SAE paper 2006-01-1087.
- Chiang, C., Stephanopoulos A. G., and Jankovic, M., "Nonlinear Control of Transitions between Thermal Equilibrium in Homogeneous Charge Compression Ignition (HCCI) Engines," 8th International Symposium on Advanced Vehicle Control, AVEC060203, 2006.
- Christensen, M., Einewall, P., and Johansson, B., "Homogeneous Charge Compression Ignition (HCCI) Using Isooctane, Ethanol, and Natural Gas - A Comparison with Spark Ignition Operation," SAE paper 972874.
- Christensen, M., Hultqvist, A., and Johansson, B., "Demonstrating the Multi Fuel Capability for a Homogeneous Charge Compression Ignition Engine with Variable Compression Ratio," SAE paper 1999-01-3679.
- Christensen, M., and Johansson, B., "Homogeneous Charge Compression Ignition with Water Injection," SAE paper 1999-01-0182.

- Christensen, M., and Johansson, B., "Influence of Mixture Quality on Homogeneous Charge Compression Ignition," SAE paper 982454.
- Christensen, M., Johansson, B., Amneus, P., and Mauss, F., "Supercharged Homogeneous Charge Compression Ignition," SAE paper 980787.
- Curran, H. J., Gaffuri, P., Pitz, W. J., and Westbrook, C. K., "A Comprehensive Modeling Study of iso-Octane Oxidation," *Combustion and Flame*, Vol. **129**, pp. 253-280, 2002.
- Dec, J. E., "A Computational Study of the Effects of Low Fuel Loading and EGR on Heat Release Rates and Combustion Limits in HCCI Engines," SAE paper 2002-01-1309.
- Dec, J. E., and Sjöberg, M., "A Parametric Study of HCCI Combustion – the Sources of Emissions at Low Loads and the Effects of GDI Fuel Injection," SAE Paper 2003-01-0752, 2003.
- Dec, J. E., and Sjöberg, M., "Isolating the Effects of Fuel Chemistry on Combustion Phasing in an HCCI Engine and the Potential of Fuel Stratification for Ignition Control," SAE paper 2004-01-0557.
- Eng, J. A., "Characterization of Pressure Waves in HCCI Combustion," SAE paper 2002-01-2859.
- Fiveland, S. B., *Modeling and Experimental Studies of a Large-Bore Natural Gas Engine Operating on Homogeneous Charge Compression Ignition*, Ph.D. Thesis, University of Michigan, Ann Arbor (2001).
- Fiveland, S. B., Assanis, D. N., "A Four-Stroke Homogeneous Charge Compression Ignition Engine Simulation for Combustion and Performance Studies," SAE Paper 2000-01-0332.

- Fiveland, S. B., Assanis, D. N., "Development of a Two-Zone HCCI Combustion Model Accounting for Boundary Layer Effects," SAE paper 2001-01-1028.
- Fiveland, S. B., Assanis, D. N., "Development and Validation of a Quasi-Dimensional Model for HCCI Engine Performance and Emissions Studies under Turbocharged Conditions," SAE paper 2002-01-1757.
- Flowers, D., Aceves, S., Martinez-Frias, J., Hessel, R., and Dibble, R., "Effect of Mixing on Hydrocarbon and Carbon Monoxide Emissions Prediction for Isooctane HCCI Engine Combustion Using a Multi-zone Detailed Kinetics Solver," SAE Paper 2003-01-1821, 2003.
- Flowers, D., Aceves, S., Smith, R., Torres, J., Girard, J., and Dibble, R., "HCCI in a CFR Engine: Experiments and Detailed Kinetic Modeling," SAE Paper 2000-01- 0328, 2000.
- Flynn, P. F., Hunter, G. L., Farrell, L., Durrett, R. P., Akinyemi, O., Zur Loye, A. O., Westbrook, C. K., and Pitz, W. J., "The Inevitability of Engine-Out NO_x Emissions from Spark-Ignited and Diesel Engines," *Proceedings of the Combustion Institute* **29**:1211-1218, 2000.
- Fuerhapter, A., Piock, W. F., and Fraidl, G. K., "CSI - Controlled Auto Ignition - the Best Solution for the Fuel Consumption - Versus Emission Trade Off?," SAE paper 2003-01-0754.
- Fuerhapter, A., Unger, E., Piock, W. F., and Fraidl, G. K., "The new AVI CSI Engine – HCCI Operation on a Multi-Cylinder Gasoline Engine," SAE paper 2004-01-0551.
- Gamma Technologies, "GT-POWER User's manual, GT-SUITE™ Version 6.1," 2004.
- Gentili, R., Frigo, S., Tognotti, L., Habert, P., and Lavy, J., "Experimental Study on ATAC (Active Thermo-Atmosphere Combustion) in a Two-Stroke Gasoline Engine," SAE Paper 970363, 1997.

- Girard, J. W., Dibble, R. W., Flowers, D. L., and Aceves, S. M., "An Investigation of the Effect of Fuel-Air Mixedness on the Emissions from an HCCI Engine," SAE Paper 2002-01-1758, 2002.
- Goldsborough, S. S., and Van Blarigan, P., "A Numerical Study of a Free Piston Engine Operating on Homogeneous Charge Compression Ignition Combustion," SAE Paper 1999-01-0619, 1999.
- Gray, A. W., and Ryan, T. W., "Homogeneous Charge Compression Ignition (HCCI) of Diesel Fuel," SAE Paper 971676, 1997.
- Guohong, T., Zhi, W., Jianxin, W., Shijin, S., and Xinliang, A., "HCCI Combustion Control by Injectio Strategy with Negative Valve Overlap in a GDI Engine," SAE paper 2006-01-0415.
- Haraldsson, G., Tunestal, P., Johansson, B., and Hyvonen, J., "HCCI Close-Loop Combustion Control using Fast Thermal Management," SAE paper 2004-01-0943.
- Haraldsson, G., Tunestal, P., Johansson, B., and Hyvonen, J., "Transient Control of a Multi Cylinder HCCI Engine During a Drive Cycle," SAE paper 2005-01-0153.
- He X., Donovan, M. T., Zigler, B. T., Palmer, T. R., Walton, S. M., Wooldridge, M. S., and Atreya, A., "An Experimental and Modeling Study of Iso-octane Ignition Delay Times at Homogeneous Charge Compression Ignition Conditions," *Combustion and Flame*, Vol. 142, pp. 266-275, 2005.
- Heywood, J. B., *Internal Combustion Engine Fundamentals* (McGraw-Hill, New York, 1988).
- Hiltner, J., Agama, R., Mauss, F., Johansson, B., and Christensen, M., "HCCI Operation with Natural Gas: Fuel Composition Implications," *Proceedings of the ASME Internal Combustion Engine Fall Technical Conference*, ASME Paper 2000- ICE-317, 2000.

- Hiraya, K., Hasegawa, K., Urushihara, T., Liyama, A. and Otoh, T., "A Study on Gasoline Fueled Compression Ignition Engine ~ A Trial of Operation Region Expansion ~," SAE Paper 2002-01-0416.
- Hong, S., Assanis, D. N., and Wooldrige, M., "Multi-Dimensional Modeling of NO and Soot Emissions with Detailed Chemistry and Mixing in a Direct Injection Natural Gas Engine," SAE paper 2002-01-1112.
- Hong, S., Wooldridge, M., and Assanis, D. N., "Modeling of Chemical and Mixing Effects on Methane Autoignition Under Direct Injection stratified Charge Conditions," Proceeding of the 29th International Symposium on Combustion, 2002.
- Hultqvist, A., Christensen, M., Johansson, B., Franke, A., Richter, M., and Alden, M., "A Study of the Homogeneous Charge Compression Ignition Combustion Process by Chemiluminescence Imaging," SAE Paper 1999-01-3680, 1999.
- Hultqvist, A., Christensen, M., Johansson, B., Richter, M., Nygren, J., Hult, J., and Alden, M., "The HCCI Combustion Process in a Single Cycle~High-Speed fuel Tracer LIF and Chemiluminescence Imaging," SAE Paper 2002-01-0424, 2002.
- Hultqvist, A., Engdar, U., Johansson, B., and Klingmann, J., "Reacting Boundary Layers in a Homogeneous Charge Compression Ignition (HCCI) Engine," SAE Paper 2001-01-1032, 2001.
- Hyvonen, J., Haraldsson, G., and Johansson, B., "Operating Conditions Using Spark Assited HCCI Combustion During Combustion Mode Transfer to SU in a Multi-Cylinder VCR-HCCI Engine," SAE paper 2005-01-0109.
- Ishibashi, Y., and Asai, M., "Improving the Exhaust Emissions of Two-Stroke Engines by Applying the Activated Radical Combustion," SAE Paper 960742, 1996.

- Ishibashi, Y., Isomura, S., Kudo, O., Tsushima, Y., "Improving the Exhaust Emissions of Two-Stroke Engines by Applying the Activated Radical Combustion," SAE Paper 972077
- Iwashiro, Y., Tsurushima, T., Nishijima, Y., Asumi, Y., and Aoyagi, Y., "Fuel Consumption Improvement and Operation Range Expansion in HCCI by Direct Water Injection," SAE Paper 2002-01-0105.
- Kaahaaina, N. B., Simon, A. J., Caton, P. A., and Edwards, C. F., "Use of Dynamic Valving to Achieve Residual-Affected Combustion," SAE Paper 2001-01-0549, 2001.
- Kaiser, E. W., Yang, J., Culp, T., Xu, N., and Maricq, M. M., "HCCI Engine-out Emissions - Does Flame Propagation Occur in HCCI?," *International Journal of Engine Research*, Vol. 3, pp. 185-195, 2002.
- Koehler, U., and Bargende, M., "A Model for a Fast Prediction of the In-Cylinder Residual Gas Mass," SAE paper 2004-01-3053.
- Kong S., C., Marriott, C. D., Rutland, C. J., and Reitz, R. D., "Experiments and CFD Modeling of Direct Injection Gasoline HCCI Engine Combustion," SAE paper 2002-01-1925.
- Kong, S.-C., and Reitz, R. D., "Application of Detailed Chemistry and CFD for Predicting Direct Injection HCCI Engine Combustion and Emissions," *Proceedings of the Combustion Institute* 29:663-669, 2002.
- Kong, S. C., and Reitz, R. D., "Modeling Direct-Injection Gasoline HCCI Combustion Using Detailed Chemistry and CFD," ASME paper 2001-UCF-415, ICE-Vol. 37-2, 2001.

- Kong S., C., Marriott, C. D., Reitz, R. D., and Christensen, M., "Modeling and Experiments of HCCI Engine Combustion Using Detailed Chemical Kinetics with Multi-dimensional CFD," SAE paper 2001-01-1026.
- Kontarakis, G., Collings, N., and Ma, T., "Demonstration of HCCI Using a Single-Cylinder, Four-Stroke SI Engine with Modified Valve Timing," SAE Paper 2000-01-2870, 2000.
- Koopmans, L., Backlund, O., and Denbratt, I., "Cycle to Cycle Variations: Their Influence on Cycle Resolved Gas Temperature and Unburned Hydrocarbons from a Camless Gasoline Compression Ignition Engine," SAE Paper 2002-01-0110.
- Koopmans L., and Denbratt, I., "A Four Stroke Camless Engine, Operated in Homogeneous Charge Compression Ignition Mode with Commercial Gasoline," SAE paper 2001-01-3610.
- Koopmans, L., Strom, H., Lundgren, S., Backlund, O., and Denbratt, I., "Demonstrating a SI-HCCI-SI Mode Change on a Volvo 5-Cylinder Electronic Valve Control Engine," SAE paper 2003-01-0753.
- Kraft, M., Maigaard, P., Mauss, F., Christensen, M., and Johansson, B., "Investigation of Combustion Emission in a HCCI Engine –Measurement and a New Computational Model," Proc. Combust. Inst. 28:1195-1202, 2000.
- Lavy, J., Dabadie, J. C., Angelberger, C., Duret, P., Willand, J., Juretzka, A., Schaflein, J., Ma, T., Lendresse, Y., Satre, A., Shulz, C., Kramer, H., Zhao, H., and Damiano, L., "Innovative Ultra-Low NO_x Controlled Auto-Ignition Combustion Process for Gasoline Engines: the 4-Space Project," SAE paper 2000-01-1837.
- Law, D., Allen, J., and Chen, R., "On the Mechanism of Controlled Auto Ignition," SAE Paper 2002-01-0421.

- Law, D., Kemp, D., Allen, J., Kirkpatrick, G., and Copland, T., "Controlled Combustion in an IC-Engine with a Fully Variable Valve Train," SAE Paper 2000- 01-0251, 2001.
- Li, J., Zhao, H., Ladommatos, N., and Ma, T., "Research and Development of Controlled Auto-Ignition (CAI) Combustion in a 4-Stroke Multi-Cylinder Gasoline Engine," SAE paper 2001-01-3608.
- Iida, N., "Combustion Analysis of Methanol-Fueled Active Thermo-Atmosphere Combustion (ATAC) Engine Using a Spectroscopic Observation," SAE Paper 940684, 1994.
- Liu, J. P., Kleeberg, H., Tomazic, D., Ciaravino, J., and Amer, A. A., "A Model for On-Line Monitoring of In-Cylinder Residual Gas Fraction (RGF) and Mass Flowrate in Gasoline Engines," SAE paper 2006-01-0656.
- Livengood, J. C., and Wu, P. C., "Correlation of Auto-ignition Phenomena in internal Combustion Engines and Rapid Compression Machines," Proceedings of 5th Symposium (International) on Combustion, pp. 347-356, 1955.
- Ma, T., Oakley, A., Zhao, H., and Ladommatos, N., "Dilution Effects on the Controlled Auto-Ignition (CAI) Combustion of Hydrocarbon and Alcohol Fuels," SAE paper 2001-01-3606.
- Marriot, C. D., and Reitz, R. D., "Experimental Investigation of Direct Injection-Gasoline for Premixed Compression Ignited Combustion Phasing Control," SAE Paper 2002-01-0418, 2002.
- Matthews, J., Santoso, H., and Cheng, W. K., "Load Control for an HCCI Engine," SAE paper 2005-01-0150.
- Milovanovic, N., Blundell, D., Gedge, S., and Turner, J., "SI-HCCI-SI Mode Transition at Different Engine Operating Conditions," SAE paper 2005-01-0156.

- Santoso, H., Matthews, J., and Cheng, W. K., "Managing SI/HCCI Dual-Mode Engine Operation," SAE paper 2005-01-0162.
- Milovanovic, N., Blundell, D., Pearson, R., Turner, J., and Chen, R., "Enlarging the Operational Range of a Gasoline HCCI Engine by Controlling the Coolant Temperature," SAE paper 2005-01-0157.
- Morel, T., and Keribar, R., "A Model for Predicting Spatially and Time Resolved Convective Heat Transfer in Bowl-in-Piston Combustion Chambers," SAE Paper 850204, 1985.
- Najt, P. M., and Foster, D. E., "Compression-Ignited Homogeneous Charge Combustion," SAE paper 830264.
- Noguchi, M., Tanaka, Y. Tanaka, T., and Takeuchi, Y., "A Study on Gasoline Engine Combustion by Observation of Intermediate Reactive Products during Combustion," SAE paper 790840.
- Nygren, J., Hult, J., Richter, M., Alden, M., Christensen, M., Hultqvist, A., and Johansson, B., "Three-Dimensional Laser Induced Fluorescence of Fuel Distributions in an HCCI Engine," *Proceedings of the Combustion Institute* **29**:679-685, 2002.
- Ognik, R., and Golovitchev, V., "Gasoline HCCI Modeling: Computer Program Combining Detailed Chemistry and Gas Exchange Process," SAE paper 2001-01-3614.
- Ogink, R., and Golovitchev, V., "Gasoline HCCI Modeling: an Engine Cycle Simulation Code with a Multi-zone Combustion Model," SAE Paper 2002-01-1745, 2002.
- Ohyama, Y., "Engine Modeling of HCCI Transient Operations," SAE paper 2005-01-0158.

- Olsson, J., Tunestal, P., and Johansson, B., "Closed-Loop Control of an HCCI Engine," SAE Paper 2001-01-1031.
- Olsson, J., Tunestal, P., Johansson, B., Fiveland, S., Agama, R., Willi, M. and Assanis, D., "Compression Ratio Influence on Maximum Load of a Natural Gas Fueled HCCI Engine," SAE Paper 2002-01-0111.
- Onishi, S., Jo, S. H., Shoda, K., Jo, P. D., and Kato, S., "Active Thermo-Atmospheric Combustion (ATAC) - A New Combustion Process for Internal Combustion Engines," SAE paper 790501.
- Persson, H., Agrell, M., Olsson, J., Johansson, B., and Strom, H., "The effect of Intake Temperature on HCCI Operation Using Negative Valve Overlap," SAE paper 2004-01-0944.
- Rausen, D. J., Stefanopoulou, A. G., Kang, J-M., Eng, J. A., and Kuo, T-W., "A Mean-Value Model for Control of Homogeneous Charge Compression Ignition (HCCI) Engines," *IEEE Proceedings of American Control Conference*, 2004.
- Reuss, D. L., and Sick, V., "Investigation of HCCI Combustion with Combined PLIF Imaging and Combustion Analysis," *Proceedings of the Third Joint Meeting of the U.S. Sections of The Combustion Institute*, Chicago, IL, 2003.
- Richter, M., Engstrom, J., Franke, A., Alden, M., Hultqvist, A., and Johansson, B., "The Influence of Charge Inhomogeneity on the HCCI Combustion Process," SAE Paper 2000-01-2868, 2000.
- Richter, M., Franke, A., Alden, M., Hultqvist, A., and Johansson, B., "Optical Diagnostics Applied to a Naturally Aspirated Homogeneous Charge Compression Ignition Engine," SAE Paper 1999-01-3649, 1999.
- Risberg, P., Kalghatgi, G., and Ångström, H.-E., "The Influence of EGR on Autoignition Quality of Gasoline-Like Fuels in HCCI Engines," SAE Paper 2004- 01-2952, 2004.

- Ryan, T. W., Callahan, T. J., "Homogeneous Charge Compression Ignition of Diesel Fuel," SAE paper 961160.
- Santoso, H., Matthews, J., and Cheng, W., "Characteristics of HCCI Engine Operating in the Negative-Valve-Overlap Mode," SAE paper 2005-02-2133.
- Shaver, G. M., "Physics-Based Modeling and Control of Residual-Affected HCCI Engines Using Variable Valve Actuation," Ph.D. Thesis, 2005, Stanford University, Palo Alto.
- Sjöberg, M., and Dec, J. E., "An Investigation of the Relationship between Measured Intake Temperature, BDC Temperature, and Combustion Phasing for Premixed and DI HCCI Engines," SAE Paper 2004-01-1900, 2004.
- Sjöberg, M., Dec, J. E., Babajimopoulos, A., Assanis, D. N., "Comparing Enhanced Natural Thermal Stratification against Retarded Combustion Phasing for Smoothing of HCCI Heat-Release Rates," SAE paper 2004-01-2994.
- Sjöberg, M., Edling, L.-O., Eliassen, T., Magnusson, L., and Angström, H.-E., "GDI HCCI: Effects of Injection Timing and Air Swirl on Fuel Stratification, Combustion and Emissions Formation," SAE Paper 2002-01-0106, 2002.
- Smith, J. R., Aceves, S. M., Westbrook, C. K., and Pitz, W. J., "Modeling of Homogeneous Charge Compression Ignition (HCCI) of Methane," *Proceedings of the ASME Internal Combustion Engine Fall Technical Conference*, ASME Paper 97-ICE-68, 1997.
- Stanglmaier, R. H., and Roberts, C. E., "Homogeneous Charge Compression Ignition (HCCI): Benefits, Compromises, and Future Engine Applications," SAE Paper 1999-01-3682, 1999.

- Strandh, P., Bengtsson, J., Johansson, R., Tunestal, P., and Johansson, B., "Variable Valve Actuation for Timing Control of a Homogeneous Charge Compression Ignition Engine," SAE paper 2005-01-0147.
- Sun, R., Thomas, R., and Gray, C. Jr., "Ann HCCI Engine: Power Plant for a Hybrid Vehicle," SAE paper 2004-01-0933.
- Swan, K., Shahbakhti, M., and Koch, C. R., "Predicting Start of Combustion Using a Modified Knock Integral Method for an HCCI Engine," SAE paper 2006-01-1086.
- Takeda, Y., Keiichi, N., and Keiichi, N., "Emission Characteristics of Premixed Lean Diesel Combustion with Extremely Early Staged Fuel Injection," SAE paper 961163.
- Thring, R. H., "Homogeneous Charge Compression Ignition (HCCI) Engines," SAE paper 892068.
- Urata, Y., Awasaka, M., Takanashi, J., Kakinuma, T., Hakozaki, T., and Umemoto, A., "A Study of Gasoline Fuelled HCCI Engine Equipped with an Electromagnetic Valve Train," SAE paper 2004-01-1898.
- Urushihara, T., Hiraya, K., Kakuhou, A., and Itoh, T., "Expansion of HCCI Operating Region by the Combustion of Direct Fuel Injection, Negative Overlap and Internal Fuel Reformation," SAE paper 2003-01-0749.
- Urushihara, T., Yamaguchi, K., Yoshizawa, K., and itoh, T., "A Study of a Gasoline-Fueled Compression Ignition Engine - Expansion of HCCI Operating Range Using SI Combustion as a Trigger of Compression Ignition -," SAE paper 2005-01-0180.
- Wilhelmsson, C., Vressner, A., Tunestal, P., Johansson, B., Sarnier, G., and Alden, M., "Combustion Chamber Wall Temperature Measurement and Modeling During Transient HCCI Operation," SAE paper 2005-01-3731.

- Willand, J., Nieberding, R.-G., Vent, G., and Enderle, C., "The Knocking Syndrome: Its Cure and Potential," SAE Paper 982483, 1998.
- Wolters, P., Salber, W., Geiger, J., Duesmann, M., Dilthey, J., "Controlled Auto Ignition Combustion Process with an Electromechanical Valve Train", SAE Paper 2003-01-0032.
- Woschni, G., "A Universally Applicable Equation for the Instantaneous Heat Transfer Coefficient in the Internal Combustion Engine," SAE paper 670931.
- Wu, B., Filipi, Z. S., Kramer, D. M., Ohl, G. L., Prucka, M. J., and DiValetin, E., "Using Neural Networks to Compensate Altitude Effects on the Air Flow Rate in Variable Valve Timing Engines," SAE paper 2005-01-0066.
- Xie, H., Hou, S., Qin, J., Zhang, Y., Li, N., and Zhao, H., "Control Strategies for Steady and Transient Operation of a 4-Stroke Gasoline Engine with CAI Combustion Using a 4-Variable Valve Actuating System (4VVAS)," SAE paper 2006-01-1083.
- Yang, J., Culp, T., and Kenney, T., "Development of a Gasoline System Using HCCI Technology - The Concept and the Test Results," SAE Paper 2002-01-2832, 2002.
- Yang, J., and Kenney, T., "Robustness and Performance Near the Boundaries of HCCI Operating Regime of a Single-Cylinder OKP Engine," SAE paper 2006-01-1082.
- Yoo, I. K., Simpson, K., Bell, M., and Majkowski, S., "An Engine Coolant Temperature Model and Application for Cooling System Diagnosis," SAE paper 2000-01-0939.
- Zhao, F., Asmus, T. W., Assanis, D. N., Dec, J. E., Eng, J. A., and Najt, P. M., Eds., *Homogeneous Charge Compression Ignition (HCCI) Engines: Key Research and Development Issues* (SAE, Warrendale, PA, 2003).
- Zhao, F., Asmus, T., Assanis, D. N., Dec, J., Eng J., and Najt, P., "Homogeneous Charge Compression Ignition (HCCI) Engines, Key Research and Development Issues," SAE PT-94, 2003.

Zhao, H., Ma, T., and Ladommatos, N., "Performance and Analysis of a 4-Stroke Multi-Cylinder Gasoline Engine with CAI Combustion," SAE paper 2002-01-0420.

Zheng, J., Yang, W., Miller D. L., and Cernansky, N. P., "Prediction of Pre-ignition Reactivity and Ignition Delay for HCCI Using a Reduced Chemical Kinetic Model," SAE 2001-01-1025.